UNIVERSITY OF SOUTHAMPTON

FACULTY OF PHYSICAL SCIENCES AND ENGINEERING

School of Physics and Astronomy

Southampton High Energy Physics Group

Distinguishing Models of New Physics at the LHC

by

Patrik Svantesson

Presented for the degree of

Doctor of Philosophy

June 2013

UNIVERSITY OF SOUTHAMPTON

ABSTRACT

FACULTY OF PHYSICAL SCIENCES AND ENGINEERING
School of Physics and Astronomy

Doctor of Philosophy

DISTINGUISHING MODELS OF NEW PHYSICS AT THE LHC

by Patrik Svantesson

The work presented in this thesis explores ways of distinguishing models of physics beyond the Standard Model at the Large Hadron Collider (LHC). The focus is put on supersymmetric models, in particular the Minimal Supersymmetric Standard Model (MSSM) and the E_6-inspired Supersymmetric Standard Model (E_6SSM), which are well known and well motivated models.

The muon decay channel of the pseudoscalar and heavy Higgs bosons in the MSSM is studied. It is shown that these decays to muons, in some scenarios, make it possible to measure the widths of these Higgs bosons at the LHC. This is the only known way of measuring this width at the LHC. The decays to muons also allow for the mass to be measured accurately which together with the width measurement offers a unique opportunity to pin down the value of the model parameter $\tan\beta$, which could be used to distinguish different scenarios within the MSSM and potentially in its extensions.

Gluino cascade decays are investigated as a tool to distinguish the MSSM from more complex models, with the E_6SSM as an example. It is shown that the longer cascade decays of the E_6SSM gluinos provide less missing transverse momentum and higher lepton multiplicity, implying the higher importance of multi-lepton searches at the LHC in models with a richer low-energy particle content. The three-lepton channel is shown to be a good discriminator between the models. In the case of a gluino discovery one would typically expect a signal in this channel if it is an E_6SSM gluino but not if it is an MSSM gluino.

Furthermore, the implications of limits from dark matter and Z' searches on the Higgs sector and other collider phenomenology are discussed. These implications are important to constrain and differentiate models. In addition, the contribution to fine-tuning from the Z' mass is discussed as an important measure of how attractive a model is, which should be considered by model builders.

To Sveta
my wonderful wife

Contents

List of Figures

List of Tables

Declaration of Authorship

I, Patrik Svantesson , declare that the thesis entitled *Distinguishing Models of New Physics at the LHC* and the work presented in the thesis are both my own, and have been generated by me as the result of my own original research. I confirm that:

- this work was done wholly or mainly while in candidature for a research degree at this University;
- where any part of this thesis has previously been submitted for a degree or any other qualification at this University or any other institution, this has been clearly stated;
- where I have consulted the published work of others, this is always clearly attributed;
- where I have quoted from the work of others, the source is always given. With the exception of such quotations, this thesis is entirely my own work;
- I have acknowledged all main sources of help;
- where the thesis is based on work done by myself jointly with others, I have made clear exactly what was done by others and what I have contributed myself;
- parts of this work have been published as: [19], [20], [21], [22] and [23]

Signed:.....

Date:.....

Acknowledgements

First of all I would like to thank my supervisor Alexander Belyaev for his enthusiasm and all guidance and motivation he has given me throughout these years in Southampton.

I am also very grateful to Steve King for sharing his knowledge and giving me inspiration.

I would like to thank Jonathan Hall for providing the initial LanHEP code for the E_6SSM and for his help in developing it further.

Furthermore, I would like to thank my collaborators in the USA, Howard Baer and Chung Kao, whose correspondence and work was of great help in the beginning of my research.

I am also thankful to all my other colleagues and collaborators in Southampton for good discussions and a great work environment.

I am thankful for the NExT institute, a part of SEPnet, for providing studentship funding.

Last but not least, a special thanks to my wife, for her love, support and patience.

Abbreviations

BSM	Beyond the Standard Model
CDM	Cold Dark Matter
COBE	Cosmic Background Explorer
CMSSM	(GUT-)Constrained Minimal Supersymmetric Standard Model
DM	Dark Matter
E_6SSM	E_6-inspired (Exceptional) Supersymmetric Standard Model
EZSSM	E_6-inspired Z_2^S-invariant Supersymmetric Standard Model
EW	ElectroWeak
EWPT	ElectroWeak Precision Tests
EWSB	ElectroWeak Symmetry Breaking
FP	Focus Point
GUT	Grand Unified Theory
HB	Hyperbolic Branch
KK	Kaluza-Klein (excitation)
LEP	Large Electron-Positron collider
LHC	Large Hadron Collider
LO	Leading Order
LSP	Lightest Supersymmetric Particle
MC	Monte Carlo
MSSM	Minimal Supersymmetric Standard Model
mSUGRA	minimal SUperGRAvity
NLL	Next-to-Leading Log
NLO	Next-to-Leading Order
NLSP	Next-to-Lightest Supersymmetric Particle
NMSSM	Next-to-Minimal Supersymmetric Standard Model
NNLO	Next-to-Next-to-Leading Order
PDF	Parton Density Function
QCD	Quantum ChromoDynamics
REWSB	Radiative ElectroWeak Symmetry Breaking
SM	Standard Model
SPS	Super Proton Synchrotron
SUSY	Supersymmetry

USSM	$U(1)'$ extended Supersymmetric Standard Model
VEV	Vacuum Expectation Value
WDM	Warm Dark Matter
WIMP	Weakly Interacting Massive Particle
WMAP	Wilkinson Microwave Anisotropy Probe

"It is too early for despair but enough for depression"

— *G. Altarelli*

Chapter 1

Introduction

We are at an important stage in the exploration of high energy physics. The Large Hadron Collider (LHC) has collected data for about three years and has delivered important results, most notably the discovery of a Higgs boson, which has been the main motivation for the experiment. The hopes and expectations of finding signs of new physics Beyond the Standard Model (BSM) have not yet been satisfied however. Currently the LHC is shut down for an upgrade to an energy of 6.5 TeV per beam, close to the full design energy of 7 TeV. This will improve chances for discoveries and increase the reach for explorations of new physics phenomena.

Many BSM models have turned less attractive after the LHC data but few are completely ruled out. Strong arguments from cosmology, such as the existence of Dark Matter (DM) and the need for Baryogenesis, points towards new physics, which very well could be accessible for the LHC. The Standard Model of particle physics (SM) also suffers from theoretical, which one might consider cosmetic, issues such as the hierarchy problem, non-unification of gauge couplings and the unexplained flavour structure, which needs to be solved in attempts of moving towards a Grand Unified Theory (GUT). Furthermore, it still remains to see whether the discovered Higgs boson is the SM Higgs boson or if it will have some significantly different properties. Not only are there many theories, e.g Supersymmetry (SUSY), Extra Dimensions and Technicolour, which contain a SM-like Higgs boson and predict other new physics, but they also come in a large number of varieties. It is therefore an important task for the future to distinguish models of new physics from each other and from the SM. We will want to determine what models are consistent with the current data and how to discover them most efficiently. In the event of signs of new physics from the next set of LHC data we will need to distinguish what kind of new physics it is just as we need to distinguish what kind of Higgs boson it is that has been discovered.

The aim of this thesis is to discuss properties of some BSM models and give examples on how one can attempt to distinguish them. The outline of the content is as follows: In

Chapter 2 the SM is introduced and some features which are important in the context of this thesis and useful in comparison with other models are illustrated. Supersymmetry and some of its most useful and important concepts for phenomenology are discussed in Chapter 3. In Chapter 4 the basic features of the Minimal Supersymmetric Standard Model (MSSM) are discussed. Methods on how to determine and gather signatures of models are discussed in Chapter 5 where also computational tools and principles of discovering, distinguishing and excluding models are presented. The basic principles of relic density and detection of dark matter are introduced in Chapter 6 where also some experimental results are presented. Chapter 7 contains work that was first published in [22]. In this work a particular DM motivated scenario in the MSSM is explored by considering the muon decay channel of a pseudoscalar Higgs boson at the LHC. In Chapter 8 the experimental status of SUSY is presented which indicates the need to go beyond the simplest SUSY models. An example of a non-minimal SUSY model, the E_6-inspired (or exceptional) supersymmetric standard model (E_6SSM), is described in Chapter 9. Parts of this chapter have previously been published in [21]. In Chapter 10, which contains work first published in [20, 19, 21], the possibilities of discovering and distinguishing E_6 inspired models via gluino decays at LHC are investigated. Chapter 11 contains work that was first published in [23]. In this work the standard class of E_6 models, but with a reduced extra g_1' gauge coupling providing a lighter and more weakly coupled Z' boson, are considered. In addition, a previously unpublished section regarding the tree-level Higgs masses in such models have been added to this chapter. Finally in Chapter 12 some concluding remarks and future prospects are given.

Additional information and diagrams of gluino decays are presented in Appendix A and details on the software implementation of the E_6SSM is presented in Appendix B.

Chapter 2

The Standard Model

The aim of physicists through many centuries has been to describe observed phenomena in Nature with a model as simple and general as possible. Until not much more than 100 years ago gravity and electromagnetism were the only known interactions, since then the weak and strong interactions have been discovered and studied extensively. The physics research of the 20th century was guided by the concept of symmetries. The understanding of the symmetry of space-time and the symmetries of the interactions among particles finally led to the formulation of what we now know as the Standard Model of particle physics (SM). The SM describe the properties of what we today consider fundamental particles and their interactions, with the exception of gravity which is much weaker then the other interactions at energies accessible by current experiments. A simplified overview of the particle content of the SM is shown in Figure 2.1. The model has been tested by a large number of experiments and most of its predictions have been confirmed and measured to an incredible precision.

2.1 Lagrangian

The SM is a quantum field theory with its Lagrangian invariant under Lorentz transformations, to agree with the Special Theory of Relativity, and under the local transformations of the SM gauge group

$$G_{SM} = SU(3)_C \times SU(2)_W \times U(1)_Y, \tag{2.1}$$

to describe the strong, and electro-weak interactions. The SM Lagrangian can be written as

$$\mathcal{L}_{SM} = \frac{1}{4}F^2 + \sum_{\psi=Q,\bar{u},\bar{d},L,\bar{e}} i\bar{\psi}\not{D}\psi + |DH|^2 + y_u H Q\bar{u} + y_d H^\dagger Q\bar{d} + y_e H^\dagger L\bar{e} - \lambda|H|^4 + \mu^2|H|^2, \tag{2.2}$$

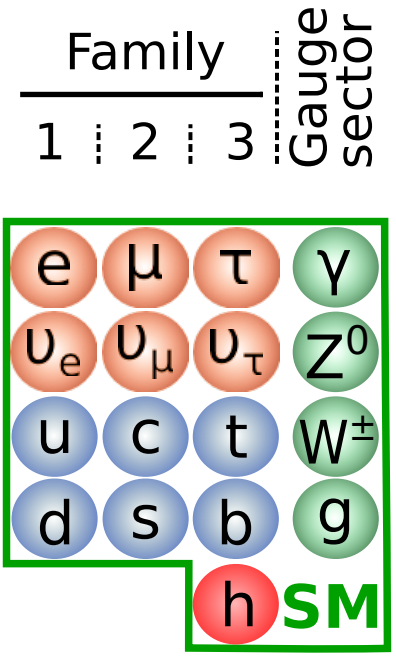

Figure 2.1: A simplified overview of the particle content of the SM. There are three generations of leptons (orange) and quarks (blue), there is one scalar (red) – the Higgs boson – and there are four kinds of gauge bosons (green). A more accurate picture of the particle content is presented in Table 2.1.

where all contracted Lorentz, gauge and family indices have been omitted for simplicity. The Fs are the gauge field strength tensors,

$$F_{\mu\nu} = \partial_\mu B_\nu - \partial_\nu B_\mu \tag{2.3}$$

$$F^a_{\mu\nu} = \partial_\mu W^a_\nu - \partial_\nu W^a_\mu + g_2 \epsilon^{abc} W^b_\mu W^c_\nu \tag{2.4}$$

$$F^a_{\mu\nu} = \partial_\mu G^a_\nu - \partial_\nu G^a_\mu + g_3 f^{abc} G^b_\mu G^c_\nu, \tag{2.5}$$

and the Ds are the covariant derivatives,

$$D_\mu = \partial_\mu - i g_1 Y B_\mu - i g_2 W^a_\mu t^a_2 - i g_3 G^a_\mu t^a_3, \tag{2.6}$$

where correct $U(1)$ charge Y and $SU(2)$ and $SU(3)$ representation should be used when acted on a particular field. The ys are the Yukawa couplings and λ and μ are the dimensionless and dimensionful parameters of the Higgs potential respectively. The matter fields, and the gauge fields are listed with their representations under the gauge groups in the top and bottom part of Table 2.1 respectively. As a convention all fermion fields are written in terms of left-handed, two-component Weyl spinors. Right-handed fields are written in terms of their charge conjugate, which transforms like a left-handed spinor under Lorentz transformations, and is denoted with a bar:

$$\bar{\psi} = \psi^c_R = -i\sigma_2 \psi^*_R, \tag{2.7}$$

Field	components	$SU(3)$	$SU(2)$	$U(1)$
Fermions	Spin 1/2			
Q^i	$\begin{pmatrix} u_L \\ d_L \end{pmatrix}^i$	**3**	**2**	$\frac{1}{6}$
$\bar{u}^i$	$u_R^{\dagger i}$	$\bar{\mathbf{3}}$	**1**	$-\frac{2}{3}$
$\bar{d}^i$	$d_R^{\dagger i}$	$\bar{\mathbf{3}}$	**1**	$\frac{1}{3}$
L^i	$\begin{pmatrix} \nu_L \\ e_L \end{pmatrix}^i$	**1**	**2**	$-\frac{1}{2}$
$\bar{e}^i$	$e_R^{\dagger i}$	**1**	**1**	1
Scalars	Spin 0			
H	$\begin{pmatrix} H^+ \\ H^0 \end{pmatrix}$	**1**	**2**	$\frac{1}{2}$
Gauge	Spin 1			
g	g	**8**	**1**	0
W	$W^\pm, W^0$	**1**	**3**	0
B	B	**1**	**1**	0

Table 2.1: The SM field content and the fields' representations under the gauge groups. Right-handed fields are written in terms of their charge conjugate.

where $\sigma_2 = \left(\begin{smallmatrix} 0 & -i \\ i & 0 \end{smallmatrix}\right)$ is one of the Pauli-matrices. The 4-component Dirac field can then be written as

$$\Psi = \begin{pmatrix} \psi_L \\ \psi_R \end{pmatrix} = \begin{pmatrix} \psi_L \\ i\sigma_2 \bar{\psi}^* \end{pmatrix}. \tag{2.8}$$

The SM Lagrangian (2.2) contains all renormalisable, gauge and Lorentz invariant terms possible with the gauge group in (2.1) and particle content defined in Table 2.1[1]. It is quite remarkable that these few fundamental principles together with the SM matter content define such a well tested model.

2.2 The Higgs boson

The 2012 discovery[24, 25] of a new boson at the LHC and later the measurements of its couplings[26, 27, 28] has pinned down the last missing piece of the SM, the Higgs boson. The Higgs boson was theorised in 1964 [29] as a part of a mechanism[2] [30, 29, 31, 32, 33] for generating masses to gauge bosons via spontaneous symmetry breaking.

The proposed mechanism is perhaps the simplest way of acquiring gauge boson masses without breaking gauge symmetry explicitly in the Lagrangian. To see the problem with massive gauge bosons one can explicitly check the gauge invariance of mass terms in a U(1) gauge theory. A matter field, e.g. a fermion ψ, is allowed by gauge invariance to

[1] Terms $\propto \epsilon^{\mu\nu\rho\sigma} F_{\mu\nu} F_{\rho\sigma}$ are possible but in the case of QCD this term has to be very suppressed, the absence of explanations for this in the SM is known as the strong CP-problem.

[2] Theorised by Brout, Englert, Higgs, Kibble, Guralnik, Haagen and Anderson.

have a mass term

$$-m\bar{\psi}\psi \tag{2.9}$$

since an Abelian gauge transformation on the matter field simply is

$$\psi \to \psi' = e^{iQ\alpha(x)}\psi. \tag{2.10}$$

The gauge field A_μ has to transform like

$$A_\mu \to A'_\mu = A_\mu + \frac{1}{g}\partial_\mu\alpha(x) \tag{2.11}$$

to keep the kinetic term for the matter field,

$$\bar{\psi}\not{D}\psi = \bar{\psi}\gamma^\mu(\partial_\mu - igQA_\mu)\psi, \tag{2.12}$$

gauge invariant. Therefore an equivalent mass term,

$$-M^2A_\mu A^\mu, \tag{2.13}$$

for the gauge boson are forbidden by the gauge symmetry. In the SM, also the fermion mass terms, like the one in (2.9), are forbidden by gauge and Lorentz invariance. However, if the SM is extended with a right-handed neutrino, which is a SM gauge singlet, this particle could have such a mass term.

2.2.1 The Higgs potential

The Higgs field in the SM will give mass to the gauge bosons Z and $W^\pm$ by spontaneously breaking the electroweak gauge symmetry by acquiring a vacuum expectation value (VEV). The Higgs doublet H can be operated on by an $SU(2)$ gauge transformation such that only the bottom component is non-zero and real. In this gauge choice the Higgs doublet can be written

$$H = \frac{1}{\sqrt{2}}\begin{pmatrix} 0 \\ v + h(x) \end{pmatrix}, \tag{2.14}$$

where v is the Higgs VEV and h the fluctuating field around it. The VEV is related to the parameters of the Lagrangian. From (2.2) one can read off the Higgs potential

$$V(H^0) = \lambda H^{0\,4} - \mu^2 H^{0\,2}, \tag{2.15}$$

where $H^0 = v + h$. Stability around the vacuum $\langle H^0 \rangle = v$ implies

$$0 = \frac{\partial V}{\partial H^0} = \sqrt{2}\lambda v^3 - \sqrt{2}\mu^2 v, \tag{2.16}$$

and solving for non-zero v gives

$$v = \sqrt{\frac{\mu^2}{\lambda}}. \tag{2.17}$$

By expanding the potential (2.15) in v and h,

$$\begin{aligned} V(h,v) =& \frac{\lambda}{4}(v^4 + 4hv^3 + 6h^2v^2 + 4h^3v + h^4) - \frac{\mu^2}{2}(v^2 + 2hv + h^2) && (2.18)\\ =& \frac{\lambda}{4}h^4 + \lambda v h^3 - \left(\frac{\mu^2}{2} - \frac{3}{2}\lambda v^2\right) h^2 - (\mu^2 - \lambda v^2)vh && (2.19)\\ =& \frac{\lambda}{4}h^4 + \lambda v h^3 + \mu^2 h^2, && (2.20) \end{aligned}$$

one can identify the mass term,

$$\frac{m_h^2}{2}h^2 = \mu^2 h^2, \tag{2.21}$$

and thus the mass,

$$m_h = \mu\sqrt{2} = v\sqrt{2\lambda}, \tag{2.22}$$

for the physical Higgs field h.

Now that the Higgs mass is measured all parameters of the Higgs potential is known. One can use the measured Higgs mass and VEV to evaluate the couplings μ and λ in a naive first approximation:

$$m_h = 126 \text{ GeV} \Rightarrow \mu = 89.1 \text{ GeV} \tag{2.23}$$

$$v = 246 \text{ GeV} \Rightarrow \lambda = 0.13. \tag{2.24}$$

More careful analysis have been made, investigating what implications different values of the Higgs mass have for the perturbativity of the self-coupling, λ, and the stability of the potential [1]. It was shown that for a Higgs mass of around 125 GeV, if the SM is supposed to be valid up to the Planck scale, the potential is at the very border of the stability bound as shown in Figure 2.2.

2.2.2 Z and W masses

If one expands the kinetic term for the Higgs doublet in (2.2) in the gauge choice (2.14) one gets

$$|DH|^2 = \left|(\partial_\mu - ig_1\frac{1}{2}B_\mu - ig_2 W_\mu^a t_2^a)\frac{1}{\sqrt{2}}\begin{pmatrix}0\\ v+h\end{pmatrix}\right|^2, \tag{2.25}$$

where the $SU(2)$ fields and generators have been expanded as

$$W_\mu^a t_2^a = \frac{1}{2}(\sqrt{2}(W_\mu^+\sigma^+ + W_\mu^-\sigma^-) + W_\mu^3\sigma^3) \tag{2.26}$$

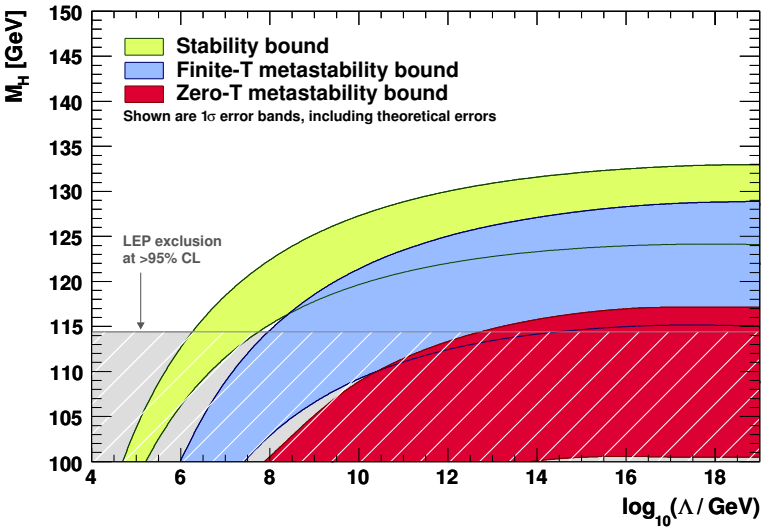

Figure 2.2: Stability and metastability bounds on the Higgs mass as a function of the cut-off scale Λ. The error bands include uncertainties in α_s, m_t and theory. The figure is taken from [1].

with $\sigma^{\pm} = \frac{1}{2}(\sigma^1 \pm i\sigma^2)$ and $W^{\pm} = \frac{1}{\sqrt{2}}(W^1 \mp iW^2)$. To see how the Higgs VEV gives mass to the gauge bosons one can ignore the derivative and h in (2.25) and focus on the quadratic terms in W and Z. Expanding the relevant terms gives

$$\begin{aligned}
\mathcal{L}_{\mathrm{W,Z-masses}} &= \frac{1}{8}\left|\left(-ig_1 B_\mu - ig_2(\sqrt{2}W^+_\mu\sigma^+ + \sqrt{2}W^-_\mu\sigma^- + W^3_\mu\sigma^3)\right)\begin{pmatrix}0\\ v\end{pmatrix}\right|^2 \\
&= \frac{1}{8}\left|\left(-ig_1 B_\mu \begin{pmatrix}0\\ v\end{pmatrix} - ig_2(\sqrt{2}W^+_\mu \begin{pmatrix}v\\ 0\end{pmatrix} + W^3_\mu \begin{pmatrix}0\\ -v\end{pmatrix})\right)\right|^2 \\
&= \frac{g_2^2v^2}{4}W^+W^- + \frac{g_1^2v^2}{8}B^2 + \frac{g_2^2v^2}{8}W^{3\,2} + \frac{g_1g_2v^2}{4}BW^3 \\
&= m_W^2 W^+W^- + \begin{pmatrix}B & W^3\end{pmatrix}\frac{v^2}{8}\begin{pmatrix}g_1^2 & g_1g_2\\ g_1g_2 & g_2^2\end{pmatrix}\begin{pmatrix}B\\ W^3\end{pmatrix}
\end{aligned} \tag{2.27}$$

from where one can read off the W mass

$$m_W = \frac{g_2 v}{2} \tag{2.28}$$

and the mass matrix

$$M_{BW^3} = \frac{v^2}{4}\begin{pmatrix}g_1^2 & g_1g_2\\ g_1g_2 & g_2^2\end{pmatrix} \tag{2.29}$$

for B and W^3, which has eigenvalues

$$m^2_{Z,\gamma} = \frac{v^2}{4}\left(\frac{g_1^2+g_2^2}{2} \pm \frac{1}{2}\sqrt{(g_1^2-g_2^2)^2 + 4g_1^2g_2^2}\right) = \frac{v^2}{8}\left(g_1^2+g_2^2\right)(1\pm 1). \tag{2.30}$$

The Z boson is the massive mixture of B and W^3 with mass

$$m_Z = \frac{v\sqrt{g_1^2 + g_2^2}}{2} = \frac{v\bar{g}}{2} \tag{2.31}$$

while the photon is the massless mixture. The weak mixing angle, θ_W, is defined as the angle between the mass eigenstates Z, γ and the weak interaction eigenstates B, W^3,

$$\begin{pmatrix} \gamma \\ Z \end{pmatrix} = \begin{pmatrix} \cos\theta_W & \sin\theta_W \\ -\sin\theta_W & \cos\theta_W \end{pmatrix} \begin{pmatrix} B \\ W^3 \end{pmatrix}. \tag{2.32}$$

By rotating the diagonal mass matrix by θ_W,

$$\begin{pmatrix} \cos\theta_W & -\sin\theta_W \\ \sin\theta_W & \cos\theta_W \end{pmatrix} \begin{pmatrix} 0 & 0 \\ 0 & m_Z^2 \end{pmatrix} \begin{pmatrix} \cos\theta_W & \sin\theta_W \\ -\sin\theta_W & \cos\theta_W \end{pmatrix} = \frac{v^2}{4} \begin{pmatrix} g_1^2 & g_1 g_2 \\ g_1 g_2 & g_2^2 \end{pmatrix} \tag{2.33}$$

one can read off

$$\cos^2\theta_W m_Z^2 = m_W^2 \quad \Rightarrow \quad \cos\theta_W = \frac{m_W}{m_Z}. \tag{2.34}$$

2.3 Experimental verifications

Many experiments have verified the validity of the SM. The Large Electron-Positron collider (LEP) made several important measurement of the electroweak theory, e.g. precise measurements [34] of the widths and masses of the Z and W bosons which had been discovered at the proton-antiproton collider Super Proton Synchrotron (SPS) [35, 36]. Another proton-antiproton collider, Tevatron, discovered the top-quark [37, 38], the last missing quark of the SM. Tevatron also made impressive precision measurements, e.g. an even more precise measurement of the W mass and width [39] than that by LEP. Finally, the last missing piece of the SM, the Higgs boson, was discovered at the LHC. The LHC has also confirmed previously measured properties of the SM and will doubtlessly contribute to the precision measurements as well.

To understand how well the SM fits to all collected data, global fits have been made. In Figure 2.3 results by the Gfitter group[2] are presented, which show a very good agreement between the data and the SM. The observables with largest pull are the forward-backward asymmetry for b-quarks at LEP , $A_{FB^{(0,b)}}$, and the ratio of partial width to b-quarks and hadrons of the Z boson at LEP, R_b^0. Another plot from the same group is presented in Figure 2.4 and shows regions of 68% and 95% confidence level for fits of m_t and M_W, with and without the measurement of M_H as input. These fits are in very good agreement with the measurements which illustrates the great consistency of the SM.

Also in the Quantum ChromoDynamics (QCD) sector the SM is verified to a great precision. As an example, results from measurements and lattice calculations of the strong gauge coupling are plotted with the predicted running coupling of QCD in Figure 2.5.

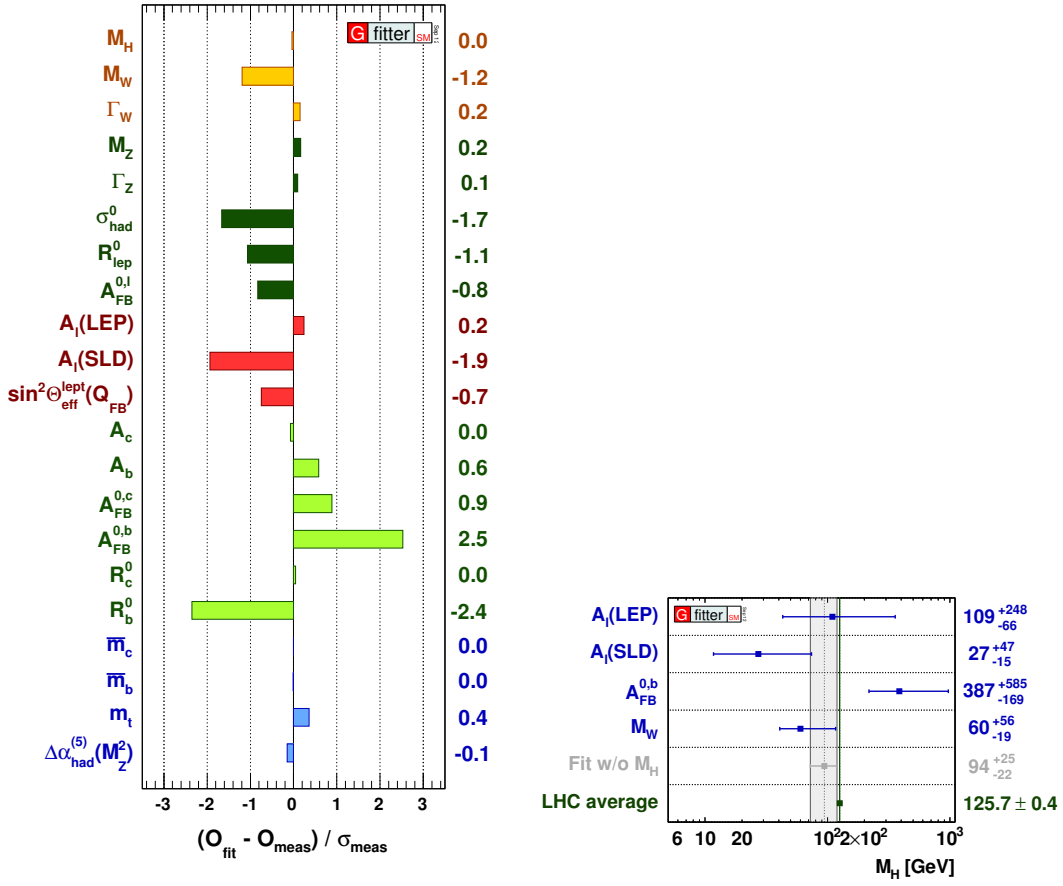

Figure 2.3: Results by global electroweak fits by the Gfitter group[2]. The left plot shows the pull between the fitted value and the experimentally measured value for the relevant observables in units of the experimental uncertainty.

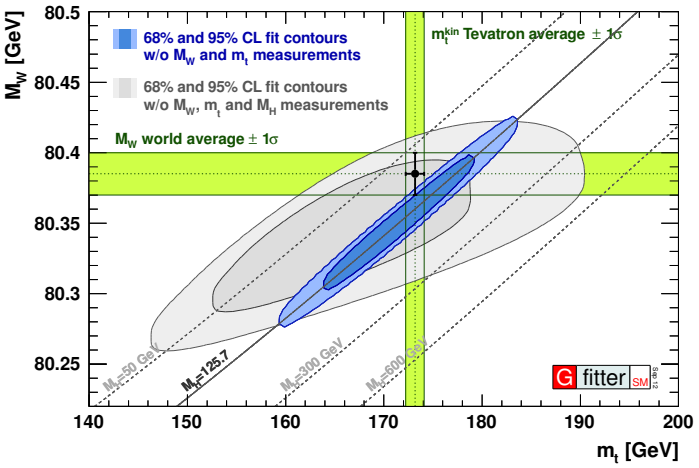

Figure 2.4: Gfitter[2] results. The shaded regions show 68% and 95% confidence levels for fits of m_t and M_W, with (blue) and without (grey) the measurement of M_H as input. The vertical and horizontal bands are direct measurements with 1σ errors.

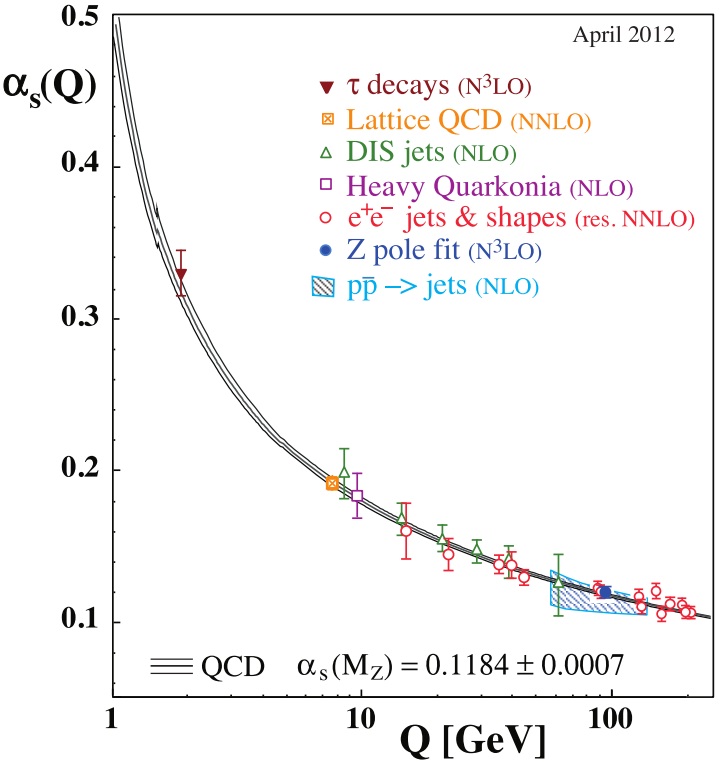

Figure 2.5: PDG[3]: Verification of the running of the strong QCD coupling from experiments and lattice simulations.

2.4 Shortcomings

Even though the SM has proven to be a good description of Nature so far, it has some flaws. Some aspects of the SM are not attractive on theoretical grounds and make it seem unnatural, fine-tuned or not well suited to fit into a GUT. Other issues are more experimental in their nature, and therefore more acute, for instance when there are necessary pieces missing in the model, such as neutrino masses or a dark matter candidate. Below follows a brief description of some of the problems with the SM and why they force us to look beyond it.

2.4.1 A hierarchy problem

The SM does not include gravity. It also does not give an explanation why gravity is so much weaker than the electroweak force. At high energies we expect that a new description of physics is necessary, at least at the Planck scale where gravity is expected to become strongly interacting. To correctly treat the SM as an effective field theory we need to assume a UV cut-off scale, Λ, where the new physics will appear. The SM Higgs mass gets loop corrections, dominantly from the top quarks as shown in Figure 2.6, which depend quadratically on the cut-off, Λ. This is the only parameter of the model that is quadratically sensitive to the UV scale. To explain the low value of the Higgs mass one needs to cancel the loop corrections of order Λ^2 with the bare mass parameter. The bare mass parameter is thus in need to be tuned very finely for these two large values to cancel and give a Higgs mass of around 125 GeV. If there would not be any need for a cut-off scale, and one would consider the model valid to arbitrarily high energies, the problem vanishes since the model is renormalisable. The divergences related to the Higgs mass can of course be removed just as other divergences related to other parameters can when renormalising the theory.

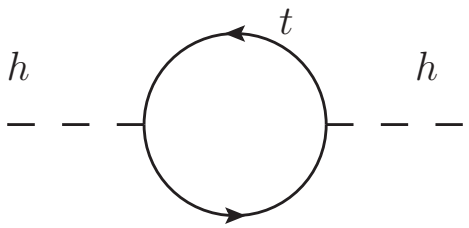

Figure 2.6: Top loop diagram contributing to the corrections of Higgs mass.

Various theories beyond the SM, e.g. supersymmetry, extra dimensions and technicolor, provide solutions on how to reduce the fine-tuning needed to explain the low mass of the Higgs boson. In supersymmetry, for example, the Higgs mass' quadratic sensitivity

to the UV scale arising from diagrams like the one depicted in Figure 2.6 is cancelled by scalar superpartners to the SM fermions, e.g. by the stop loop shown in Figure 2.7.

Figure 2.7: Stop loop diagram contributing to the corrections of Higgs mass with opposite sign compared to the top loop, in Figure 2.6.

2.4.2 No Dark Matter candidate

Dark matter is a hypothetical neutral massive particle not contained within the SM. It is however a key component for the standard model of cosmology to work. There are many cosmological and astronomical evidence for such a particle from observations on very different scales. I will briefly mention the most classical and strongest arguments for such a dark matter particle.

The oldest evidence of dark matter comes from the observation of galactic rotation curves[40] which do not agree with naive prediction of Newtonian gravity. Although dark matter is the most accepted explanation for the observed galactic rotation curves modifying the theory of gravity could provide a possible solution [41].

The strongest evidence for dark matter in the form of a new particle comes from gravitational lensing associated with galaxy clusters. Specifically the Bullet cluster[42], where two colliding clusters separate visible and dark matter, provides evidence that is not explained by models of modified gravity.

Another strong evidence of dark matter comes from the measurements of the cosmic microwave background (CMB) by the Cosmic Background Explorer (COBE), the Wilkinson Microwave Anisotropy Probe (WMAP)[15] and later the Planck telescope[43]. The power spectrum of the anisotropies in the CMB can be used to calculate components of the density of the universe. With the Planck measurement [43] the Universe is observed to consist of 69% dark energy ($\Omega_\Lambda = 0.692 \pm 0.010$), 26% dark matter ($\Omega_c h^2 = 0.1187 \pm 0.0017$) and 4.8% baryons ($\Omega_b h^2 = 0.02214 \pm 0.00024$).

The standard model of cosmology also needs a component of dark matter to allow for the observed galaxy and galaxy cluster structure formation in the early universe[44].

Given these evidence for dark matter it obvious that there is at least one missing component in the SM. Many BSM models predict stable neutral particles which are good

DM candidates, e.g. the Kaluza-Klein (KK) excitation of the photon in models of extra dimensions or the superpartner to the Z or Higgs in SUSY models. More general details about dark matter will be discussed in Chapter 6 and specific DM scenarios will be discussed in Chapter 7 and Chapter 10.

2.4.3 No baryogenesis

To explain the absence of antimatter in the universe a mechanism known as baryogenesis is supposed to have occurred in the early Universe. Baryogenesis would have provided the necessary asymmetry between baryons and anti-baryons. An interaction that would provide an excess of baryons against anti-baryons and thus lead to baryogenesis is required to satisfy the three Sakharov conditions:

- Baryon number (B) violation – since the total baryon number went from 0 to positive
- C and CP-violation – since otherwise particles and antiparticles would always interact in the same way
- Out of equilibrium – since particles and antiparticles have the same mass and abundances in thermal equilibrium only depends on the mass.

There have been attempts of incorporating baryogenesis within the SM, but there are difficulties. CP-violations exist in the SM but not enough to generate the observed asymmetry. Furthermore, SM baryogenesis would rely on electroweak baryogenesis but in this case the baryon violating processes will not be out of equilibrium since at the electroweak scale the expansion of the Universe is small compare to the interaction rate and the SM does not provide a strong enough electro-weak phase transition to otherwise allow for non-equilibrium processes (see e.g. [45]).

2.4.4 No neutrino masses

The SM, as defined by (2.2) and Table 2.1, does not include mass terms for the neutrinos. However, the experimentally observed neutrino oscillations require that neutrinos do have a mass. The neutrino masses therefore require some extension to the SM but it does not need to be a big or complex one in principle. Adding right-handed neutrinos, providing a seesaw mechanism, would explain the small neutrino masses well. The right handed neutrinos are gauge singlets and could have a Majorana mass term,

$$\bar{\nu}_R M_{RR} \nu_R, \tag{2.35}$$

but are also allowed to form Dirac masses,

$$\bar{\nu}_L m_{LR} \nu_R, \tag{2.36}$$

equivalent to the charged lepton masses. The neutrino mass terms could then be written as

$$\begin{pmatrix} \bar{\nu}_L & \bar{\nu}_R \end{pmatrix} \begin{pmatrix} 0 & m_{LR} \\ m_{LR}^T & M_{RR} \end{pmatrix} \begin{pmatrix} \nu_L \\ \nu_R \end{pmatrix}, \tag{2.37}$$

where contracted family indices are omitted. The Majorana masses, M_{RR}, are not associated with the electroweak scale but are free parameters here and are expected to be of the order of the cut-off scale of the SM, e.g. M_{GUT}. In the case that the Majorana mass is much larger than the electro-weak scaled m_{LR}, generated by the Higgs mechanism, the matrix (2.37) can be block diagonalised to

$$\begin{pmatrix} -m_{LR} M_{RR}^{-1} m_{LR}^T + \mathcal{O}(m_{LR}^3 M_{RR}^{-1\,2}) & 0 \\ 0 & M_{RR} + m_{LR} M_{RR}^{-1} m_{LR}^T + \mathcal{O}(m_{LR}^3 M_{RR}^{-1\,2}) \end{pmatrix}. \tag{2.38}$$

The mass matrix for the light neutrinos is of order

$$\frac{m_{LR}^2}{M_{RR}} \sim \frac{v^2}{M_{GUT}} \sim \frac{(10^2 \text{ GeV})^2}{10^{16} \text{ GeV}} \sim 10^{-3} \text{ eV} \tag{2.39}$$

which is naturally below the observed upper cosmological limit of about 0.3 eV [46]. The effective Majorana masses for the light neutrinos allow for neutrino-less double beta decay. Searches for this process by the NEMO experiment sets an upper limit of about 0.5-1.0 eV on these Majorana masses [47].

2.4.5 No gauge coupling unification

In the aim of finding a Grand Unified Theory where the SM gauge groups are contained in a larger symmetry group one would expect the gauge couplings of the SM to run towards the same magnitude at the unification scale. In the SM, the gauge couplings do not unify well, as depicted by the dashed lines in Figure 2.8 from [4]. The intersection of the $SU(2)$ coupling with the $U(1)$ and $SU(3)$ couplings occur at energies which differ by 10^3 GeV. Supersymmetry, which will be introduced in the following chapter, changes the running of the couplings so that they all unify around 10^{16} GeV. The supersymmetric prediction is presented as solid lines in Figure 2.8 where the sparticle threshold has been varied between 500 GeV (blue) and 1.5 TeV (red).

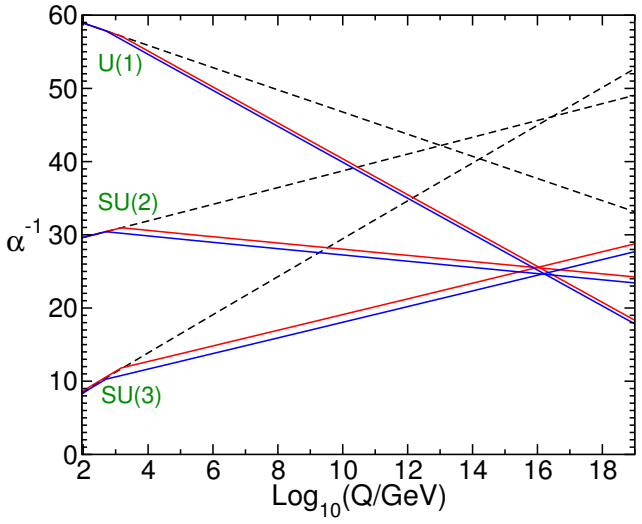

Figure 2.8: The running of the gauge couplings in the SM and in the Minimal Supersymmetric Standard Model. The plot is taken from [4].

Chapter 3

Supersymmetry

It was shown in the early 1970's that the Poincaré algebra, which determines the space-time symmetries of quantum field theories, can be extended by introducing anticommuting spinorial generators [48, 49, 50]. Earlier it had been shown that there could not be any non-trivial extensions of the Poincaré algebra[51] and in 1975 it was shown that the only way to extend the algebra was to introduce a so-called superalgebra with spinorial generators[52]. Supersymmetry has been studied extensively within string theory and quantum field theory and has shown to have both theoretically and phenomenologically appealing properties. We have already mentioned, in Section 2.4, that SUSY might provide a solution to the hierarchy problem, gauge coupling unification and dark matter. There are many books and reviews covering the topic, e.g. [4], and this chapter will just present a pragmatic overview of the basic components of supersymmetric field theories.

The generators of supersymmetry take a bosonic state into a fermionic and vice versa and are denoted Q_α and $\bar{Q}_{\dot{\alpha}}$, where the barred one is the Hermitian conjugate. These supersymmetry generators satisfy the supersymmetry algebra

$$\begin{aligned} \{Q_\alpha, \bar{Q}_{\dot{\alpha}}\} &= 2\sigma^\mu_{\alpha\dot{\alpha}} P_\mu \\ \{Q_\alpha, Q_\beta\} = \{\bar{Q}_{\dot{\alpha}}, \bar{Q}_{\dot{\beta}}\} &= 0 \\ [P^\mu, Q_\alpha] = [P^\mu, \bar{Q}_{\dot{\alpha}}] &= 0, \end{aligned} \tag{3.1}$$

where P_μ is the usual four-momentum operator, generating translations in space-time. One might use more than one pair of generators Q and $\bar{Q}$ to form an extended supersymmetry but in the case of a four dimensional field theory it is then not possible to describe chiral fermions or parity violation which we know exist in nature.

The particles of a supersymmetric theory end up in supermultiplets containing both fermions and bosons. Particles in such a multiplet belong to the same irreducible representations of both the supersymmetry algebra and the gauge groups of the theory. The

particle states in a supermultiplet are related to each other by applications of the supercharges Q and $\bar{Q}$, thus, since they commute with the mass operator P^2, the particles also have the same mass.

3.1 Superfields

A convenient way to describe supersymmetric theories is by using the superfield formulation. Superfields contain both fermionic and bosonic components that transform into each other under supersymmetry transformations. As oppsed to ordinary fields, superfields are not only functions of space-time x_μ but over superspace, $z = (x, \theta, \bar{\theta})$, where θ and $\bar{\theta}$ are spinorial, anticummuting variables. It is natural to think of the fermionic supersymmetry operators Q and $\bar{Q}$ as generating translations in the space parameterised by θ and $\bar{\theta}$. The ordinary unitary translation operator e^{ixP} might then be changed into a new one, generating translations in superspace, parameterized by $z = (x, \theta, \bar{\theta})$, as

$$U(x, \theta, \bar{\theta}) = e^{ixP} e^{i\theta Q} e^{i\bar{\theta}\bar{Q}}$$

With $U(x, \theta, \bar{\theta})$ we can now define a *superfield* as

$$\Psi(x, \theta, \bar{\theta}) = U(x, \theta, \bar{\theta}) \Psi(0) U^{-1}(x, \theta, \bar{\theta}) \tag{3.2}$$

Taylor expanding a general superfield in θ and $\bar{\theta}$, it can be written in terms of nine functions of x,

$$\begin{aligned} \Psi(x, \theta, \bar{\theta}) =& f(x) + \theta\eta(x) + \bar{\theta}\bar{\chi}(x) + \theta\theta m(x) + \bar{\theta}\bar{\theta} n(x) + \theta\sigma^\mu\bar{\theta} v_\mu(x) \\ &+ \theta\theta\bar{\theta}\bar{\lambda}(x) + \bar{\theta}\bar{\theta}\theta\psi(x) + \theta\theta\bar{\theta}\bar{\theta} d(x), \end{aligned}$$

since the fermionic property of the superspace coordinates makes the higher order terms vanish. This is because a term with a higher power of θ, e.g. $\theta_\alpha\theta_\beta\theta_\gamma$, has to contain at least two factors of the same component of θ, e.g. $\theta_1\theta_1 = -\theta_1\theta_1 = 0$.

Two kinds of superfields are needed to describe the supermultiplets in which the particles of the SM lies. All the matter particles will be described by *chiral superfields* and the gauge bosons by *vector superfields*.

Chiral superfields

The chiral superfields are defined by

$$\bar{D}_{\dot{\alpha}} \Phi = 0\,, \tag{3.3}$$

where D and $\bar{D}$ are the differential operators

$$\begin{aligned} D_\alpha =& \frac{\partial}{\partial\theta^\alpha} + i\sigma^\mu_{\alpha\dot{\alpha}}\bar{\theta}^{\dot{\alpha}}\partial_\mu = \partial_\alpha + i\sigma^\mu_{\alpha\dot{\alpha}}\bar{\theta}^{\dot{\alpha}}\partial_\mu \\ \bar{D}_{\dot{\alpha}} =& -\frac{\partial}{\partial\bar{\theta}^{\dot{\alpha}}} - i\theta^\alpha\sigma^\mu_{\alpha\dot{\alpha}}\partial_\mu = -\bar{\partial}_{\dot{\alpha}} - i\theta^\alpha\sigma^\mu_{\alpha\dot{\alpha}}\partial_\mu \,, \end{aligned}$$

satisfying

$$\begin{aligned} \{D_\alpha, \bar{D}_{\dot{\alpha}}\} =& -2i\sigma^\mu_{\alpha\dot{\alpha}}\partial_\mu \\ \{D_\alpha, D_\beta\} = \{\bar{D}_{\dot{\alpha}}, \bar{D}_{\dot{\beta}}\} =& 0 \\ \{D_\alpha, Q_\beta\} = \{\bar{D}_{\dot{\alpha}}, \bar{Q}_{\dot{\beta}}\} = \{D_\alpha\, \bar{Q}_{\dot{\beta}}\} = \{\bar{D}_{\dot{\alpha}}, Q_\beta\} =& 0\,. \end{aligned}$$

A chiral superfield can be written in terms of its component fields

$$\begin{aligned} \Phi =& \varphi(x) + i\theta\sigma^\mu\bar{\theta}\partial_\mu\varphi(x) + \frac{1}{4}\theta^2\bar{\theta}^2\partial^2\varphi(x) \\ &+ \sqrt{2}\theta\psi(x) - \frac{i}{\sqrt{2}}\theta^2\partial_\mu\psi(x)\sigma^\mu\bar{\theta} + \theta^2 F(x), \end{aligned} \tag{3.4}$$

where $\theta\theta = \theta^\alpha\theta_\alpha = \theta^2$. That (3.4) is a general solution to (3.3) can be seen by noticing that

$$\bar{D}_{\dot{\alpha}} y^\mu \equiv \bar{D}_{\dot{\alpha}}(x^\mu + i\theta\sigma^\mu\bar{\theta}) = 0 \quad \text{and} \quad \bar{D}_{\dot{\alpha}}\theta = 0\,,$$

then expanding

$$\Phi = \varphi(y) + \sqrt{2}\theta\psi(y) + \theta^2 F(y)$$

around x gives (3.4). The component fields of (3.4) describe a supermultiplet in which we have a chiral fermion, ψ, and its complex, scalar superpartner, φ. For example ψ could be the field for the electron and φ the field for the selectron. Superpartners to SM particles are generally called sparticles (or supersymmetric particles). The field F is an auxiliary (non-propagating) field, i.e. it has algebraic equations of motion. With the help of integrals over Grassmann variables we may write the most general form[1] of a supersymmetric renormalisable theory of chiral fields Φ_i as

$$\mathcal{L}_{WZ} = \int d^2\theta d^2\bar{\theta}\, \Phi^i\Phi_i^\dagger + \int d^2\theta\, W(\Phi) + \int d^2\bar{\theta}\, W^\dagger(\Phi^\dagger)\,, \tag{3.5}$$

where W is the *superpotential*

$$W(\Phi) = \frac{1}{3}y^{ijk}\Phi_i\Phi_j\Phi_k + \frac{1}{2}M^{ij}\Phi_i\Phi_j + L^i\Phi_i\,.$$

It should be noted that SUSY invariance require that the superpotential is a holomorphic function of the superfields, i.e. only a function of superfields and not also of their Hermitian conjugates, $W \neq W(\Phi, \Phi^\dagger)$.

[1] Here only the simplest Kähler potential $K(\Phi, \Phi^\dagger) = \Phi\Phi^\dagger$ is assumed.

Vector superfields

The vector superfields, which contain the SM gauge bosons, are defined by

$$V = V^\dagger. \tag{3.6}$$

We may write a superfield, satisfying (3.6), as

$$\begin{aligned} V =& A(x) + i\theta\chi(x) - i\bar{\theta}\bar{\chi}(x) + \frac{i}{2}\theta^2\big[B(x) + iC(x)\big] \\ &- \frac{i}{2}\bar{\theta}^2\big[B(x) - iC(x)\big] - \theta\sigma^\mu\bar{\theta}V_\mu(x) + i\theta^2\bar{\theta}\big[\bar{\lambda}(x) + \frac{i}{2}\bar{\sigma}^\mu\partial_\mu\chi(x)\big] \\ &- i\bar{\theta}^2\theta\big[\lambda(x) + \frac{i}{2}\sigma^\mu\partial_\mu\bar{\chi}(x)\big] + \frac{1}{2}\theta^2\bar{\theta}^2\big[D(x) + \frac{1}{2}\partial^2 A(x)\big]\,, \end{aligned} \tag{3.7}$$

where A, B, C, D and V_μ are real. Looking for the supersymmetric generalization of a gauge transformation, we note that if we take the usual transformation $\Phi \to \Phi' = e^{-i\Lambda^a t_a}\Phi$, we need $\Lambda = \Lambda(x, \theta, \bar{\theta})$ to be a chiral superfield in order to keep Φ' a chiral superfield. This is necessary since a product of chiral superfields is a chiral superfield. But since Λ is complex we have for the kinetic part of (3.5)

$$\bar{\Phi}\Phi \to \bar{\Phi}e^{i\bar{\Lambda}^a t_a}e^{-i\Lambda^a t_a}\Phi \neq \bar{\Phi}\Phi\,.$$

We make the kinetic term invariant under the gauge transformation by inserting a factor e^V between the chiral fields and defining the gauge transformation for the vector superfield as

$$e^V \to e^{-i\bar{\Lambda}}e^V e^{i\Lambda}\,.$$

For an Abelian group this means simply $V \to V' = V + i\Lambda - i\bar{\Lambda}$. The Hermitian field constructed by the sum of the chiral field $i\Lambda$ and its conjugate is

$$\begin{aligned} i(\Lambda - \bar{\Lambda}) =\ & i\big[\varphi(x) - \varphi^*(x) + \sqrt{2}\big(\theta\psi(x) - \bar{\theta}\bar{\psi}(x)\big) + \theta^2 F(x) - \bar{\theta}^2 F^*(x) \\ &+ i\theta\sigma^\mu\bar{\theta}\partial_\mu\big(\varphi(x) + \varphi^*(x)\big) - \frac{i}{\sqrt{2}}\theta^2\partial_\mu\psi(x)\sigma^\mu\bar{\theta} \\ &+ \frac{i}{\sqrt{2}}\bar{\theta}^2\partial_\mu\bar{\psi}(x)\bar{\sigma}^\mu\theta + \frac{1}{4}\theta^2\bar{\theta}^2\partial^2\big(\varphi(x) - \varphi^*(x)\big)\big]\,. \end{aligned}$$

We see now that the coefficient of the $\theta\sigma^\mu\bar{\theta}$-term, which the vector field V_μ is associated with, is $-\partial_\mu(\varphi + \varphi^*)$ implying that we get the usual gauge transformation for the vector field

$$V_\mu \to V'_\mu = V_\mu + \partial_\mu\alpha\,,$$

where $\alpha = -(\varphi + \varphi^*)$. Using the gauge transformations for the rest of the component fields in the vector superfield (3.7) we may choose a gauge in which we are left with only three non-zero fields. This gauge is known as the Wess-Zumino gauge, and it gives V

the form

$$V = -\theta\sigma^{\mu}\bar{\theta}V_{\mu}(x) + i\theta^2\bar{\theta}\bar{\lambda}(x) - i\bar{\theta}^2\theta\lambda(x) + \frac{1}{2}\theta^2\bar{\theta}^2 D(x)\,, \tag{3.8}$$

where the component fields are the gauge boson V_μ, its superpartner, the gaugino, λ, and the auxiliary field D. To construct the gauge invariant, supersymmetric free theory for the vector superfield we use a chiral superfield W_α, known as the supersymmetric field strength, that will contain the field strength tensor. It is defined as

$$W_\alpha = -\frac{1}{4}\bar{D}^2 e^{-V} D_\alpha e^{V}$$

and transforms as

$$W_\alpha \to W'_\alpha = e^{-i\Lambda} W_\alpha e^{i\Lambda}\,.$$

The free theory for the vector superfield is described by

$$\mathcal{L}_{gauge,free} = \frac{1}{16g^2}\int d^2\theta\ \mathrm{Tr}\ W^\alpha W_\alpha + \frac{1}{16g^2}\int d^2\bar{\theta}\ \mathrm{Tr}\ \bar{W}_{\dot{\alpha}}\bar{W}^{\dot{\alpha}} \tag{3.9}$$

3.2 Superpotential

From the superpotential it is straightforward to read off the component field terms of the Lagrangian. If one writes the general superpotential[2],

$$W(\Phi) = \frac{\lambda_{ijk}}{6}\Phi_i\Phi_j\Phi_k + \frac{\mu_{ij}}{2}\Phi_i\Phi_j \tag{3.10}$$

in terms of the scalar component fields φ_i, such that $W = W(\varphi)$, the terms of the Lagrangian originating from the superpotential can be derived by

$$\mathcal{L}_W = -\frac{1}{2}\left(\frac{\partial^2 W(\varphi)}{\partial\varphi_i\partial\varphi_j}\psi_i\psi_j + h.c.\right) - \left(\frac{\partial W(\varphi)}{\partial\varphi_i}\right)\left(\frac{\partial W(\varphi)}{\partial\varphi_i}\right)^{\dagger}, \tag{3.11}$$

where the first term contains standard Yukawa interactions and fermionic masses and the second term contains scalar interactions and masses. More explicitly the Lagrangian from (3.10) would be

$$\begin{aligned}\mathcal{L}_W = &-(\frac{\lambda_{ijk}}{2}\varphi_i\psi_j\psi_k + \frac{\mu_{ij}}{2}\psi_i\psi_j + h.c.)\\ &-(\frac{\lambda_{ijk}}{2}\varphi_j\varphi_k + \mu_{ij}\varphi_j)(\frac{\lambda_{ijk}}{2}\varphi_j\varphi_k + \mu_{ij}\varphi_j)^{\dagger}.\end{aligned} \tag{3.12}$$

[2]Possible linear terms due to gauge singlets are omitted here since such models will not be discussed.

3.3 Gauge interactions

Apart from gauge boson and gaugino interactions, which are given by (3.9), the gauge sector in SUSY models imply extra matter interactions, namely scalar quartic interactions. These interactions are due to auxiliary component fields, D, of the vector superfields, appearing in (3.8), which when eliminated by use of their algebraic equations of motion give rise to quartic interactions proportional to the gauge coupling squared,

$$\mathcal{L}_D = -\frac{1}{2}\sum_G g_G^2 \sum_a \left(\sum_i \varphi_i^\dagger T_G^a \varphi_i\right)^2 \tag{3.13}$$

among scalars, φ_i, which transform under the relevant gauge group, G, in a representation with generators T^a. In the MSSM for example, the D-terms for the group $G = SU(2)_W$ are

$$\begin{aligned}
\mathcal{L}_{D_Y} =& -\frac{g_2^2}{2}\left(\left(\varphi_i^\dagger \frac{\sigma_1}{2}\varphi_i\right)^2 + \left(\varphi_i^\dagger \frac{\sigma_2}{2}\varphi_i\right)^2 + \left(\varphi_i^\dagger \frac{\sigma_3}{2}\varphi_i\right)^2\right) \\
=& -\frac{g_2^2}{8}\left(\left(\varphi_i^\dagger \sigma_1 \varphi_i\right)^2 + \left(\varphi_i^\dagger \sigma_2 \varphi_i\right)^2 + \left(\varphi_i^\dagger \sigma_3 \varphi_i\right)^2\right) \\
=& -\frac{g_2^2}{8}\Big(\left(\tilde{Q}^\dagger\sigma_1\tilde{Q} + \tilde{L}^\dagger\sigma_1\tilde{L} + H_u^\dagger\sigma_1 H_u + H_d^\dagger\sigma_1 H_d\right)^2 + \\
& \left(\tilde{Q}^\dagger\sigma_2\tilde{Q} + \tilde{L}^\dagger\sigma_2\tilde{L} + H_u^\dagger\sigma_2 H_u + H_d^\dagger\sigma_2 H_d\right)^2 + \\
& \left(\tilde{Q}^\dagger\sigma_3\tilde{Q} + \tilde{L}^\dagger\sigma_3\tilde{L} + H_u^\dagger\sigma_3 H_u + H_d^\dagger\sigma_3 H_d\right)^2\Big),
\end{aligned} \tag{3.14}$$

where the σ_a are the Pauli matrices.

3.4 Soft supersymmetry breaking terms

Supersymmetry predicts that superpartners have the same mass, therefore since no sparticles have been observed, it has to be broken. There are various theories on how SUSY breaking could take place. SUSY breaking is supposed to have happened in a hidden sector, from which the breaking is mediated to the visible sector, e.g. via gravitational[53, 54, 55, 56, 57, 58, 59, 60] or SM gauge [61] interactions. There are however great uncertainties in how SUSY is broken and how the breaking is mediated so a common approach is to define a softly broken theory. This means that one introduces all possible supersymmetry breaking terms which will not reintroduce any quadratic sensitivity to the UV scale. To do this one includes supersymmetry breaking terms which are renormalisable but which have dimensionful couplings. Dimensionful couplings are needed to naturally maintain a hierarchy between the electroweak scale and the supersymmetry breaking scale. The possible soft supersymmetry breaking terms are therefore scalar trilinear and bilinear interactions and gaugino masses. The soft terms

with scalars appear in the same form as the superpotential (3.10) but with dimensionful parameters,

$$\mathcal{L}_{\text{soft}\,W} = -\frac{A_{ijk}}{6}\varphi_i\varphi_j\varphi_k - \frac{B_{ij}}{2}\varphi_i\varphi_j + \text{c.c.}, \tag{3.15}$$

and equivalent non-holomorphic terms,

$$\mathcal{L}_{\text{soft non}-\text{hol.}} = -\frac{C_{ijk}}{2}\varphi_i^*\varphi_j\varphi_k + \text{c.c.} - m_{ij}^2\varphi_i^*\varphi_j. \tag{3.16}$$

Finally, for completeness, the gauginos for each gauge group G get soft mass terms,

$$\mathcal{L}_{\text{soft gaugino}} = -\frac{M_G}{2}\lambda^G\lambda^G + \text{c.c.}. \tag{3.17}$$

It has been shown in [62] that the inclusion of these soft supersymmetry breaking terms does not reintroduce quadratic sensitivity to the UV scale for scalar masses.

Chapter 4

The MSSM

The MSSM is the Minimal Supersymmetric Standard Model. It contains all SM particles and the minimal amount of new particles. All SM fields, ϕ, are promoted to superfields, Φ, and contain the superpartners of the SM particles. A simplified overview, showing how the SM is extended to the MSSM is presented in Figure 4.1. Since the superpotential is required to be holomorphic in the superfields an extra Higgs doublet, with opposite hypercharge to the SM Higgs, is needed to couple to the down-type fermions and replace $H^\dagger$ in the SM Lagrangian[1]. The complete set of fields in the MSSM are listed in Table 4.1.

4.1 Superpotential and R-parity

The MSSM superpotential is defined as

$$W = y_u \bar{u} Q H_u + y_d \bar{d} Q H_d + y_e \bar{e} L H_d + \mu H_u H_d. \tag{4.1}$$

There are however other renormalisable, gauge invariant terms that one can write down with the MSSM matter content. These terms,

$$W_{\text{dangerous}} = \mu' L H_u + y' L L \bar{e} + y'' L Q \bar{d} + y''' \bar{u} \bar{d} \bar{d}, \tag{4.2}$$

are dangerous and one typically assumes they are forbidden by some symmetry. The first three terms in (4.2) are lepton number (L) violating and the last term is baryon number (B) violating. No L or B violating process has yet been verified in any experiment. Furthermore, more drastically, if *both* B and L were violated, e.g. by the two last terms in (4.2), it would lead to tree-level proton decay. An order of magnitude estimate can be made for the proton decay width from tree-level processes arising from the dangerous

[1]The extra Higgs doublet is required also to provide anomaly cancellations.

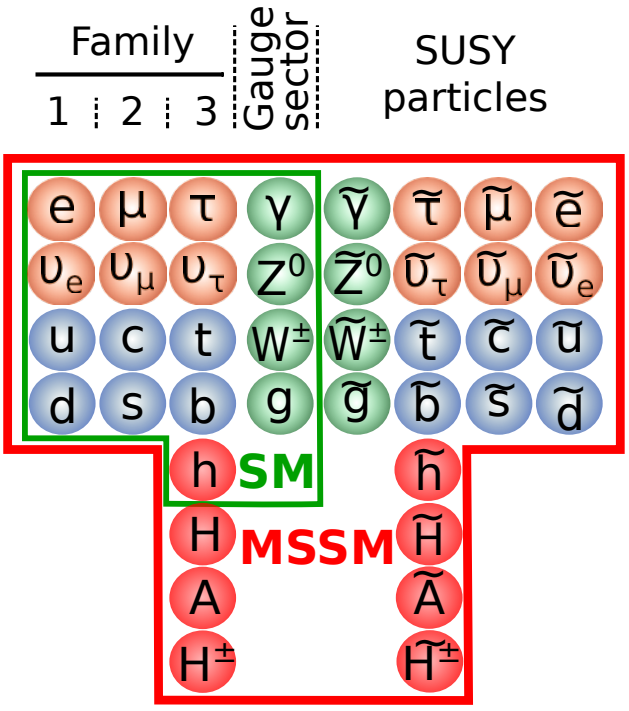

Figure 4.1: A very simplified overview of the particle content of the MSSM. The three generations of leptons (orange) and quarks (blue), the Higgs bosons (red) and the gauge bosons (green) all get superpartners only differing by their spin and mass. The picture is merely aimed at providing an impression of what sectors and to what extent the MSSM is extending the SM. A more accurate picture of the particle content is presented in Table 4.1.

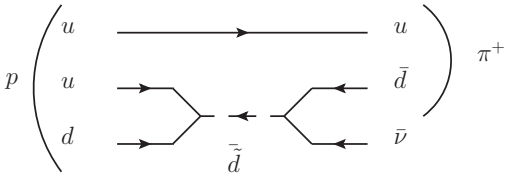

Figure 4.2: A tree-level proton decay diagram arising from the two last terms in (4.2)

terms in (4.2) such as the one represented by the diagram in Figure 4.2. With $y'' \sim y''' \sim y$ the decay width for $p \to \pi^+ \bar{\nu}$ is

$$\Gamma_{p\to\pi^+\bar{\nu}} \sim \frac{y^4}{M_{\tilde{q}}^4} m_p^5. \tag{4.3}$$

There are very strong constraints on the partial widths for the proton decays, e.g. the partial mean life for $p \to \pi^+ \bar{\nu}$ is $\tau > 25 \times 10^{30}$ y $\approx 80 \times 10^{37}$ s [3]. The limit on the partial decay width is therefore

$$\Gamma_{p\to\pi^+\bar{\nu}} \approx \frac{\hbar}{\tau} \lesssim \frac{7 \times 10^{-25}}{8 \times 10^{38}} \sim 10^{-63} \text{ GeV} \tag{4.4}$$

Field	Boson	Fermion	$SU(3)$	$SU(2)$	$U(1)$
Chiral	Spin 0	Spin 1/2			
Q^i	$\begin{pmatrix}\tilde{u}_L \\ \tilde{d}_L\end{pmatrix}^i$	$\begin{pmatrix}u_L \\ d_L\end{pmatrix}^i$	$\mathbf{3}$	$\mathbf{2}$	$\frac{1}{6}$
$\bar{u}^i$	$\tilde{\bar{u}}^i$	$\bar{u}^i$	$\bar{\mathbf{3}}$	$\mathbf{1}$	$-\frac{2}{3}$
$\bar{d}^i$	$\tilde{\bar{d}}^i$	$\bar{d}^i$	$\bar{\mathbf{3}}$	$\mathbf{1}$	$\frac{1}{3}$
L^i	$\begin{pmatrix}\tilde{\nu}_L \\ \tilde{e}_L\end{pmatrix}^i$	$\begin{pmatrix}\nu_L \\ e_L\end{pmatrix}^i$	$\mathbf{1}$	$\mathbf{2}$	$-\frac{1}{2}$
$\bar{e}^i$	$\tilde{\bar{e}}^i$	$\bar{e}^i$	$\mathbf{1}$	$\mathbf{1}$	1
H_u	$\begin{pmatrix}H_u^+ \\ H_u^0\end{pmatrix}$	$\begin{pmatrix}\tilde{H}_u^+ \\ \tilde{H}_u^0\end{pmatrix}$	$\mathbf{1}$	$\mathbf{2}$	$\frac{1}{2}$
H_d	$\begin{pmatrix}H_d^0 \\ H_d^-\end{pmatrix}$	$\begin{pmatrix}\tilde{H}_d^0 \\ \tilde{H}_d^-\end{pmatrix}$	$\mathbf{1}$	$\mathbf{2}$	$-\frac{1}{2}$
Gauge	Spin 1	Spin 1/2			
g	g	$\tilde{g}$	$\mathbf{8}$	$\mathbf{1}$	0
W	$W^\pm, W^0$	$\tilde{W}^\pm, \tilde{W}^0$	$\mathbf{1}$	$\mathbf{3}$	0
B	B	$\tilde{B}$	$\mathbf{1}$	$\mathbf{1}$	0

Table 4.1: The MSSM field content and the fields' representations under the gauge groups. Right-handed fields are written in terms of their charge conjugate and are denoted with a bar. The same notation is used for a superfield and its contained SM field.

and thus from (4.3) we get a rough limit on the ratio of the squark mass to the B and L violating couplings

$$\frac{M_{\tilde{q}}}{y} \gtrsim 10^{16} \text{ GeV}. \tag{4.5}$$

If squarks exist at the TeV scale these y-couplings have to be extremely suppressed. Rather than to tune these couplings small it is preferred to impose a symmetry which explains the absence of the dangerous terms. In MSSM this symmetry is a discrete symmetry known as R-parity. All SM fields, including the two scalar Higgs doublets, carry charge $+1$ (even under R-parity) under this symmetry while all their superpartners, known as sparticles, carry charge -1 (odd under R-parity). The R-parity of a particle can be defined by the its baryon number, B, lepton number, L, and spin, s, as

$$P_R = (-1)^{3(B-L)+2s}. \tag{4.6}$$

All terms in (4.2) are odd under R-parity and are thus forbidden while all terms in (4.1) are allowed since they are all even. R-parity was introduced to ensure the stability of the proton but it has some other very important implications. Since R-parity only allows interactions with an even number of sparticles it implies that

- sparticles are produced in even numbers at collider experiments,
- sparticles decay to SM particles and an odd number of sparticles,
  $\Rightarrow$ the lightest sparticle (LSP) is stable.

These are very important properties, which much of experimental searches and phenomenological studies of supersymmetry rely on. The fact that the LSP is expected to be stable is probably the most important side-effect of R-parity. For cosmology it means that if the LSP would be electrically neutral but weakly interacting and of the right mass it could be a good dark matter candidate. For collider experiments it means that since all produced sparticles eventually would decay into an odd number of LSPs, if it is neutral they should look for events with large missing momentum.

One should emphasise that there is no strict reason why all R-parity violating terms in (4.2) should be neglected or suppressed. The real danger lies in allowing for *both* B and L violation with these terms as demonstrated above. There are many studies on R-parity violating SUSY models where some, but not all of the couplings in (4.2) are non-zero (see e.g. [63]).

4.2 Soft supersymmetry breaking terms

For completeness, following Section 3.4, the soft supersymmetry breaking terms of the MSSM are

$$\begin{aligned}\mathcal{L}_{\text{soft}} = &- A_u \tilde{\bar{u}} \tilde{Q} H_u - A_d \tilde{\bar{d}} \tilde{Q} H_d - A_e \tilde{\bar{e}} \tilde{L} H_d - B H_u H_d \\ &+ \sum_{\phi=\tilde{Q},\tilde{\bar{u}},\tilde{\bar{d}},\tilde{L},\tilde{\bar{e}},H_u,H_d} m_\phi^2 \phi^\dagger \phi \\ &+ \sum_{\lambda=\tilde{B},\tilde{W},\tilde{g}} m_\lambda \bar{\lambda} \lambda.\end{aligned} \tag{4.7}$$

These terms are important, for example, for the tree and loop level Higgs masses as illustrated below.

4.3 The Higgs sector

The MSSM has two Higgs doublets, H_u and H_d, which will take part in electroweak symmetry breaking and give masses to the Z and W bosons. Three of the eight degrees of freedom within the two complex doublets will go to the gauge boson masses, the remaining five will appear as the physical scalar states h, H, A and $H^\pm$. The h and H are a light and a heavy CP-even Higgs bosons, the A is a CP-odd Higgs boson and $H^\pm$ is a charged Higgs boson.

4.3.1 The Higgs potential

The Higgs potential in MSSM is determined by the supersymmetry breaking parameters. The potential for all Higgs components can be written

$$\begin{aligned} V =&(|\mu|^2 + m_{H_u}^2)(|H_u^0|^2 + |H_u^+|^2) + (|\mu|^2 + m_{H_d}^2)(|H_d^0|^2 + |H_d^-|^2) \\ &+ [B(H_u^+ H_d^- - H_u^0 H_d^0) + \text{c.c.}] + \frac{1}{8}(g^2 + g'^2)(|H_u^0|^2 + |H_u^+|^2 - |H_d^0|^2 - |H_d^-|^2)^2 \\ &+ \frac{1}{2}g^2 |H_u^+ H_d^{0*} + H_u^0 H_d^{-*}|^2. \end{aligned} \tag{4.8}$$

Since electromagnetism should not be broken we can remove the charged Higgs bosons from this potential when considering its minimum and the neutral masses. The Higgs potential then simplifies to

$$\begin{aligned} V =&(|\mu|^2 + m_{H_u}^2)|H_u^0|^2 + (|\mu|^2 + m_{H_d}^2)|H_d^0|^2 \\ &- [BH_u^0 H_d^0 + \text{c.c.}] + \frac{1}{8}(g^2 + g'^2)(|H_u^0|^2 - |H_d^0|^2)^2. \end{aligned} \tag{4.9}$$

The potential is required to be stable or at least metastable at the minimum and therefore one has

$$\begin{aligned} \frac{\sqrt{2}}{v_u}\frac{\partial V}{\partial H_u} &= (|\mu|^2 + m_{H_u}^2) - B\frac{v_d}{v_u} + \frac{1}{4}(g^2 + g'^2)\frac{v_u^2 - v_d^2}{2} = 0 \\ \frac{\sqrt{2}}{v_d}\frac{\partial V}{\partial H_d} &= (|\mu|^2 + m_{H_d}^2) - B\frac{v_u}{v_d} - \frac{1}{4}(g^2 + g'^2)\frac{v_u^2 - v_d^2}{2} = 0. \end{aligned} \tag{4.10}$$

4.3.2 The μ-problem and the little fine-tuning problem

Adding the equations in (4.10) gives the relation

$$B\left(\frac{v_d}{v_u} + \frac{v_u}{v_d}\right) = 2|\mu|^2 + m_{H_u}^2 + m_{H_d}^2 \tag{4.11}$$

and another linear combination gives

$$\frac{1}{8}(g^2 + g'^2)v^2 \cos 2\beta(1 + \tan^2\beta) + |\mu|^2(1 - \tan^2\beta) + (m_{H_d}^2 - m_{H_u}^2 \tan^2\beta) = 0, \tag{4.12}$$

where $\tan\beta = \frac{v_u}{v_d}$ and $v_u^2 + v_d^2 = v^2$ has been used. Using $M_Z^2 = \frac{1}{4}(g^2 + g'^2)v^2$ one can rewrite (4.12) as

$$\frac{M_Z^2}{2} = -|\mu|^2 + \frac{m_{H_d}^2 - m_{H_u}^2 \tan^2\beta}{\tan^2\beta - 1}. \tag{4.13}$$

This equation relates the Z boson mass to the soft supersymmetry breaking parameters m_{H_d} and m_{H_u} and implies that there is a potential source of fine-tuning in the MSSM if the supersymmetry breaking scale is large. This is known as *the little fine-tuning*

problem. This type of fine-tuning, which appears in the minimization conditions of the Higgs potential, will be given more attention towards the end of this Thesis where modifications of the Higgs potential by new components in the theory will be studied.

The supersymmetry preserving parameter μ also appears in (4.13) and has to be of the same scale as the supersymmetry breaking parameters or less. There is however no reason why μ should be associated with the supersymmetry breaking scale rather than to be of the order of the cut-off scale which could be the Planck scale. The unexplained preference of a low value of the μ-parameter is known as *the μ-problem* and is addressed in many models beyond the MSSM, some of which will be mentioned below.

4.3.3 Tree level masses

The CP-odd Higgs boson A is a linear combination of the imaginary parts of the neutral components of H_u and H_d. The mass matrix for these imaginary parts can be written as

$$M_{odd} = \begin{pmatrix} |\mu|^2 + m_{H_u}^2 - \frac{M_Z^2}{2}\cos 2\beta & B \\ B & |\mu|^2 + m_{H_d}^2 + \frac{M_Z^2}{2}\cos 2\beta \end{pmatrix}. \tag{4.14}$$

The diagonal elements can be rewritten in terms of B by using the minimisation conditions (4.11) and (4.12),

$$M_{odd} = B \begin{pmatrix} \cot\beta & 1 \\ 1 & \tan\beta \end{pmatrix}. \tag{4.15}$$

The eigenvalues are

$$M_{G^0}^2 = 0 \quad \text{and} \quad M_A^2 = B(\cot\beta + \tan\beta) = \frac{2B}{\sin 2\beta}. \tag{4.16}$$

The zero eigenvalue belongs to the Goldstone boson which ends up being the longitudinal mode of the Z boson. The simple expression for the mass of the pseudoscalar Higgs boson is often used to exchange the soft parameter B in favour of the physical tree-level mass M_A^2.

The light and heavy Higgs bosons are linear combinations of the real parts of the neutral components of H_u and H_d. Using (4.16), their mass matrix can be written as

$$M_{even} = \begin{pmatrix} M_A^2\cos^2\beta + M_Z^2\sin^2\beta & -(M_A^2 + M_Z^2)\frac{\sin 2\beta}{2} \\ -(M_A^2 + M_Z^2)\frac{\sin 2\beta}{2} & M_A^2\sin^2\beta + M_Z^2\cos^2\beta \end{pmatrix}. \tag{4.17}$$

The eigenvalues for the CP-even states are thus

$$m_{h,H} = \frac{1}{2}\left(M_A^2 + M_Z^2 \mp \sqrt{(M_A^2 + M_Z^2)^2 - 4\cos^2 2\beta M_A^2 M_Z^2}\right). \tag{4.18}$$

The lightest Higgs mass, m_h, is increasing with $\cos 2\beta$ and reaches its maximum $m_h = M_Z$ at $\cos 2\beta = 1$. A SM-like Higgs mass less than the Z boson mass has been ruled out for a long time, however loop corrections, dominantly from stops due to their large Yukawa coupling, will make the Higgs mass larger and, in particular, a Higgs mass of 125 GeV can be accommodated in the MSSM. The one-loop limit, taking into account stop and top loops only is

$$m_h^2 < M_Z^2 \cos^2 2\beta + \frac{3}{2\pi^2}\frac{m_t^4 \sin^4 \beta}{v^2}\left(\log\frac{m_{\tilde{t}^2}}{m_t^2} + \frac{X_t^2}{m_{\tilde{t}}^2}\left(1 - \frac{X_t^2}{12 m_{\tilde{t}}^2}\right)\right), \tag{4.19}$$

where $X_t = A_t - \mu \cot \beta$ is the stop mixing parameter. The limit is maximised in the so called maximal mixing scenario where $X_t = \sqrt{6} M_{\tilde{t}}$.

The mixing angle α relates the mass eigenstates with the interaction states,

$$\begin{pmatrix} h \\ H \end{pmatrix} = \begin{pmatrix} \cos\alpha & -\sin\alpha \\ \sin\alpha & \cos\alpha \end{pmatrix} \begin{pmatrix} \mathrm{Re}H_u^0 \\ \mathrm{Re}H_d^0 \end{pmatrix}, \tag{4.20}$$

and satisfies

$$\sin 2\alpha = -\frac{M_A^2 + M_Z^2}{m_H^2 - m_h^2} \sin 2\beta. \tag{4.21}$$

If $M_A \gg M_Z$, $\sin 2\alpha = -\sin 2\beta$ which implies that $\alpha \approx \beta - \frac{\pi}{2}$, in which case

$$\begin{aligned} \sin\alpha &\approx -\cos\beta \\ \cos\alpha &\approx \sin\beta. \end{aligned} \tag{4.22}$$

Finally, the charged Higgs, $H^\pm$, is a linear combination of H_u^+ and H_u^-, which mass matrix is

$$M_{charged} = (M_A^2 + M_W^2) \begin{pmatrix} \cos^2\beta & \frac{\sin 2\beta}{2} \\ \frac{\sin 2\beta}{2} & \sin^2\beta \end{pmatrix}, \tag{4.23}$$

where the expression for the W mass, $M_W = \frac{g_2 v}{2}$, has been used. The eigenvalues are

$$M_{G^\pm} = 0 \quad \text{and} \quad M_{H^\pm}^2 = M_W^2 + M_A^2 \tag{4.24}$$

which corresponds to the Goldstone bosons for the longitudinal modes for the $W^\pm$ and the charged Higgs $H^\pm$, respectively.

4.3.4 Couplings to SM fermions

The couplings of the Higgs boson to the SM fermions is rather different in the MSSM compared to the SM due to the extended Higgs sector and the two VEVs. The Yukawa

couplings for up- and down-type fermions are now

$$y_u = \frac{m_u\sqrt{2}}{v_u} = \frac{m_u\sqrt{2}}{v\sin\beta} \qquad \text{and} \qquad y_d = \frac{m_d\sqrt{2}}{v_d} = \frac{m_d\sqrt{2}}{v\cos\beta}. \tag{4.25}$$

Using (4.20) the coupling between the lightest Higgs boson, h, and up-type fermions can be written as

$$-\frac{m_u\sqrt{2}}{v}\frac{\cos\alpha}{\sin\beta} \tag{4.26}$$

and the coupling to down-type fermions,

$$\frac{m_d\sqrt{2}}{v}\frac{\sin\alpha}{\cos\beta}. \tag{4.27}$$

If $M_A \gg M_Z$, then (4.22) holds and both the couplings to up- and down-type fermions are approximately the standard model result

$$-\frac{m\sqrt{2}}{v}. \tag{4.28}$$

Equivalently, the couplings of the heavy Higgs boson, H, can be found to be

$$-\frac{m_u\sqrt{2}}{v}\frac{\sin\alpha}{\sin\beta} \qquad \text{and} \qquad -\frac{m_d\sqrt{2}}{v}\frac{\cos\alpha}{\cos\beta} \tag{4.29}$$

to up- and down-type fermions respectively. Thus in the large M_A limit the H-coupling to up-type fermions is proportional to $\cot\beta$ and the coupling to down-type fermions proportional to $\tan\beta$. Since the equivalent mixing angle between the longitudinal mode of the Z and the pseudoscalar Higgs boson A, i.e. the angle of the rotation which diagonalises (4.15), is simply β, the A-couplings to up- and down-type fermions are always proportional to $\cot\beta$ and $\tan\beta$ respectively.

Chapter 5

Collider signatures

The models MSSM and E_6SSM, that were introduced in Chapter 4 and Chapter 9, are examples of models beyond the SM. As was argued in Chapter 2, there seems to be a need of physics beyond the SM and these particular models might provide solutions to some of the problems discussed in Section 2.4. The MSSM and E_6SSM are specific examples of supersymmetric models but whatever theory or principles determine the structure of the underlying physics beyond the SM we must develop ways to discover, distinguish and verify such models. The correct description of new physics could indeed be provided by a supersymmetric theory but there are many alternatives, such as models of extra dimensions, technicolour or something unthought of. There is a huge set of models proposed by model builders and even though the models might be constructed in very different ways they can give rise to very similar phenomenology. Phenomenologists and experimentalists therefore face a difficult problem of distinguishing many models. The classical example of this concerns models of supersymmetry and extra dimensions. Both theories predict a new coloured particle, associated with the gluon, known as the gluino in the case of supersymmetry and as a KK-gluon in the case of extra dimensions. Both are expected to be pair-produced at colliders and to typically decay into jets and missing energy, the only difference is the spin of the particles. The similarity of their decay is illustrated in the Feynman diagrams in Figure 5.1. With all these models on the market

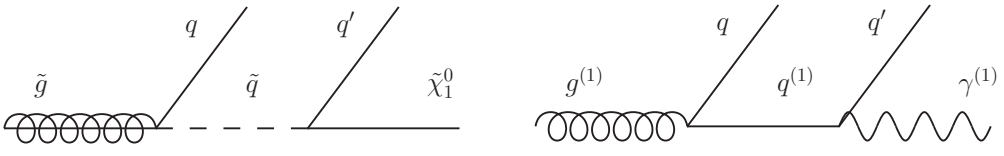

Figure 5.1: The similarity between the final states of the simplest decays of gluinos of supersymmetry (Left) and KK-gluons of extra dimensions (Right). Both theories predicts a signature of four jets and missing energy for the pair-productions of respective particle.

it is a big project to characterise all and find ways how to discover and distinguish them

from each other. For a given model one needs to pin down what specific features it has that makes it different from the SM as well as other BSM models to make it discoverable and distinguishable. The most obvious and direct way to discover parts of a model is by collider experiments but for example predictions regarding the neutrino mass spectrum or observables related to cosmology and dark matter are important aspects that help verifying or excluding models.

5.1 Characterising models by collider signals

To be able to confirm the validity of a model at a collider one needs to specify its characteristics in terms of experimental observables. Collision events are collected and analysed based on various kinematical variables. To have an idea of what can be measured at colliders it is good to have an idea idea of how the detectors at the experiments work. The collisions occur somewhere in the centre of a cylindrically shaped detector which has many parts,

- the innermost part of the detector is the *tracker*, it records tracks of charged particles in the presence of a magnetic field,
- the *electromagnetic calorimeter* surrounds the tracking chamber and is made of a dense energy absorbing metal, e.g. lead or compounds thereof, it precisely records the amount and location of energy deposits from electromagnetically interacting particles, e.g electrons and photons,
- the next layer is the *hadronic calorimeter*, which has layers of metals, e.g. steel, that absorbs energy from particles that penetrate through the electromagnetic calorimeter, typically hadrons such as pions, neutrons and kaons, which may interact via the strong force,
- the outer layer is the *muon detector*, which detects the comparatively heavy, long-lived and deeply penetrating muons, which pass through the calorimeters.

To give an example of a detector at LHC, a slice of the CMS detector is illustrated in Figure 5.2, where the detection of different types of particles in different layers is shown. The data from the different components of the detector is then analysed and interpreted as physical objects, such as electrons, muons, photon and (hadronic) jets.

5.1.1 Kinematical variables

There are many kinematical variables that are frequently used in context of collider experiments. The variables describe the properties of objects in an event, the event itself

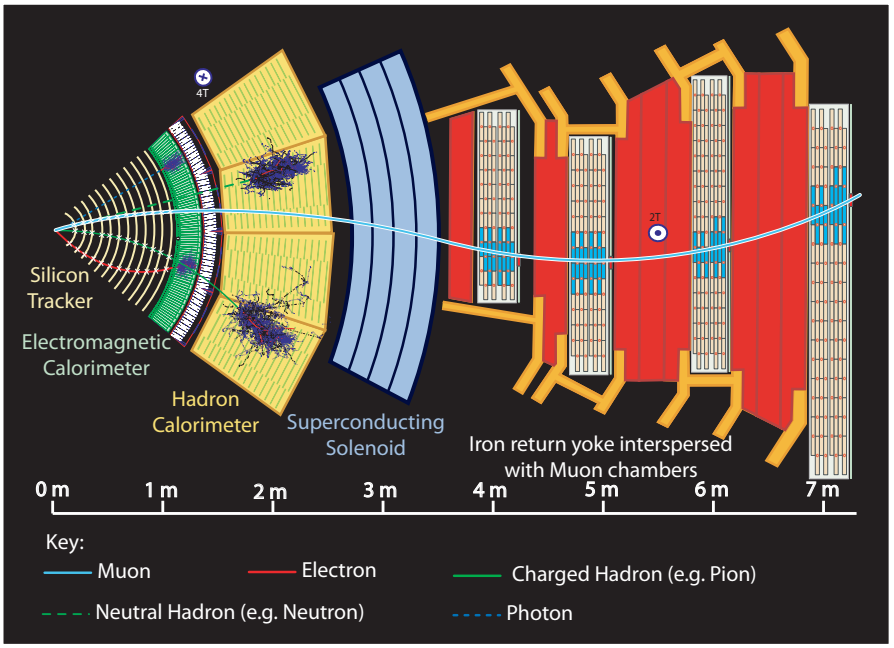

Figure 5.2: The different layers of the CMS detector. The different behaviours of different types of particles are shown. [Courtesy of CERN, CMS].

or even of a set of a large number of events. In hadron colliders there is little knowledge of the momentum component along the beam axis (defined as the z-axis) of the colliding partons and final state particles can escape the detectors if they are produced close to the beam axis. To be able to correctly assume momentum conservation and have control of the events one is therefore forced to consider variables in the plane transverse to the beam axis. The transverse momentum of particles in an event contain more information regarding the physics in the interaction while the z-component is strongly correlated with the initial momenta of the incoming partons. Below follows brief definitions and explanations of the most commonly used kinematical variables.

- The *transverse momentum*, p_T, is the momentum of an object projected on to the x–y plane, transverse to the beam axis. Where there is no risk of confusion, the magnitude of the transverse momentum is denoted in the same way, i.e. $|p_T| = p_T$.

- The *azimuthal angle*, ϕ, is the polar angle in the x–y plane of the transverse momentum. The x and y components of the momentum are thus

$$p_x = p_T \cos\phi \tag{5.1}$$

$$p_y = p_T \sin\phi. \tag{5.2}$$

- The *pseudorapidity*, η, is a measure of how close an object is to the beam axis. It is related to the angle θ to the beam axis by

$$\eta = -\ln(\tan\frac{\theta}{2}) \tag{5.3}$$

and can be expressed in terms of the momentum and z component of the momentum by

$$\eta = \frac{1}{2}\ln(\frac{|p| + p_z}{|p| - p_z}). \tag{5.4}$$

The z component of the momentum can thereby be expressed in terms of p_T and η via

$$p_z = p_T \sinh \eta. \tag{5.5}$$

- The *missing transverse momentum*, p_T^{miss}, is the momentum in the transverse plane not accounted for by the detected objects. It is defined as the negative vectorial sum of the observed particles' p_T,

$$p_T^{\text{miss}} = -\sum_i p_T^i. \tag{5.6}$$

The source of missing transverse energy could be neutrinos, instrumental errors or new physics. The missing transverse momentum is sometimes, rather confusingly, called the missing transverse energy vector. The magnitude of the missing transverse momentum is also often called the missing energy, denoted MET or E_T^{miss}.

- The *hadronic transverse momentum*, H_T, is defined as the scalar sum of the transverse momentum of the visible jets,

$$H_T = \sum_{i \in \text{jets}} |p_T^i|. \tag{5.7}$$

- The *effective mass*, M_{eff}, is defined as the scalar sum of the transverse momentum of the visible particles and the missing transverse momentum,

$$M_{\text{eff}} = |p_T^{\text{miss}}| + \sum_i |p_T^i|. \tag{5.8}$$

If an analysis only considers events with no leptons, i.e. a lepton veto is applied, the missing transverse momentum is sometimes denoted $\not{H}_T$, and the effective mass may then be defined as $M_{\text{eff}} = H_T + \not{H}_T$. One should note that the requirements for the objects that are included in the sums for H_T and $\not{H}_T$ may vary between each other and between analyses and M_{eff} is often not defined in exactly the same way.

- The *invariant mass*, M, is the centre-of-mass energy of a system. For two particles it is simply

$$\begin{aligned} M^2 &= (E_1 + E_2)^2 - (p_1 + p_2)^2 \\ &= m_1^2 + m_2^2 + 2(E_1 E_2 - p_1 \cdot p_2), \end{aligned} \tag{5.9}$$

which is easily generalised for more particles.

- The *transverse mass*, M_T, is a useful variable when looking for a heavy particle which is produced alone or with visible particles and which decays into one visible and one invisible particle. The transverse mass is defined by

$$\begin{aligned} M_T^2 &= (E_T^{\text{miss}} + E_T)^2 - (p_T^{\text{miss}} + p_T)^2 \\ &= m^{\text{miss}^2} + m^2 + 2(E_T^{\text{miss}} E_T - p_T^{\text{miss}} \cdot p_T). \end{aligned} \tag{5.10}$$

  If both the visible and invisible particles are massless the expressions simplifies to

$$M_T^2 = 2|p_T||p_T^{\text{miss}}|(1 - \cos\phi_{1,\text{miss}}) \tag{5.11}$$

  where $\cos\phi_{1,\text{miss}}$ is the angle between the visible and invisible particles in the x–y plane. The maximum value M_T can acquire is the mass of the mother particle, M. The M_T distribution over a large number of events will thus provide an endpoint $M_T^{\max} \approx M$.

- The *M_{T2}-variable* is an extension of the concept of transverse mass. It is very suitable when a particle of mass M is pair-produced and decays into an invisible particle of mass m and a visible particle. Details on this variable can be found in reference [64, 65].

5.1.2 Signatures

With the knowledge of what can be measured and searched for at colliders one can relate the new components of a BSM model to specific features in kinematical variables. Some particles are more straightforward to search for than others. If a particle can be produced on-shell through an s-channel resonance and if it decays to visible particles it is a matter of looking for a bump in the invariant mass spectrum of its decay products. The location of the bump would provide a mass measurement and the shape would give information of the strength of its couplings. This method is well tested and used in the discoveries of the Z and Higgs boson. It is more tricky when you expect particles to decay only partially to visible particles. The transverse mass variables mentioned above will however be good tools in such searches. The transverse mass was for example used for the discovery of the W boson via its semi-leptonic decays. In theories where you predict pair-production of a heavy particle which will decay to an invisible particle, e.g. supersymmetry or extra dimensions, the M_{T2}-variable is often very suitable.

In general, in models which predicts a DM candidate, accessible to the collider, one can assume some amount of missing transverse momentum and use that as a requirement when selecting events. Usually the validity of the assumption of large missing momentum

is very dependent on the mass spectrum of the models which will be discussed in more detail in Chapter 10.

When searching for heavy particles, which are pair produced and will decay to a lot of jets (or leptons) and perhaps missing particles, it is difficult to directly measure its mass by any of the transverse or invariant mass variables. Typically one can instead use the effective mass or transverse hadronic mass where you would expect to see a broad excess at large values, related to the particle's mass, of the variable.

These are basic features that are common to look for in searches for BSM particles. By applying cuts on the variables, restricting them by some limits, one is able to save and analyse events of interest which provide better signal-to-background ratio. Usually these cuts on the variables appear in various complex combinations to enhance the signal to background ratio for various models and regions of their parameter space.

5.2 The Tools

One can of course draw some qualitative conclusions regarding a model just by looking at its Lagrangian, e.g. one might easily see that there is a stable neutral particle which would give rise to missing transverse momentum. It is not trivial to verify such conclusions, however, and to quantitatively understand what to expect at collider experiments one needs to simulate the events that a model predicts. To study how and whether a model could be discovered one therefore need to use some computational tools.

5.2.1 Feynman Rules Generators and Matrix Element Calculators

To do numerical simulation of a model one needs to extract the mass terms and Feynman rules from it and use them to evaluate the mass spectrum and relevant cross sections. There are a few software tools available, e.g. `LanHEP` [66], `FeynRules` [67] and `SARAH` [68], which evaluates the Feynman rules of model, given the Lagrangian or superpotential. The calculation of diagrams, matrix elements and cross sections are performed by other available packages such as `CalcHEP` [69], `MadGraph` [70], `FeynArts` [71], `FeynCalc` [72]. At this stage one can evaluate partial widths and cross sections for parton level final states, e.g. quarks, gluons and leptons. This is often enough for a good quantitative analysis but sometimes it is necessary to go beyond the parton level.

5.2.2 Monte Carlo Events and Beyond the Parton Level

Many of the available matrix element calculators mentioned above offer an option to generate MC events. These events simulate what could occur at a collider experiment.

The events are based on the cross sections for the involved subprocesses and sometimes branching ratios and widths of intermediate particles in a decay chain. The events contain all relevant information about the particles involved in the event. The events may be treated in a similar way to experimental data and once one has generated events for backgrounds and signal one can apply suitable cuts on these events as mentioned in Section 5.1.2.

To use parton level events is sometimes not accurate enough and could be completely misleading in some cases. Using for example `PYTHIA` [73] or `Sherpa` [74, 75] one can generate events which simulate hadronisation, jet formation and initial and final state radiation. These beyond the parton level events can then be fed to a detector simulator, e.g. `PGS` [76] or `DELPHES` [77], for even more realistic results.

5.2.3 Databases of models

Even though there are efficient tools for model implementation and event generation the process can be cumbersome and time consuming. Because of this reason and to get an overview of what models already have been implemented and what their signatures are a High Energy Models DataBase (HEPMDB) [78] has been created. The data base allows you to browse and download existing models which are tagged with some typical predicted signatures. You are also allowed to contribute by uploading your own model and share your work. The database is hosted on the cluster Iridis and users are allowed to submit jobs via an online web browser to the cluster for event generations using the accessible models. Thereafter, simple analysis of the events are available online or the event files can be downloaded for analysis on your local computer.

There are also other databases with collections of models, e.g. FeynRules model database [79] which hosts FeynRules implementations of models.

5.3 Discoveries and significant observations

The easy access of models and computer power via HEPMDB simplifies the procedure of gathering signatures from known models. Whether one does the event generation and analysis on HEPMDB or on another machine one will need to specify a search strategy and a set of cuts which enhances the signal-to-background ratio for the specific model. Then the surviving Monte Carlo events in the specified search region will determine at what amount of collected data that benchmark of the model will be discoverable or ruled out. After collecting and analysing data from experiment one will be able to determine how well the data agreed with certain predictions.

5.3.1 Significance and criteria for exclusions and discoveries

The convention for discovery is that the data should deviate with a significance of more than five standard deviations, σ, from the expected background and for exclusion that the data should deviate more than two standard deviations from the new physics benchmark prediction. There are however different ways of how to define an estimate, S, for the significance of an experimental measurement. A general event-counting approach is to consider an observation to be of a significance of $S_\kappa\sigma$ if the signal plus background has a statistical downward fluctuation of $(1-\kappa)S_\kappa\sigma$ and still is equal to the background only model with a upward fluctuation of $\kappa S_\kappa\sigma$,

$$N_b + N_s - (1-\kappa)S_\kappa\sqrt{N_b+N_s} = N_b + \kappa S_\kappa\sqrt{N_b}, \quad \kappa \in [0,1]. \tag{5.12}$$

The N_b and N_s are the number of observed background and signal events, respectively, and κ is a weight, determining how you define your significance in terms of fluctuations away from the background-only model rather than from the signal-plus-background model. Counting all significance in terms of fluctuations of the background only, i.e. $\kappa = 1$, one gets the commonly used estimator

$$S_1 = \frac{N_s}{\sqrt{N_b}}. \tag{5.13}$$

Instead, counting all significance in terms of fluctuations of the signal plus background model, $\kappa = 0$, one arrives at another commonly used estimator

$$S_0 = \frac{N_s}{\sqrt{N_b+N_s}}. \tag{5.14}$$

An intermediate choice, $\kappa = \frac{1}{2}$, is sometimes used,

$$S_{1/2} = 2(\sqrt{N_b+N_s} - \sqrt{N_b}), \tag{5.15}$$

which is suitable for small statistics and has been shown to be robust against downward fluctuations of the background [80, 81].

The numerical difference between the definitions of significance is illustrated in Figure 5.3

The estimated number of background and signal events, $N_b = \mathcal{L}\sigma_b$ and $N_s = \mathcal{L}\sigma_s$ for a given integrated luminosity $\mathcal{L}$ can be evaluated by calculating the cross sections for respective processes, σ_b and σ_s. From any of definitions of the estimator of significance S_κ in (5.13), (5.14) or (5.15) it can be seen that

$$S_\kappa \propto \sqrt{\mathcal{L}}. \tag{5.16}$$

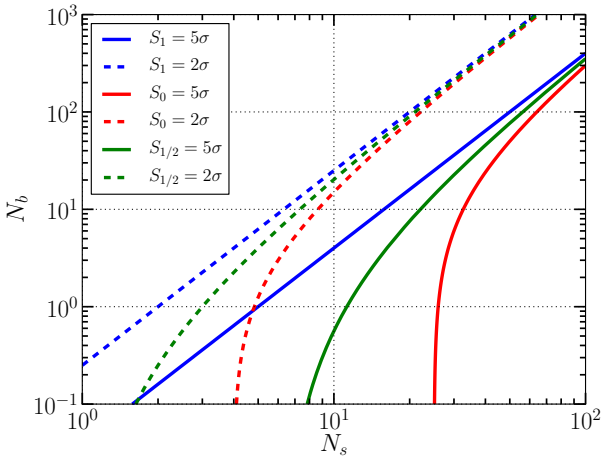

Figure 5.3: The 5 and 2 σ contours for the three estimators of significance, $S_1 = \frac{N_s}{\sqrt{N_b}}$, $S_0 \frac{N_s}{\sqrt{N_b+N_s}}$ and $S_{1/2} = 2(\sqrt{N_b + N_s} - \sqrt{N_b})$, in the plane of signal and background events, N_s and N_b. For $N_b \gg N_s$ they all approach S_1.

After counting the number of observed event and comparing it to the number of expected events from the background model one can deduce whether there are any signs of a signal. If there are no hints of a signal at all one can go ahead a place limits on models which predict a signal. In the absence of discoveries in supersymmetry searches some examples of exclusion limits is presented in Section 8. If it is a strong signal, but not quite a 5σ deviation from the background you might want to improve your analysis and focus on the particular signal region. Once there is a 5σ deviation or more there has been a discovery. Now the question is what it is that has been discovered.

5.4 Distinguishing scenarios from data

After a discovery it is rarely obvious exactly what it is one has discovered. Therefore further measurements and improved analysis is usually required to determine what model describes the new phenomenon most accurately. There is hopefully an observable or more that will serve as a good discriminator between models. As an example, recall the case of the very similar signatures of decaying KK-gluons and gluinos, where the major difference between the models were the spin of the particles. Proposed solutions on how to determine the spin of the decaying particle are related to angular correlations of visible decay products [82] and the invariant mass distributions of the jets [83].

As will be discussed in detail in Chapter 10, lepton multiplicity is a good discriminator between standard MSSM-like supersymmetric models and more complex models, such as E_6 inspired models which has a richer particle spectrum. The importance of multi-lepton searches for discovering and distinguishing models are shown by a concrete example in Chapter 10 but the principle can be generalized. Recently mass limits of squarks and gluinos from different search channels were studied for a set of simplified models[5]. The

results show how the importance of lepton channels increase as the complexity of the simplified model increases. This behaviour can be seen in Figure 5.4 (taken from [5]) where exclusion confidence levels are plotted for different search channels against model complexity. A preference of signal in multi-lepton channels can thus quite generically be used to distinguish more complex models from simpler ones.

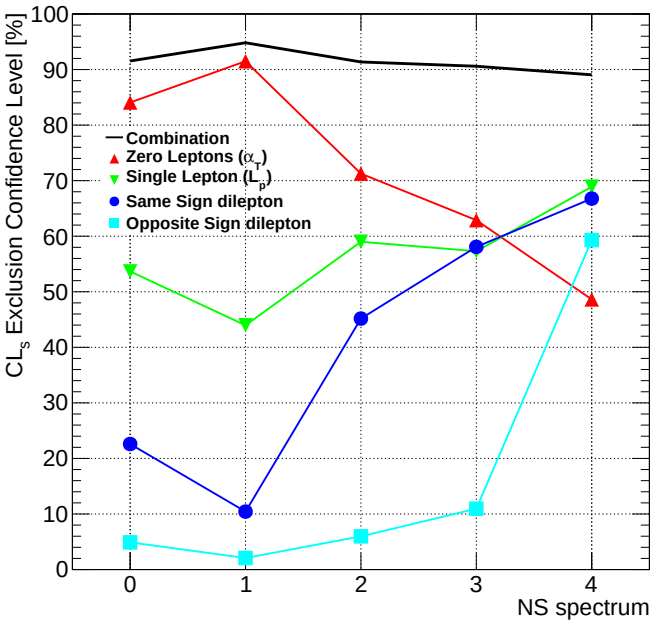

Figure 5.4: A figure from [5] showing the exclusion confidence limits for different search channels for a particular benchmark versus the model complexity. The model complexity goes from NS0, a model of gluino, stops and LSP only, to NS4, a model of gluinos, stops, sbottoms, sleptons, two neutralinos and one chargino.

Chapter 6

Dark Matter signatures

Many BSM models provide a dark matter candidate to explain the compelling observations mentioned in Section 2.4.2. The dark matter predictions of models can be tested by experiments and in conjunction with collider studies it can play an important role in favouring some models before others. It is however difficult to make any strict conclusion regarding a BSM model's validity at as description of collider phenomenology from dark matter arguments since small modifications or extensions to the DM sector of the model might affect its collider predictions very little. Since DM is a strong motivation for many theories, tests regarding DM properties still serve as an important test of how attractive theories are.

6.1 Freeze-out

In the early Universe particles are in thermal equilibrium and interact with a rate,

$$\Gamma = \langle \sigma v \rangle n_\chi, \tag{6.1}$$

where $\langle \sigma v \rangle$ is the thermal averaged cross section and relative speed of the particles. The number density, n_χ, for the DM candidate χ is determined by

$$n_\chi = \frac{g_\chi}{(2\pi)^2} \int f_\chi(p) d^3p \tag{6.2}$$

in thermal equilibrium, where g_χ is the number of internal degrees of freedom of χ and $f_\chi(p)$ is the distribution function

$$f_\chi(p) = \frac{1}{e^{\frac{E_\chi - \mu_\chi}{T}} \pm 1} \tag{6.3}$$

with $-$ if χ is a boson and $+$ if it is a fermion. In the early Universe, when $T \gg m_\chi$, the number density is $n_\chi \propto T^3$ and later, when $T \ll m_\chi$, it is exponentially suppressed,

$n_\chi \propto e^{-m_\chi/T}$, under the assumption of equilibrium. However, if the annihilation rate (6.1), turns smaller than the expansion rate of the universe, $H = \frac{\dot{a}}{a}$, where a is the scale of the Universe, the particle does not annihilate and departs from equilibrium and the exponential Boltzmann suppression is discontinued. The particle is in this case said to *freeze out*. The Boltzmann equation for the DM candidate χ, describing this behaviour, is

$$\frac{dn_\chi}{dt} + 3Hn_\chi = -\langle\sigma v\rangle \left(n_\chi^2 - n_\chi^{\mathrm{eq}2}\right), \tag{6.4}$$

where no particle-antiparticle asymmetry is assumed, i.e. $n_\chi = n_{\bar{\chi}}$. The terms in (6.4) describe the change of the number density in terms of the expansion of the Universe, the annihilation rate and the production rate. The Boltzmann equation can be solved numerically to evaluate the relic density, Ω_χ of the dark matter candidate. To get the right amount of dark matter relic density the thermal averaged cross section and speed should be $\langle\sigma v\rangle \sim 1$ pb$\cdot c$, which suggests that the particle would be weakly interacting. Depending on whether a particle is relativistic or not at freeze-out it is called a hot or cold relic respectively. Experimental observations, e.g. by the 2dF Galaxy Redshift Survey [84], and simulations, e.g. [44], show that hot dark matter, e.g. neutrinos, is not a dominant component of dark matter and that it can not provide the observed galaxy structure formation in the early universe. Observations are however in good agreement with Cold Dark Matter (CDM) and Warm Dark Matter (WDM), where typical DM particle masses are in the GeV-TeV and keV scales respectively. Because of these rough coupling and mass requirements, Weakly Interacting Massive Particles (WIMPs), such as the neutralino of supersymmetric theories, have been a very popular subject of study to explain dark matter.

There are several available software tools that calculate the annihilation cross section, σ, for the particle χ in a BSM model. There are SUSY specific software, such as `DarkSUSY` [85], or software aimed at wider range of models, such as `MicrOMEGAs` [14], where one can use model implementations in the `CalcHEP` format. These software also calculate the cross sections limited by direct DM detection experiments, discussed below.

6.2 Typical annihilation channels

What determines the relic density of a models dark matter candidate is its couplings and the particle spectrum. The LSP in SUSY models has, as mentioned above, roughly the right properties for providing the right amount of relic dark matter. The relic density is however quite sensitive to the model parameters. In fact, the typical scenario in SUSY is to create an overabundance of dark matter. To predict the right amount of dark matter some specific annihilation mechanism has to have taken place in the early Universe to have allowed for the LSP to annihilate quickly enough. In an accurate calculation one

has to take into account a large number of Feynman diagrams but usually some diagrams are particularly important in certain regions of the parameter space.

One plausible, but largely excluded region of the parameter space is where there is at least one light sparticle which makes t-channel exchange annihilation via this sparticle efficient. Example of such diagrams are shown in Figure 6.1. If the LSP has a significant Higgsino or Wino component, it couples efficiently to W bosons and the right diagram in Figure 6.1 is particularly important. Another possibility is that the LSP is not very

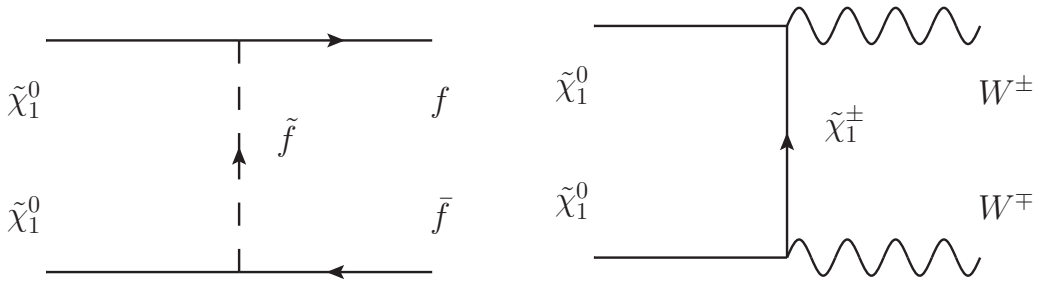

Figure 6.1: Diagram contributing to LSP annihilation via t-channel with light sfermion (Left) and chargino (Right). The decay into WW via t-channel exchange of $\tilde{\chi}_1^{\pm}$ is particularly important if the LSP has a significant Higgsino/Wino component.

far from an s-channel resonance annihilation via a massive boson, e.g. Z, light or heavy Higgs, as depicted in Figure 6.2. This means that the LSP has a mass, $m_{\tilde{\chi}_1^0} \approx \frac{M}{2}$, where M is the mass of the heavier boson. Finally, something which can enhance the

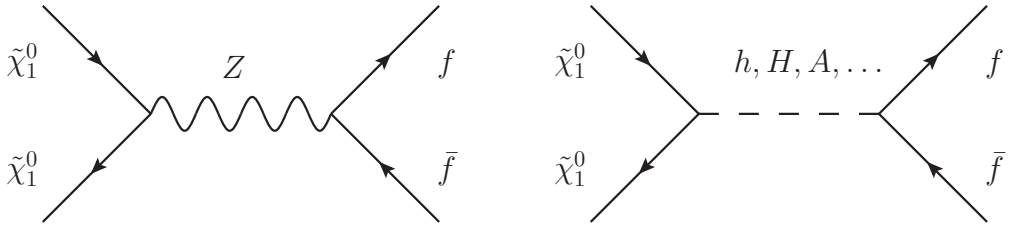

Figure 6.2: Examples of diagrams contributing to LSP annihilation via s-channel Z resonance (Left) and scalar resonance (Right), e.g. via light, heavy or pseudoscalar Higgs bosons, into SM fermions.

annihilation further is if there is a particle just a little bit heavier than the LSP. In this case, co-annihilation diagrams, such as those shown in Figure 6.3 give important contributions to the annihilation cross section. Again, if the LSP has a sizable Higgsino or Wino component the first diagram in Figure 6.3, involving a W, is extra important.

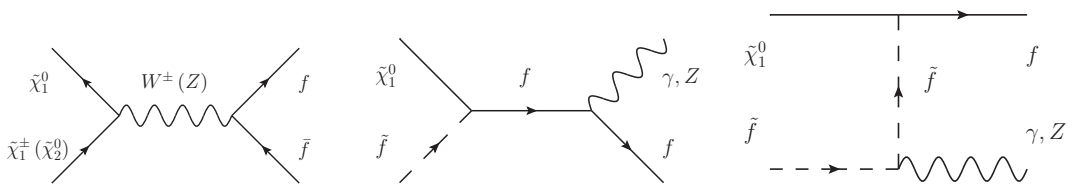

Figure 6.3: Examples of diagrams for LSP coannihilation with a fermion (Left), e.g. neutralino or chargino, and a scalar (Centre and Right), e.g. stau, into a SM fermion and boson.

6.3 Typical detection channels

Since dark matter is expected to pass through our solar system and the Earth itself many experiments are designed to directly detect dark matter passing through their detectors via elastic scattering of the dark matter particle with nuclei. The expected cross sections for such scatterings are often related to the annihilation cross section. For instance, if the annihilation is made efficient by a light sparticle or an enhanced coupling to the Higgs boson, these intermediate particles typically give important contributions to the detection cross section. The annihilation diagram is thus turned on its side to represent scattering with the quarks (or potentially gluons) in the nucleus. The scatterings of an LSP with a proton or neutron via a t-channel Higgs exchange and via an s-channel squark are depicted in Figure 6.4.

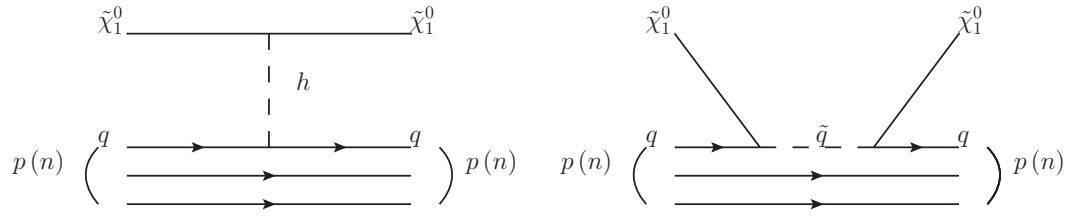

Figure 6.4: The Feynman diagram for an LSP scattering off an nucleon by interacting via a Higgs boson (Left) and via a squark (Right).

Another way of observing dark matter is by indirect detection of its annihilation or decay products in outer space. Experiments look for signals from regions of space where the DM density is expected to be high, e.g. the galactic centre. In these regions annihilation of DM particles to SM particles could take place via the same annihilation channels that was important at the time of freeze-out. Typically one is looking for so-called gamma-ray lines in the gamma-ray spectrum from $\tilde{\chi}\tilde{\chi} \to \gamma\gamma$ or a broader peak from $\tilde{\chi}\tilde{\chi} \to Z\gamma$, which would be proportional to the mass of the DM particle, or an excess of anti-particles, e.g. positrons from $\tilde{\chi}\tilde{\chi} \to e^+e^-$. Examples of loop-diagrams contributing to $\tilde{\chi}\tilde{\chi} \to \gamma\gamma$ are shown in Figure 6.5. Three-body final state including a photon will also

give very important photon signatures since these processes will not be loop suppressed.

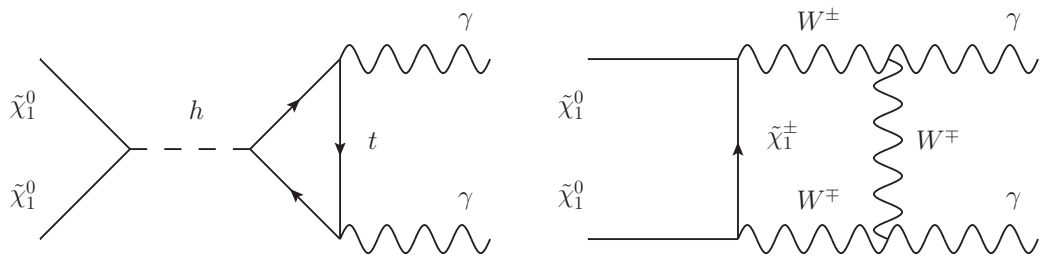

Figure 6.5: The Feynman diagram for two LSPs annihilating into photons via a Higgs boson (Left) and via a chargino/W-loop (Right).

6.4 Experimental constraints

Apart from the information given by the observations discussed in Section 2.4.2, e.g the measurement of the DM relic density $\Omega_c h^2 = 0.1187 \pm 0.0017$, other properties are explored by several other experiments. There are many experiments aiming to measure the mass and interaction cross section with nucleons via direct detection. Some interesting, but somewhat confusing results, are listed below in chronological order, and a summary plot of limits and signal regions in the mass – cross section plane is shown in Figure 6.6.

- 2010-02-04: The DAMA and LIBRA collaborations claim a 8.9σ observation of the expected annual modulation [86] due to the sum of the Earth's velocity with respect to sun and the solar system's velocity with respect to the galaxy, which is compatible with e.g. a WIMP of mass 10 GeV and spin-independent cross section of $\sigma_{SI} = 10^{-40}$ cm^2.
- 2010-02-25: The CoGeNT collaboration reported a hint of a WIMP with mass of $\sim$ 10 GeV and a spin-independent cross section $\sigma_{SI} \approx 7 \times 10^{-41}$ cm^2 using a Germanium detector [87].
- 2011-04-21: The CDMS collaboration has set a limit of the spin-independent cross section for a WIMP with mass of 10 GeV to $\sigma_{SI} < 2 \times 10^{-41}$ cm^2 based on 241 kg days data collected in 2006-2008 with Germanium detectors [88].
- 2011-06-03: The CoGeNT collaboration 2-3σ hint of annual modulation consistent with a WIMP of mass 7-8 GeV and spin-independent cross section $\sigma_{SI} \sim 10^{-4}$pb= 10^{-40} cm^2 with their germanium detectors[89].

- 2011-09-04: The CRESST collaboration observes a 4.2σ signal of a WIMP of mass 11.6 GeV and WIMP-nucleon cross section $\sigma = 3.7 \times 10^{-5}pb= 3.7 \times 10^{-41}$ cm^2 in the 730 kg days of data from 2011 [90]

- 2012-07-25: The XENON 100 collaboration sets a limit $\sigma_{SI} < 3 \times 10^{-43}$ cm^2 for WIMPs with a mass of 10 GeV [6].

- 2013-04-12: The CDMS collaboration has set a limit of the spin-independent cross section for a WIMP with mass of 10 GeV to $\sigma_{SI} < 1.7 \times 10^{-41}$ cm^2 based on 55.9 kg-days data collected in 2006-2007 with silicon detectors. The limit improves to $\sigma_{SI} < 8.3 \times 10^{-42}$ cm^2 when combined with previous silicon data from CDMS[91].

- 2013-04-16: The CDMS collaboration has set a limit of the spin-independent cross section for a WIMP with mass of 10 GeV to $\sigma_{SI} < 2.4 \times 10^{-41}$ cm^2 based on 140.2 kg-days data collected in 2007-2008 with silicon detectors and report a 2-3σ hint of a WIMP with a mass of 8.6 GeV and cross section $\sigma_{SI} = 1.9 \times 10^{-41}$ cm^2 [92].

There are surprisingly many observed hints of DM candidates with a mass of around 10 GeV. Few of these hints are consistent with each other in terms of cross section however and furthermore, all seem to be excluded by the XENON limits. One should note that a recent analysis of data show that XENON10/100 do not exclude the entire signal region determined from CDMS data[93]. We will hopefully see soon in which direction this tension will go, otherwise the DM sector is more complicated than we think, or the sources of background need to be better understood.

There are hints of dark matter, also from the indirect detection experiments. The Large Area Telescope of the Fermi Gamma-ray Space Telescope have observed a narrow excess around 130-135 GeV in the gamma spectrum near the galactic centre. This has been interpreted as a hint of a DM candidate with a mass around 130 GeV [94, 95].

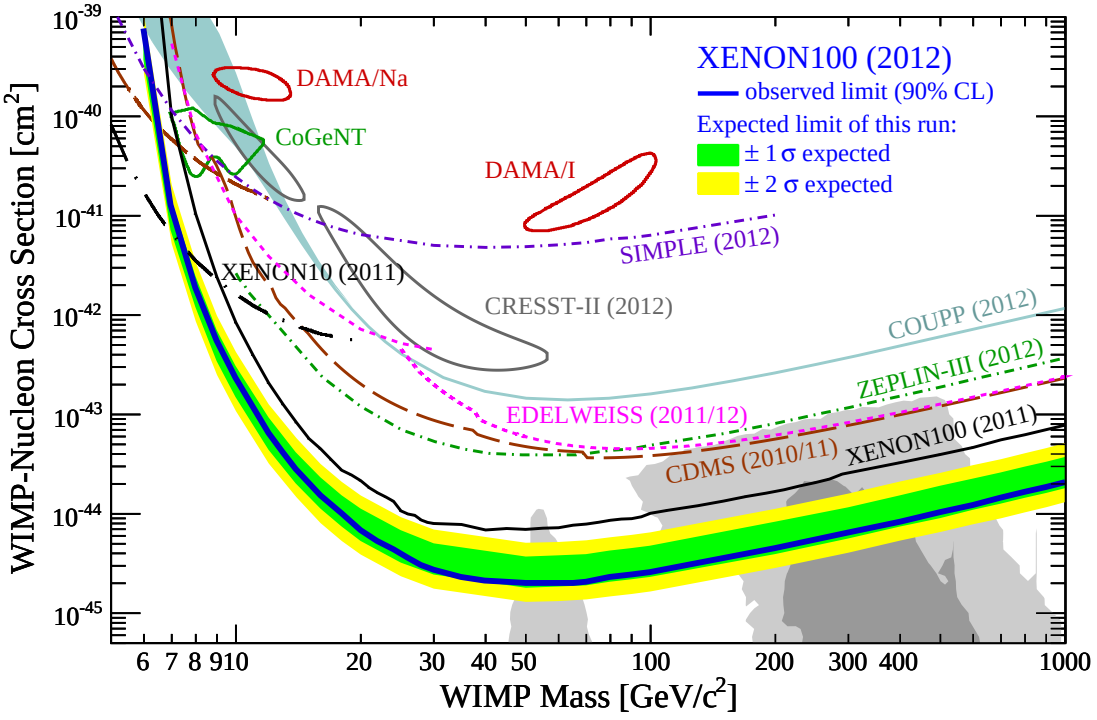

Figure 6.6: Limits and observations in the mass – nucleon cross section plane for the WIMP. The plot is taken from [6].

Chapter 7

Exploring DM resonance annihilation via $H, A \to \mu^+\mu^-$ at the LHC

When one wants to distinguish different new physics scenarios from each other it boils down to measure one or more observables and determine some model parameters. In this chapter the possibility of distinguishing certain scenarios within the MSSM is explored. The scenario of particular interest here is associated with the so-called A-funnel region of the Constrained MSSM (CMSSM) or minimal Supergravity (mSUGRA) parameter space, which will be discussed in more detail below. In this region the dominant annihilation mechanism of dark matter in the early universe is a resonant s-channel annihilation. An important parameter to determine for distinguishing this scenario in particular, but also other instances of proposed SUSY models, is $\tan\beta$. This parameter is however not easy to determine directly. What will be shown below is how the measurement of the width, Γ_A, of the heavy or pseudoscalar Higgs, A, of the MSSM helps determining $\tan\beta$ via its correlation with Γ_A. Much in the procedure in this chapter relies on the fact that the coupling between the pseudoscalar Higgs boson and down-type fermions, e.g. b-quarks and muons, is proportional to $\tan\beta$ as was shown in Section 4.3.4. It is a difficult task to measure Γ_A but we show that by using the $\tan\beta$-enhancement, the rare muonic decays of the Higgs bosons and the precision of the muon detectors it is possible at the LHC.

As was mentioned in Chapter 6, the lightest neutralino $\tilde{\chi}_1^0$ of R-parity conserving SUSY models is often touted as an excellent WIMP candidate for cold dark matter in the universe. However, in SUSY models where the $\tilde{\chi}_1^0$ is mainly bino-like, the natural value of the relic density $\Omega_{\tilde{\chi}_1^0}h^2$ is in the 1-100 range [96, 97], which is far beyond the WMAP observation [15],

$$\Omega_{CDM}h^2 = 0.1123 \pm 0.0035 \quad 68\%\ CL, \tag{7.1}$$

where $h = 0.74 \pm 0.03$ is the scaled Hubble constant[98, 99]. To gain accord between theory and observation, special neutralino annihilation mechanisms must be invoked. These include: (*i*). co-annihilation (usually involving $\tilde{\chi}_1^0$ with a stau[100, 101, 102, 103, 104, 105], stop[106, 107, 108] or chargino[109, 110]), (*ii*). tempering the neutralino composition[111, 112, 113] so it is a mixed bino-higgsino (as occurs in the hyperbolic branch/focus point (HB/FP) region of mSUGRA[114, 115, 116, 117, 118, 119, 120]) or mixed bino-wino state or (*iii*). annihilation through the light (h) or heavy Higgs boson resonance (A *and/or* H) [121, 122, 123, 124, 125, 126, 127, 128].

In this chapter, we are concerned with testing the latter annihilation mechanism, which occurs if $2m_{\tilde{\chi}_1^0} \simeq m_A$. The A-resonance annihilation mechanism already occurs in the paradigm minimal supergravity (mSUGRA or CMSSM) model, which serves as a template for many investigations into SUSY phenomenology. The mSUGRA parameters at GUT scale include

$$m_0,\ m_{1/2},\ A_0,\ \tan\beta \ \text{ and } \ \text{sign}(\mu), \tag{7.2}$$

where m_0 is a common scalar mass, $m_{1/2}$ is a common gaugino mass, A_0 is a common trilinear term and $\tan\beta$ is the ratio of Higgs field VEVs. The superpotential Higgs mass term μ has its magnitude, but not sign, determined by radiative breaking of electroweak symmetry (REWSB), which is seeded by the large top quark Yukawa coupling.

In mSUGRA, as $\tan\beta$ increases, the b- and τ- Yukawa couplings – f_b and f_τ – also increase, and in fact their GUT scale values may become comparable to f_t for $\tan\beta \sim 50$. In this case, the up and down Higgs soft masses $m_{H_u}^2$ and $m_{H_d}^2$ run under renormalization group evolution to nearly similar values at the weak scale. Since at the weak scale $m_A^2 \sim m_{H_d}^2 - m_{H_u}^2$[129, 130], we find that as $\tan\beta$ increases, the value of m_A decreases[131], until finally the condition $2m_{\tilde{\chi}_1^0} \simeq m_A$ is reached, whereupon neutralino annihilation through the A-resonance may take place. Another condition that occurs at large $\tan\beta$ is that since the b- and τ Yukawa couplings are growing large, the partial widths $\Gamma(A \to b\bar{b})$ and $\Gamma(A \to \tau\bar{\tau})$ also grow, and the A width becomes very large (typically into the tens of GeV range). In this case, a wide range of parameter space actually accommodates $\tilde{\chi}_1^0\tilde{\chi}_1^0$ annihilation through A, H, and the value of $2m_{\tilde{\chi}_1^0}$ may be a few partial widths off resonance since in the relic density calculation the $\tilde{\chi}_1^0\tilde{\chi}_1^0$ annihilation rate times relative velocity must be thermally averaged. The question we wish to address here is: how well may one identify the cosmological scenario of *neutralino annihilation through the heavy Higgs resonance* via measurements at the CERN LHC?

Since the b-quark Yukawa coupling increases with $\tan\beta$, so do the Yukawa-induced Higgs production cross sections such as $b\bar{b} \to A$, $bg \to bA$ and $gg, q\bar{q} \to b\bar{b}A$. The presence of additional high p_T b-jets in the final state for the second and third of these reactions allows one to tag the b-quark related production mechanisms, and also allows for a cut which rejects SM backgrounds – which don not involve the enhanced b Yukawa coupling – at low cost to signal. The second of these reactions, which is tagged by a single b-jet in

the final state, occurs at an order of magnitude greater cross section than $b\bar{b}A$ production at the LHC[132].

To be accurate, the process $b\bar{b} \to A$ also predicts b-jets associated with A. This happens due to jets appearing as a result of initial state radiation from gluon splitting, which gives rise to the b-quark PDF. The p_T of those b-jets will however not be described correctly in the high p_T region ($p_T^b > 30$ GeV). We will consider the channel bA rather than $b\bar{b}A$, a choice which is based on the fact that this process provide a higher significance. The channel bA and $b\bar{b}A$ should preferably be combined, but then the proper combination requires subtraction of the double counting these processes give rise to and taking into account higher order corrections to bA. This can however be avoided by considering just the bA process and choosing the factorization and renormalization scale to be $\mu_F = \mu_R = m_\phi/4$ with $\phi = A, H$ which reproduces higher order corrections[132].

The A and H Higgs bosons are expected to dominantly decay to $b\bar{b}$ and $\tau\bar{\tau}$ final states. Then, the $bb\bar{b}$ or $b\tau\bar{\tau}$ modes offer a substantial LHC reach for A and H, especially at large $\tan\beta$[133, 134]. Along with these decay modes, the decay $A,\ H \to \mu^+\mu^-$ has been found to be very useful [135]. Since the f_μ Yukawa coupling constant also increases with $\tan\beta$, this mode maintains its branching fraction – typically at the 10^{-4} level – even in the face of increasing $A \to b\bar{b}$ partial width. It also offers the advantages in that the two high p_T isolated muons are easy to tag, and the reconstruction of the invariant mass of muon pair, $m_{\mu^+\mu^-}$, allows a high precision measurement of the A mass and width, Γ_A. In fact, is was shown in Ref. [136, 137] that the LHC discovery potential for $A \to \mu^+\mu^-$ is greatest in the $b\mu^+\mu^-$ mode at large $\tan\beta$, compared to $\mu^+\mu^-$, or $b\bar{b}\mu^+\mu^-$. We will adopt the $pp \to bA,\ bH$ production mode along with decay to muon pairs as a key to explore neutralino annihilation via the A-resonance in this chapter.

In Figure 7.1, we show the leading order cross section for $pp \to b\phi \to b\mu^+\mu^-$ production versus m_A at LHC with $\sqrt{s} = 14$ TeV. We show curves for $\phi = A$ and H, and for $\tan\beta = 10$ and 55. Several features are worth noting.

- The cross sections for A and H production are nearly identical, except at very low m_A values, where substantial mixing between h and H occurs.
- The total production cross section increases by a factor of ~ 30 in moving from $\tan\beta = 10$ to $\tan\beta = 55$. This reflects the corresponding increase in b-quark Yukawa coupling f_b, and goes as f_b^2 in the total production cross section.
- In spite of the small $A,\ H \to \mu^+\mu^-$ branching fraction of $\sim 10^{-4}$, the cross section for $b\mu^+\mu^-$ production via the Higgs remains large, varying between over 10^2 fb for low m_A to $\sim 10^{-1}$ fb for $m_A \sim 1$ TeV when $\tan\beta$ is large. For LHC integrated luminosities (L) of order $10^2 - 10^3$ fb^{-1}, these rates should be sufficient at least to extract the A and/or H mass bump.

- In addition, the factorization scale and the renormalization scale are chosen to be $\mu_F = \mu_R = m_\phi/4$ with $\phi = A, H$. This choice of scale effectively reproduces the effects of next-to-leading order (NLO) corrections[132].

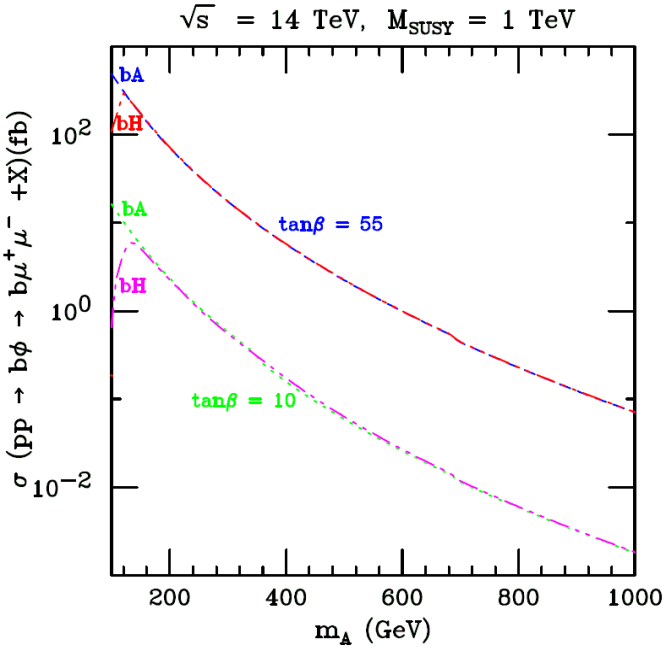

Figure 7.1: The total production cross section for $pp \to b\phi \to b\mu^+\mu^-$ versus m_A in fb at LHC with $\sqrt{s} = 14$ TeV. We show results for $\phi = A$ and H, and for $tan\beta = 10$ and 55.

The remainder of this chapter is organized as follows. In Section 7.1, we review neutralino annihilation via the A-resonance in the mSUGRA model, and the reach of LHC for $A,\ H \to \mu^+\mu^-$ in mSUGRA parameter space for various values of integrated luminosities. In Section 7.2, we present our methods and results from Monte Carlo simulations for $A,\ H$ production and decay to muons. In Section 7.3 we present our strategy to extract Higgs masses ($m_{A,H}$) and Higgs widths ($\Gamma_{A,H}$), and show the expected precision that LHC might be expected to attain in measuring m_A and Γ_A. In Section 7.4 (Conclusions), we comment on how these measurements will help ascertain when A-resonance annihilation might be the major annihilation reaction for neutralino dark matter in the early universe.

7.1 The A-resonance annihilation region in mSUGRA

In this section, we would like to map out the portions of the A-resonance annihilation parameter space which are potentially accessible to LHC searches. Figure 7.2 shows our results in the $(m_0, m_{1/2})$ plane of the mSUGRA model for $A_0 = 0$, $\tan\beta = 55$ and $\mu > 0$. The green-shaded region has a relic density[1] of $0.1 < \Omega_{\tilde{\chi}_1^0} h^2 < 0.12$, while the

[1] The neutralino relic density is computed with the IsaReD[138] subroutine of Isajet 7.80[139, 140].

yellow-shaded region has $\Omega_{\tilde{\chi}_1^0}h^2 < 0.1$. The red-shaded region has too large a thermal neutralino abundance $\Omega_{\tilde{\chi}_1^0}h^2 > 0.12$, and so is excluded under the assumption of a standard cosmology with neutralino dark matter. The gray region is excluded because either REWSB breaks down (right side), or we find a stau as the LSP (left side). The blue shaded region is excluded by LEP2 searches for chargino pair production, *i.e.* $m_{\widetilde{W}_1} < 103.5$ GeV.

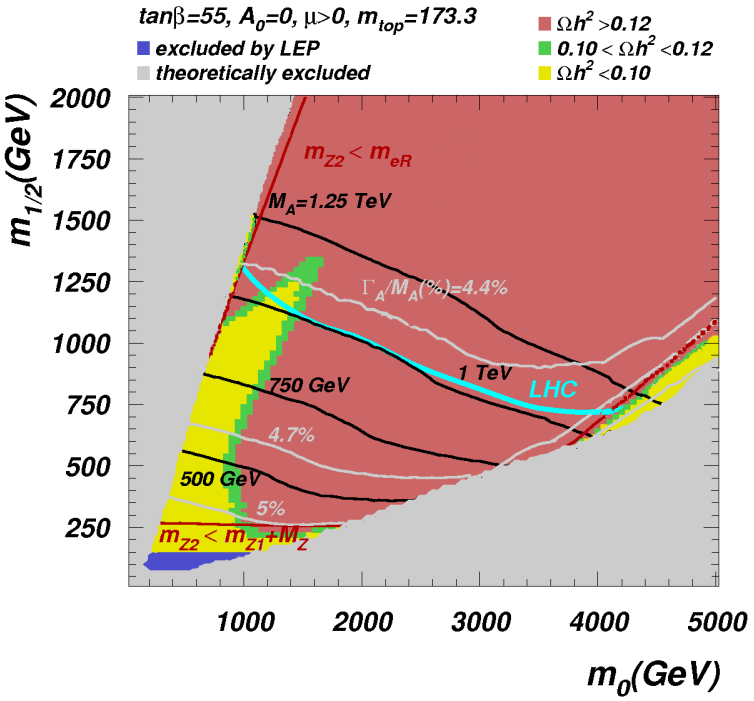

Figure 7.2: The m_0 *vs.* $m_{1/2}$ frame of the mSUGRA model for $\tan\beta = 55$, $A_0 = 0$, $\mu > 0$ and $m_t = 173.3$ GeV. The green and yellow regions provide a thermal neutralino abundance in accord with WMAP measurements of the dark matter density. We also show contours of m_A and Γ_A/m_A, and also show the LHC reach for SUSY with 100 fb^{-1} and $\sqrt{s} = 14$ TeV.

The A-resonance annihilation region is plainly visible on the plot. We also show the SUSY reach of the CERN LHC assuming $\sqrt{s} = 14$ TeV and 100 fb^{-1} of integrated luminosity, taken from Fig. 5 of Ref. [141]. The LHC reach is mainly determined by the total cross section for $\tilde{g}\tilde{g}$, $\tilde{g}\tilde{q}$ and $\tilde{q}\tilde{q}$ production, followed by their subsequent cascade decays[142, 143, 144, 145] into final states with multi-jets plus multi-isolated leptons plus missing transverse energy. A hypercube of cuts is examined to extract signal and background rates over a variety of cascade decay signal channels. We see that with $L = 100$ fb^{-1}, LHC can nearly cover the entire A-funnel. Doubling the integrated luminosity would allow for complete exploration of this DM-allowed region. Meanwhile, much of the HB/FP region is inaccessible to LHC searches, although it should be completely covered by ongoing and future WIMP searches by Xenon-100 and Xenon-1-ton experiments[146, 147, 148, 149].

We also show the contour where $m_{\tilde{\chi}_2^0} > m_{\tilde{e}_R}$ and where $m_{\tilde{\chi}_2^0} < m_{\tilde{\chi}_1^0} + M_Z$. In the former region, the decay $\tilde{\chi}_2^0 \to e\tilde{e}_R \to e^+e^-\tilde{\chi}_1^0$ will be kinematically open while in the latter region the 3-body decay $\tilde{\chi}_2^0 \to \tilde{\chi}_1^0 e^+e^-$ should be visible. In either case, the dilepton mass edge $m_{\ell^+\ell^-}$ should provide information on $m_{\tilde{\chi}_2^0}$ and $m_{\tilde{\chi}_1^0}$[150, 151, 152, 153, 154, 155, 156].

Next, we would like to know how much of the A-funnel region is open to heavy Higgs detection in the $A \to \mu^+\mu^-$ mode. A parton level study has been performed in Ref. [136, 137] for m_A values up to 600 GeV. Here, we wish to extend these results to much higher m_A values. In Ref. [136, 137], the maximal reach for the $A,\ H \to \mu^+\mu^-$ mode was found to be in the $pp \to b\phi$ channel, where $\phi = A$ or H.

The study in Ref. [136, 137] evaluated $pp \to b\phi \to b\mu^+\mu^-$ production against SM backgrounds coming from $bg \to b\mu\mu$, from $gg,\ q\bar{q} \to b\bar{b}W^+W^-$ and from $gb \to bW^+W^-$ (followed by $W \to \mu\nu_\mu$ decay). Here, at the first stage of our analysis, we repeat this calculation, although we extend the results to much higher values of m_ϕ and higher integrated luminosities. We also evaluate additional possible backgrounds to determine whether their contributions are important or negligible. We require the presence of

- two isolated opposite-sign muons with $p_T > 20$ GeV and pseudorapidity $|\eta_\mu| < 2.5$,
- one tagged b-jet, with $p_T > 15$ (30) GeV and $|\eta_b| < 2.5$ and b-jet detection efficiency of $\epsilon_b = 60$ (50)% for low (high) integrated luminosity regimes,
- $p_T^{\rm miss} < 20$ GeV (40 GeV), to reduce backgrounds from $t\bar{t}$ production for low (high) integrated luminosity regimes.

Furthermore a signal region was defined by the mass window $m_\phi \pm \Delta M_{\mu^+\mu^-}$, where, $\Delta M_{\mu^+\mu^-} = 1.64\left[(\Gamma_\phi/2.36)^2 + \sigma_m^2\right]^{1/2}$, with Γ_ϕ is the total width of the Higgs boson, and the muon mass resolution is taken to be $\sigma_m = 0.02 m_\phi$. To determine the observability of the signal we use the intermediate, $\kappa = \frac{1}{2}$, definition of significance discussed in Section 5.3.1. The signal is thus considered to be observable at the $2N\sigma$ level if the lower limit on the signal plus background is larger than the corresponding upper limit on the background with equal statistical fluctuations

$$L(\sigma_s + \sigma_b) - N\sqrt{L(\sigma_s + \sigma_b)} \geq L\sigma_b + N\sqrt{L\sigma_b} \tag{7.3}$$

or equivalently,

$$\sigma_s \geq \frac{N}{L}\left[N + 2\sqrt{L\sigma_b}\right] . \tag{7.4}$$

Here L is the integrated luminosity, σ_s is the cross section of the signal, and σ_b is the background cross section.

In our analysis, we use the CTEQ6L set for Parton Density Functions (PDFs) [157] and the QCD scale is set equal to $m_A/4$ for signal and $\hat{s}$ for backgrounds. The following

backgrounds have been evaluated with the respective K-factors applied to take into account Higher order corrections:

- $gg+q\bar{q} \to W^+W^-b\bar{b} \to \mu^+\mu^-\nu\bar{\nu}$ ($K = 2$): this is the dominant background coming mainly from $t\bar{t}$ production and decay,
- $bg \to W^+W^-b \to \mu^+\mu^-\nu\bar{\nu}$ ($K = 1.3$): this background is typically at least one order of magnitude below the first one,
- $bg \to b\mu^+\mu^-\nu\bar{\nu}$ ($K = 1.3$): this background is of the same order of magnitude as previous one,
- $b\gamma \to b\mu^+\mu^-\nu\bar{\nu}$ ($K = 1.3$): this background is several times lower than the previous one and can be considered as a subdominant one, contributing to the total background at the percent level. It was evaluated using the photon distribution function of the proton available in CalcHEP,
- $cg \to c\mu^+\mu^-\nu\bar{\nu}$ ($K = 1.3$): this background is of the same order as the previous one and therefore, again contributing to the total background at the percent level. It was evaluated using a mis-tagging probability for c-jet equal to 10%.
- $qg \to q\mu^+\mu^-\nu\bar{\nu}$ ($K = 1.3$): also, this background is of the same order as the previous one, contributing to the total background at the percent level. It was evaluated using mis-tagging probability for light q-jet equal to 1%.

Figure 7.3 presents $pp \to \phi^0 b \to \mu^+\mu^- b$ signal rates versus m_A, where $\phi^0 = A, H, h$ after application of kinematical cuts and efficiency of b-tagging for $\tan\beta = 5$ (black lines) and $\tan\beta = 55$ (red lines). Results for low and high luminosity regimes are denoted by solid and dashed lines respectively.

In Figure 7.4, we present rates for various backgrounds described above for $\mu^+\mu^- b$ signature versus m_A after application of kinematical cuts and efficiency of b-tagging for an intermediate value of $\tan\beta = 30$. Results for low and high luminosity regimes are presented in top and bottom frames respectively. One can see that indeed the contributions from the last three subdominant backgrounds discussed above are at the percent level.

Using signal and background rates from these calculations, we derive the LHC discovery reach. The results are shown in Figure 7.5. One should notice an important effect of the cuts for low and high luminosity regimes. The main effect for LHC reach comes from the $p_T^{\rm miss}$ cut. We require $p_T^{\rm miss} < 20$ GeV for low luminosity which should leave signal intact assuming that instrumental missing transverse momentum is under control above 20 GeV in the low luminosity regime. This cut significantly suppresses the leading $t\bar{t}$ background. For high luminosity regime we apply $p_T^{\rm miss} < 40$ GeV which does not affect signal but significantly increases background. The overall effect of high luminosity cuts

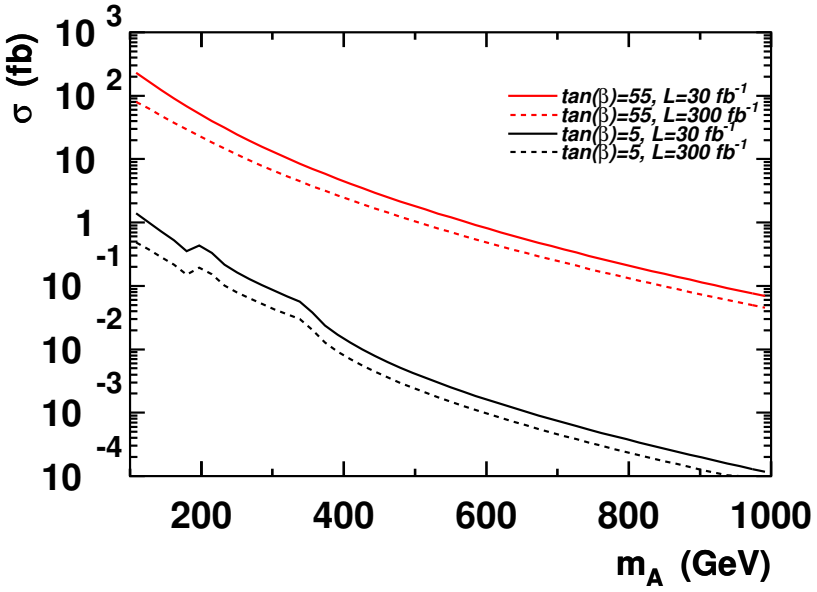

Figure 7.3: $pp \to \phi b \to \mu^+\mu^- b$ signal rates versus m_A, where $\phi = A,\ H,\ h$ after application of kinematical cuts and efficiency of b-tagging for $\tan\beta = 5$ (black lines) and $\tan\beta = 55$ (red lines). Results for low and high luminosity regimes are denoted by solid and dashed lines respectively. The kink at about 350 GeV for low $\tan\beta$ is due to reduced branching ratios to muons when the $t\bar{t}$-channel opens up. The increase of cross section just below 200 GeV for low $\tan\beta$ is due to H becoming more degenerate with A as m_A increases and thus contributing more to the cross section in the defined mass window. Subsequent downward kinks are due to the channels WW, ZZ and hh opening up for H.

is an increase of the background and decrease of the signal. Therefore, the discovery potential of the LHC at $L = 100$ fb^{-1} is slightly lower than at $L = 30$ fb^{-1}. But in the region sufficiently above the border-line for LHC discovery potential shown in Figure 7.5, say for $m_A = 400$ GeV and $\tan\beta = 55$, LHC at $L = 100$ fb^{-1} provides better statistics and significance as compared to the $L = 30$ fb^{-1} case as we show below.

Here, we see that for $L = 100$ fb^{-1}, the reach for $b\phi \to b\mu^+\mu^-$ at $\tan\beta \sim 55$ extends to $m_A \simeq 550$ GeV. For $L = 300$ fb^{-1}, the reach extends to $m_A \simeq 730$ GeV, and for $L = 1000$ fb^{-1}, the reach extends to ~ 925 GeV.

From the results of Figure 7.5, we can now compare against Figure 7.2 to see how much of the A-funnel can be explored via the $A,\ H \to \mu^+\mu^-$ decay mode. To illustrate, we show contours of $m_A = 500,\ 750,\ 1000$ and 1250 in Figure 7.2. Thus, for 100 fb^{-1} of integrated luminosity, we expect LHC to be sensitive to a $A,\ H \to \mu^+\mu^-$ bump for about half of the A-funnel. An integrated luminosity of 300 fb^{-1} covers about three-quarters of the A-funnel, while well over 1000 fb^{-1} will be needed to cover the entire funnel region.

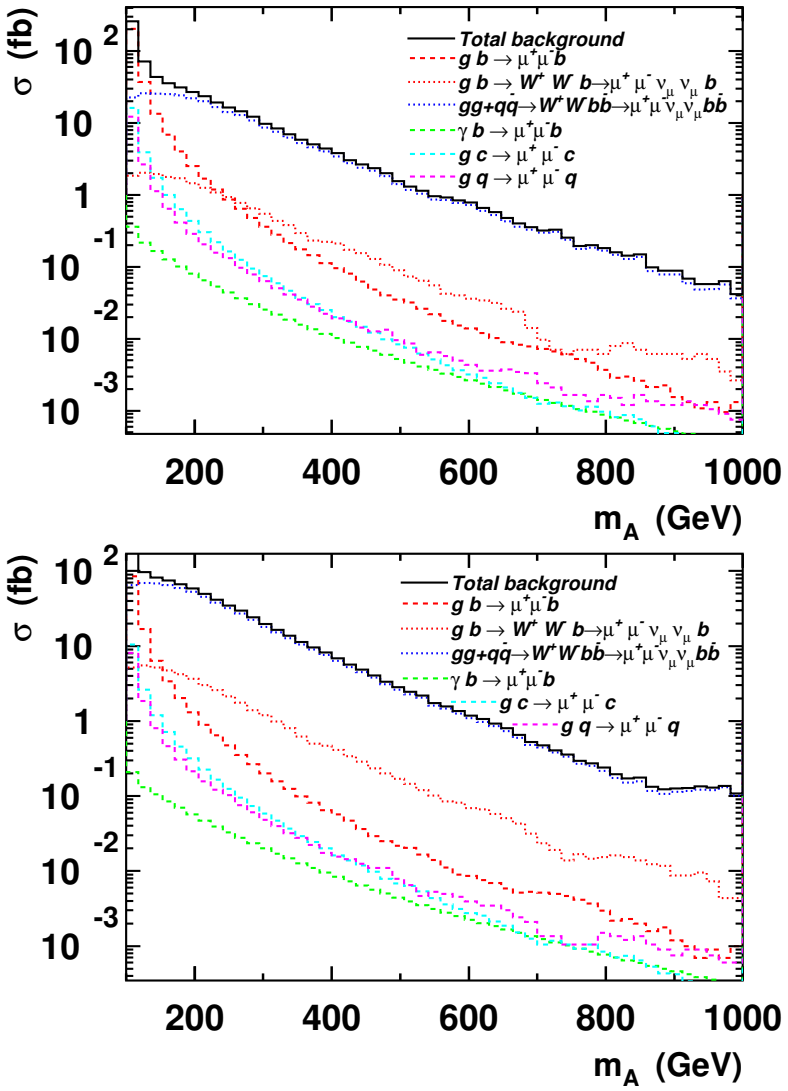

Figure 7.4: Rates for various backgrounds for $\mu^+\mu^- b$ signature versus m_A after application of kinematical cuts and efficiency of b-tagging for $\tan\beta = 30$. Results for low and high luminosity regimes are presented in top and bottom frames respectively.

It should be noted once more that there are other channel, more promising in terms of discovery. For example, we shall see in Chapter 8 that much of the parameter space shown in Figure 7.5 is already excluded, e.g. by the recent $\tau\tau$-results shown in Figure 8.6. Nevertheless, the muon channel is interesting in its own right.

In addition to measuring the value of $m_{A,H}$ via a dimuon mass bump, one may be able to extract information on the A, H widths from the dimuon channel, if LHC experiments have sufficiently good muon energy reconstruction. To illustrate the values of Γ_A that are expected, we plot contours of Γ_A/m_A in Figure 7.2. These range from about 5% for low $m_{1/2} \sim 250$ GeV, corresponding to $\Gamma_A \sim 15-20$ GeV, to about 4.4% for $m_{1/2} \sim 1200$ GeV, where $\Gamma_A \sim 50$ GeV. To better illustrate the range of Higgs widths expected in mSUGRA, we show in Figure 7.6 the value of Γ_A versus m_A after a scan over mSUGRA

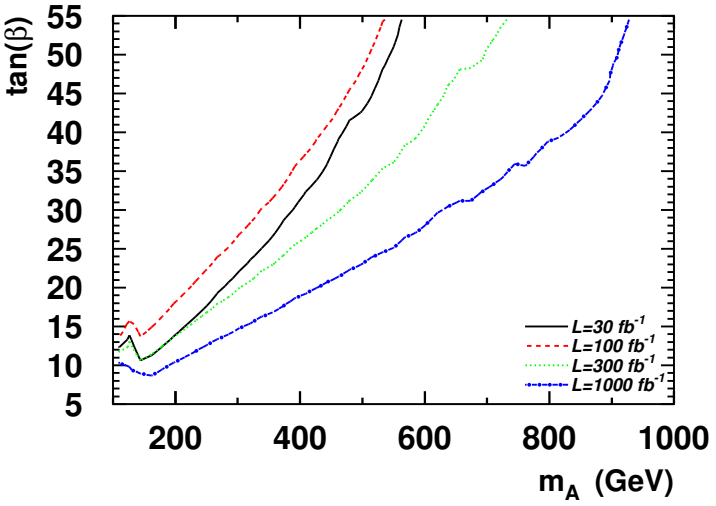

Figure 7.5: LHC reach for the pseudoscalar Higgs A via $pp \to bA \to b\mu^+\mu^-$ in the m_A *vs.* $\tan\beta$ plane for various possible values of integrated luminosity. The 30 fb^{-1} reach exceeds the 100 fb^{-1} reach because we use harder cuts in the high luminosity case.

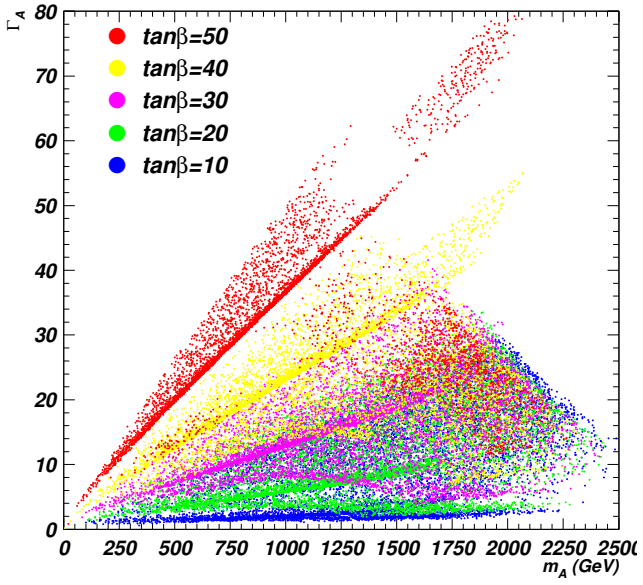

Figure 7.6: Plot of Γ_A versus m_A from a scan over mSUGRA model parameters for $\tan\beta = 10,\ 20,\ 30,\ 40$ and 50.

parameter space for various fixed values of $\tan\beta$. Here, we see that indeed as $\tan\beta$ grows, so too does Γ_A. In fact, for a measured value of m_A, a measurement of Γ_A will

indicate a rather small window of allowed $\tan\beta$ values. Naively, one might expect a one-to-one correspondence between $\tan\beta$ and Γ_A for fixed m_A. However, two effects that spread out the correlation include: (i). weak scale threshold corrections to f_b that are large at large $\tan\beta$, and depend on the entire SUSY spectrum via loop effects [158], and (ii). various additional SUSY decay modes of the A and H may open up [159, 160], depending on sparticle masses and mixings. For instance, if $m_A > 2m_{\widetilde{W}_1}$, then the decay mode $A \to \widetilde{W}_1^+\widetilde{W}_1^-$ opens up and contributes to the A width. Thus, models with lighter SUSY particles should correspond to larger Γ_A values for a given m_A and $\tan\beta$ value, whereas if all non-standard decay modes are closed, then the lower range of Γ_A that is shown may be expected to occur. The loop corrections to f_b tend to enhance f_b for $\mu > 0$ and diminish f_b for $\mu < 0$, leading to somewhat separated bands for each $\tan\beta$ value.

7.2 Detailed simulations for $pp \to bA,\ bH$

In this section, we present a detailed Monte Carlo study of detection of $b\phi \to b\mu^+\mu^-$ for a particular case study. The benchmark point we adopt is known as LCC4 in the study by Battaglia *et al.*, Ref. [161]. Some of the mSUGRA parameters and sparticle masses as generated by Isajet 7.80 are given in Table 7.1. We use a value of $m_t = 175$ GeV instead of 178 GeV as in Ref. [161] since the latest Isasugra/IsaReD code gives a relic density of $\Omega_{\widetilde{\chi}_1^0}h^2 = 0.1$ for the 175 GeV value, and 0.16 for the 178 GeV value. We also examine later how well the value of Γ_A can be measured for benchmark point BM600 with $m_A = 608$ GeV. The benchmarks LCC4 and BM600 have now been excluded by LHC data but will still serve as good examples on how well the Higgs mass and width can be measured at LHC.

The resolution of the dimuon invariant mass, and hence an accurate measurement of m_A and especially Γ_A, depends on the LHC detector's ability to measure the muon's momentum. The muon momentum is measured from its amount of bending in the magnetic field of the detector. Thus, for low energy muon, with a highly curved track, the muon $\vec{p}$ measurement should be more precise than for high energy muons, which have very little track curvature. For our studies, we use a CMS muon smearing subroutine, where the smearing as a function of $|\eta(\mu)|$ is displayed in Figure 7.7, for several muon p_T values [162, 163].

We begin our MC simulation by calculating $bg \to b\mu^+\mu^-$ production for pp collisions at $\sqrt{s} = 14$ TeV using CalcHEP[164]. The relevant Feynman diagrams are displayed in Figure 7.8. They include not only A and H production and decay, but also background contributions from γ^*, Z^* and h production.

In Figure 7.9, we plot the invariant mass distribution of muon pairs $m_{\mu^+\mu^-}$ for $L = 30$ fb^{-1}. For all distributions now and hereafter, we take into account detector effects of

parameter	LCC4	BM600
m_0	380	900
$m_{1/2}$	420	650
A_0	0	0
$\tan\beta$	53	55
μ	528.2	750.7
$m_{\tilde{g}}$	991.5	1502.6
$m_{\tilde{u}_L}$	973.0	1609.0
$m_{\tilde{t}_1}$	713.4	1167.9
$m_{\tilde{b}_1}$	798.9	1309.5
$m_{\tilde{e}_L}$	475.4	998.2
$m_{\tilde{e}_R}$	412.5	931.5
$m_{\tilde{\tau}_1}$	206.6	541.7
$m_{\widetilde{W}_1}$	325.7	520.1
$m_{\tilde{\chi}_2^0}$	325.4	519.5
$m_{\tilde{\chi}_1^0}$	172.5	274.7
m_A	420.7	607.9
m_H	423.5	612.0
m_h	115.1	117.1
Δa_μ	35×10^{-10}	11×10^{-10}
$BF(b \to s\gamma)$	1.9×10^{-4}	2.8×10^{-4}
$BF(B_s \to \mu^+\mu^-)$	2.8×10^{-8}	1.1×10^{-8}
$\Omega h^2_{\tilde{\chi}_1^0}$	0.096	0.089
$\sigma(\tilde{\chi}_1^0 p)$ pb	1.1×10^{-8}	1.7×10^{9}
Γ_A	19.1 GeV	31.9 GeV
Γ_H	19.2 GeV	32.1 GeV

Table 7.1: Masses and parameters in GeV units for Benchmark points LCC4 (with $m_t = 175$ GeV) and BM600 (with $m_t = 173.3$ GeV) using Isajet 7.80.

muon momenta resolution according to Figure 7.7 using Gaussian smearing applied to the particle's momentum generated by CalcHEP at the parton level. What is clear from the plot is that the γ, $Z \to \mu^+\mu^-$ peaks stand out; but also the A, $H \to \mu^+\mu^-$ overlapping peak stands out well above background levels at $m_A \sim 420$ GeV.

In Figure 7.10, we plot the muon p_T distribution (solid line) and b-jet p_T distribution (dashed line) from $pp \to bA \to b\mu^+\mu^-$ production for the LCC4 benchmark. The muon p_T distribution peaks at around $p_T \sim m_A/2$, but with substantial smearing to either side due to the momentum of the A. Since the b-jets are emitted preferentially in the forward direction, the $p_T(b)$ distribution peaks at low values, with some smearing out to values over a hundred GeV. In Figure 7.11, we plot the muon (solid line) and b-jet (dashed line) pseudo-rapidity distributions from $pp \to bA \to b\mu^+\mu^-$ for the LCC4 benchmark. The muon η distribution is clearly more central, while $\eta(b)$ is less central due to its role as an element in QCD initial state radiation.

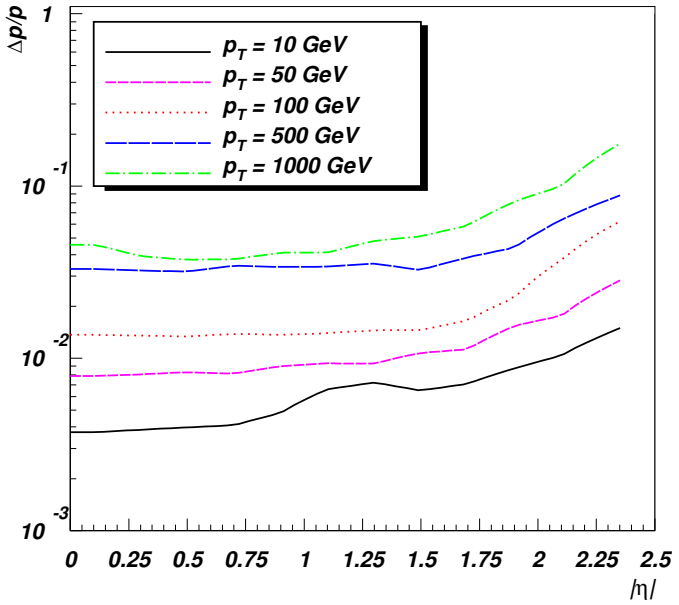

Figure 7.7: Plot of CMS muon smearing function versus $|\eta(\mu)|$ for various muon P_T values.

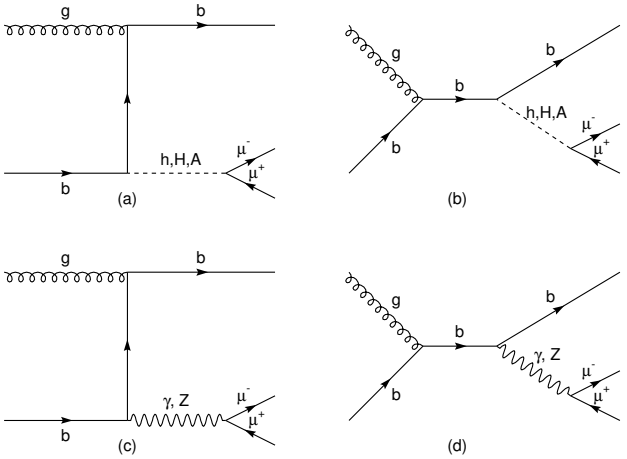

Figure 7.8: Feynman diagrams for $bg \to b\mu^+\mu^-$ in the MSSM.

7.3 Extracting $m_{A,H}$ and $\Gamma_{A,H}$

Once a dimuon mass bump has been established, the next step is to fit the invariant mass distribution with a curve which depends on the Higgs mass and width. A complication occurs because in our case the A and H masses are only separated by ~ 3 GeV, and so the two peaks are highly overlapping, and essentially indistinguishable. To see what this means for an ideal measurement, we plot in Figure 7.12 for LCC4 the dimuon invariant mass from just the reaction $pp \to bA \to b\mu^+\mu^-$ (red curve), and also the distribution from $pp \to bH \to b\mu^+\mu^-$ (blue curve), along with the sum (black curve). A direct measurement of these idealized distributions of full-width-at-half-max shows indeed that $\Gamma_A \simeq 430 - 410 = 20$ GeV, while $\Gamma_H \simeq 433 - 413 = 20$ GeV. A measure

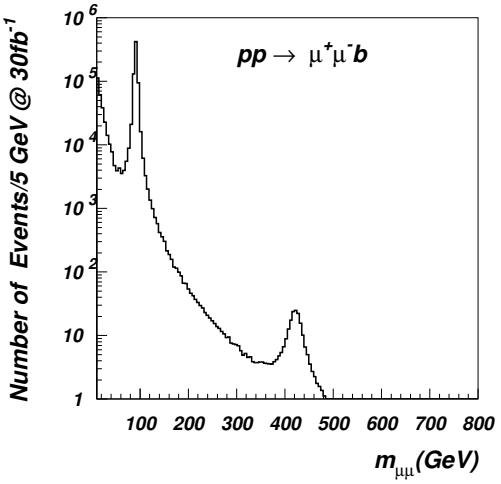

Figure 7.9: Plot of invariant mass distribution of muon pairs $m_{\mu^+\mu^-}$ from a CalcHEP MC computation using benchmark LCC4.

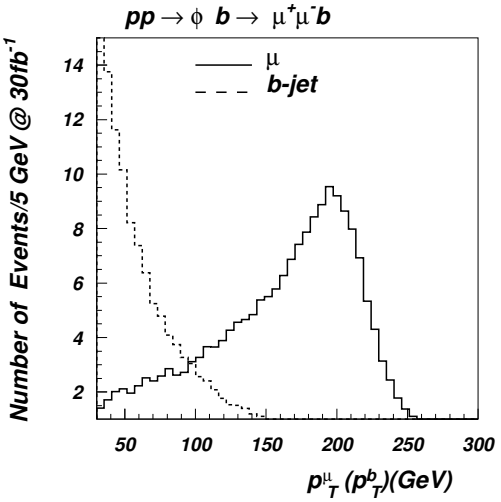

Figure 7.10: Plot of distribution in $p_T(\mu)$ (solid line) and $p_T(b)$ (dashed line) from a CalcHEP MC computation using benchmark LCC4.

of the summed distributions provides $\Gamma_{A,H} \simeq 433 - 410 = 23$ GeV, *i.e.* the idealized width expectation expanded by the A, H mass splitting. We fit the dimuon invariant mass distribution from all diagrams of Figure 7.8 along with muon smearing with the following function F of dimuon mass m and 6 fitting parameters $\Gamma, M, N, \sigma, N_{p1}, N_{p2}$:

$$F(m;\Gamma,M,N,\sigma,N_{p1},N_{p2}) = N\int B(m',\Gamma,M)\times G(m',m,\sigma)dm' + N_{p1}\exp(-N_{p2}m), \tag{7.5}$$

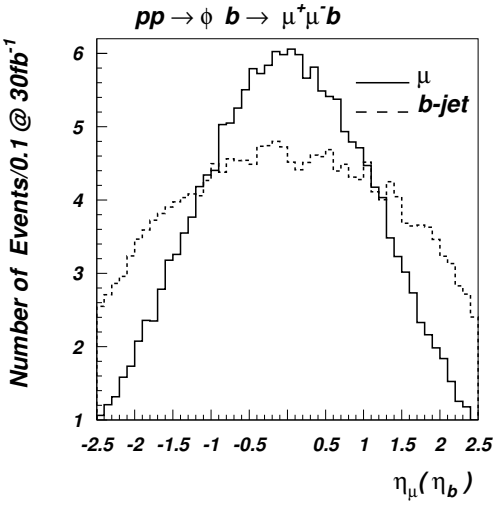

Figure 7.11: Plot of distribution in $\eta(\mu)$ (solid line) and $\eta(b)$ (dashed line) from a CalcHEP MC computation using benchmark LCC4.

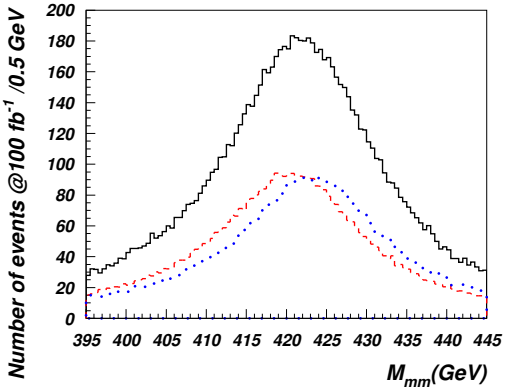

Figure 7.12: Plot of dimuon invariant mass ($M_{\mu^+\mu^-}$) from bA production (red), bH production (blue) and sum (black) for benchmark LCC4 with no smearing.

where N is just a normalization parameter,

$$B(m', \Gamma, M) = \frac{2}{\pi} \frac{\Gamma^2 M^2}{(m'^2 - M^2)^2 + m'^4(\Gamma^2/M^2)},$$

$$G(m', m, \sigma) = \frac{1}{\sqrt{2}\pi\sigma} \exp\left[-\frac{(m' - m)^2}{2\sigma^2}\right].$$

One can see that $F(m; \Gamma, M, N, \sigma, N_{p1}, N_{p2})$ is a convolution of the Breit-Wigner resonance function along with Gaussian detector smearing plus an exponentially dropping function describing the background shape.

The results from the χ^2 fits of signal-plus-background are presented in Figure 7.13 for different integrated luminosities of L =30, 100, 300 and 1000 fb^{-1}. The left side of the

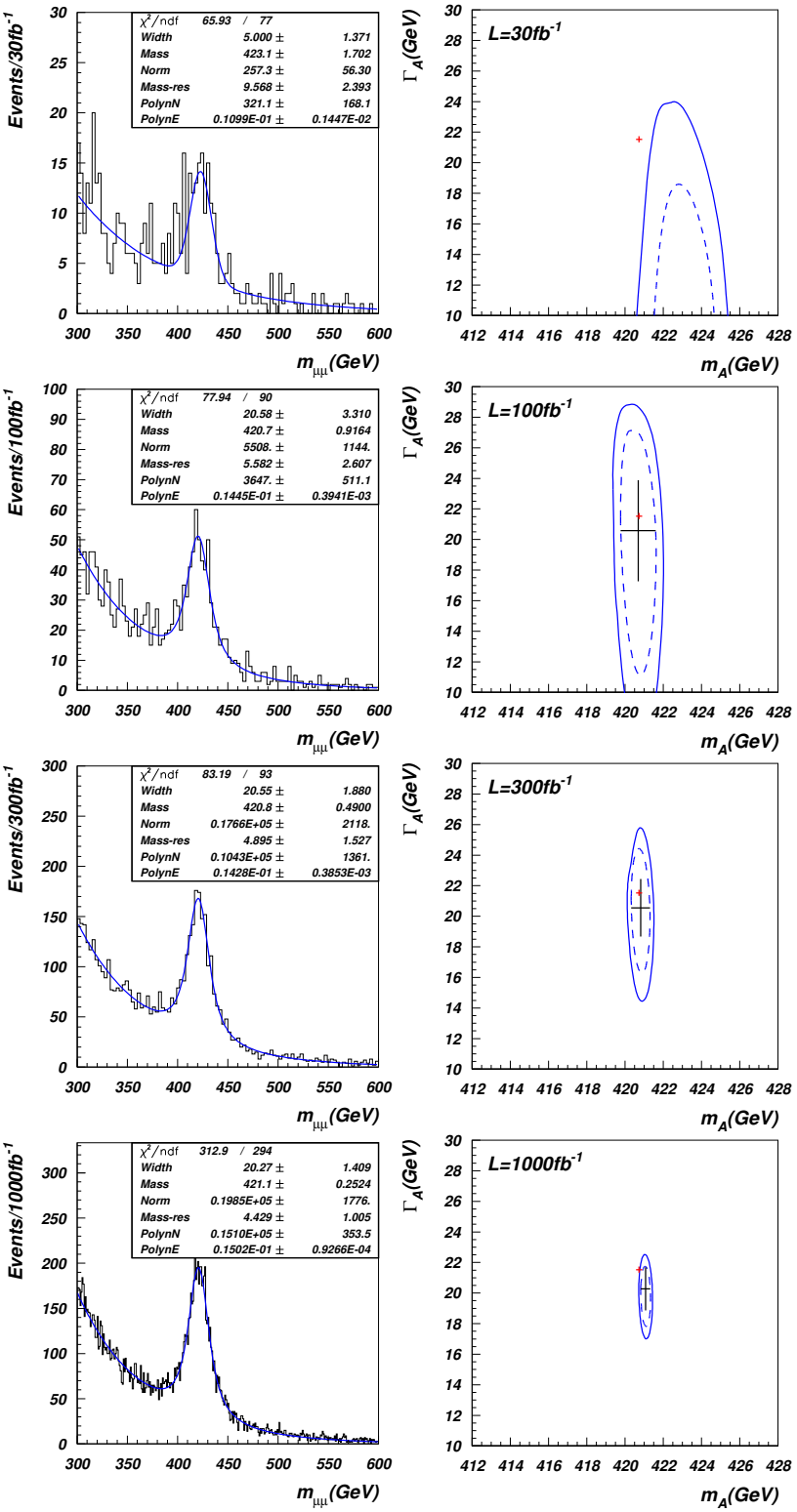

Figure 7.13: Left : best fit of Monte Carlo data for LCC4 for $pp \to bA, H \to b\mu^+\mu^-$ production including muon smearing. Right: corresponding contours of fit to m_A and Γ_A values for Monte Carlo data for LCC4 from $pp \to bA, H \to b\mu^+\mu^-$ production including muon smearing.

Figure 7.13 shows the fit to Monte Carlo data for LCC4 with $pp \to bA, H \to b\mu^+\mu^-$ production including muon smearing. It also shows the values of the fitted parameters $(\Gamma, M, N, \sigma, N_{p1}, N_{p2})$ together with their standard deviations according to the fit. The fit has been performed using the MINUIT program from CERN library which properly takes into account the correlation matrix of the fit parameters, which is crucial for the evaluation of the corresponding contours in the Γ_A *vs.* m_A plane at 1σ and 2σ confidence levels; these are shown on the right side of the Figure 7.13. The black crosses show the width measurement assuming the Higgs masses are known to perfect accuracy. From

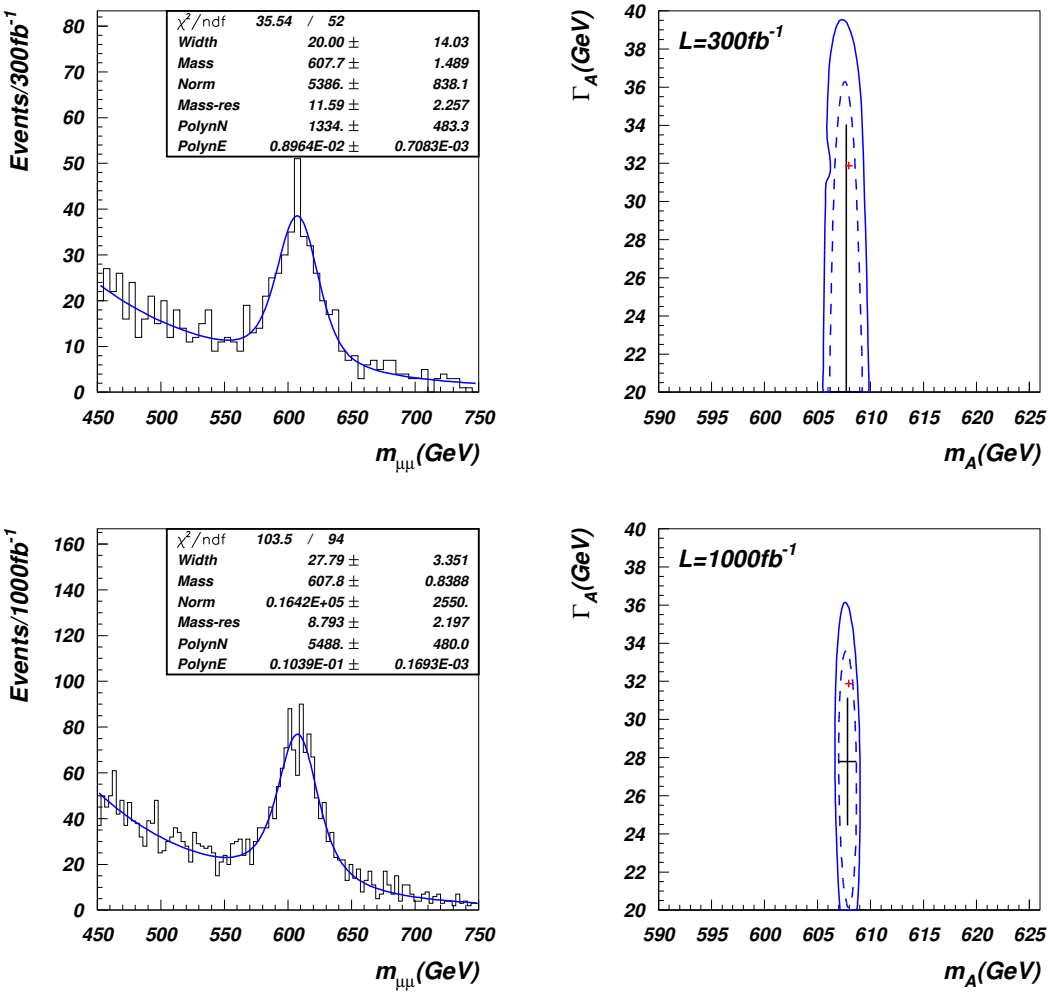

Figure 7.14: Left : best fit of Monte Carlo data for BM600 for $pp \to bA, H \to b\mu^+\mu^-$ production including muon smearing. Right: corresponding contours of fit to m_A and Γ_A values for Monte Carlo data for BM600 from $pp \to bA, H \to b\mu^+\mu^-$ production including muon smearing.

Figure 7.13, one can see that for L =30 fb^{-1} of data, the statistics only provide a rough fit to the A, H width. On the other hand, moving to L =100 fb^{-1}, our fit provides promising results for Γ_A. We see that with L =100 fb^{-1}, m_A can be measured to 1 GeV accuracy, or 0.25%. Meanwhile, the A, H width is measured at $\Gamma_{A,H} \simeq 20 \pm 8$ GeV, or 40% level. At higher integrated luminosity values of L =300 fb^{-1}, the accuracy

on $m_{A,H}$ is improved to sub-GeV levels and $\Gamma_{A,H}$ is found to be $\sim 20 \pm 4$ GeV, a 20% measurement. At L =1000 fb^{-1}, which might be reached in ~ 10 years of LHC running, the measurement of $\Gamma_{A,H}$ can be improved to about 20 ± 1.75 GeV, or $\sim 8\%$ accuracy. The $\Gamma_{A,H}$ accuracy is expected to approach $\sim 7\%$ level for infinite integrated luminosity, and is mainly limited by the detector muon energy resolution of 4%, which is actually quite close to Γ_A/m_A.

The results from the χ^2 fits to m_A and Γ_A of signal-plus-background for benchmark point BM600 are shown in Figure 7.14 for integrated luminosities of L =300 and 1000 fb^{-1}. In this case, the heavy Higgs masses are $m_{A,H} = 608,\ 612$ GeV, while the widths from CalcHEP are $\Gamma_{A,H} = 31.9$ (32.1) GeV. We find for 10^3 fb^{-1} of integrated luminosity, that Γ_A is extracted to be $\Gamma_A = 28 \pm 5.5$ GeV, a 17% measurement.

7.4 Conclusions

To investigate dark matter properties at colliders is a hard task and requires many different measurement. It is however possible that with certain measurements one could determine features of the DM candidate from which one could infer its annihilation mechanism and perhaps even relic density. To distinguish the scenario of resonance annihilation through the pseudoscalar Higgs boson the most important test would be to confirm the condition $2m_{\tilde{\chi}_1^0} \approx m_A$.

A variety of techniques have been proposed for extracting the SUSY particle masses, including $m_{\tilde{\chi}_1^0}$, in sparticle cascade decay events at the LHC [165]. Extracting the heavy Higgs masses is also possible provided that m_A is small enough and that $\tan\beta$ is large enough. Mass measurements of heavy Higgs decays into $b\bar{b}$ and $\tau^+\tau^-$ are fraught with uncertainties from multi-particle production and energy loss from neutrinos. We focused instead on the suppressed decay $A,\ H \to \mu^+\mu^-$, since it allows for both highly accurate heavy Higgs mass and width reconstructions. Production of A and H in association with a single b-jet offers a large background rejection at small cost to signal, especially in the large $\tan\beta$ regime, where Higgs production in association with bs is expected to be enhanced by large Yukawa couplings. This is also the regime in models such as mSUGRA where neutralino annihilation through the heavy Higgs resonance is expected to occur.

In this chapter, we have computed regions of m_A *vs.* $\tan\beta$ parameter space where $pp \to b\phi, \phi = H, A$ production followed by $H,\ A \to \mu^+\mu^-$ should be visible for various integrated luminosities. We have also performed detailed Monte Carlo simulations of signal and background for the LCC4 and BM600 benchmark points. Fits of the dimuon mass spectra allow for sub-percent determinations of the (nearly overlapping) H and A masses. The $A,\ H$ overlapping widths were determined to $\sim 8\%$ ($\sim 17\%$) accuracy in the case of LCC4 (BM600) with 10^3 fb^{-1} of integrated luminosity. We conclude that

indeed the study of $pp \to b\phi, \phi = H, A$ production followed by $H,\ A \to \mu^+\mu^-$ offers a unique opportunity to directly measure $A(H)$ Higgs width. This process also allows to measure the A (H) mass with unprecedented precision. Both these measurements would provide crucial information to connect the cosmological *A-funnel* scenario of dark matter annihilation with LHC data. Combining these measurements with SUSY particle mass measurements such as the mass edge in $m_{\ell^+\ell^-}$ from $\tilde{\chi}_2^0 \to \tilde{\chi}_1^0\ell^+\ell^-$ decay would go a long way towards determining the parameter $\tan\beta$, and also whether or not neutralino annihilation through the A resonance (with $2m_{\tilde{\chi}_1^0} \sim m_A$) is the operative mechanism in the early universe to yield the measured abundance of neutralino dark matter.

Recent exclusion limits in the $\tan\beta$–m_A plane are not far away from excluding the whole 5σ reach region for the dimuon Higgs decay at 1000 fb^{-1} of 14 TeV data. While some of the parameter space is left there is little hope for determining the pseudoscalar Higgs width of the MSSM in this way in the near future at LHC.

Chapter 8

Exclusion limits in supersymmetric models

8.1 Model assumptions

When placing limits one needs to make some assumptions regarding the mass spectrum and couplings of the sparticles. Therefore, exclusion limits typically apply to a particular model with a specific set of parameter values. The CMSSM and mSUGRA models used to be the standard models to apply exclusion limits on. Global fits[166, 167, 168] and direct exclusions in the $m_0 - m_{1/2}$ plane as shown in Figure 8.1 indicates that the CMSSM has a bad goodness-of-fit or a large fine-tuning, e.g. due to heavy squarks. Since these models are no longer favourable by experimental data and the need to explore wider classes of supersymmetric models has risen, one typically focus on so called simplified models. In order to assume more general mass relations in the spectrum, other simplifications have to be made. Therefore the full sparticle spectrum is not included in these models, only the most relevant particles for the particular search. It is also common to simplify the assumptions regarding branching ratios, e.g. such that a dominant branching ratio is exactly 1. One may for example study a model where gluinos only decay via a virtual stop to $t\bar{t}\tilde{\chi}_1^0$. Below follow some example of exclusion limits on sparticle masses.

8.2 Gluinos and squarks

As mentioned, exclusion limits on the CMSSM have not been published recently since the model no longer seems very attractive. For illustrative purposes exclusion limits from a combination of 0-lepton searches by ATLAS[7] are presented in Figure 8.1. One

can see that already at an integrated luminosity of $\mathcal{L} = 5.8$ fb^{-1} gluino masses below ~ 1 TeV and squark masses below ~ 1.5 TeV were excluded in this model.

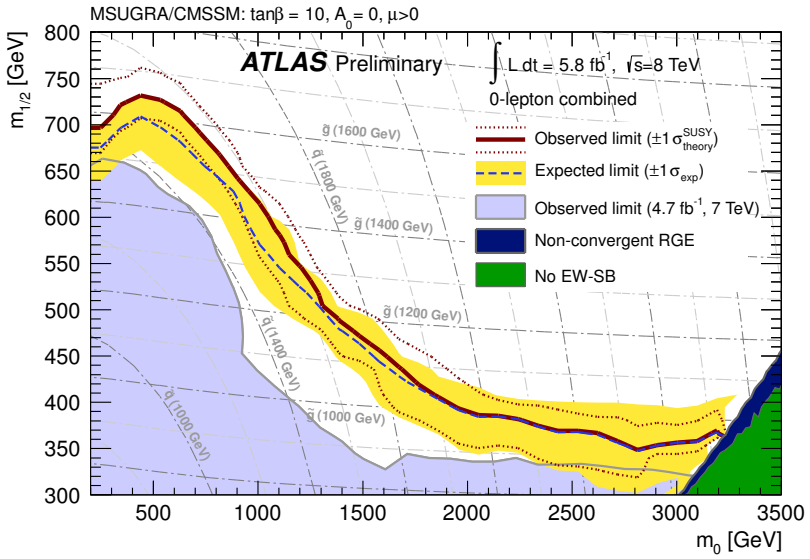

Figure 8.1: Combinations of exclusion limits in the CMSSM from 0-lepton searches by ATLAS [7]

Recent limits are typically made on models where the mass relations between the particles are not constrained. These models need to be simplified in terms of particle content, however. Exclusion limits for a common simplified model for gluino production and decay is presented in Figure 8.2. In this model, known as T1tttt, the gluinos are assumed to be pair-produced at LHC and decay only to $t\bar{t}\tilde{\chi}_1^0$. The gluino decays into tops are motivated by the fact that most models predict the stop to be the lightest squark which would imply a preferred intermediate decay $\tilde{g} \to \tilde{t}\bar{t}$. Then if the stop is not kinematically allowed to decay into any other sparticle than the LSP it will decay into a top and LSP, $\tilde{t} \to t\tilde{\chi}_1^0$. The model does not include any virtual stop particles however and contains just two BSM particles, gluinos and LSPs. From the assumptions of the model follows that $m_{\tilde{g}} > 2m_t + m_{\tilde{\chi}_1^0}$, therefore exclusions on configurations with small mass gap between the LSP and gluino cannot be made. From Figure 8.2 one can read of a strict limit of ~ 1 TeV for the mass of a gluino in the T1tttt model. If the LSP mass is less than 600 GeV however, the gluino mass limit is as large as 1.3 TeV.

A similar kind of analysis occurs for the direct stop searches. Limits on a model where the stop decays only to top and LSP are shown in the right plot in Figure 8.3. For LSP masses below 200 GeV the stop is limited to be heavier than about 650 GeV. In the left plot of Figure 8.3 limits on slightly more complex stop models are shown where the stop decays via a chargino. In these scenarios the limit on the stop mass is weakened to about 500 GeV. In both of these types of decays one is unable to set limits for very small mass gaps between the stop and LSP.

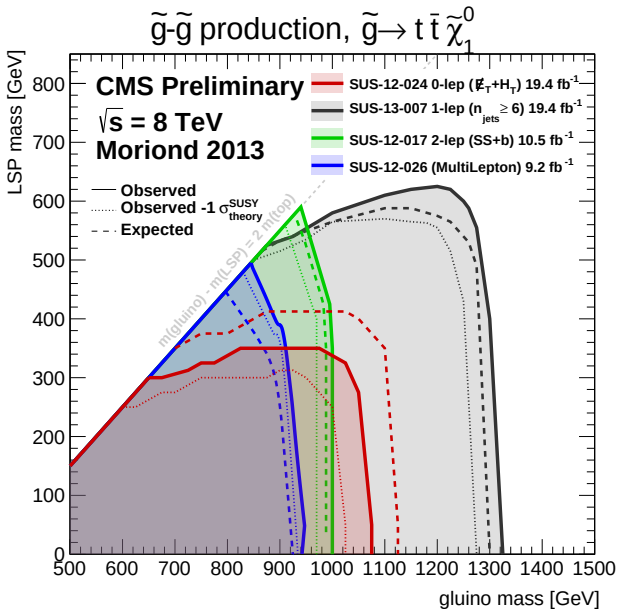

Figure 8.2: A figure combining results from CMS[8, 9, 10, 11] showing exclusion limits in the $m_{\tilde{g}} - m_{\tilde{\chi}_1^0}$ plane for the T1tttt model where $\tilde{g} \to t\bar{t}\tilde{\chi}_1^0$ is the only decay channel.

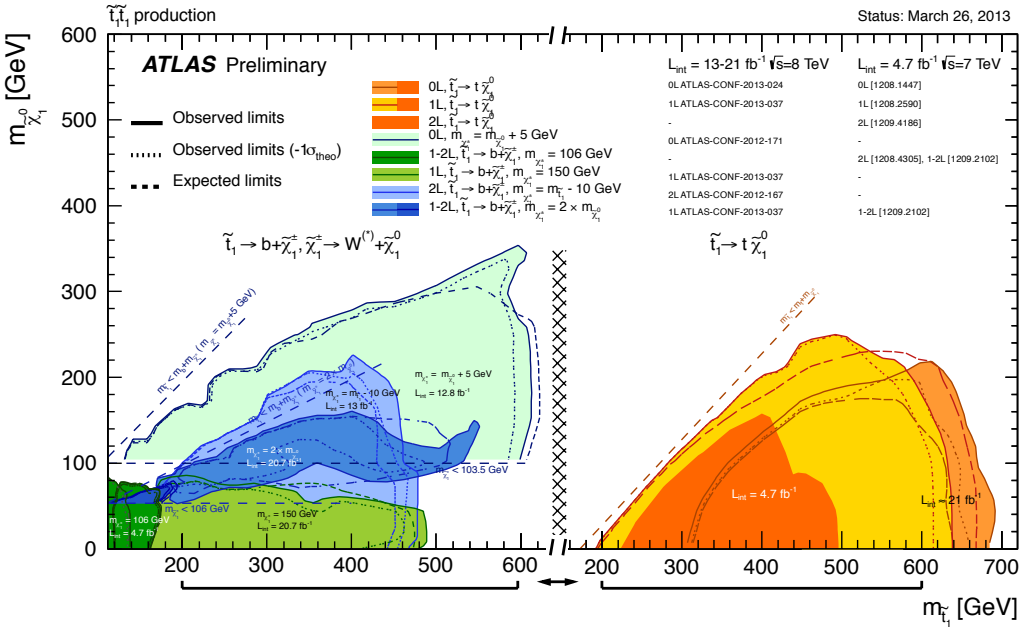

Figure 8.3: A figure combining exclusion limits from direct stop production searches by ATLAS in simplified models.

8.3 Electro-weak sparticle production

If the coloured sparticles are very heavy and perhaps out of reach for the LHC, the most promising way of discovering supersymmetry might be via direct production of sparticles charged under the electroweak groups, i.e. charginos, neutralinos and sleptons. In Figure 8.4 limits on some specific scenarios by CMS are presented. They are all some

kind of wino pair-production, either $\tilde{\chi}_2^0\tilde{\chi}_1^\pm$ or $\tilde{\chi}_1^\pm\tilde{\chi}_1^\mp$. The exclusion limits for the wino mass are not very strong. All scenarios except one presented in Figure 8.4 assume that a slepton of mass $m_{\tilde{l}} = \frac{1}{2}(m_{\tilde{\chi}_1^\pm} + m_{\tilde{\chi}_1^0})$ take part in the decay. If no light slepton is assumed, the mass limit is approximately $m_{\tilde{\chi}_1^\pm} > 330$ GeV for $m_{\tilde{\chi}_1^0} < 100$ GeV. Again, if the mass spectrum is very degenerate it is very difficult to set limits since visible particles will be very soft.

Another scenario which has been studied is the direct production of sleptons which of course would be important if not only the coloured sparticles but also the charginos are heavy. Figure 8.5 shows limits on the slepton masses in the case of selectron or smuon pair-production. The limits here are even weaker than the chargino mass limits in Figure 8.4, the slepton mass is only about $m_{\tilde{l}} > 250$ GeV for $m_{\tilde{\chi}_1^0} < 100$ GeV. This is due to the reduced lepton multiplicity in these decays compared to the scenarios with charginos. However, if one considered pair-production of $\tilde{\chi}_1^\pm$ without assuming any light sleptons even weaker limits for $m_{\tilde{\chi}_1^\pm}$ is expected since not only is the maximum number of final state leptons reduced but since the decay will occur via W-bosons the branching ratios to quarks will suppress the essential lepton signatures.

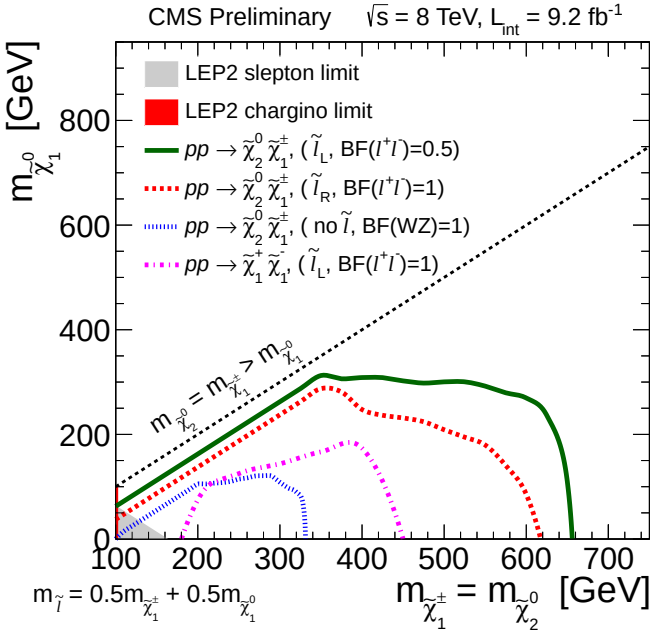

Figure 8.4: A figure combining results from CMS[12] showing limits from searches for direct production of charginos and neutralinos

8.4 Extra Higgs bosons

The exclusion limits on the pseudoscalar Higgs boson, A, of the MSSM are typically presented in the $M_A - \tan\beta$ plane. A search for $A \to \tau^+\tau^-$ by CMS gave the limits presented in Figure 8.6. The $\tau\tau$ channel is expected to be an efficient search channel

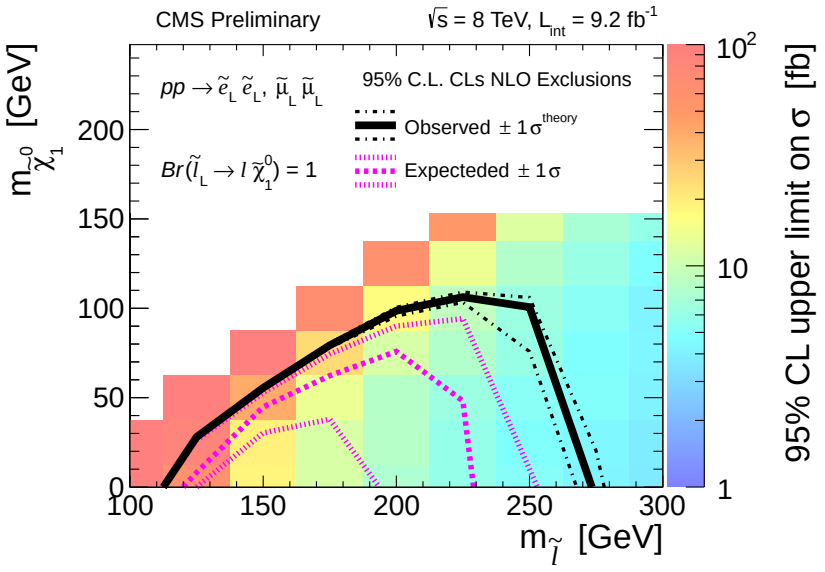

Figure 8.5: Exclusion limits on slepton pair-production by CMS[12] in simplified models.

since the Higgs coupling will be proportional to the fermion mass and enhanced by large $\tan\beta$ in the case of a down-type fermion. Since this parameter space is already largely excluded for large $\tan\beta$ it is not likely that the measurements by the decays to muons which was discussed in detail in Chapter 7 will be possible in the near future.

8.5 Non-minimal SUSY models

The exclusion limits presented in this chapter are made on very minimal models such as the CMSSM, simplified models and the MSSM. Because constrained models such as the CMSSM are no longer favourable the simplified models provide a fairly general way of placing limits on SUSY. However these models will not capture all features that are contained in the MSSM and even less so for more complex models. Therefore models beyond the MSSM, which may be motivated on theoretical grounds, require individual studies. Next chapter will introduce one such non-minimal and in Chapter 10 some of its LHC phenomenology will be compared with that of the MSSM.

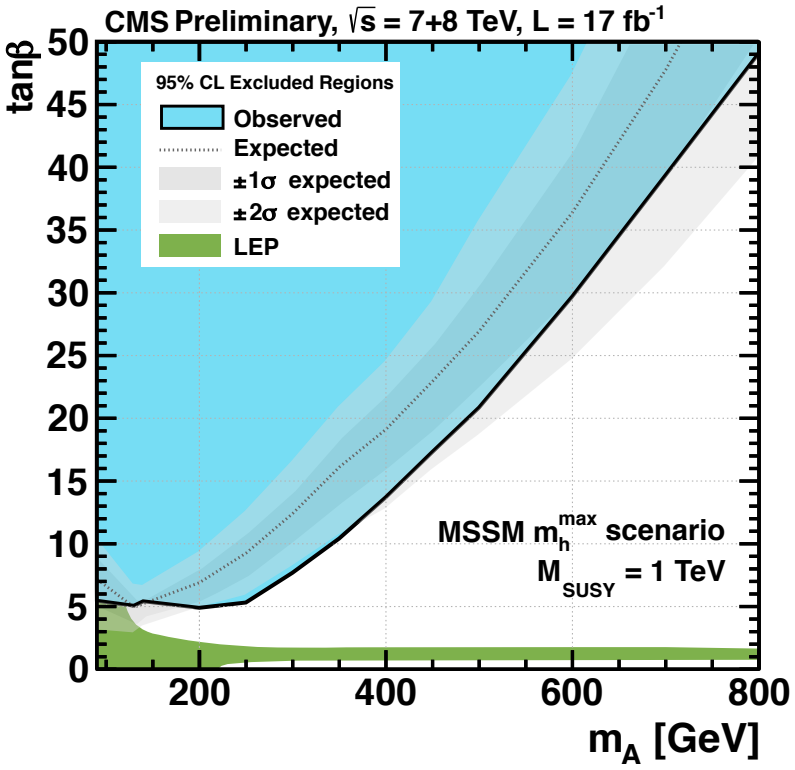

Figure 8.6: Exclusion limits in the $M_A - \tan\beta$ plane of the MSSM from a $A \to \tau\tau$ search by CMS[13]. The maximal mixing scenario, mentioned in Section 4.3.3, is chosen here (denoted $m_h^{\max}$).

Chapter 9

The E_6SSM

Despite its many attractive features, the MSSM suffers from the μ problem. The superpotential of the MSSM contains the bilinear term $\mu H_d H_u$, where H_d and H_u are the Higgs doublet superfields. In order to get the correct pattern of electroweak (EW) symmetry breaking the parameter μ is required to be in the TeV region. At the same time, the incorporation of the MSSM into grand unified theories GUT or string theory implies that μ could be of the order of the GUT or Planck scales, or possibly zero. None of these possibilities is phenomenologically and theoretically acceptable. There are various proposed solution to the μ-problem, e.g. the Giudice-Masiero mechanism [169] in which the μ-term is a result of SUSY breaking. The Next-to-Minimal Supersymmetric Standard Model (NMSSM) [170, 171, 172, 173, 174, 175, 176, 177] attempts to address this problem by postulating an additional gauge singlet superfield S with the interaction $\lambda S H_d H_u$ in the superpotential together with an S^3 interaction in order to break an accidental global $U(1)$ symmetry to a discrete Z_3 symmetry. At low energies ($\sim$ TeV) the scalar component of S acquires a non-zero VEV, s, giving an effective μ term. However the resulting Z_3 discrete symmetry is broken at the same time, leading to potentially dangerous cosmological domain walls [170]. There are however proposed solutions to the cosmological domain wall problem, e.g due to Z_3 breaking by suppressed, non-renormalisable operators[178].

A solution to the μ problem which does not suffer from the problems of the NMSSM arises within E_6 inspired SUSY models. At high energies the E_6 gauge symmetry arising from GUTs or string theory in extra dimensions can be broken to the rank-5 subgroup $SU(3)_c \times SU(2)_L \times U(1)_Y \times U(1)'$, where in general

$$U(1)' = U(1)_\chi \cos\theta + U(1)_\psi \sin\theta \tag{9.1}$$

and the two anomaly-free $U(1)_\psi$ and $U(1)_\chi$ symmetries originate from the breakings $E_6 \to SO(10) \times U(1)_\psi$, then $SO(10) \to SU(5) \times U(1)_\chi$. The extra $U(1)'$ gauge symmetry forbids S^3 interactions since the SM-singlet superfield S is now charged under $U(1)'$. In

addition the bilinear μ term is also forbidden if $\theta \neq 0$ or π, while the interaction $\lambda S H_d H_u$ is allowed in the superpotential.

At low energies ($\sim$ TeV) the scalar component of S acquires a non-zero VEV $\langle S \rangle = \frac{s}{\sqrt{2}}$ breaking $U(1)'$ and giving rise to a massive Z' gauge boson together with an effective μ term. Within the class of rank-5, E_6 inspired SUSY models with an extra $U(1)'$ gauge symmetry, there is a unique choice of the extra Abelian gauge group that allows right-handed neutrinos to be uncharged. This is the $U(1)_N$ gauge symmetry given by $\theta = \arctan\sqrt{15}$ [179, 180]. In this particular case, called the Exceptional Supersymmetric Standard Model (E$_6$SSM), based on the $SU(3)_c \times SU(2)_L \times U(1)_Y \times U(1)_N$ gauge group, the right-handed neutrinos may be superheavy, allowing a high scale see-saw mechanism in the lepton sector [179, 180].

An elegant feature of the E_6 inspired models with an extra Z' gauge boson at the TeV scale is that the conditions of anomaly cancellation may be satisfied by matter content filling out complete 27 representations of E_6 surviving to the TeV scale. One can therefore have three 27 representations, with each containing a generation of SM matter and fields with the quantum numbers of Higgs doublets and SM-singlets. Thus such models predict, in addition to three SUSY families of quarks and leptons, also three SUSY families of Higgs doublets of type H_u, three SUSY families of Higgs doublets of type H_d, three SUSY SM singlets S_i, and three SUSY families of charge $\mp 1/3$ colour triplet and anti-triplet states D and $\overline{D}$, which can get large mass terms due to the (third) singlet VEV $\langle S_3 \rangle = s/\sqrt{2}$ which is also responsible for the μ term. A simplified overview of the particle content and how it contains the MSSM is shown in Figure 9.1.

9.1 Field content

As discussed above, the E$_6$SSM involves a unique choice for the extra Abelian gauge group that allows zero charges for right-handed neutrinos, namely $U(1)_N$. To ensure anomaly cancellation the particle content of the E$_6$SSM at the TeV scale is extended to include three complete fundamental 27 representations of E$_6$, apart from the three right-handed neutrinos which are singlets and do not contribute to anomalies and so may be much heavier. The 27 representations of E_6 decompose under the $SU(5) \times U(1)_N$ subgroup of E$_6$ as follows:

$$27_i \to (10,1)_i + (5^*,2)_i + (5^*,-3)_i + (5,-2)_i + (1,5)_i + (1,0)_i\,. \tag{9.2}$$

The first and second quantities in brackets are the $SU(5)$ representation and extra $U(1)_N$ charge (where a GUT normalisation factor of $1/\sqrt{40}$ is omitted [179, 180]) respectively, while i is a family index that runs from 1 to 3. An ordinary SM family, which contains the doublets of left-handed quarks Q_i and leptons L_i, right-handed up- and down-quarks

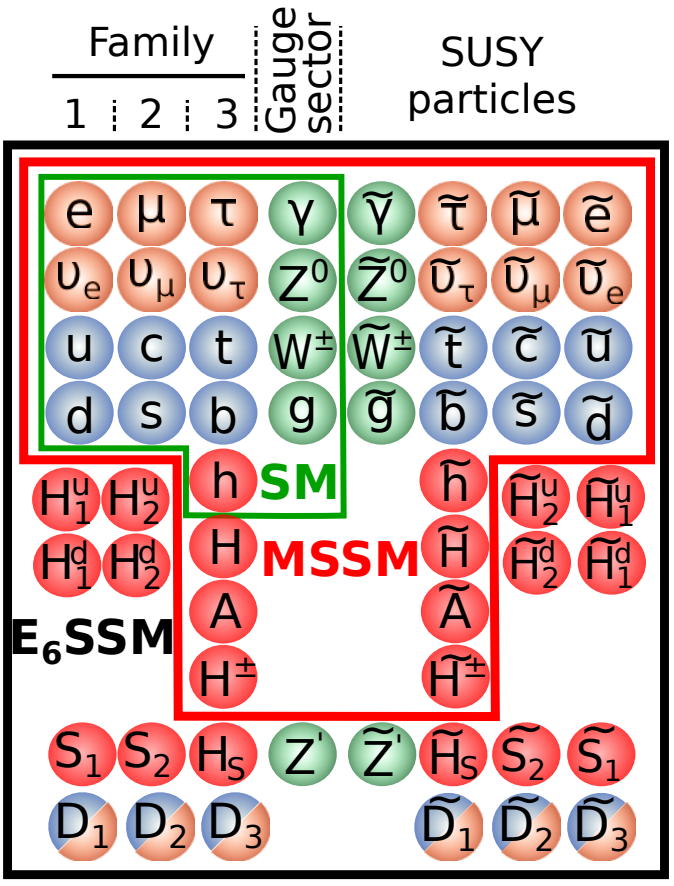

Figure 9.1: A simplified overview of the particle content of the E$_6$SSM and how it contains the MSSM and SM. All matter particles come in three generations, including the Higgs bosons. The Higgs/scalar sector (red) is greatly extended. Only the third generation scalars, which acquire VEVs, are expanded in their physical states. Extra coloured states, leptoquarks or diquarks (orange/blue), D_i, as well as a Z' boson are predicted. For a more complete and accurate description of the field content see Section 9.1 and Table 9.1.

($\bar{u}_i$ and $\bar{d}_i$), and right-handed charged leptons is assigned to $(10,1)_i + (5^*,2)_i$. Right-handed neutrinos $\bar{N}_i$ should be associated with the last term in (9.2), $(1,0)_i$. The next-to-last term, $(1,5)_i$, represents SM-singlet fields S_i, which carry non-zero $U(1)_N$ charges and therefore survive down to the EW scale. The pair of $SU(2)_L$-doublets (H_i^d and H_i^u) that are contained in $(5^*,-3)_i$ and $(5,-2)_i$ have the quantum numbers of Higgs doublets. They form either Higgs or inert Higgs $SU(2)_L$ multiplets. Other components of these fundamental $SU(5)$ multiplets form colour triplet and anti-triplet of exotic coloured particles D_i and $\overline{D}_i$ with electric charges $-1/3$ and $+1/3$ respectively. These exotic quark states carry a $B-L$ charge $\mp 2/3$, twice that of ordinary quarks. In addition to the complete 27_i multiplets the low energy matter content of the E$_6$SSM can be supplemented by an $SU(2)_L$ doublet L_4 and anti-doublet $\overline{L}_4$ from extra $27'$ and $\overline{27'}$ representations to preserve gauge coupling unification [181]. These states will typically be much heavier than the gluino and so will play no role in the present analysis, although

Field	Boson	Fermion	$SU(3)$	$SU(2)$	$U(1)$	$U(1)'$
Chiral	Spin 0	Spin 1/2				
Q^i	$\begin{pmatrix}\tilde{u}_L \\ \tilde{d}_L\end{pmatrix}^i$	$\begin{pmatrix}u_L \\ d_L\end{pmatrix}^i$	**3**	**2**	$\frac{1}{6}$	1
$\bar{u}^i$	$\tilde{\bar{u}}^i$	$\bar{u}^i$	$\bar{\mathbf{3}}$	**1**	$-\frac{2}{3}$	1
$\bar{d}^i$	$\tilde{\bar{d}}^i$	$\bar{d}^i$	$\bar{\mathbf{3}}$	**1**	$\frac{1}{3}$	2
L^i	$\begin{pmatrix}\tilde{\nu}_L \\ \tilde{e}_L\end{pmatrix}^i$	$\begin{pmatrix}\nu_L \\ e_L\end{pmatrix}^i$	**1**	**2**	$-\frac{1}{2}$	2
$\bar{e}^i$	$\tilde{\bar{e}}^i$	$\bar{e}^i$	**1**	**1**	1	1
$\bar{N}^i$	$\tilde{\bar{N}}^i$	$\bar{N}^i$	**1**	**1**	0	0
S^i	S^i	$\tilde{S}^i$	**1**	**1**	0	5
H_u^i	$\begin{pmatrix}H_u^+ \\ H_u^0\end{pmatrix}^i$	$\begin{pmatrix}\tilde{H}_u^+ \\ \tilde{H}_u^0\end{pmatrix}^i$	**1**	**2**	$\frac{1}{2}$	-2
H_d^i	$\begin{pmatrix}H_d^0 \\ H_d^-\end{pmatrix}^i$	$\begin{pmatrix}\tilde{H}_d^0 \\ \tilde{H}_d^-\end{pmatrix}^i$	**1**	**2**	$-\frac{1}{2}$	-3
D^i	D^i	$\tilde{D}^i$	**3**	**1**	$-\frac{1}{3}$	-2
$\bar{D}^i$	$\bar{D}^i$	$\tilde{\bar{D}}^i$	$\bar{\mathbf{3}}$	**1**	$\frac{1}{3}$	-3
Gauge	Spin 1	Spin 1/2				
g	g	$\tilde{g}$	**8**	**1**	0	0
W	$W^{\pm,0}$	$\tilde{W}^{\pm,0}$	**1**	**3**	0	0
B	B	$\tilde{B}$	**1**	**1**	0	0
B'	B'	$\tilde{B}'$	**1**	**1**	0	0

Table 9.1: The E_6SSM field content and the fields' representations under the gauge groups. Right-handed fields are written in terms of their charge conjugate and are denoted with a bar. The same notation is used for a superfield and its contained SM field (or R-parity even field).

they may play a role in leptogenesis [182]. The field content and their representations for the E_6SSM are summarised in Table 9.1.

9.2 Superpotential and Z_2-symmetries

Just as in the MSSM, the gauge symmetry of the E_6SSM does not forbid lepton and baryon number violating operators that result in rapid proton decay. The situation is somewhat different in the E_6SSM however, since the renormalisable superpotential of the model automatically preserves R-parity because of the enlarged gauge symmetry. Although the $B-L$ violating operators of the R-parity violating MSSM are forbidden by the gauge symmetry, there are new B and L violating interactions involving the new exotic particles. In the E_6SSM these terms are removed by imposing an exact Z_2 symmetry on the superpotential. There are two options for this symmetry under which the exotic coloured states are either interpreted as diquarks or leptoquarks, leading to B and L conservation. Furthermore, the extra particles present in E_6 inspired SUSY

models give rise to new Yukawa interactions that in general induce unacceptably large non-diagonal flavour transitions. To suppress these effects in the E$_6$SSM an additional approximate Z_2^H symmetry is imposed. Under this symmetry all superfields except one pair of H_d^i and H_u^i (say $H_d \equiv H_d^3$ and $H_u \equiv H_u^3$) and one SM-type singlet field ($S \equiv S^3$) are odd. Ignoring L_4 and $\overline{L}_4$, the Z_2^H symmetry reduces the structure of the Yukawa interactions to

$$\begin{aligned} W_{\rm E_6SSM} \;\simeq\; & \lambda S(H_u H_d) + \lambda_{\alpha\beta} S(H_d^\alpha H_u^\beta) + f_{u\alpha\beta} S^\alpha (H_d^\beta H_u) + f_{d\alpha\beta} S^\alpha (H_d H_u^\beta) \\ + \;\; & y_{ij}^U (H_u Q_i)\bar{u}_j + y_{ij}^D (H_d Q_i)\bar{d}_j + y_{ij}^E (H_d L_i)\bar{e}_j + y_{ij}^N (H_u L_i)\bar{N}_j \\ + \;\; & \frac{1}{2} M_{ij} \bar{N}_i \bar{N}_j + \kappa_i S(D_i \overline{D}_i)\,, \end{aligned} \tag{9.3}$$

where hats denote superfields, $\alpha, \beta = 1, 2$ and $i, j = 1, 2, 3$. The inert Higgs doublets and SM-singlets have suppressed couplings to matter, whereas the third generation $SU(2)_L$ doublets H_u and H_d and SM-type singlet field S, that are even under the Z_2^H symmetry, play the role of Higgs fields and acquire VEVs. At the physical vacuum their scalar components develop VEVs

$$\langle H_d \rangle = \frac{1}{\sqrt{2}} \begin{pmatrix} v_1 \\ 0 \end{pmatrix}, \qquad \langle H_u \rangle = \frac{1}{\sqrt{2}} \begin{pmatrix} 0 \\ v_2 \end{pmatrix}, \qquad \langle S \rangle = \frac{s}{\sqrt{2}}, \tag{9.4}$$

generating the masses of the quarks, leptons and gauge bosons. Instead of v_1 and v_2 it is more convenient to use $\tan\beta = v_2/v_1$ and $v = \sqrt{v_1^2 + v_2^2} = 246\,\text{GeV}$. The VEV of the SM-singlet field, s, breaks the extra $U(1)_N$ symmetry, generating exotic fermion masses and also inducing a mass for the Z' boson. Therefore the singlet field S must acquire a large VEV in order to avoid conflict with direct particle searches at present and past accelerators.

The superpotential (9.3) is only containing terms allowed by the Z_2^H symmetry. We will later on also be considering odd terms under this symmetry, specifically terms in the Higgs and neutralino sector,

$$\lambda_{ijk} S_i H_{dj} H_{uk}, \tag{9.5}$$

which also contains the first row of (9.3). Let us therefore define the notation for these coupling here in Table 9.2 for future reference.

λ_{333}	λ
$\lambda_{3\alpha\beta}$	$\lambda_{\alpha\beta}$
$\lambda_{\alpha 3\beta}$	$f_{d\alpha\beta}$
$\lambda_{\alpha\beta 3}$	$f_{u\alpha\beta}$
$\lambda_{3\alpha 3}$	$x_{d\alpha}$
$\lambda_{33\alpha}$	$x_{u\alpha}$
$\lambda_{\alpha 33}$	z_α
$\lambda_{\alpha\beta\gamma}$	

Table 9.2: Different notations for Yukawa couplings in the terms $\lambda_{ijk}S_iH_{dj}H_{uk}$, where again Greek generation indices take values $\alpha = 1, 2$ and Latin indices, $i = 1, 2, 3$. Couplings in the top half appear in the Z_2^H-even terms in the top row of (9.3) while those in the bottom half appear in Z_2^H-odd terms and are expected to be small.

9.3 Soft supersymmetry breaking terms

The soft supersymmetry breaking terms of the E_6SSM are

$$\begin{aligned}\mathcal{L}_{\rm soft} =& - A_u\tilde{\bar{u}}\tilde{Q}H_u - A_d\tilde{\bar{d}}\tilde{Q}H_d - A_e\tilde{\bar{e}}\tilde{L}H_d + \text{c.c.}\\ & - A_{\lambda_{ijk}}S_iH_{uj}H_{dk} + A_{\kappa_i}SD_i\bar{D}_i + \text{c.c.}\\ & + \text{scalar and gaugino masses.}\end{aligned} \tag{9.6}$$

For simplicity one can assume that A_λ is a universal scale multiplying the Yukawa couplings λ_{ijk}, $A_{\lambda_{ijk}} = A_\lambda\lambda_{ijk}$, in generalising the assumption of Yukawa proportionality for the trilinear squark and slepton couplings, e.g. $A_{u\,ij} = A_u y^U_{ij}$, to assure suppression of flavour changing neutral currents.

9.4 The Higgs sector

As mentioned above, the Higgs sector of the E_6SSM is largely extended to that of the MSSM. The sector becomes particularly complicated if all the Z_2^H-violating parameters are included. It is often reasonable to assume that these couplings are very small, in which case only the third generation Higgs bosons and SM-singlet are relevant. The extra degrees of freedom in this Higgs sector compared to the one in the MSSM, introduced by the complex scalar field S, results in a mass for the Z' and an extra heavy, CP-even Higgs state. Some features of the potential and masses of this neutral Higgs sector are discussed below. Including all Higgs bosons and singlets, there would be 9 CP-even states, h_i, 7 CP-odd states, A_i, and 5 charged states, $H_i^\pm$, in total.

9.4.1 Higgs potential

Assuming a universal soft parameter A_λ, providing all soft SUSY breaking terms $A_\lambda \lambda_{ijk} S_i H_{dj} H_{uk}$, the neutral Higgs potential is

$$\begin{aligned} V =& m^2_{H_{ui}} {H^0_{ui}}^2 + m^2_{H_{di}} {H^0_{di}}^2 + m^2_{S_i} {S_i}^2 - 2A_\lambda \lambda_{ijk} S_i H^0_{dj} H^0_{uk} \\ &+ \frac{g^2+g_y^2}{8}\left(\sum_i {H^0_{iu}}^2 - {H^0_{id}}^2\right)^2 + \frac{g'^2}{2}\left(\sum_i {H^0_{iu}}^2 Q_u + {H^0_{id}}^2 Q_d + S_i^2 Q_s\right)^2 \\ &+ \lambda_{ijk}\lambda_{ilm} H_{dj} H_{uk} H_{dl} H_{um} + \lambda_{ijk}\lambda_{ljm} S_i H_{uk} S_l H_{um} + \lambda_{ijk}\lambda_{lmk} S_i H_{dj} S_l H_{dm}, \end{aligned} \tag{9.7}$$

where $i = 1,2,3$ is the generation index. After inserting the VEVs $\langle H_{di}\rangle = \frac{v_d}{\sqrt{2}}\delta_{r3}$, $\langle H_{ui}\rangle = \frac{v_u}{\sqrt{2}}\delta_{3i}$ and $\langle S_i\rangle = \frac{s}{\sqrt{2}}\delta_{3i}$ one can apply the vacuum stability conditions for the first and second generation of scalars and find the six equations

$$0 = \frac{\partial V}{\partial S_\alpha} = -\lambda_{\alpha 33} A_\lambda v_d v_u + \lambda_{\alpha i3}\lambda_{3i3}\frac{s v_u^2}{\sqrt{2}} + \lambda_{\alpha 3i}\lambda_{33i}\frac{s v_d^2}{\sqrt{2}}, \tag{9.8}$$

$$0 = \frac{\partial V}{\partial H_{u\alpha}} = -\lambda_{33\alpha} A_\lambda s v_d + \lambda_{i3\alpha}\lambda_{i33}\frac{v_u v_d^2}{\sqrt{2}} + \lambda_{3i\alpha}\lambda_{3i3}\frac{v_u s^2}{\sqrt{2}}, \tag{9.9}$$

$$0 = \frac{\partial V}{\partial H_{d\alpha}} = -\lambda_{3\alpha 3} A_\lambda s v_u + \lambda_{i\alpha 3}\lambda_{i33}\frac{v_d v_u^2}{\sqrt{2}} + \lambda_{3\alpha i}\lambda_{33i}\frac{v_d s^2}{\sqrt{2}}. \tag{9.10}$$

These six equations could for example be used to express the six Z_2^H-breaking Yukawa couplings, $x_{d\alpha}$, $x_{u\alpha}$ and z_α, in terms of the other parameters. The equivalent equations for the third generation scalars are

$$\begin{aligned} 0 = \frac{\partial V}{\partial S} =& m_S^2 s\sqrt{2} + \frac{g_1'^2}{2}(Q_d v_d^2 + Q_u v_u^2 + Q_s s^2) Q_s s\sqrt{2} \\ &- \lambda_{333} A_\lambda v_d v_u + \lambda_{3i3}\lambda_{3i3}\frac{s v_u^2}{\sqrt{2}} + \lambda_{33i}\lambda_{33i}\frac{s v_d^2}{\sqrt{2}}, \end{aligned} \tag{9.11}$$

$$\begin{aligned} 0 = \frac{\partial V}{\partial H_u} =& m^2_{H_u} v_u\sqrt{2} + \frac{g_1'^2}{2}(Q_d v_d^2 + Q_u v_u^2 + Q_s s^2) Q_u v_u\sqrt{2} + \frac{\bar{g}^2}{8}(v_u^2 - v_d^2) v_u\sqrt{2} \\ &- \lambda_{333} A_\lambda s v_d + \lambda_{i33}\lambda_{i33}\frac{v_u v_d^2}{\sqrt{2}} + \lambda_{3i3}\lambda_{3i3}\frac{v_u s^2}{\sqrt{2}}, \end{aligned} \tag{9.12}$$

$$\begin{aligned} 0 = \frac{\partial V}{\partial H_d} =& m^2_{H_d} v_d\sqrt{2} + \frac{g_1'^2}{2}(Q_d v_d^2 + Q_u v_u^2 + Q_s s^2) Q_d v_d\sqrt{2} - \frac{\bar{g}^2}{8}(v_u^2 - v_d^2) v_d\sqrt{2} \\ &- \lambda_{333} A_\lambda s v_u + \lambda_{i33}\lambda_{i33}\frac{v_d v_u^2}{\sqrt{2}} + \lambda_{33i}\lambda_{33i}\frac{v_d s^2}{\sqrt{2}}. \end{aligned} \tag{9.13}$$

The Higgs mass matrix is given by second derivatives of the potential with respect to the different fields. After substituting the soft scalar masses using the tree-level vacuum stability conditions the third generation scalars have a mass matrix in the (v_d, v_u, s)-basis

with elements

$$\begin{aligned}
M_{11}^2 =& \frac{\lambda A_\lambda}{\sqrt{2}}\frac{v_u s}{v_d} + v_d^2\left(\frac{\bar{g}^2}{4} + g_1'^2 Q_d^2\right)\\
M_{12}^2 =& -\frac{\lambda A_\lambda}{\sqrt{2}}s + v_u v_d\left(-\frac{\bar{g}^2}{4} + g_1'^2 Q_u Q_d + \lambda^2 + \lambda_{233}^2 + \lambda_{133}^2\right)\\
M_{22}^2 =& \frac{\lambda A_\lambda}{\sqrt{2}}\frac{v_d s}{v_u} + v_u^2\left(\frac{\bar{g}^2}{4} + g_1'^2 Q_u^2\right)\\
M_{13}^2 =& -\frac{\lambda A_\lambda}{\sqrt{2}}v_u + s v_d\left(g_1'^2 Q_s Q_d + \lambda^2 + \lambda_{332}^2 + \lambda_{331}^2\right)\\
M_{23}^2 =& -\frac{\lambda A_\lambda}{\sqrt{2}}v_d + s v_u\left(g_1'^2 Q_s Q_u + \lambda^2 + \lambda_{323}^2 + \lambda_{313}^2\right)\\
M_{33}^2 =& \frac{\lambda A_\lambda}{\sqrt{2}}\frac{v_u v_d}{s} + s^2 g_1'^2 Q_s^2.
\end{aligned} \tag{9.14}$$

Neglecting the Z_2^H breaking Yukawa couplings and applying a rotation

$$\begin{pmatrix} \cos\beta & -\sin\beta & 0\\ \sin\beta & \cos\beta & 0\\ 0 & 0 & 1\end{pmatrix} \tag{9.15}$$

to the mass matrix, the $(v, 0, s)$-basis is chosen, in which the matrix elements are

$$\begin{aligned}
M_{11}'^2 =& \frac{\lambda^2}{2}v^2\sin^2 2\beta + \frac{\bar{g}^2}{4}v^2\cos^2 2\beta + g_1'^2 v^2(\tilde{Q}_1\cos^2\beta + \tilde{Q}_2\sin^2\beta)^2\\
M_{12}'^2 =& \left(\frac{\lambda^2}{4} - \frac{\bar{g}^2}{8}\right)v^2\sin 4\beta + \frac{g_1'^2}{2}v^2(\tilde{Q}_2 - \tilde{Q}_1)(\tilde{Q}_1\cos^2\beta + \tilde{Q}_2\sin^2\beta)\sin 2\beta\\
M_{22}'^2 =& \frac{\sqrt{2}\lambda A_\lambda}{\sin 2\beta}s + \left(\frac{\bar{g}^2}{4} - \frac{\lambda^2}{2}\right)v^2\sin^2 2\beta + \frac{g_1'^2}{4}(\tilde{Q}_2 - \tilde{Q}_1)^2 v^2\sin^2 2\beta\\
M_{13}'^2 =& -\frac{\lambda A_\lambda}{\sqrt{2}}v\sin 2\beta + \lambda^2 v s + g_1'^2(\tilde{Q}_1\cos^2\beta + \tilde{Q}_2\sin^2\beta)\tilde{Q}_S v s\\
M_{23}'^2 =& -\frac{\lambda A_\lambda}{\sqrt{2}}v\cos 2\beta + \frac{g_1'^2}{2}(\tilde{Q}_2 - \tilde{Q}_1)\tilde{Q}_S v s\sin 2\beta\\
M_{33}'^2 =& \frac{\lambda A_\lambda}{2\sqrt{2}s}v^2\sin 2\beta + g_1'^2\tilde{Q}_S^2 s^2
\end{aligned} \tag{9.16}$$

where the first diagonal element no longer contains the singlet VEV, s. Since $s \gg v$, and since the smallest eigenvalue of a Hermitian matrix is bounded from above by the smallest diagonal element, the tree-level lightest Higgs mass should satisfy

$$m_h^2 \leq \frac{\lambda^2}{2}v^2\sin^2 2\beta + \frac{\bar{g}^2}{4}v^2\cos^2 2\beta + g_1'^2 v^2(\tilde{Q}_1\cos^2\beta + \tilde{Q}_2\sin^2\beta)^2. \tag{9.17}$$

The terms contributing to this bound are the MSSM term, proportional to M_Z, the F-term proportional to λv and the D-term proportional to $g_1' v$. Since the tree-level bound on the Higgs mass is increased above the MSSM bound M_Z by two terms it is in general easier to acquire a larger Higgs mass in the E_6SSM.

9.5 The neutralino and chargino sector

In the MSSM [183] there are four neutralino interaction states, the neutral wino, the bino, and the two neutral Higgsinos. In the E$_6$SSM the neutralino sector is extended to include 8 additional states. There are four extra higgsinos, $\tilde{H}_u^\alpha$, $\tilde{H}_d^\alpha$, from the inert neutral Higgs bosons and one singlino, $\tilde{S}$, for each generation and finally a bino$'$ from the extra gauge boson. All the twelve neutralino interaction states are then taken into account in the column vector

$$\tilde{\chi}^0_{\rm int} = (\ \tilde{B}\ \ \tilde{W}^3\ \ \tilde{H}^0_d\ \ \tilde{H}^0_u \,\big|\, \tilde{S}\ \ \tilde{B}' \,\big|\, \tilde{H}^0_{d2}\ \ \tilde{H}^0_{u2}\ \ \tilde{S}_2 \,\big|\, \tilde{H}^0_{d1}\ \ \tilde{H}^0_{u1}\ \ \tilde{S}_1\ )^{\rm T}. \tag{9.18}$$

The first four states are the MSSM interaction states, $\tilde{S}$ is the third generation singlino and $\tilde{B}'$ is the new gaugino. The remaining six states are the extra inert doublet Higgsinos and Higgs singlinos that come with the full E$_6$SSM. Under the assumption that only the third generation Higgs doublets and singlet acquire VEVs the full Majorana mass matrix is then [184]

$$M^n_{\rm E_6SSM} = \begin{pmatrix} M^n_{\rm USSM} & B_2 & B_1 \\ B_2^{\rm T} & A_{22} & A_{21} \\ B_1^{\rm T} & A_{21}^{\rm T} & A_{11} \end{pmatrix}, \tag{9.19}$$

where the sub-matrix containing the mixings of states from the third generation and gauginos is

$$M^n_{\rm USSM} = \left(\begin{array}{cccc|cc} M_1 & 0 & -m_Z s_W c_\beta & m_Z s_W s_\beta & 0 & 0 \\ 0 & M_2 & m_Z c_W c_\beta & -m_Z c_W s_\beta & 0 & 0 \\ -m_Z s_W c_\beta & m_Z c_W c_\beta & 0 & -\mu & -\mu_s s_\beta & g'_1 v c_\beta Q^N_d \\ m_Z s_W s_\beta & -m_Z c_W s_\beta & -\mu & 0 & -\mu_s c_\beta & g'_1 v s_\beta Q^N_u \\ \hline 0 & 0 & -\mu_s s_\beta & -\mu_s c_\beta & 0 & g'_1 s Q^N_s \\ 0 & 0 & g'_1 v c_\beta Q^N_d & g'_1 v s_\beta Q^N_u & g'_1 s Q^N_s & M'_1 \end{array}\right), \tag{9.20}$$

where M_1, M_2, and M'_1 are the soft gaugino masses and $\mu_s = \lambda v/\sqrt{2}$. The variables $s_{\beta(W)}$ and $c_{\beta(W)}$ stand for sin and cos of β(the weak mixing angle θ_W) and $Q^N_{(d,u,S)}$ are the (H_d, H_u, S) $U(1)_N$ charges $(-3, -2, 5)/\sqrt{40}$. The sub-matrices in (9.19) involving only the inert interaction states are given by

$$A_{\alpha\beta} = A^{\rm T}_{\beta\alpha} = -\frac{1}{\sqrt{2}} \begin{pmatrix} 0 & \lambda_{\alpha\beta} s & f_{u\beta\alpha} v \sin\beta \\ \lambda_{\beta\alpha} s & 0 & f_{d\beta\alpha} v \cos\beta \\ f_{u\alpha\beta} v \sin\beta & f_{d\alpha\beta} v \cos\beta & 0 \end{pmatrix} \tag{9.21}$$

and the Z_2^H breaking sub-matrices are given by

$$B_\alpha = -\frac{1}{\sqrt{2}} \begin{pmatrix} 0 & 0 & 0 \\ 0 & 0 & 0 \\ 0 & x_{d\alpha} s & z_\alpha v \sin\beta \\ x_{u\alpha} s & 0 & z_\alpha v \cos\beta \\ x_{u\alpha} v \sin\beta & x_{d\alpha} v \cos\beta & 0 \\ 0 & 0 & 0 \end{pmatrix} \tag{9.22}$$

and involve the small Z_2^H violating Yukawa couplings that were neglected in (9.3), $x_{u\alpha}$, $x_{d\alpha}$, and z_α. Since these coupling are small, the six states of the inert neutralino sector is only weakly coupled to the six first states of (9.18), and may be considered separately from them to good approximation. In the limit of exact Z_2^H symmetry the neutralino sector is that of the USSM [185], a model similar to the NMSSM, but where the $U(1)$, introduced by adding the singlet field S, is gauged instead of reduced to a Z_3 However we emphasise that the Z_2^H violating couplings are essential in order for the lightest neutralino from the USSM sector to be able to decay into inert neutralinos and that these couplings are not expected to be zero. Exact Z_2^H would also render exotic D and $\overline{D}$ states stable.

Similarly, we take our basis of chargino interaction states to be

$$\tilde{\chi}^{\pm}_{\rm int} = \begin{pmatrix} \tilde{\chi}^{+}_{\rm int} \\ \tilde{\chi}^{-}_{\rm int} \end{pmatrix},$$

where

$$\tilde{\chi}^{+}_{\rm int} = \begin{pmatrix} \tilde{W}^{+} \\ \tilde{H}^{+}_{u} \\ \tilde{H}^{+}_{u2} \\ \tilde{H}^{+}_{u1} \end{pmatrix} \quad \text{and} \quad \tilde{\chi}^{-}_{\rm int} = \begin{pmatrix} \tilde{W}^{-} \\ \tilde{H}^{-}_{d} \\ \tilde{H}^{-}_{d2} \\ \tilde{H}^{-}_{d1} \end{pmatrix}. \tag{9.23}$$

The corresponding mass matrix is then

$$M^{c}_{\rm E_6SSM} = \begin{pmatrix} & C^{\rm T} \\ C & \end{pmatrix},$$

where

$$C = \begin{pmatrix} M_2 & \sqrt{2} m_W \sin\beta & 0 & 0 \\ \sqrt{2} m_W \cos\beta & \mu & \frac{1}{\sqrt{2}} x_{d2} s & \frac{1}{\sqrt{2}} x_{d1} s \\ 0 & \frac{1}{\sqrt{2}} x_{u2} s & \frac{1}{\sqrt{2}} \lambda_{22} s & \frac{1}{\sqrt{2}} \lambda_{21} s \\ 0 & \frac{1}{\sqrt{2}} x_{u1} s & \frac{1}{\sqrt{2}} \lambda_{12} s & \frac{1}{\sqrt{2}} \lambda_{11} s \end{pmatrix}. \tag{9.24}$$

It is clear that a generic feature of the E_6SSM is that the LSP is usually (naturally) composed mainly of inert singlino and ends up being typically very light. One can see this by inspecting the new sector blocks of the extended neutralino mass matrix in

(9.19), such as A_{11}, and assuming a hierarchy of the form $\lambda_{\alpha\beta}s \gg f_{u\alpha\beta}v, f_{d\alpha\beta}v$. This is a natural assumption since we already require that $s \gg v$ in order to satisfy the current experimental limit on the Z' mass of around 2.5 TeV, as discussed below and for example in Ref. [186].

We emphasise again that for both the neutralinos and the charginos we see that if the Z_2^H breaking couplings are exactly zero then the new part of the E$_6$SSM neutralino mass matrix becomes decoupled from the USSM mass matrix. However, although approximate decoupling is expected, exact decoupling is not, and will therefore not be considered.

9.6 The software implementation of the E$_6$SSM

To scan parameter spaces of models and generate Monte Carlo (MC) events the models have to be transferred from paper to computer. There are various ways of doing this. Some principles and tools for this processes will be discussed in Section 5.2. Many implementations of the MSSM have already been created, but for the E$_6$SSM there are no available sources. We have chosen to use the software package `LanHEP` [187] to calculate the Feynman rules for the E$_6$SSM. `LanHEP` finds the interactions and mass mixings between the particle states in the model and writes an output which can be read by a Feynman diagram calculator or Monte Carlo event generator.

In the `LanHEP` implementation of the model the particle content and Lagrangian is specified. We have used a slightly stripped down version of the E$_6$SSM, suitable for our purposes, which is called `E6SSM-12.02` [188] and which now has an updated version `E6SSM-13.04` [189]. What is not included from the three families of 27 representations of the E_6 group in this implementation are the exotic coloured states [1], their superpartners, and the inert Higgs doublets and SM-singlets from the two first families. However, one should note that we are including the superpartners of these inert Higgs and singlet states which, as described in Section 9.5, extends the neutralino and chargino sectors. The diagonalisation of large mass matrices appearing in the model, e.g. the 12×12 neutralino mass matrix, is performed with routines available from the `SLHAplus` [190] package which is well integrated with `LanHEP` and the matrix element calculator and event generator `CalcHEP` [69].

The Z_2^H violating Yukawa couplings, x_u, x_d, and z, connecting the inert neutralino sector with the USSM sector, have been included in the `LanHEP` model. Turning on these couplings causes the neutralino mass matrix to leave its block-diagonal form and acquire non-zero off-block-diagonal elements. The model is parameterised such that the dimensionless input parameters of the model are the Yukawa couplings λ_{ijk} from the SH_uH_d-terms in the superpotential, the ratio of the Higgs doublet VEVs, $\tan\beta$, and the

[1] These can be diquarks or leptoquarks depending on the model definition.

gauge couplings. Dimensionful input parameters of the model are the third generation soft trilinear scalar A-couplings, the soft masses of the squarks and sleptons, and the soft gaugino masses at the electroweak scale. One should note that we use the notation of the physical gluino mass, $m_{\tilde{g}}$ (`MGo`) instead of M_3. The soft trilinear coupling A_λ associated with the SH_uH_d-term is exchanged for the pseudo-scalar Higgs mass M_A.

The details and notations of the `CalcHEP` model `E6SSM-12.02` described above can be found in Appendix B and the model files are accessible from the High Energy Physics Model DataBase (HEPMDB)[78].

Chapter 10

Discovering E_6 SUSY models in gluino cascade decays at the LHC

In the previous chapter we discussed methods of measuring the mass and width of a pseudoscalar Higgs boson which could lead to determination of $\tan\beta$ and subsequently distinguish scenarios within the MSSM. In this chapter we go beyond the MSSM and study gluino production and decay within the non-minmal SUSY model E_6SSM, which is expected to be the main discovery channel for this model. We aim to quantify the difference between this model and the MSSM in this particular process. In fact the analysis also applies to a larger class of E_6 models in which the matter content of three 27 representations of E_6 survives to the TeV scale. We study the E_6SSM as a concrete example and at the same time demonstrate the use of the `E6SSM-12.02 CalcHEP` model that we have now made publicly available on HEPMDB. After extensive scans over the parameter space we create a number of representative benchmarks for different E_6SSM scenarios, considering Z' and Higgs boson physics, the LSP dark matter relic density and direct detection cross-section, and the perturbativity of dimensionless couplings. We then analyse representative MSSM and E_6SSM benchmarks consistent with the recently discovered Higgs boson at the LHC.

This chapter also illustrates the model dependence of limits on SUSY particles. For example, searches at ATLAS [191, 192] and CMS [9, 10], under certain assumptions, constrain the gluino mass to be greater than about 900 – 1300 TeV. This mass limit range reflects the fact that the precise limit depends crucially on the assumptions one makes about the rest of the SUSY spectrum, in particular the mass spectrum of the squarks, charginos, and neutralinos. As we emphasise in this chapter, mass limits and the LHC discovery potential also depend on the particular SUSY model under consideration and the quoted mass limits strictly only apply to the constrained MSSM or simplified models of SUSY[193] with very few particles. In other, well motivated, non-minimal SUSY extensions of the SM, such as those discussed in Chapter 9 and below, the enriched

particle content alters the SUSY discovery potential at the LHC and this should be taken into account in phenomenological and experimental studies.

The focus on gluinos in this analysis is motivated by the fact that these particles are the expected to be the lightest strongly interacting particles in E_6 models [194], so one should expect them to have the largest production rate. In particular, we are interested in gluino cascade decays which not only provide observable signatures, but are also important for distinguishing the E_6 inspired models from the MSSM. As we shall see, there are important differences between the two cases, which can affect the respective search strategies. The differences arise because of the extra Higgsino and singlino states predicted to be part of the E_6 matter content, as above. In particular, in the E_6 inspired models, relative to the MSSM, there are two extra families of Higgsinos, $\tilde{H}_u^\alpha$ and $\tilde{H}_d^\alpha$, together with two extra singlinos, $\tilde{S}^\alpha$, where $\alpha = 1, 2$ [1]. There is also a third singlino, $\tilde{S}^3$, similar to the NMSSM singlino, which mixes with the bino$'$, both states having a large mass of order the effective μ parameter. The remaining extra Higgsinos and singlinos may be lighter than the gluino. Indeed, it is possible to show that at least two linear combinations of the states $\tilde{H}_u^\alpha$, $\tilde{H}_d^\alpha$, $\tilde{S}^\alpha$ must be lighter than or of order $M_Z/2$. If these states mix with the usual neutralinos of the MSSM or NMSSM then the LSP will inevitably be one of these states, leading to longer decay chains. For example, in regions of MSSM parameter space where the bino is the LSP the gluino typically undergoes a cascade decay to the bino. In the E_6 inspired models the bino will mix with the extra Higgsinos and singlinos and the predominantly bino state will subsequently decay into some lighter state having a mass of order $M_Z/2$, thereby typically giving a longer gluino cascade decay chain and producing less missing energy due to the lighter mass of the LSP [2]. For simplicity we shall assume that the D and $\overline{D}$ states, as well as the NMSSM type singlino $\tilde{S}^3$, are all heavier than the gluino and so are irrelevant for gluino cascade decays. Similarly we shall also assume all squarks and sleptons and Higgs scalars and pseudoscalars (with the exception of the SM-like Higgs boson) to be heavier than the gluino. These assumptions are motivated by the parameter space of the constrained E_6 inspired models [194, 195, 196].

The main result of our analysis is that in E_6 inspired models the gluino decays into the LSP with longer chains which involve more jets and leptons and less missing energy than in the MSSM. This happens because the would-be LSP (e.g. an MSSM-like bino dominated neutralino) undergoes further decays to the extra light neutralinos and charginos predicted by the E_6 inspired models. As a result, the characteristics of the signal, such as lepton and jet multiplicity, missing transverse momentum, effective mass, etc., are altered in the E$_6$SSM as compared to the MSSM case even after the matching of the

[1] Note that the first and second family of Higgs doublet and singlet fields H_u^α, H_d^α, and S^α predicted by the E$_6$SSM do not develop VEVs and are called "inert".

[2] The decay to bino is expected to happen before the subsequent decay into a lighter state since these lighter states are expected to have small mixing to the MSSM-like sector, for reasons explained in section II.

gaugino masses in both models. Therefore, the search strategies designed for the MSSM need to be modified for the E$_6$SSM case, while one should stress that the gluino mass limits for the MSSM are not applicable to the E$_6$SSM gluinos.

The layout of the remainder of this chapter is as follows: In Section 10.1 the theoretical and experimental constraints of the E$_6$SSM, not relating to gluino detection, are discussed. We also present the results of parameter scans and discuss the viable parameter space, before going on to introduce a set of benchmark points, including those which form the basis of our analysis. The analysis of the different signatures and search prospects for different strategies for each model are presented in Section 10.2. The conclusions are in Section 10.3.

10.1 Model Setup and Parameter Space

Before going on to consider the prospects for the production and detection of gluinos, which are the main focus of this chapter, discussed in Section 10.2, we must first determine the limits on the E$_6$SSM from other experimental, and cosmological, considerations. We discuss experimental constraints relating to Z' and Higgs boson physics and to exotic coloured particles in Section 10.1.1 before going on to discuss dark matter considerations in Section 10.1.2. In light of these discussions we then show the results of some parameter space scans in Section 10.1.3 and produce a set of benchmark points in Section 10.1.4. These benchmarks example various viable scenarios for the E$_6$SSM and we explain their features and issues. Although the benchmarks presented look very different from each other from many points of view, it turns out that they look very similar in terms of their gluino decay signatures. In Section 10.2 we therefore mostly show results for two particular benchmarks that demonstrate the qualitative differences between the MSSM and E_6 models for gluino searches.

In this study Higgs – Singlet superfield couplings, appearing in the first line of (9.3), will be of great importance. These are the couplings of the form $S^i H_d^j H_u^k$, where $i, j, k = 1, 2, 3$ label the three families of Higgs doublet and singlet superfields predicted in the E$_6$SSM. In particular we shall be concerned with the resulting chargino and neutralino mass terms coming from such couplings involving one third-family scalar component and two fermion components, i.e. $S\tilde{H}_d^j \tilde{H}_u^k$, $\tilde{S}^i H_d \tilde{H}_u^k$, and $\tilde{S}^i \tilde{H}_d^j H_u$. In the E$_6$SSM the presence of the extra Higgsinos and singlinos $\tilde{H}_u^\alpha$, $\tilde{H}_d^\alpha$, and $\tilde{S}^\alpha$ means that the chargino and neutralino mass matrices are extended, as was discussed in Section 9.5.

We shall assume that the κ_i are sufficiently large that the exotic $D_i, \overline{D}_i$ states are much heavier than the gluino and so will play no role in gluino decays. Similarly the right-handed neutrinos N_i will be neglected since they are assumed to be very heavy.

10.1.1 Experimental constraints

The most recent limit on the $U(1)_N$ Z' mass, set by the CMS [197], searching for dilepton resonances, is $m_{Z'} \gtrsim 2600$ GeV at a confidence level of 95%. Although the limit on the mass of the Z' boson associated with the extra $U(1)_N$ of the E$_6$SSM can be inferred from this analysis, this analysis neglects any other matter beyond that of the SM. When decays of the Z' boson into inert neutralinos (inert Higgsino and singlino dominated mass eigenstates) are considered the Z' width tends to increase by a factor of about 2 (see for example Ref. [196], although we confirm the result in our analysis). This then means that the branching ratio into leptons is decreased by a factor of about 2. Estimating the effect of halving this expected branching ratio on the analysis in Ref. [197] one can read off a 95% confidence level lower bound of around 2400 GeV. This implies $s \gtrsim 6600$ GeV.

When the singlet VEV is this large, as required by experiments, the Higgs boson spectrum typically becomes rather hierarchical with a lightest mass eigenstate that participates in interactions as a SM-like Higgs boson and much heavier Higgs boson states that are approximately decoupled. Indeed the Higgs candidate recently discovered at the LHC can easily be accommodated in the E$_6$SSM [198]. Although in the MSSM large loop corrections are required in order for this limit to be satisfied, in the E$_6$SSM this is easier to achieve since there are extra contributions to the SM-like Higgs mass at tree-level due to $U(1)_N$ D-terms.

If the exotic diquarks (or leptoquarks) are light enough they would produce spectacular signatures at the LHC and these exotic states already have strong limits on their masses. The E_6 diquarks are excluded for masses below 3.5 TeV [199]. Since these particles' masses must be so large they do not play a role in gluino cascade decays and are excluded from our analysis.

10.1.2 Dark matter considerations

Stringent constraints on the E$_6$SSM inert parameter space come from considerations relating to dark matter. In the E$_6$SSM as described thus far the LSP is typically one of the two necessarily light states from the inert neutralino sector. As such this inert neutralino LSP becomes a dark matter candidate. The E$_6$SSM has been previously studied as a model attempting to explain the observed amount of thermal relic cold dark matter [184, 200]. Unfortunately this dark matter scenario is now severely challenged by the most recent XENON100 dark matter direct detection limits [16]. The reason is essentially as outlined in the following paragraph and a more detailed analysis can be found in Ref. [200].

In the E$_6$SSM the LSP is generically singlino dominated, a situation which arises from the extended neutralino mass matrix in (9.19) under the condition $s \gg v$. One can show

that [184, 200] if there is no hierarchy in the Yukawa couplings then the LSP would not annihilate very efficiently at the time of thermal freeze-out and would therefore lead to an unacceptable overabundance of dark matter in the Universe. On the other hand, by allowing the largest $f_{d\alpha\beta}$ and $f_{u\alpha\beta}$ couplings to be significantly larger than the largest $\lambda_{\alpha\beta}$ couplings and $\tan\beta$ to be less than about 2 the observed amount of dark matter can be predicted. In this case the LSP is heavier and, although still inert singlino dominated, has substantial inert Higgsino admixtures and can annihilate efficiently enough in the early universe via an s-channel Z boson. The largest $\lambda_{\alpha\beta}$ coupling cannot be too small, otherwise the inert charginos would be too light to have so far escaped detection. At the same time the largest $f_{d\alpha\beta}$ and $f_{u\alpha\beta}$ couplings cannot be too large if it is required that perturbation theory remains valid up to the GUT scale. This being the case, the LSP and the NLSP cannot be made much larger than about 60 GeV [200]. In this dark matter scenario there should be some suppression of the coupling of the LSP to the Z boson, by partial cancellation between the up-type and down-type inert Higgsino components, in order to be consistent with the precision measurement of the invisible Z boson width from LEP, if the LSP mass is below half of the Z mass. For given Yukawa couplings increasing $\tan\beta$ has the effect of both suppressing the LSP mass and increasing the coupling to the Z boson, lessening this cancellation. Although this partial cancellation can occur in the coupling of the LSP to the Z boson, the coupling of the LSP to the SM-like Higgs boson is necessarily large if the LSP is to produce the observed amount of dark matter (due to its inert Higgsino admixtures). This in turn means a large spin-independent direct detection cross-section, larger than is now consistent with experiment. However, if the relic abundance is less than the observed value, then the direct detection constraint can be avoided, and that is the strategy that we follow for benchmark points of this kind, as we now discuss in more detail.

It is important to note that for both the MSSM and the standard E$_6$SSM we analyse points where less than the observed amount of dark matter is predicted and assume that the majority of dark matter is not made up of MSSM/E$_6$SSM neutralinos. This choice of the parameter space is actually dictated by limits from direct detection experiments: if less than the total amount of the dark matter in the universe is made up of LSPs, then the expected number of events for a direct detection experiment for a given LSP direct detection cross-section will be correspondingly smaller. In the E$_6$SSM such points require the previously discussed hierarchy of Yukawa couplings appearing in the inert block of the neutralino mass matrix and in this case if the LSP mass is below half of the Z mass then $\tan\beta$ still cannot be too large in order for the LSP not to contribute too much to the invisible width of the Z boson, as measured at LEP. Large values of $\tan\beta$ mean that the up-type inert Higgsino admixture in the LSP greatly outweighs the down-type inert Higgsino admixture, necessarily leading to a too large coupling to the Z boson.

Alternatively, in a variation of the model known as the EZSSM [201] the situation is

quite different and the model may be responsible for all dark matter and consistent with all experiment. Here an extra discrete symmetry Z_2^S is imposed that forbids the terms in the superpotential involving the inert singlet superfields, i.e. the $f_{u\alpha\beta}$ and $f_{d\alpha\beta}$ and Z_2^H violating $x_{u\alpha}$ and $x_{d\alpha}$ Yukawa couplings are forced to be zero. This then means that the inert singlinos are exactly massless and decoupled from the rest of the neutralinos. In this variation of the model the lightest non-inert-singlino LSP is absolutely stable. If this stable particle is the bino and there are a pair of inert Higgsinos close by in mass then the bino can be responsible for all of dark matter [201]. The massless inert singlinos themselves slightly increase the expansion rate of the universe prior to nucleosysnthesis in agreement with observation of the ^{4}He relic abundance and in this scenario there would currently be a cosmic inert singlino background slightly colder than the cosmic neutrino background. The singlinos contribute a small amount to the effective number of neutrino species but are consistent with the measured $N_{\rm eff}$ [201]. The phenomenology of this scenario as regards the gluino cascade decay is essentially identical to MSSM one and we do not make of point of trying to distinguish this type of scenario from the MSSM in this study.

Finally we shall consider a scenario where the two lightest (predominantly inert singlino) neutralinos are both very light, with one around a GeV, and one much lighter, in principle in the keV range. In this case, interesting phenomenology can emerge in the gluino cascade decays as in the usual case where the lightest neutralino states are around half the Z mass. However, unlike that case, the lightest neutralino is not subject to direct detection limits. Moreover, it is possible to arrange for the correct relic abundance in such a scenario, where the lightest neutralino in the keV mass range is stable and constitutes Warm Dark Matter (WDM) [202]. The idea is that both the light neutralinos are thermally produced in the early Universe due to their couplings to the Z and Z' gauge bosons, but the GeV state decays late (due to its weak couplings) after both of the neutralinos have gone out of thermal equilibrium, and reheats the Early Universe, effectively diluting the number density of the stable keV neutralinos, such that they are responsible for the observed relic abundance. It is very interesting to compare the gluino cascade decays in this case to that where the lightest neutralinos are around half the Z mass, in order to provide an experimental "confirmation" of keV dark matter at the LHC.

10.1.3 Parameter space under study

In this study we consider a pattern of low energy soft gaugino masses that is consistent with E_6 grand unification [179]. This typically implies that at the EWSB scale $M_2 \approx 2M_1$ and if $M_1 = 150$ GeV the physical gluino mass is around 800 GeV. In order to have a direct comparison, M_1 is made equal in both the MSSM and E$_6$SSM, 150 GeV in the following analysis. For large μ in the MSSM, and given that the effective μ in the

E_6SSM is large due to the limit on s coming from the limit on the Z' mass, there will be a neutralino that is almost the bino with a mass very close to M_1. For lower values of μ in the MSSM bino-Higgsino mixing occurs. We fix the physical gluino mass to be equal in the two models and then consider various scenarios where we independently change the gluino mass to values in the range 700 GeV to 1500 GeV.

We also consider large squark masses, with all squarks heavier than the gluino. This is motivated by the GUT constrained E_6SSM, where such large squark masses are a feature, although it should be noted that although the EZSSM scenario is consistent with such GUT constraints it has not been shown that a GUT constrained standard E_6SSM scenario consistent with dark matter observations exists. Nonetheless we assume heavy squarks for all scenarios.

In Figure 10.1 we present the results of scans over the MSSM and the E_6SSM parameter space in the $(\Omega_\chi h^2, \sigma_{\rm SI})$ plane. The parameter space scanned over is shown in Table 10.1 and Table 10.2 and points are linearly distributed over these ranges. The ranges chosen are motivated from the discussions in the previous two subsections. For both the MSSM and E_6SSM the points are shown as long as they are consistent with the LEP limit on the SM-like Higgs boson mass, applicable even if the Higgs has large invisible branching fractions, but we also highlight benchmark points that are consistent with the particle recently discovered at the LHC being the SM-like lightest Higgs boson. For the E_6SSM, where the LSP mass may be less than half of the Z mass, points are only shown if they are consistent with LEP limits on the invisible Z width, contributing less than 1-sigma. For both scans squark soft masses are set to 2 TeV, although the effects of squark mixing on the mass eigenstates are included. The physical gluino mass is set to 800 GeV and the $U(1)_Y$ gaugino mass is set to 150 GeV in both cases. We do not consider scenarios in which any squarks are less massive than the gluino.

We define the length of a gluino decay chain to be the number of decays after the virtual squark as in Figure 10.2. We then also define an effective chain length for each point in parameter space

$$l_{\rm eff} = \sum_l l \cdot P(l), \tag{10.1}$$

where $P(l)$ is the probability of having a decay chain of length l for that point. Intervals of effective chain length are colour/shape coded in Figure 10.1. These scans indicate that in the E_6SSM these decay chains are typically longer due to the bino decaying into the lower mass inert states. The distribution of effective chain lengths for these scans are also plotted in Figure 10.3(a).

In the MSSM, for the parameters chosen, the typical decay length is 2, with the lightest chargino being initially produced from the virtual squark decay before subsequently itself decaying to the bino LSP. When the magnitude of μ is small the mixing between the gauginos (bino and wino) and the Higgsinos increases and the entire neutralino and

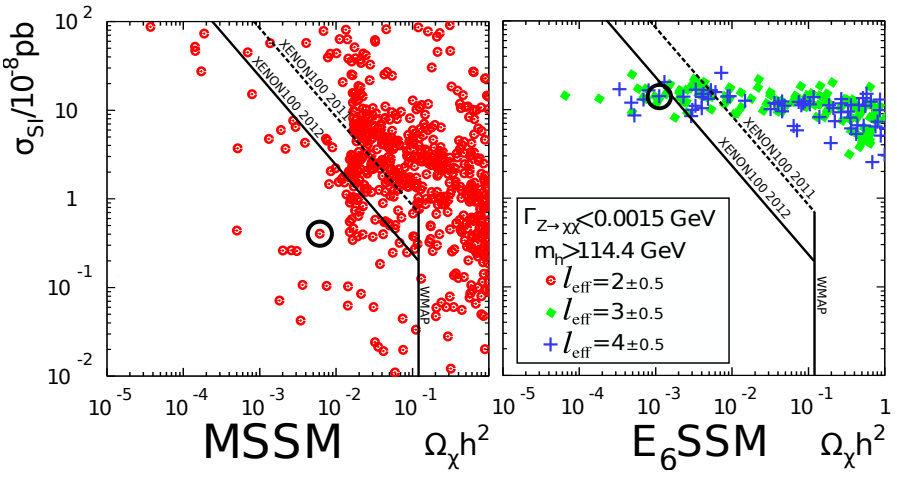

Figure 10.1: The scanned regions of the parameter spaces projected onto the plane spanned by the spin-independent cross-section, σ_{SI}, and the relic density of the LSP, $\Omega_{\tilde{\chi}_1^0}h^2$, calculated with MicrOMEGAs [14]. The area right of the vertical solid line is excluded by WMAP [15] and the area above the diagonal line is excluded by XENON100, where the LSP direct detection cross-section exclusion gets weighted by its relic density. The 90% confidence level limit on the spin-independent LSP-nucleon cross section for a weakly interacting LSP with mass around 50 GeV and which makes up all of the observed amount of DM has been pushed down from $0.7 \times 10^{-44}\text{cm}^2 = 0.7 \times 10^{-8}\text{pb}$ in 2011 [16] to $0.2 \times 10^{-44}\text{cm}^2 = 0.2 \times 10^{-8}\text{pb}$ in 2012 [6]. The LEP constraints on chargino masses ($m_{\tilde{\chi}_1^\pm} > 103$ GeV) and invisble Z width ($\Gamma(Z \to \tilde{\chi}^0\tilde{\chi}^0) < 1.5$ MeV) have been applied. The constraint on the Higgs mass is also taken from LEP since it holds for invisible Higgs decays, a common feature among the E$_6$SSM points. The colours/shapes represent the effective gluino decay chain length $l_{\text{eff}} = \sum_l l \cdot P(l)$ for each point, where $P(l)$ is the probability for a chain length of l, as defined in Figure 10.2. The benchmarks entitled MSSM and E$_6$SSM-I, which are consistent with the particle recently discovered at the LHC being the SM-like lightest Higgs boson, are encircled.

chargino spectrum is pushed down. Specifically the heavier neutralinos and chargino are brought down below the gluino mass causing extra steps in the gluino decay chain.

In the E$_6$SSM the effective decay length is typically either 3 or 4. Initially an either charged or neutral wino is produced and this subsequently decays to the bino. The bino then decays into either of the two light inert neutralinos that are the LSP and NLSP. Which of these the bino preferentially decays into depends on the values of the Z_2^H violating couplings in blocks B_α in the neutralino mass matrix in (9.19). Therefore in the E$_6$SSM we typically expect the gluino cascade decays to be either one or two steps longer than in the MSSM.

parameter	min	max	
$\tan\beta$	2	60	
$A_t = A_b = A_\tau = A_\mu$	-3	3	
M_A	0.1	2	[TeV]
μ	-2	2	

Table 10.1: The MSSM scanning region. A common squark and slepton mass scale was fixed to $M_S = 2$ TeV. The gaugino masses were fixed to $M_1 = 150$ GeV, $M_2 = 285$ GeV, and $M_3 = 619$ GeV, providing a gluino mass close to 800 GeV.

parameter	min	max	
$\tan\beta$	1.4	2	
$\lvert\lambda\rvert$	0.3	0.7	
λ_{22}	0.0001	0.01	
λ_{21}	0.01	0.1	
λ_{12}	0.01	0.1	
λ_{11}	0.0001	0.01	
f_{d21}	0.0001	0.01	
f_{d21}	0.1	1	
f_{d12}	0.1	1	
f_{d11}	0.0001	0.01	
f_{u22}	0.0001	0.01	
f_{u21}	0.1	1	
f_{u12}	0.1	1	
f_{u11}	0.0001	0.01	
x_{d2}	10^{-4}	10^{-2}	
x_{d1}	10^{-4}	10^{-2}	
x_{u2}	10^{-4}	10^{-2}	
x_{u1}	10^{-4}	10^{-2}	
z_1	10^{-3}	10^{-1}	
z_2	10^{-3}	10^{-1}	
$A_t = A_b = A_\tau$	-3	3	
M_A	1	5	[TeV]
s	3.7	8	

Table 10.2: The E_6SSM scanning region. A common squark and slepton mass scale was fixed to $M_S = 2$ TeV. The gaugino masses were fixed to $M_1 = 150$ GeV, $M_1' = 150$ GeV, $M_2 = 300$ GeV, and $M_{\tilde{g}} = 800$ GeV.

10.1.4 Benchmarks

Below follow descriptions of the main features of the chosen benchmarks. The details of their spectrum and parameter values are given in Table 10.3. In the table the benchmarks are defined with a gluino mass of 800 GeV but we consider also analogous benchmarks, independently varying the gluino masses between 700 GeV and 1500 GeV, leaving other parameters fixed. The diagrams for the main decay channels of the gluinos are shown in Figure 10.4 for the two main benchmarks, MSSM and E_6SSM-I, discussed below. The branching ratios for production of particles are denoted in brackets. The decay chains for both benchmarks are essentially the same up to the first two steps, with just a slight difference in branching ratios. The essential difference is that, in the case of the E_6SSM, the lightest MSSM-like neutralino is no longer stable and decays in two steps to the lightest E_6SSM neutralino. About 20% of the gluino decays go directly

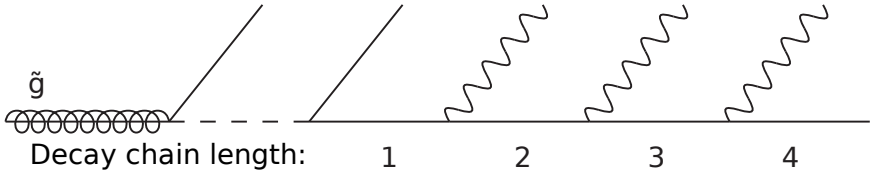

Figure 10.2: In the first step in a gluino decay chain the gluino decays into a quark and a squark (in our scenario it will be a virtual squark) which in turn decays into a second quark and a neutralino or chargino. This is the shortest possible gluino decay chain, which we define as having length $l = 1$. The neutralino or chargino can then decay into lighter neutralinos or charginos by radiating W, Z, or Higgs bosons, which typically decay into pairs of fermions. For each such decay the decay chain length is taken to increase by one. The radiated bosons could be on-shell or off-shell depending on the mass spectrum of the model. Light squarks or leptons could appear further along in the decay chain, leading to radiation of SM fermions without intermediate W, Z, or Higgs bosons, but in our study squarks and sleptons are heavy so this is not relevant.

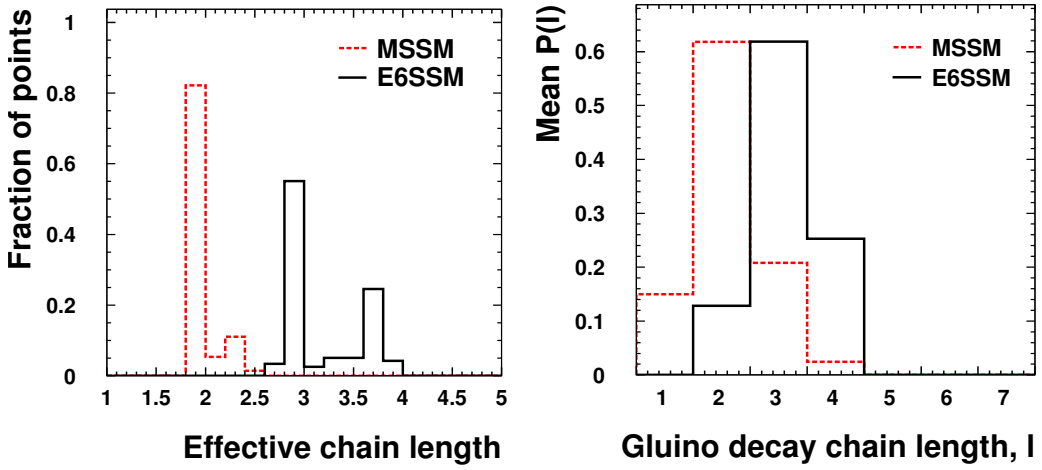

(a) The distribution of the effective chain length, $l_{\text{eff}} = \sum_l l \cdot P(l)$, where $P(l)$ is the probability of length, averaged over all points in the parameter scan, satisfying dark matter and collider constraints.

(b) The probability for a certain gluino decay chain having a decay chain of length l for a point in parameter space.

Figure 10.3: Statistical properties of the gluino decay chain length in the scanned parameter space. Figure 10.3(a) shows how the effective gluino decay chain length evaluated at each point is distributed over the scanned parameter space. Most points have an effective decay chain length close to an integer indicating that there usually is a largely dominant decay chain length. The two peaks just below 3 and 4 clearly show how the E_6SSM generally introduces one or two extra steps in the chain. Figure 10.3(b) show the average probabilities of different gluino decay chain lengths for both models' parameter spaces. Again, the E_6SSM is shown to shift the probabilities to longer decay chain lengths.

into the lightest MSSM-like neutralino implying a chain length $l = 1$ for the MSSM and $l = 3$ for the E_6SSM. On the other hand, about 80% of the gluino decays are into a heavier neutralino or chargino, which subsequently decays into the lightest MSSM-like neutralino state giving the MSSM a chain length $l = 2$ and the E_6SSM $l = 4$. More

complete diagrams showing how the gluinos decay for the different benchmarks (below) are shown in Figure A.1 in Appendix A.

MSSM:

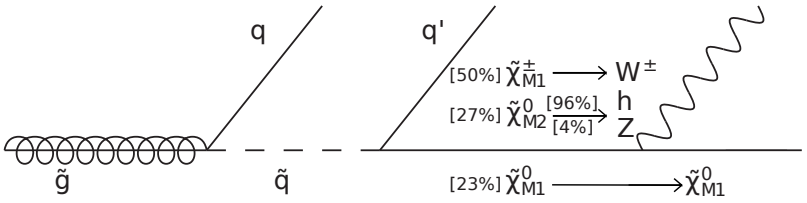

E_6SSM-I:

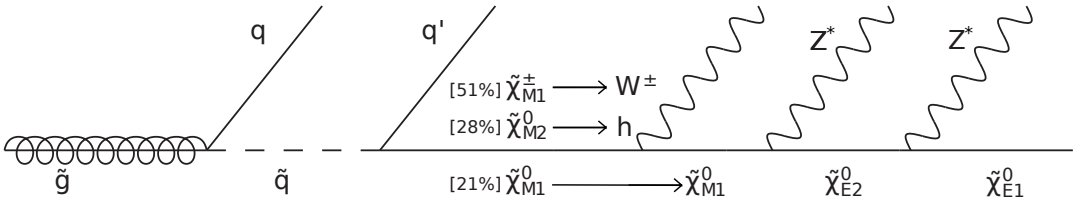

Figure 10.4: Feynman diagrams for the leading gluino decay chains for our two main benchmarks, MSSM and E_6SSM-I. The branching ratios for production of particles are denoted in brackets. The decay chains for both benchmarks are essentially the same up to the first two steps, with just a slight difference in branching ratios. The essential difference is that, in the case of the E_6SSM, the lightest MSSM-like neutralino is no longer stable and decays in two steps to the lightest E_6SSM neutralino. About 20% of the gluino decays go directly into the lightest MSSM-like neutralino implying a chain length $l = 1$ for the MSSM and $l = 3$ for the E_6SSM. On the other hand, about 80% of the gluino decays into a heavier neutralino or chargino, which subsequently decays into the lightest MSSM-like neutralino state, giving the MSSM a chain length $l = 2$ and the E_6SSM $l = 4$.

The following benchmarks provide the main focus of our study:

- MSSM:
  In this benchmark we have an LSP with a mass of 150 GeV. The low dark matter relic density is achieved via LSP resonance annihilation through the CP-odd and heavy Higgs bosons, A and H. The lightest Higgs boson, h, has a mass of 124.4 GeV and can be produced in gluino decay chains. This happens when the gluino decays via the next to lightest neutralino $\tilde{\chi}^0_2$. The gluino decay chain length is dominantly $l = 2$ for this benchmark as for all the MSSM points scanned over.

- E_6SSM-I:
  In this benchmark the LSP and NLSP annihilate efficiently through the Higgs boson resonance leaving a relic density less than the observed relic density of dark matter. The lightest Higgs mass is around 125 GeV and the two lightest inert neutralino state masses are slightly above half of the Higgs mass. In this case the Higgs is SM-like in both its composition and its decays, since only decays into SM final states are kinematically allowed. If the LSP mass was to be slightly below

half of the Higgs mass then the Higgs boson would decay invisibly. In order for the two lightest inert neutralino states to be heavy enough some of the $f_{u\alpha\beta}$ and $f_{d\alpha\beta}$ are required to be large enough such that Yukawa coupling running becomes non-perturbative on the way up to the GUT scale. Using a numerical code to evaluate the running of the couplings we estimate that here the Yukawa couplings remain purtubative up to an energy scale of order 10^{12} GeV. Compared to the MSSM benchmark there are typically two extra steps in the decay chain as the bino-like neutralino decays into first the NLSP which subsequently decays into the LSP. The two extra steps in the chain make the most common total gluino decay chain length $l = 4$. The decay of the bino into the NLSP is preferred over the decay directly into the LSP because of the structure of the Z_2^H breaking trilinear Higgs Yukawa couplings given in Table 10.4.

- E_6SSM-II:
  This benchmark represents a typical scenario, with decay chain features similar to in the E_6SSM-I benchmark, where the most common decay length is 4. Yukawa coupling running remains perturbative up to the GUT scale, as it does in all of the following benchmarks. Just as in previous benchmark the gluino decay chain length here is typically two steps longer than in the MSSM because of the two extra light neutralino states, but here their masses are smaller. The LSP mass is below half of the Z boson mass, but decays of the Z boson into LSP-LSP contribute to the effective number of neutrinos as measured at LEP less than 1-sigma. Because the LSP and NLSP have masses not very far away from half of the Z mass they are able to annihilate relatively efficiently via an s-channel Z boson in the early Universe and the LSP contributes much less than the observed relic density of dark matter. This benchmark has a rather heavy lightest Higgs with a mass around 134 GeV. This Higgs decays dominantly invisibly into a pair LSPs and is ruled out if the boson candidate discovered at the LHC is interpreted as a SM-like Higgs boson.

- E_6SSM-III:
  In contrast to previous benchmarks this benchmark represents the other typical E_6SSM scenario where the bino-like neutralino decays straight to the LSP (not via the NLSP). In this case there is only one extra step compared to the MSSM and the most common decay length is 3. Points with this shorter decay length are slightly more common when one scans over the Z_2^H breaking Yukawa couplings. In the same way as in E_6SSM-II the LSP annihilates efficiently via an s-channel Z boson, even though it is farther away from resonance, and contributes much less than the observed relic density of dark matter. In this benchamark the lightest Higgs has a mass around 116 GeV, much lighter than in E_6SSM-II. As above, this is ruled out if the boson candidate discovered at the LHC is interpreted as a SM-like Higgs boson. This benchmark represent the slightly more common scenario

in the parameter space where the typical decay chain has one extra step after the 150 GeV bino-like neutralino.

- E_6SSM-IV (EZSSM-I):
  This benchmark represents an EZSSM dark matter scenario as described in Ref. [201]. Here the bino-like neutralino is stable and makes up all of the observed dark matter relic density. A low enough relic density is achieved via the bino-like neutralino upscattering into the inert Higgsino pseudo-Dirac pair $\tilde{\chi}^0_{E3}$ and $\tilde{\chi}^0_{E4}$. Since the bino is stable the gluino decays of this benchmark are essentially identical to those of the MSSM benchmark and also have the same dominant decay chain length $l = 2$. The bino-like neutralino's direct detection cross-section is small.

  This benchmark looks very similar to the MSSM benchmark and cannot be distinguished from it purely by analysis of gluino cascade decays. However, if a heavy or CP-odd Higgs around 300 GeV was to be excluded then the MSSM, but not the EZSSM, benchmark would be excluded. This relies on the fact that the EZSSM can have a stable bino at 150 GeV without requiring resonance annihilation through heavy Higgs boson states, which in contrast is required in the MSSM. The Higgs boson has a mass around 125 GeV and is SM-like in its composition and decays.

- E_6SSM-V (EZSSM-II):
  This is another benchmark of the EZSSM, but here the dark matter relic density is not explained. Here the inert Higgsino pseudo-Dirac pair have masses around 120 GeV, well below the bino-like neutralino. These states co-annihilate efficiently in the early universe and contribute a dark matter relic density less than the total observed dark matter relic density. The effective decay chain length is about 4. The complete decay modes for the gluino are shown in Figure A.1(f) in Appendix A. This benchmark provides an example of heavier lightest inert neutralino masses (excluding the decoupled inert singlinos) without requiring non-perturbatively large Yukawa couplings as in the non-EZSSM benchmark E_6SSM-I. Because the lightest inert-Higgsino-like neutralinos have masses much larger than half of the lightest Higgs mass, which is 126 GeV, the Higgs will decay very SM-like.

- E_6SSM-VI (approximate Z_2^S):
  In this benchmark the inert singlino decoupling is not exact and the inert singlino-like LSP mass is not zero, but has been pushed down to the 100 keV scale. This point represents the scenario where the lightest neutralino in the keV mass range is stable and and WDM candidate [202], as described earlier, although we do not calculate the relic density here.

  The approximate decoupling leads to a quite long-lived bino (with a width of order 10^{-11} GeV) and the step in the decay after the bino appears as a displaced vertex at the order of 0.1 mm from the previous step. The decay chain length is typically 4. The complete decay modes for the gluino is shown in Figure A.1(g) in

Appendix A. As remarked, the observed relic density could be achieved by pushing the LSP mass down to the keV scale. In this case the last steps of the gluino decay would be likely to occur outside the detector and one would be left with something that looks like the MSSM. The lightest Higgs has a mass of 126 GeV and decays to the LSP are very suppressed due to its small mass. The Higgs could decay to the GeV scale NLSP, which in turn would decay to the LSP outside the detector since its width is of the order 10^{-20} GeV, leading to invisible Higgs decays. The branching ratio for $h \to \tilde{\chi}_2^0 \tilde{\chi}_2^0$ is however around 6% and is not excluded by current Higgs data.

In the following analysis, in section IV, we use MSSM and E_6SSM-I as our main benchmarks. With the exception of E_6SSM-IV (EZSSM-I) the results obtained for each of the E_6SSM benchmarks are very similar. (E_6SSM-IV on the other hand looks very similar to the MSSM, since the bino is stable.) We therefore mainly give just the results for MSSM and E_6SSM-I, demonstrating the qualitative difference between the MSSM and E_6 models. We also include some results for the E_6SSM-VI to demonstrate the effects of having an even less compact spectrum and also to show how little our conclusions depend on the exact spectrum of the E_6 model.

10.2 Gluino Production and Decays in the MSSM and E_6SSM

The most important processes for supersymmetry searches at hadron colliders are the production of gluinos and squarks, provided that they are not much heavier than charginos and neutralinos. We consider here the case where all of the squarks are heavier than the gluino, which is motivated by the GUT constrained E_6SSM as discussed in Section 10.1.3, which makes the pair-production of gluinos the most attractive process for E_6SSM search and discovery.

10.2.1 Production cross-sections

The tree-level cross section for gluino pair-production at the LHC at 7, 8, and 14 TeV is shown as a function of the gluino mass in Figure 10.5. The CTEQ6LL [203] PDFs are used and the cross section is evaluated at the QCD scales $Q = \sqrt{\hat{s}}$ and $Q = m_{\tilde{g}}$ [3].

In Figure 10.5 one can see a large scale dependence of the cross section due to the uncertainty in the leading order calculation, which is substantially reduced at NLO level [17, 204, 205, 206]. At $Q = m_{\tilde{g}}$, for which the cross section is about 50% larger than at $Q = \sqrt{s}$ at tree level, the product of NLO and NLL K-factors is in the 2.5–5 range for

[3] Both renormalisation and factorisation scales were chosen to be equal.

	MSSM	E_6SSM-I	E_6SSM-II	E_6SSM-III	E_6SSM-IV	E_6SSM-V	E_6SSM-VI	
$\tan\beta$	10	1.5	1.42	1.77	3	1.42	1.42	
λ	-	0.497	0.598	-0.462	-0.4	0.598	0.598	
s	-	5180	5268	5418	5500	5268	5268	
μ	1578	(1820)	(2228)	(1770)	(-1556)	(2228)	(2228)	
A_t	-2900	-3110	-3100	476.2	4638	-2684	-2684	
M_A	302.5	3666	4365	2074	4341	4010	4000	[GeV]
M_1	150	150	150	150	150	150	150	
M_2	285	300	300	300	300	300	300	
$M_{1'}$	-	151	151	151	151	151	151	
$m_{\tilde{g}}$	800	800	800	800	800	800	800	
$m_{\tilde{\chi}^0_{M1}}$	148.7	148.9	149.1	151.2	150.6	149.1	149.1	
$m_{\tilde{\chi}^0_{M2}}$	302.2	296.1	296.8	303.7	301.7	296.8	296.8	
$m_{\tilde{\chi}^0_{M3}}$	1582	1763	2233	1766	1557	2233	2233	
$m_{\tilde{\chi}^0_{M4}}$	1584	1823	2246	1771	1558	2246	2246	
$m_{\tilde{\chi}^\pm_{M1}}$	302.2	299.0	299.2	300.9	300.4	299.2	299.2	
$m_{\tilde{\chi}^\pm_{M2}}$	1584	1822	2229	1771	1557	2229	2229	
$m_{\tilde{\chi}^0_{U1}}$	-	1878	1835	1909	1937	1835	1835	[GeV]
$m_{\tilde{\chi}^0_{U2}}$	-	1973	2003	2062	2087	2003	2003	
$m_{\tilde{\chi}^0_{E1}}$	-	62.7	43.5	45.2	0	0	0.00011	
$m_{\tilde{\chi}^0_{E2}}$	-	62.8	48.6	53.2	0	0	1.53	
$m_{\tilde{\chi}^0_{E3}}$	-	119.8	131.3	141.6	164.1	119.9	120.1	
$m_{\tilde{\chi}^0_{E4}}$	-	121.0	163.6	187.4	164.1	119.9	122.8	
$m_{\tilde{\chi}^0_{E5}}$	-	183.0	197.0	227.8	388.9	185.8	185.8	
$m_{\tilde{\chi}^0_{E6}}$	-	184.4	224.3	265.6	388.9	185.8	187.0	
$m_{\tilde{\chi}^\pm_{E1}}$	-	109.8	119.9	122.7	164.1	119.9	119.9	
$m_{\tilde{\chi}^\pm_{E2}}$	-	117.7	185.8	225.1	388.9	185.8	185.8	
m_h	124.4	125.4	133.8	116.3	124.7	126.1	125.8	
$P(l=1)$	0.188	$< 10^{-9}$	$< 10^{-5}$	$< 10^{-5}$	0.1727	$< 10^{-8}$	$< 10^{-12}$	
$P(l=2)$	0.812	$< 10^{-4}$	0.01524	0.1723	0.8273	0.01	$< 10^{-5}$	
$P(l=3)$	0	0.1746	0.2336	0.7986	$< 10^{-6}$	0.2	0.1721	
$P(l=4)$	0	0.8196	0.7512	0.02915	$< 10^{-15}$	0.8	0.8280	
$P(l=5)$	0	0.0058	$< 10^{-7}$	0	0	$< 10^{-15}$	0	
Ωh^2	0.00628	0.00114	0.0006842	0.0006937	0.101	0.00154		
σ_{SI}	0.401×10^{-9}	15.34×10^{-8}	9.35×10^{-8}	16.35×10^{-8}	3.75×10^{-11}	3.98×10^{-13}		[pb]

Table 10.3: Benchmarks motivated by the parameter scans presented in Figure 10.1 and Table 10.1 and Table 10.2. From top to bottom the classes of parameters are dimensionless input parameters; dimensionful input parameters; neutralino, chargino, and lightest Higgs masses (in absolute values); probabilities for certain gluino decay chain lengths; and finally dark matter properties. The $\tilde{\chi}^{0(\pm)}_{Mi}$ are MSSM-like states, the $\tilde{\chi}^0_{Ui}$ are USSM-like states, being mainly mixtures of $\tilde{S}$ and $\tilde{B}'$. The $\tilde{\chi}^{0(\pm)}_{Ei}$ are states introduced by the inert sector of E_6SSM. The scale for squark and slepton masses is $M_S = 2$ TeV in all benchmarks. The benchmarks are here defined with a gluino mass of 800 GeV but can easily be generalised to other masses. For such scenarios, we will use the same names for the benchmarks but clearly state what gluino mass is used.

	E$_6$SSM-I	E$_6$SSM-II	E$_6$SSM-III	E$_6$SSM-IV	E$_6$SSM-V	E$_6$SSM-VI
λ	3.93×10^{-1}	5.98×10^{-1}	-4.77×10^{-1}	-4.0×10^{-1}	5.98×10^{-1}	5.98×10^{-1}
λ_{22}	-3.57×10^{-4}	-4.48×10^{-3}	5.14×10^{-3}	1.0×10^{-1}	-4.48×10^{-3}	-4.48×10^{-3}
λ_{21}	3.0×10^{-2}	-4.34×10^{-2}	-8.77×10^{-2}	0	-4.34×10^{-2}	-4.34×10^{-2}
λ_{12}	3.21×10^{-2}	-3.83×10^{-2}	6.40×10^{-2}	0	-3.83×10^{-2}	-3.83×10^{-2}
λ_{11}	7.14×10^{-4}	-1.25×10^{-2}	-3.36×10^{-2}	4.22×10^{-2}	-1.25×10^{-2}	-1.25×10^{-2}
f_{d22}	1×10^{-3}	-9.02×10^{-3}	7.06×10^{-3}	0	0	2.0×10^{-1}
f_{d21}	6.844×10^{-1}	-3.48×10^{-1}	6.10×10^{-1}	0	0	-3.48×10^{-3}
f_{d12}	6.5×10^{-1}	6.92×10^{-1}	-7.64×10^{-1}	0	0	6.92×10^{-3}
f_{d11}	1×10^{-3}	6.17×10^{-3}	9.26×10^{-3}	0	0	6.17×10^{-5}
f_{u22}	1×10^{-3}	-6.77×10^{-3}	3.93×10^{-3}	0	0	1.0×10^{-1}
f_{u21}	6.7×10^{-1}	-7.86×10^{-1}	-8.56×10^{-1}	0	0	-7.86×10^{-3}
f_{u12}	6.4×10^{-1}	2.52×10^{-1}	-2.71×10^{-1}	0	0	2.52×10^{-3}
f_{u11}	1×10^{-3}	8.59×10^{-3}	-2.24×10^{-3}	0	0	8.59×10^{-5}
x_{d2}	7.14×10^{-4}	4.04×10^{-3}	2.35×10^{-4}	4.04×10^{-5}	4.04×10^{-5}	4.04×10^{-5}
x_{d1}	7.14×10^{-4}	5.11×10^{-4}	2.96×10^{-4}	5.11×10^{-6}	5.11×10^{-6}	5.11×10^{-6}
x_{u2}	7.14×10^{-4}	-2.01×10^{-3}	9.04×10^{-4}	-2.01×10^{-5}	-2.01×10^{-5}	-2.01×10^{-5}
x_{u1}	7.14×10^{-4}	1.01×10^{-3}	-2.21×10^{-3}	1.01×10^{-5}	1.01×10^{-5}	1.01×10^{-5}
z_2	1×10^{-3}	6.02×10^{-2}	4.16×10^{-3}	0	0	6.02×10^{-4}
z_1	1×10^{-3}	2.63×10^{-3}	1.18×10^{-2}	0	0	2.63×10^{-5}

Table 10.4: Trilinear Higgs Yukawa couplings in the E$_6$SSM benchmarks. The couplings λ_{ijk} come from the terms $\lambda_{ijk}S_iH_{dj}H_{uk}$ in the superpotential. Here $\lambda_{333}=\lambda$, $\lambda_{3\alpha\beta}=\lambda_{\alpha\beta}$, $\lambda_{\alpha3\beta}=f_{d\alpha\beta}$, $\lambda_{\alpha\beta3}=f_{u\alpha\beta}$, $\lambda_{33\alpha}=x_{d\alpha}$, $\lambda_{3\alpha3}=x_{u\alpha}$, and $\lambda_{\alpha33}=z_\alpha$.

$\sqrt{s}=7$ TeV for the 500–1500 GeV mass range [206]. The large K-factor indicate a large one-loop contribution to the cross section. Apart from the squark and gluino masses the K-factors also depend on the PDF parameterisation. To be on the conservative side we use LO cross sections evaluated at $Q=m_{\tilde{g}}$ in our analysis. For our benchmarks with a gluino mass of 800 GeV, the production cross sections are 20.6 fb, 47.5 fb, and 839 fb for the $\sqrt{s}=7$, 8 and 14 TeV respectively. So, with an integrated luminosity of about 20 fb^{-1} at 8 TeV which is roughly what the experiments had at the end of 2012 about 1000 gluino pairs would have been produced.

10.2.2 Signatures and distributions

Since the E$_6$SSM introduces new neutralinos, naturally lighter than the MSSM-like LSP, the gluino decay chains will be longer than in the MSSM in general. This is confirmed and illustrated by the parameter scans in Figure 10.1 and the benchmarks defined in Table 10.3. In order to study the LHC phenomenology of gluino cascade decays of the E$_6$SSM, and the MSSM for comparison, we have performed Monte Carlo analyses using the `CalcHEP` [69] package with CTEQ6LL [203] PDFs. With the exception of the multi-jet analysis in Section 10.2.4, we restrict ourselves to a parton-level analysis. We do however take into account a realistic electromagnetic energy resolution, given by $0.15/\sqrt{E(\mathrm{GeV})}$, typical for the ATLAS and CMS detectors, as well as their typical hadronic energy resolution of $0.5/\sqrt{E(\mathrm{GeV})}$ and perform the respective Gaussian

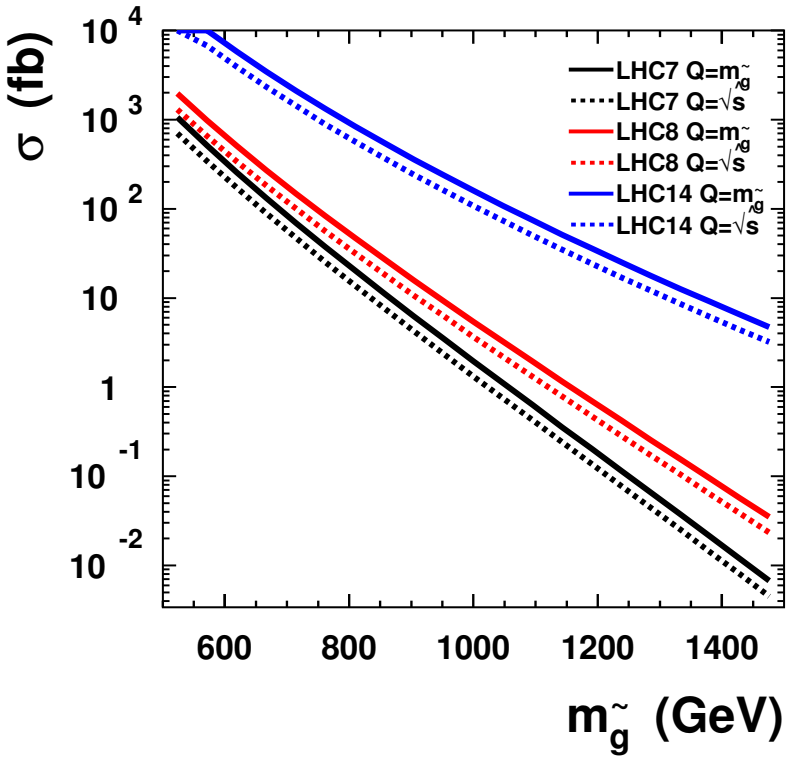

Figure 10.5: The tree-level cross section for gluino pair production as a function of the gluino mass, $m_{\tilde{g}}$. The solid (or dashed) lines represent, from bottom to top, the LHC at 7 TeV (black), 8 TeV (red), and 14 TeV (blue). The CTEQ6LL set is used for PDFs. The QCD scale, Q, is set to the gluino mass, $Q = m_{\tilde{g}}$, for the solid lines and to the centre of mass energy, $Q = \sqrt{\hat{s}}$, for the dashed lines. The scale dependence of the cross section is an effect of the uncertainty of the leading order calculation. Including NLO corrections is known to bring up the cross section by at least a factor 2 [17], so we are underestimating the production rate for gluinos slightly with this leading order calculation.

smearing for leptons and quarks. We define leptons (jets) by requiring $p_T > 10$ GeV (20 GeV) and $|\eta| < 2.5$ (4.5) and a lepton isolation of $\Delta R(\text{lepton}, \text{jet}) > 0.5$.

The longer decay chains of gluinos lead to less missing momentum, p_T^{miss}, and larger effective mass $M_{\text{eff}} = p_T^{\text{miss}} + \sum_{\text{visible}} |p_T^{\text{visible}}|$, as measured in the detector as one can see in Figure 10.6 which presents the respective distributions for our main benchmarks (MSSM and E_6SSM-I). Although the p_T^{miss} distribution is quite different, one should note that the effective mass distribution is not significantly different between the models. This happens because the effect from the suppressed missing momentum in the case of the E_6SSM is partially cancelled by the effect of the increase of visible momentum, due to the longer gluino cascade decay. There is a slight overall increase of the effective mass due to the fact that visible momenta are added up as magnitudes while the missing

momentum is a vectorial sum. The reduced amount of missing transverse momentum in the E$_6$SSM makes it less discoverable, compared to the MSSM, in typical SUSY searches which focus on all-hadronic events with large missing momentum.

Another important feature of the long decay chains of the E$_6$SSM is the increase in lepton as well as jet multiplicity, as shown in Figure 10.7, again for the benchmarks MSSM and E$_6$SSM-I. This feature allows us to rely on multi-lepton requirements for background reduction rather than cuts on missing energy. There is a significant loss of statistics by using this strategy, however it turns out to be a very important channel for discovery of gluinos with long decay chains and indeed a channel in which the E$_6$SSM is largely dominant compared to the MSSM. This makes the multi-lepton channels essential for distinguishing the models.

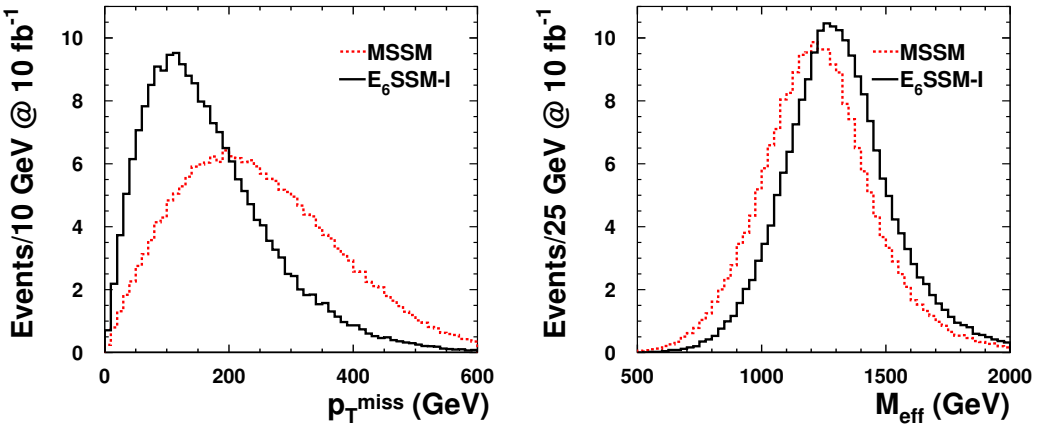

Figure 10.6: Missing transverse momentum (left) and the effective mass (right) before cuts for the MSSM and E$_6$SSM-I benchmark with $m_{\tilde{g}} = 800$ GeV at $\sqrt{s} = 7$ TeV. The E$_6$SSM predicts significantly less missing transverse momentum and slightly larger effective mass compared to the MSSM. The longer gluino decay chains of the E$_6$SSM, with a lighter LSP in the end, provide less missing and more visible transverse momentum. The effective mass does not distinguish the features of these models since it is a sum of visible and missing transverse momenta.

10.2.3 Searches at $\sqrt{s} = 7$ TeV LHC

There has not been any indications of SUSY from the LHC during its run at $\sqrt{s} = 7$ TeV. We have investigated different SUSY search channels at this energy to understand the status of our benchmarks and what limits can be put on the E$_6$SSM and which channels we expect to be the most favourable for discovery and distinguishing the models. We compare our signals with published backgrounds used by CMS and ATLAS at this energy. We have scaled all the channels to an integrated luminosity of 10 fb^{-1} for

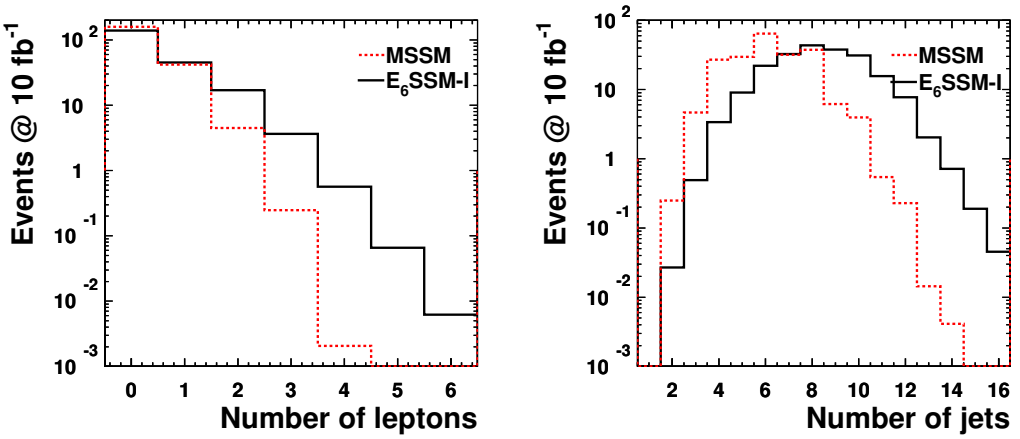

Figure 10.7: Lepton multiplicity (left) and jet multiplicity (right), requiring $p_T > 10$ GeV, $|\eta| < 2.5$, and $\Delta R(\text{lepton}, \text{jet}) > 0.5$ for leptons and $p_T > 20$ GeV and $|\eta| < 4.5$ for jets. The benchmarks considered are the MSSM and E$_6$SSM-I as presented in Table 10.3 with $m_{\tilde{g}} = 800$ GeV. The LHC setup is used with $\sqrt{s} = 7$ TeV and normalised to 10 fb^{-1} of integrated luminosity. Due to the longer gluino decay chains of the E$_6$SSM it predicts many more visible particles in collider experiments, both leptons and jets. This suggests that searches for E$_6$SSM gluinos should be more favourable in multi-lepton and multi-jet searches.

comparison, which is approximately the amount of 7 TeV data acquired by the two experiments. Benchmarks with an 800 GeV gluino mass are considered here.

0 leptons

The long gluino cascade decays with less missing momentum would be less visible in the main SUSY searches based on jets and missing energy (see e.g. [192] and [207]) which provide the best statistics and strongest exclusions for MSSM. In these searches the E$_6$SSM parameter space is less constrained as compared to the MSSM and the acquired exclusions do not hold for this model. The main reason for this is the hard cuts on missing energy and its ratio to the effective mass since the distributions for these variables are significantly different for MSSM versus E$_6$SSM as we demonstrate here.

The effective mass distribution for our benchmarks for an 800 GeV gluino mass is plotted on the top of the backgrounds from ATLAS and CMS in Figure 10.8(a) and Figure 10.8(b) after all cuts have been applied except for the final selection cut on the effective mass itself. The signal from E$_6$SSM is suppressed as compared to the MSSM and, more importantly, both benchmarks are well below the background, illustrating the difficulty of discovering SUSY at the 7 TeV LHC in the case where the gluino mass is around 800 GeV, assuming the squarks to be much heavier.

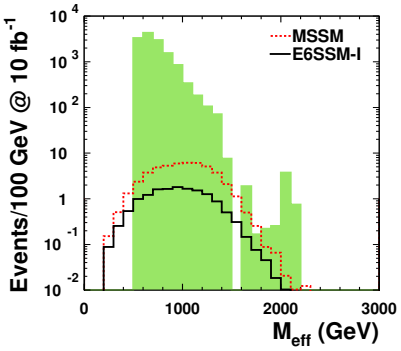

(a) 0 leptons, 4 jets: Backgrounds from ATLAS [192].

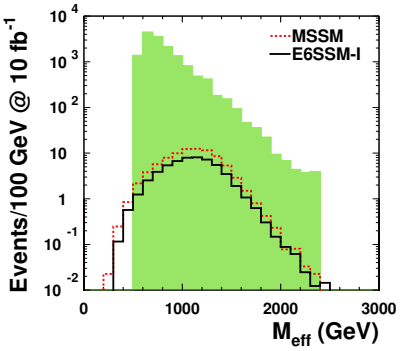

(b) 0 leptons, 3 jets: Backgrounds from CMS[207].

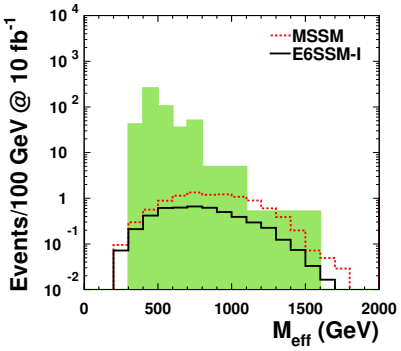

(c) 1 muon, 4 jets: Backgrounds from ATLAS [208]

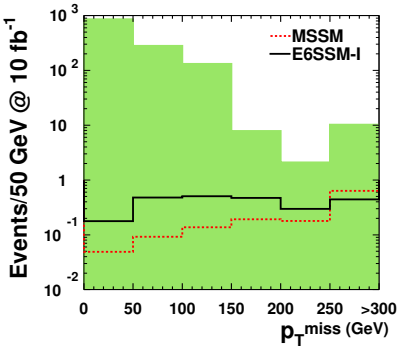

(d) 2SS leptons: SS-SR2. Backgrounds from ATLAS [209]

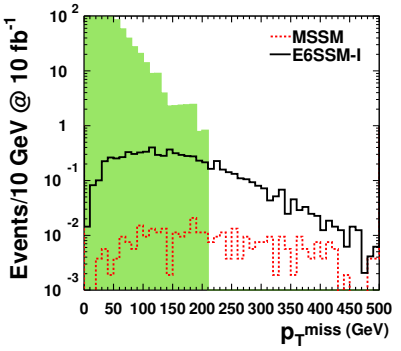

(e) 3 leptons: Backgrounds from CMS [210]

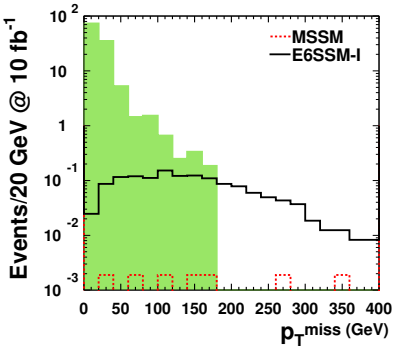

(f) 4 leptons: Backgrounds from ATLAS [211]

Figure 10.8: Distributions for published 0–4 lepton searches at 7 TeV, scaled to 10 fb^{-1} for comparison. The signal contributions from the MSSM and E$_6$SSM-I benchmarks with $m_{\tilde{g}} = 800$ GeV are plotted on top of published backgrounds. The absence of backgrounds at high $M_{\rm eff}$ or $p_T^{\rm miss}$ is because backgrounds in these regions were not published by the experiments. The distributions shown are after all cuts except the final selection cut on the plotted distribution. 0 lepton searches (with jets$\leq$4) give bad background suppression and favour MSSM. Requiring two or more leptons makes MSSM more suppressed. For multi-lepton searches the signal to background ratio for the E$_6$SSM is better but the signal statistics is low.

Even though the 0-lepton signature with a jet multiplicity of about four is not favoured for E_6SSM hunting, the 0-lepton signature for this model could be still interesting for the cases of larger jet-multiplicity. For multi-jet channels, analyses beyond the parton level are essential. We discuss this in detail for the case of $\sqrt{s} = 8$ TeV in Section 10.2.4 where we perform one example of a beyond-the-parton level analysis. Apart from this, we restrict ourselves here by the parton level analysis and in particular we shall focus on the tri-lepton signature.

1–2 leptons

The selection of events with leptons provides easy triggering and efficient background suppression at the cost of worse statistics. To exemplify this we compare the signal distributions for the benchmarks versus the backgrounds for two ATLAS searches, a single lepton search in Figure 10.8(c) and a two same-sign lepton search in Figure 10.8(d). One can see that the signal-to-background ratio is better in these leptonic searches compared to the all-hadronic searches. In the effective mass distribution of the 1 muon channel from ATLAS's 1 lepton plus 4 jets search shown in Figure 10.8(c) one can see that the signal level is not extremely far below the background level in the high effective mass region. The E_6SSM signal is still suppressed as compared to the MSSM in this one lepton search, however, considering the $p_T^{\rm miss}$ distribution for the two same-sign lepton search by ATLAS in Figure 10.8(d), one sees how the E_6SSM signal overtakes the MSSM benchmark's by requiring one more lepton. This is due to the fact that two same-sign leptons in the final state become more likely in the E_6SSM than in the MSSM, simply because it predicts more leptons in general. Even though the E_6SSM signal has got stronger than the MSSM signal in this 2SS channel compared to the one lepton channel, the signal-to-background ratio now looks worse. This is because the choice of using the missing momentum instead of the effective mass as the variable to define the signal region is not favourable for the E_6SSM since the respective signal is very vulnerable to hard cuts on this variable. Also for higher multiplicity searches, using the effective mass to define the signal region allows for the signal-to-background ratio to be improved as we will show below.

3–4 leptons

Requiring additional leptons makes the statistics even worse, but it allows the signal to appear above the background enough to allow a reasonable signal significance in order to test the models under study. Comparison of the benchmark signals with the background from a 3 lepton search by CMS is shown in Figure 10.8(e) and from a 4 lepton search

by ATLAS in Figure 10.8(f). The three lepton channel defined by the cuts

$$\begin{aligned} p_T(l_1) &> 20 \text{ GeV} \\ p_T(l_2) &> 10 \text{ GeV} \\ p_T(l_3) &> 10 \text{ GeV} \end{aligned} \tag{10.2}$$

where $l = \mu$ or e with $|\eta| < 2.5$, and $\Delta R(\text{lepton}, \text{jet}) > 0.5$, seems promising, showing a possible excess in the high missing transverse momentum region. The background used by CMS is not evaluated for large enough missing transverse momentum however. To explore the large missing transverse momentum region and to expand the analysis further we have produced backgrounds for this channel, including several processes, using `CalcHEP`.

The dominant backgrounds come from ZWj and $t\bar{t}V$. Other important contributions come from ZW and $t\bar{t}$. We also considered backgrounds such as $ZWjj$, ZZ and ZZZ which we found to be subleading. Our background predictions at $\sqrt{s} = 7$ TeV agree well with backgrounds used in the multi-lepton searches by CMS [210] and ATLAS [211]. They only major difference is in the very low end of the p_T^{miss} distribution where the `CalcHEP` generated backgrounds are suppressed.

This difference in the transverse missing momentum distribution between our results and the results from the full detector simulation occurs because we do not simulate any source of instrumental missing energy in our analysis. However, this difference does not affect the our results since we are not using missing p_T information directly, similar to approach of [212], and, moreover, this difference effectively vanishes after the cut is applied on the effective mass variable as used at last stage of our analysis.

We would like to stress that parton level analysis is quite accurate to the tri-lepton signature we study in this chapter. Signatures with lower lepton multiplicity require considerations of QCD backgrounds from jets faking leptons and instrumental defects which could affect the low p_T^{miss} region. This background is difficult to take into account at the parton-level event generator and even at the level of fast detector simulation. Therefore analysis of signatures with lepton multiplicities below three are outside of the scope of this study. When we compare signal versus background for these signatures for illustration purposes we therefore chose to rely on published backgrounds for those channels.

The result for the p_T^{miss} distribution is shown in Figure 10.9(a). One can see that the E_6SSM signal is now at the same level as the background and maybe a little higher for large p_T^{miss}. If one instead considers the effective mass as a selection variable for the three lepton channel, the situation looks much more promising, at least for the E_6SSM. This can be seen from the effective mass distribution presented in Figure 10.9(b). CMS has not been using the effective mass to define the signal region for this channel but uses the missing transverse energy and the hadronic transverse energy instead. Our

way of defining the signal region by the effective mass is on the other hand much closer to the way presented by ATLAS in [211] or as suggested in [212]. A cut on M_{eff} at 950 GeV gives $S = 11.5$ signal events for the 800 GeV gluino mass E_6SSM-I benchmark and $B = 0.4$ background events, providing an expected 5.7σ excess at 10 fb^{-1}, using the definition of statistical significance $S_{12} = 2(\sqrt{S+B} - \sqrt{B})$ valid for small statistics [80, 81].

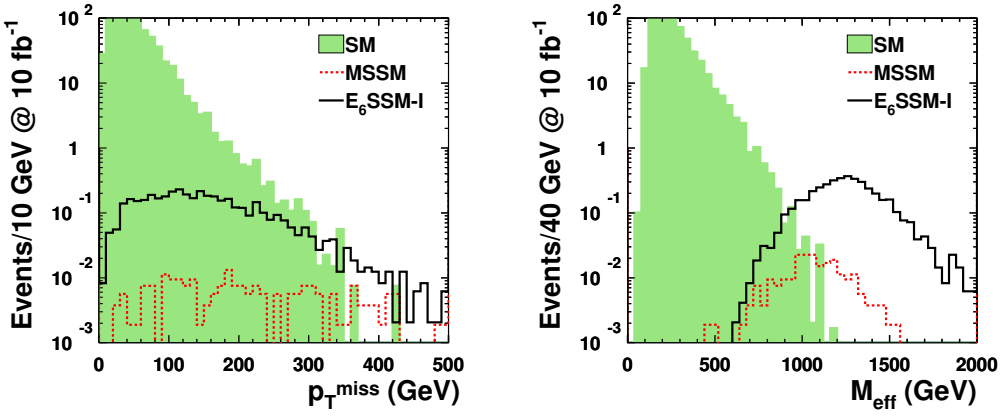

(a) (b)

Figure 10.9: Distributions for p_T^{miss} (a) and M_{eff} (b) at the LHC with 10 fb^{-1} at $\sqrt{s} = 7$ TeV after requiring at least three leptons. The benchmarks both have a gluino mass $m_{\tilde{g}} = 800$ GeV. Backgrounds have been generated by `CalcHEP` and agree well with published ones such the ones by CMS, shown in Figure 10.8(e). The E_6SSM-I benchmark is shown to present a signal larger than the background for large missing momentum (a) even though it is a model that predicts quite small amounts of missing momentum. The signal presents itself more strongly in the effective mass variable where there is no need for a cut on the missing transverse momentum.

10.2.4 Searches at $\sqrt{s} = 8$ TeV LHC

6 jets

Since the multi-jet channels could provide good prospects of discovery of and differentiation between benchmarks we investigate the effect of the cuts,

$$\begin{aligned} E_T^{\rm miss} &> 160 \text{ GeV} \\ p_T(j_1) &> 130 \text{ GeV} \\ p_T(j_2) &> 60 \text{ GeV} \\ p_T(j_3) &> 60 \text{ GeV} \\ p_T(j_4) &> 60 \text{ GeV} \\ p_T(j_5) &> 60 \text{ GeV} \\ p_T(j_6) &> 60 \text{ GeV} \\ \Delta\phi(\text{jet}, p_T^{\rm miss})_{\rm min} &> 0.4(i = \{1,2,3\}), 0.2(p_T > 40 \text{ GeV jets}) \\ E_T^{\rm miss}/m_{\rm eff} &> 0.25(6j) \\ m_{\rm eff} &> 1300 \text{ GeV}, \end{aligned} \tag{10.3}$$

used by ATLAS [7] for 6-jets analysis applied to our benchmarks. To perform this kind of multi-jet analysis we are forced to go beyond our parton-level analysis. The need for a more dedicated analysis, with hadronisation and detector effects, comes mainly from the importance of initial and final state radiation that plays an important role when requiring more than four jets in the gluino decays. This is because the first four jets are well approximated by our parton level analysis since they typically are the ones that originate straight from the gluino decay. To generate the events at the level of fast detector simulation we fed events from `CalcHEP` to the `PGS` [76] package. We also compare the signal from the MSSM and E_6SSM with an mSUGRA point which is excluded, but very close to the limit. The result for the effective mass distribution for the signals before and after cuts are shown in Figure 10.10.

Our result, produced with `CalcHEP` and `PGS`, is in good agreement with the ATLAS result and is consistent with the experimental data.

Our analysis shows that, also in the multi-jet channels, the E_6SSM will be suppressed compared to the MSSM and mSUGRA models, mostly because of its small missing transverse momentum. The larger jet multiplicity of the E_6SSM at the parton level turns to be not such a great discriminator between two models, at least for this signature, because the initial and final state radiation allows most of the signal from the MSSM model to pass the 6-jets selection requirement. Even though it might still be a good discovery channel for different selection/analysis for the E_6SSM, we note that, for the current selection, the E_6SSM signal from an 800 GeV gluino is about at the same level

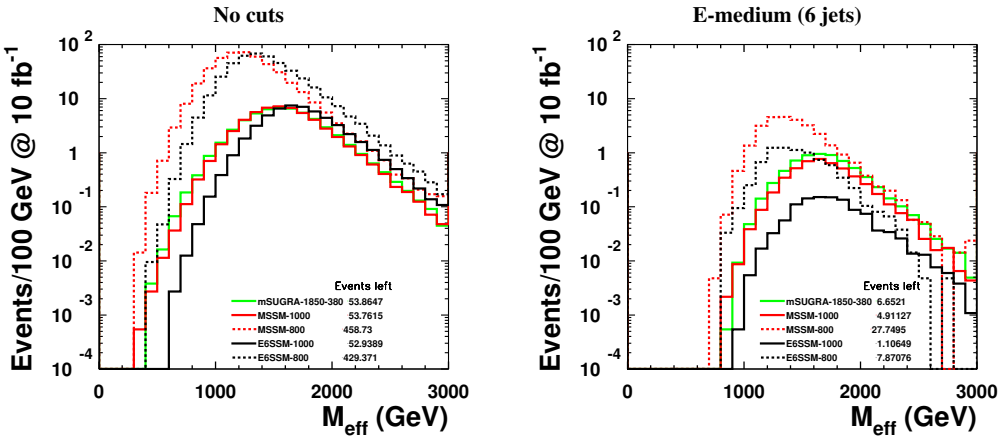

(a) (b)

Figure 10.10: Comparison between mSUGRA, MSSM, and E_6SSM benchmarks in the 6 jet channel, E-medium, used by ATLAS [7]. The effective mass distribution for the gluino signal are plotted before (a) and after (b) cuts at $\sqrt{s} = 8$ TeV and 10 fb^{-1} of integrated luminosity. The events left after the last signal region cut on the effective mass, $M_{\rm eff} > 1300$ GeV, are given in Table 10.5. The benchmarks with solid lines all have a gluino mass of 1 TeV while the benchmarks with dashed lines have a gluino mass of 800 GeV. After cuts (b) the E_6SSM benchmark with an 800 GeV gluino mass has a distribution not very different from the mSUGRA point with a 1 TeV gluino mass.

as the signal from the mSUGRA model with a 1 TeV gluino. This is the very important point we would like to convey in this section: the MSSM limits are not quite applicable to the E_6SSM, for example the gluino mass limit could easily differ by about 200 GeV between two models in the heavy squark limit as we demonstrate above. Therefore the status of the E_6SSM is quite different even from generic MSSM one for the current LHC analysis, which needs to be tuned in order to explore E_6SSM parameter space.

	$m_{\tilde{g}}$/TeV	Events
mSUGRA (1850,380)	1	6.18
MSSM	1	5.59
	0.8	18.16
E_6SSM	1	1.05
	0.8	5.58

Table 10.5: The events left at 8 TeV and 10 fb^{-1} for benchmarks from three models after the E-medium set of cuts, including the final cut on the effective mass, $M_{\rm eff} > 1300$ GeV. Here the E_6SSM benchmark with a 800 GeV gluino mass is left with fewer events than the mSUGRA benchmark with a 1 TeV gluino mass.

3 leptons

Performing the same analysis for the promising 3 lepton channel at the LHC with $\sqrt{s} =$ 8 TeV as was done for the case with $\sqrt{s} = 7$ TeV we are able to calculate the discovery prospects for our benchmarks. Again, the 3 lepton signature is defined by the cuts in Section 10.2. In Figure 10.11 the effective mass distributions are plotted for our benchmarks and SM backgrounds for 20 fb^{-1} of integrated luminosity. The different plots show how the effective mass distributions change for the benchmarks if the gluino mass is varied.

In these plots we have included another benchmark, E$_6$SSM-VI, for comparison with the E$_6$SSM-I and MSSM benchmarks. This benchmark gives a signal slightly above that of the E$_6$SSM-I. This is because the E$_6$SSM-VI benchmark has a long gluino decay chain with an even less compact spectrum. The larger mass difference between the MSSM-like lightest neutralino and the inert singlinos implies that higher p_T leptons can be radiated from that step in the decay chain. This causes an increase in the number of lepton surviving the lepton identification cuts.

A final cut, defining the signal region, is made on the effective mass. We let the signal region cut depend on the gluino mass to enhance the expected significance and define it as $M_{\text{eff}} > 1.4 m_{\tilde{g}}$. Using the definition of statistical significance, $S_{12} = 2(\sqrt{S+B} - \sqrt{B})$, valid for small statistics [80, 81], we calculate the expected excess for different gluino masses using our mass dependent signal region cut. The significance is plotted as a function of the gluino mass in Figure 10.12(a) where a K-factor of 3 has been applied to the signal. The expected number of events for the E$_6$SSM-I and E$_6$SSM-VI benchmarks with gluino mass $m_{\tilde{g}} = 900$ GeV and the background before and after the final cut on the effective mass ($M_{\text{eff}} > 1.4 m_{\tilde{g}} = 1260$ GeV) are presented in Table 10.6. The table also lists the expected significances with and without a K-factor of 3 for the two benchmarks. The integrated luminosity needed for discovery and exclusion of a particular gluino mass in the E$_6$SSM in the 3 lepton channel is shown in Figure 10.12(b), where again a K-factor of 3 has been applied to the signal. The plot shows that a 2σ exclusion of gluino masses below 1 TeV is possible with data acquired by ATLAS or CMS at the end of the year 2012. The MSSM benchmark is still well below the background at this stage and is therefore not included in these plots.

10.2.5 3 lepton searches at $\sqrt{s} = 14$ TeV LHC

At higher collider energy the cross section for gluino production increases considerably. This causes both our MSSM and E$_6$SSM benchmarks to be clearly visible above the background, as can be seen in Figure 10.13. The figure shows the effective mass distribution for the MSSM, E$_6$SSM-I, and E$_6$SSM-VI benchmarks for different gluino masses in different subfigures, where a requirement of at least three leptons has been applied in

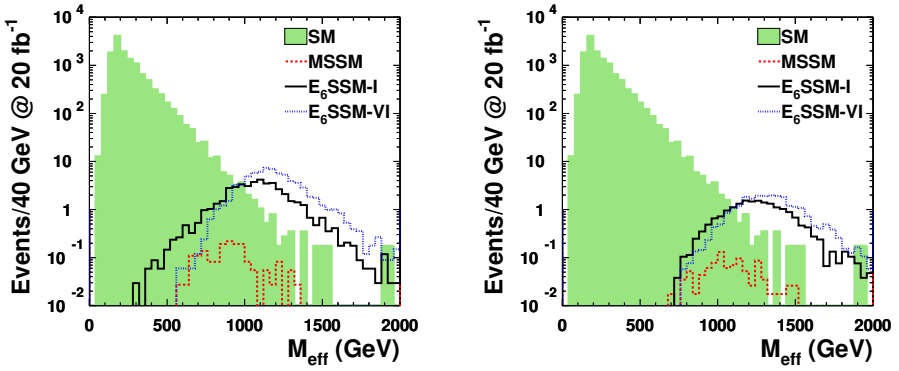

(a) $m_{\tilde{g}} = 700$ GeV (b) $m_{\tilde{g}} = 800$ GeV

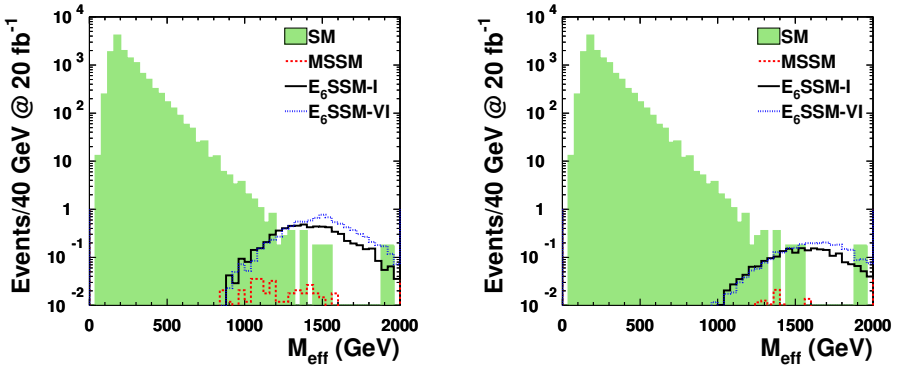

(c) $m_{\tilde{g}} = 900$ GeV (d) $m_{\tilde{g}} = 1000$ GeV

Figure 10.11: Plots of M_{eff} after requiring at least 3 leptons at LHC at $\sqrt{s}$ =8 TeV. The integrated luminosity is taken to be 20 fb^{-1}. The different subfigures show the signal distributions for the MSSM, E$_6$SSM-I, and E$_6$SSM-VI benchmarks for different values of the gluino mass. The E$_6$SSM-VI benchmark is similar to E$_6$SSM-I, but the lighter LSP mass, and thus larger mass gap between it and the bino-like neutralino, causes the signal to be stronger since higher p_T leptons are more likely to be produced. The distributions for gluino masses of 700 GeV (a), 800 GeV (b), 900 GeV (c), and 1000 GeV (d) show that the signal to background ratio is not affected much as the gluino mass increases, but the statistics become low since the cross section gets small.

the same way as in the 8 TeV analysis. For all gluino masses the E$_6$SSM-VI benchmark gives the largest signal, just as in the 8 TeV scenario discussed in section Section 10.2.4. The 14 TeV collider at such a large integrated luminosity as 100 fb^{-1}, which is used in Figure 10.13, allows for statistics needed for discovery of high mass gluinos. Heavier gluinos would push the effective mass distribution to higher values where there is essentially no background and where it is just a matter of acquiring enough statistics, but once that is done one expects a very clean signal.

	$N_{\text{lep}} \geq 3$	$M_{\text{eff}} > 1.4m_{\tilde{g}}$	$\sigma_{K=1}$	$\sigma_{K=3}$
E_6SSM-I	6.72	5.08	2.80	5.88
E_6SSM-VI	8.95	7.60	3.71	7.57
BG	8.66×10^3	1.25		

Table 10.6: The expected number of events after the first and second cuts in the 3 lepton analysis for the E_6SSM-I and E_6SSM-VI benchmarks with $m_{\tilde{g}} =$ 900 GeV and SM background at 20 fb^{-1} and 8 TeV. Also the significance, based on signal and background events after the second cut, with K-factors of 1 and 3 applied to the signal.

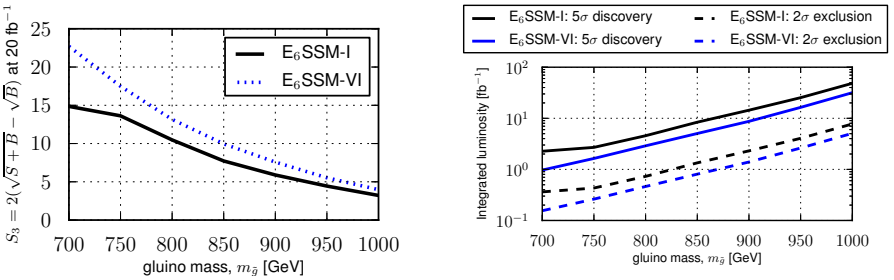

(a) Expected significance at 20 fb^{-1}, $\sqrt{s}$ = 8 TeV

(b) Luminosity required for 5σ discovery and 2σ exclusion, $\sqrt{s} = 8$TeV

Figure 10.12: The gluino mass reach at $\sqrt{s}$ =8 TeV for the three lepton channel. The gluino mass is varied for the benchmarks E_6SSM-I and E_6SSM-VI to estimate the expected significance for different gluino masses. The significance is calculated with the events remaining after a selection cut requiring $M_{\text{eff}} > 1.4m_{\tilde{g}}$. A K-factor of 3 has been applied to the signal. The E_6SSM-VI benchmark (shown in blue) is more accessible for exclusion or discovery than benchmark E_6SSM-I since it has a bigger mass gap between the bino-like and inert-singlino-like neutralinos, providing higher p_T leptons.

In Figure 10.14 the gluino reach for the benchmarks at the 14 TeV collider is presented in the same way as was done for the 8 TeV collider in Figure 10.12, again with a K-factor of 3 applied to the signal. The only difference is that the gluino mass dependent cut on the effective mass which defines the signal region is taken to be $M_{\text{eff}} > m_{\tilde{g}}$ instead of $M_{\text{eff}} > 1.4m_{\tilde{g}}$. For the MSSM benchmark, which has become accessible at this energy, one will be able to exclude gluino masses up to ∼1400 GeV through this channel for an integrated luminosity of 100 fb^{-1}. The expected significance for the MSSM is however about an order of magnitude below the E_6SSM benchmarks as shown in Figure 10.14(a). An order of magnitude difference in significance implies two orders of magnitude difference for the integrated luminosity required for exclusion of a particular gluino mass, as can be seen in Figure 10.14(b). For the E_6SSM-I and E_6SSM-VI the 100 fb^{-1} of data at 14 TeV allows not only for exclusion, but potentially for a 5σ discovery for the whole gluino mass range up to 1.5 TeV. In fact, we estimate that the discovery reach for the E_6SSM in the 3 lepton channel at 100 fb^{-1} is almost 1.7 TeV.

It should be stressed once more that the results for the MSSM benchmark are different

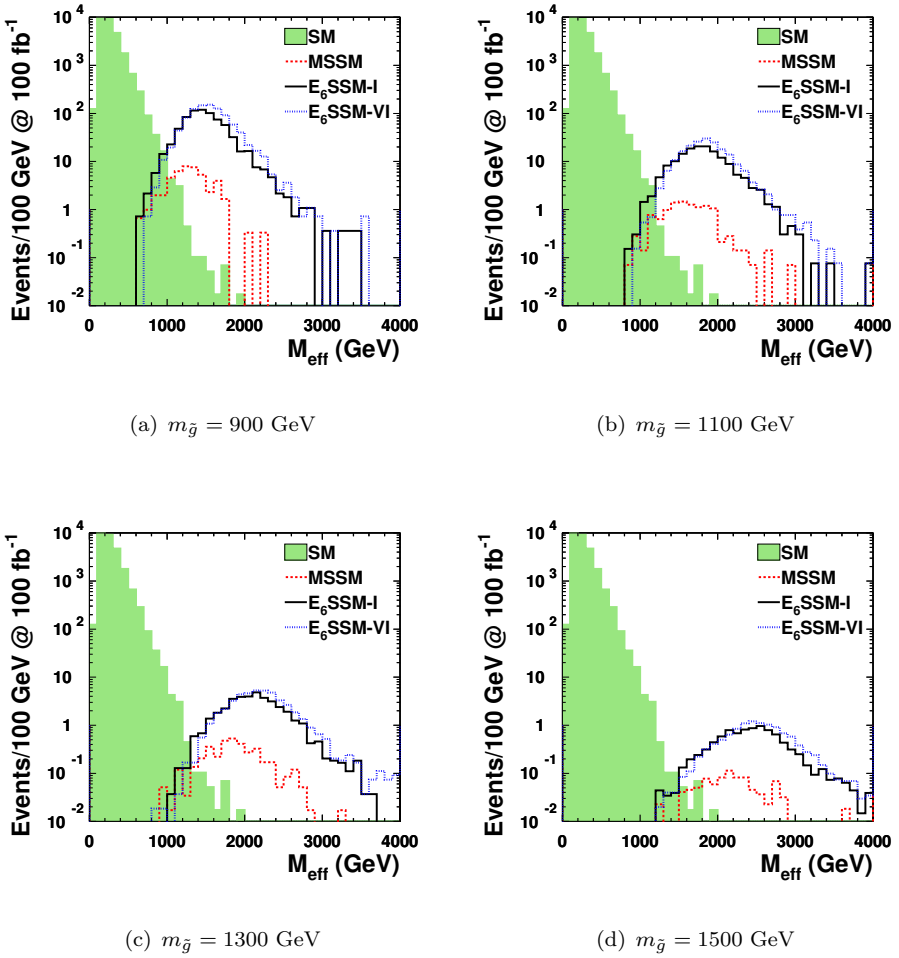

(a) $m_{\tilde{g}} = 900$ GeV

(b) $m_{\tilde{g}} = 1100$ GeV

(c) $m_{\tilde{g}} = 1300$ GeV

(d) $m_{\tilde{g}} = 1500$ GeV

Figure 10.13: These plots show the evolution of the effective mass distribution after requiring at least three leptons for the benchmarks MSSM, E_6SSM-I, and E_6SSM-VI as the gluino mass changes. In Figure 10.13(a) the gluino mass is 900 GeV and at this large integrated luminosity of 100 fb^{-1} at $\sqrt{s} = 14$ TeV the MSSM benchmark is almost discoverable. The E_6SSM benchmarks are both well above the background and clear signals are expected due to the good statistics.

from other studies since we are not dealing with a GUT constrained model, but an electro-weak scale model and the spectrum is more general. Our study focuses on a specific scenario in which the squarks are two to three times heavier than the gluino. Therefore, typical results obtained in previous multi-lepton analyses for SUSY searches differ from our results. As an example, the three lepton signals derived for the mSUGRA points in [212] are larger than the signals for the benchmarks considered in this chapter with the same gluino mass. This is mainly due to the lighter squark masses assumed in that study, giving rise to a larger cross section, but also partly due to the entire assumed spectrum being very different. These differences plays a crucial role in providing different p_T distributions for the leptons arising from gluino cascade decays between the different models.

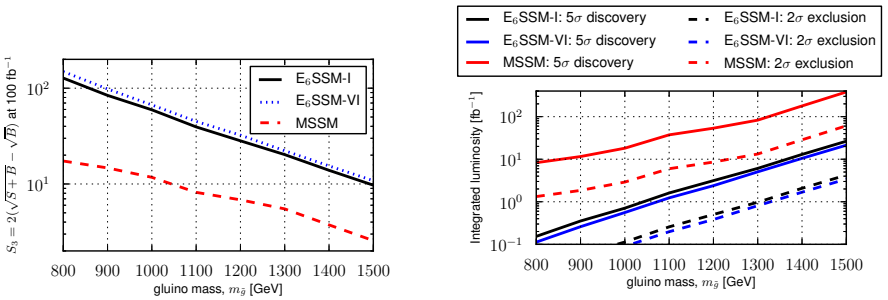

(a) Expected significance at 100 fb^{-1}, $\sqrt{s}$ = 14TeV

(b) Luminosity required for 5σ discovery and 2σ exclusion, $\sqrt{s} = 14$TeV

Figure 10.14: The gluino mass reach at $\sqrt{s}$ =14 TeV for the three lepton channel. The gluino mass has been varied for the benchmarks E$_6$SSM-I, E$_6$SSM-VI, and MSSM. The expected significance is calculated using the signal and background events surviving the cut $M_{\text{eff}} > m_{\tilde{g}}$. A K-factor of 3 has also been applied to the signal. Here at the higher collider energy the MSSM benchmark also becomes discoverable through this 3 lepton channel. The E$_6$SSM benchmarks are discoverable up to almost a 1500 GeV gluino mass.

10.3 Conclusions

There are many well motivated SUSY models and even though many are severely constrained by data, few are ruled out completely. If a SUSY discovery would occur it would be a delicate task to determine what model is correct. It is therefore important to investigate the differences between model predictions and how to tell them apart. This knowledge will also be important when interpreting limits on SUSY particles, which are very model dependent.

A generic prediction of all SUSY models is the gluino, which can be produced with a large cross-section at the LHC due to its colour octet nature. Moreover, in many SUSY models it may be the lightest coloured SUSY particle, which could make it the first SUSY particle to be discovered. However the gluino typically decays in cascade decays, via a chain of charginos and neutralinos, emitting jets or leptons at each stage of the decay chain, with the chain ending when the LSP is produced which is typically the lightest neutralino.

In this chapter we have discussed the gluino cascade decays in E_6 models, which include matter and Higgs filling out three complete 27 dimensional representations close to the TeV scale. In such models there are three families of Higgs doublets of both H_u and H_d kinds, plus three Higgs SM-singlets, similar to the NMSSM field, S. Only the third family acquire VEVs and the other two families do not and are called inert. All these Higgs states are accompanied by spin-1/2 SUSY partners, the Higgsinos. The extra inert charged and neutral Higgsinos, some of which are necessarily light, will mix with the usual MSSM charginos and neutralinos, yielding extra light states, providing extra

links in the gluino cascade decays, and hence extra jets and leptons, with less missing energy.

The extra neutralinos and charginos generically appearing in a large class of E_6 inspired models lead to distinctive signatures from gluino cascade decays in comparison to those from the MSSM. These signatures involve longer decay chains, more visible transverse energy, higher multiplicities of jets and leptons, and less missing transverse energy than in the MSSM. We have studied this effect in gluino cascade decays for the MSSM and E_6SSM and have shown that it can provide a characteristic and distinctive signature of the model, enabling an early discovery of the E_6SSM which may be discriminated from the MSSM.

In order to demonstrate this, we have first defined a rather large set of benchmark points within the E_6SSM. These benchmark points are chosen for the variety of ways in which the inert charginos and neutralinos can appear, and they all are chosen to have a nominal gluino mass of about 800 GeV, although this can be varied while keeping the inert chargino and neutralino masses unchanged. The results discussed below are remarkably robust, and apply to all of the E_6 benchmark points. These E_6 benchmarks are also compared to an MSSM benchmark which is chosen to have similar conventional (non-inert) chargino and neutralino masses to the E_6 ones, as well as mSUGRA points, in order to verify the model independence of the conclusions.

Given this set of benchmark points, we have then studied gluino pair production and decay at the LHC, first at 7 TeV, then at 8 TeV, and eventually at 14 TeV using a Monte Carlo analysis. We already know that the gluino was not discovered at 7 TeV, which motivates the nominal choice of gluino mass of 800 GeV. For this gluino mass, we have first studied the missing transverse momentum and effective mass distributions for representative benchmark points, and seen that the former has a softer spectrum in the E_6 models when compared to the MSSM, as expected, while the latter has a similar or slightly harder distribution in the effective mass variable. Staying at 7 TeV, we then calculated the lepton and jet multiplicities in E_6 models and showed that they are significantly higher than in the MSSM. This motivated a study of lepton channels with increasing numbers of leptons, and decreasing statistics, where we showed that the 3 lepton channel provided a very good discriminator between the MSSM and the E_6 models, although the statistics are rather too low at 7 TeV.

At 8 TeV we studied the 6 jet channel and showed that, in an effective mass analysis, a 1 TeV MSSM gluino may provide a similar limit to that of an 800 GeV E_6 gluino. Turning to the promising 3 lepton channels at 8 TeV, we find increased statistics and possible observable signals in this channel for a range of gluino masses, which would provide a striking confirmation of E_6 models. We calculate the required integrated luminosity in order to either discover or exclude the E_6 gluino in this channel at 8 TeV. We emphasise again that the MSSM gluino is unobservable in the 3 lepton channel.

Finally we have repeated the analysis for the promising 3 lepton channel at 14 TeV and found analogous results for required integrated luminosity to discover or exclude the E_6 gluino there as well.

In conclusion, the E_6 inspired models are clearly distinguishable from the MSSM in gluino cascade decays at the LHC with the full data set at 8 TeV, and certainly at 14 TeV, using the three lepton channel that we have proposed. Moreover, the present limits on the gluino mass, for example from a multijet analysis, are weaker (and therefore not applicable) for E_6 models in comparison with the MSSM, due to the longer decay chains with less missing transverse energy that is expected in E_6 models. We emphasise to the LHC experimental groups that the distinctive features present in gluino cascade decays, resulting in different search strategies including the choice of the kinematical variables, such as those discussed here, not only represents a unique footprint of a particular model but also may provide the key to an earlier discovery of supersymmetry.

Chapter 11

Little Z' models

So far in this thesis we have focused on the exploration of properties of typical SUSY particles, e.g. gluinos, neutralinos and pseudoscalar Higgs bosons. In this chapter we will instead focus on an extended gauge sector, specifically on the extra $U(1)'$ of E_6 inspired SUSY models and its Z' boson. Mass limits on extra gauge bosons give important information about BSM physics. In many models Z' bosons are linked with other sectors of the theory. For example, if the Z' gets its mass from a VEV, the mass limits constrain this VEV which in turn affects the Higgs sector. The E$_6$SSM is an example of such a model where the singlet VEV, which is responsible for the Z' mass, affect the Higgs sector and also many other particle masses of the model and will furthermore affect the fine-tuning of the model as will be discussed below. Measurements and limits on the Z' bosons are therefore very powerful when constraining and distinguishing models. In this chapter the effects of having a lighter and more weakly coupled Z' are discussed in terms of contributions to fine-tuning of the model and current exclusion limits.

The recently observed SM-like Higgs boson has a mass, $m_h = 125 - 126$ GeV [24, 25], which is within the range for it to be consistent with the lightest Higgs in supersymmetric models. In the MSSM the light Higgs mass at tree-level is bounded from above by the Z boson mass, M_Z, as we saw in Section 4.3.3. The large radiative contributions from stops needed to raise it to the observed value typically imply very large fine-tuning.

Conventional E_6 inspired SUSY models involve both a singlet generated μ term, denoted μ_{eff}, and a massive Z' gauge boson at the TeV scale. Such models can increase the tree level physical Higgs boson mass above the M_Z limit of the MSSM, due to both F-term contributions of the singlet and the D-term contributions associated with the Z', allowing lighter stop masses and hence reducing fine-tuning due to stop loops. The E$_6$SSM is an example of such a model, inspired by the E_6 group. It involves an extra singlet responsible for μ_{eff} and an extra $U(1)$ gauge symmetry at low energy, giving both new F-term and D-term contributions at tree level to the light Higgs mass, which is larger

than both the MSSM and the NMSSM. In the E$_6$SSM the light Higgs mass is given by,

$$m_h^2 \approx M_Z^2 \cos^2 2\beta + \frac{\lambda^2}{2} v^2 \sin^2 2\beta + g_1'^2 v^2 (Q_1 \cos^2\beta + Q_2 \sin^2\beta)^2 + \Delta m_h^2, \tag{11.1}$$

where Δm_h^2 represents loop corrections.

In (11.1) there are two extra terms proportional to v^2, relative to the MSSM, which contribute at tree level to the Higgs mass squared. This means that the E$_6$SSM permits lower stop masses than in the MSSM (or the NMSSM) corresponding to lower values required for the radiative correction term Δm_h^2. However, as we shall discuss, one of the minimisation conditions of the E$_6$SSM can be written in the form,

$$c\frac{M_Z^2}{2} = -\mu_{\text{eff}}^2 + \frac{(m_d^2 - m_u^2 \tan^2\beta)}{\tan^2\beta - 1} + d\frac{M_{Z'}^2}{2}, \tag{11.2}$$

where c, d are functions of $\tan\beta$ which are of order $\sim \mathcal{O}(1)$, m_d^2, m_u^2 are soft Higgs mass squared parameters, $M_{Z'} \sim g_1' s$ and $\mu_{\text{eff}} \sim \lambda s$ arise from the singlet VEV s. Written in this form it is clear that there is a new source of tree-level fine-tuning, due to the Z' mass squared term in (11.2), which will increases quadratically as $M_{Z'}^2$, eventually coming to dominate the fine-tuning for large enough values of $M_{Z'}$. This tree-level fine-tuning can be compared to that due to μ_{eff} which typically requires this quantity to be not much more than 200 GeV, and similar limits also apply to $M_{Z'}$. With the current CMS experimental mass limit for the Z' in the E$_6$SSM of $M_{Z'} \gtrsim 2.08$ TeV [213] it is clear that there is already a significant, perhaps dominant, amount of fine-tuning due to the Z' mass limit, and furthermore this source of fine-tuning increasing quadratically with $M_{Z'}$ will rapidly overtake the logarithmic fine-tuning due to the stop mass limits, as the experimental mass limits of both types of particles increases in the future. This was first pointed out in [214] and has been discussed quantitatively [215] in the framework of the constrained E$_6$SSM [196], where it has been verified that this new source of fine-tuning dominates over all other sources.

In this chapter we propose a new class of models called Little Z' models which differ from the usual class of E_6 models by having a reduced gauge coupling g_1' leading to the possibility of lower mass Z' bosons. Such a reduction in the gauge coupling g_1' at the unification scale has some motivation from F-theory constructions [216]. We show that reducing g_1' relaxes the experimental limit on the Z' mass, allowing a lighter value and hence reducing the tree-level fine-tuning associated with E_6 models. We show that, although for sufficiently small values of g_1' the new source of fine-tuning due to the Z' mass can be essentially eliminated, it does so at the expense of increasing the singlet vacuum expectation value, leading to overall fine-tuning similar to that in the MSSM. We emphasise that the main prediction of Little Z' models is the presence of weakly coupled low mass Z' resonances, perhaps as low as 200 GeV.

The layout of the remainder of the chapter is as follows. In Section 11.1 we discuss the Electroweak Symmetry Breaking (EWSB) conditions and the impact of the Z' mass on fine-tuning. Little Z' models are introduced in Section 11.2, where the experimental limits on such a boson are studied as a function of its mass and (reduced) gauge coupling. In Section 11.3 we briefly investigate the consequences of a reduced g_1' coupling in the Higgs sector. Section 11.4 concludes the chapter.

11.1 The Higgs potential and the EWSB conditions

The scalar Higgs potential is,

$$\begin{aligned} V(H_d, H_u, S) = {} & \lambda^2|S|^2(|H_d|^2 + |H_u|^2) + \lambda^2|H_d.Hu|^2 \\ & + \frac{g_2^2}{8}(H_d^\dagger \sigma_a H_d + H_u^\dagger \sigma_a H_u)(H_d^\dagger \sigma_a H_d + H_u^\dagger \sigma_a H_u) \\ & + \frac{g'^2}{8}(|H_d|^2 - |H_u|^2)^2 + \frac{g_1'^2}{2}(Q_1|H_d|^2 + Q_2|H_u|^2 + Q_s|S|^2)^2 \\ & + m_s^2|S|^2 + m_d^2|H_d|^2 + m_u^2|H_u|^2 \\ & + [\lambda A_\lambda S H_d.H_u + c.c.] + \Delta_{\text{Loops}} \end{aligned} \tag{11.3}$$

where, g_2, $g'(=\sqrt{3/5}g_1)$, and g_1' are the gauge couplings of $SU(2)_L, U(1)_Y$ (GUT normalized), and the additional $U(1)_N$, respectively. $Q_1 = -3/\sqrt{40}, Q_2 = -2/\sqrt{40}$, and $Q_s = 5/\sqrt{40}$ are effective $U(1)_N$ charges of H_u, H_d and S, respectively. m_s is the mass of the singlet field, and $m_{u,d} \equiv m_{H_{u,d}}$.

The Higgs field and the SM singlet acquire VEVs at the physical minimum of this potential,

$$< H_d >= \frac{1}{\sqrt{2}}\begin{pmatrix} v_1 \\ 0 \end{pmatrix}, \quad < H_u >= \frac{1}{\sqrt{2}}\begin{pmatrix} 0 \\ v_2 \end{pmatrix}, < S >= \frac{s}{\sqrt{2}}, \tag{11.4}$$

It is reasonable exploit the fact that $s \gg v$, which will help in simplifying our master formula for fine-tuning as will be seen in Section 4. Then, from the minimisation conditions,

$$\frac{\partial V_{E_6SSM}}{\partial v_1} = \frac{\partial V_{E_6SSM}}{\partial v_2} = \frac{\partial V_{E_6SSM}}{\partial s} = 0, \tag{11.5}$$

the Electroweak Symmetry Breaking (EWSB) conditions are,

$$\frac{M_Z^2}{2} = -\frac{1}{2}\lambda^2 s^2 + \frac{(m_d^2 - m_u^2\tan^2\beta)}{\tan^2\beta - 1} + \frac{g_1'^2}{2}\left(Q_1 v_1^2 + Q_2 v_2^2 + Q_s s^2\right)\frac{(Q_1 - Q_2\tan^2\beta)}{\tan^2\beta - 1} \tag{11.6}$$

$$\sin 2\beta \approx \frac{\sqrt{2}\lambda A_\lambda s}{m_d^2 + m_u^2 + \lambda^2 s^2 + \frac{g_1'^2}{2} Q_s s^2 (Q_1 + Q_2)}, \tag{11.7}$$

$$m_s^2 \approx -\frac{1}{2} g_1'^2 Q_s^2 s^2 = -\frac{1}{2} M_{Z'}^2, \tag{11.8}$$

where $M_Z^2 = \frac{1}{4}(g'^2 + g_2^2)(v_2^2 + v_1^2)$ and $M_{Z'}^2 \approx g_1'^2 Q_s^2 s^2$.

The condition (11.6) can be written,

$$\frac{M_Z^2}{2}\left(1 - \frac{g_1'^2}{g'^2 + g_2^2} P(\tan\beta) R(\tan\beta)\right) = -\left(\frac{\lambda s}{\sqrt{2}}\right)^2 + \frac{m_d^2 - m_u^2 \tan^2\beta}{\tan^2\beta - 1} + \frac{M_{Z'}^2}{2} R(\tan\beta) \tag{11.9}$$

where

$$R(\tan\beta) = \frac{Q_1 - \tan^2\beta Q_2}{\tan^2\beta - 1} \tag{11.10}$$

and

$$P(\tan\beta) = 4\left(\frac{Q_1(1 - \frac{Q_1}{Q_S}) + \tan^2\beta Q_2(1 - \frac{Q_2}{Q_S})}{\tan^2\beta + 1}\right) \tag{11.11}$$

If one takes $g_1' = 0$ we have $M_{Z'} = 0$ and the factor in front of M_Z^2 in (11.9) is equal to one and we recover the well known MSSM relation between M_Z, $\mu (= s\lambda/\sqrt{2})$ and the soft Higgs masses m_1, m_2 we derived in (4.13). Written in this form, which may be compared to (11.2) but with the coefficients c, d explicitly given, it is clear that fine-tuning will increase quadratically as $M_{Z'}$ increases.

To avoid any fine-tuning we would like to keep $\mu \sim M_{Z'} \sim 200$ GeV or less. This motivates the main idea of this chapter, namely to relax the CMS experimental mass limit of $M_{Z'} \gtrsim 2.08$ TeV [213] down to $M_{Z'} \sim 200$ GeV by reducing its gauge coupling g_1'. Indeed, as we shall see, such a low value of $M_{Z'} \sim 200$ GeV may be made consistent with the experimental limit by choosing $g_1' \sim 10^{-2} \times 0.46$ and $s \sim 20 \times 2.75 \sim 55$ TeV. In order to keep μ close to the electroweak scale this requires a very small value of $\lambda \sim g_1'$. In Figure 11.1 the contribution $\Delta_{M_{Z'}}$ to fine-tuning from $M_{Z'}$ is plotted, where the measure of fine-tuning[217] due to $M_{Z'}$, $\Delta_{M_{Z'}}$ is defined as

$$\Delta_{M_{Z'}} = \frac{M_{Z'}^2}{M_Z^2}\frac{\partial M_Z^2}{\partial M_{Z'}^2} = \frac{\partial \log M_Z^2}{\partial \log M_{Z'}^2}. \tag{11.12}$$

We emphasise that the appearance of $M_{Z'}$ in the tree-level minimisation condition is characteristic of all SUSY Z' models where the usual Higgs doublets carry $U(1)'$ charges (e.g. it applies to all E_6 models but not, for example the $U(1)_{B-L}$ model.) This provides a motivation for Little Z' models in which the extra gauge coupling g_1' is reduced and the experimental lower bound on $M_{Z'}$ may be relaxed.

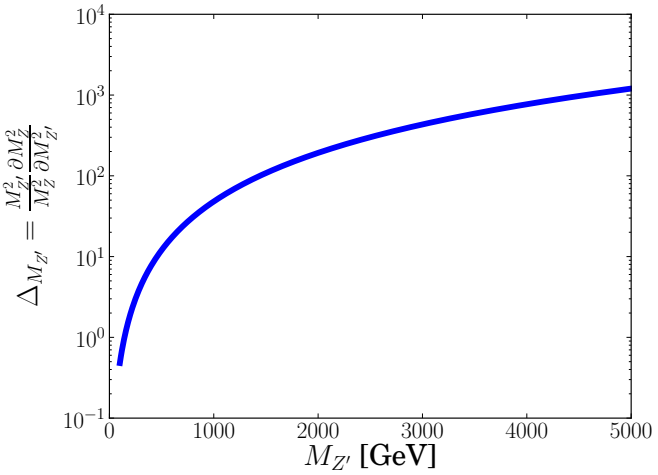

Figure 11.1: Contribution to fine-tuning from the Z' mass.

11.2 Little Z' Models

In general Little Z' Models can be defined by the gauge group

$$SU(3)_c \times SU(2)_L \times U(1)_Y \times U(1)' \tag{11.13}$$

where the SM is augmented by an additional $U(1)'$ gauge group with a gauge coupling g'_1 which is significantly smaller than the hypercharge gauge coupling g'. The $U(1)'$ gauge group is broken at low energies giving rise to a massive Z' gauge boson with couplings to a SM fermion f given by [186]:

$$\mathcal{L}_{NC} = \frac{g'_1}{2} Z'_\mu \bar{f} \gamma^\mu (g_V^f - g_A^f \gamma^5) f.$$

The values of g_V^f, g_A^f depend on the particular choice of $U(1)'$ and on the particular fermion f. We assume universality amongst the three families. More explicitly, this assumption implies that $g_V^u = g_V^c = g_V^t$, $g_V^d = g_V^s = g_V^b$, $g_V^e = g_V^\mu = g_V^\tau$, and $g_V^{\nu_e} = g_V^{\nu_\mu} = g_V^{\nu_\tau}$ for up-quarks, down-quarks, charged leptons and neutrinos respectively. The axial couplings, g_A^f, behave accordingly.

In a given model there are eight model dependent couplings of the extra Z' boson to SM fermions, that is $g_{V,A}^f$ with $f = u, d, e, \nu_e$. These are fixed by group theory, so cannot be changed for a given model. However the low energy $U(1)'$ gauge coupling g'_1 is fixed by a unification condition. E.g. in E$_6$SSM $g'_1 \approx 0.46$ which is approximately equal to the (GUT normalised) hypercharge gauge coupling. If unification of g'_1 with the other gauge couplings is relaxed, then g'_1 becomes a free parameter. In this chapter we are interested in taking it to be smaller than the GUT prediction, namely we shall consider $g'_1 \ll g' \approx 0.46$, keeping g_V^f, g_A^f fixed at their model predictions.

Specializing to the charged lepton pair production cross-section relevant for the first runs at the LHC, the cross-section may be written at the leading order (LO) as [186]:

$$\sigma^{LO}_{\ell^+\ell^-} = \frac{\pi}{48s}\left[c_u w_u(s, M^2_{Z'}) + c_d w_d(s, M^2_{Z'})\right] \tag{11.14}$$

where the coefficients c_u and c_d are given by:

$$c_u = \frac{g_1'^2}{2}(g_V^{u\,2} + g_A^{u\,2})Br(\ell^+\ell^-), \qquad c_d = \frac{g_1'^2}{2}(g_V^{d\,2} + g_A^{d\,2})Br(\ell^+\ell^-), \tag{11.15}$$

and $w_u(s, M^2_{Z'})$ and $w_d(s, M^2_{Z'})$ are related to the parton luminosities $\left(\frac{dL_{u\bar{u}}}{dM^2_{Z'}}\right)$ and $\left(\frac{dL_{d\bar{d}}}{dM^2_{Z'}}\right)$ and therefore only depend on the collider energy and the Z' mass. All the model dependence of the cross-section is therefore contained in the two coefficients, c_u and c_d. These parameters can be calculated from g^f_V, g^f_A and g'_1, assuming only SM decays of the Z' boson. Note that the cross-section is proportional to g'^2_1 and will therefore be reduced in Little Z' models in which $g'_1 \ll g' \approx 0.46$.

A given model such as the E_6SSM [179] appears as a point in the $c_d - c_u$ plane, assuming that the low energy $U(1)'$ gauge coupling g'_1 is fixed by a unification condition. If we relax the unification condition then the point will become a line in the $c_d - c_u$ plane, since each of c_u and c_d are proportional to g'^2_1 and the points on the line will approach the origin as $g'_1 \to 0$. For example in the E_6SSM we have:

$$c_u = 5.94 \times 10^{-4}\left[\frac{g'_1}{0.46}\right]^2, \quad c_d = 1.48 \times 10^{-3}\left[\frac{g'_1}{0.46}\right]^2. \tag{11.16}$$

Since the experimental Z' mass contours in the $c_d - c_u$ plane are fixed for a given limit on the cross-section, the effect of reducing g'_1 will not change those contours. The only effect of reducing g'_1 is to move the model point in the $c_d - c_u$ plane closer to the origin, resulting in a reduced experimental limit on the Z' mass. See for example [186] where this approach is followed for conventional Z' models. Although this provides a simple way to understand qualitatively why the experimental limits are relaxed by reducing g'_1, it turns out that for the lower mass Z' signal regions backgrounds and other constraints become more important for this reason we shall not present our results in the $c_d - c_u$ plane.

In the E_6SSM the Z' mass is given to good approximation by:

$$M^2_{Z'} = g'^2_1 v^2\left(\tilde{Q}_1^2 \cos^2\beta + \tilde{Q}_2^2 \sin^2\beta\right) + g'^2_1 \tilde{Q}_S^2 s^2 \approx g'^2_1 \tilde{Q}_S^2 s^2\,, \tag{11.17}$$

where the charges are $\tilde{Q}_S = 5/\sqrt{40}$, $\tilde{Q}_1 = -3/\sqrt{40}$, $\tilde{Q}_2 = -2/\sqrt{40}$. The last approximation in (11.17) assumes $s \gg v$ where we can neglect the terms involving the electroweak VEV $v = 246$ GeV. What is the effect of reducing g'_1 in this model? On the one hand,

reducing g'_1 will reduce $M_{Z'}$ in direct proportion, since $M_{Z'} \propto g'_1$ for a fixed value of s. On the other hand, reducing g'_1 will reduce the cross-section since $c_{u,d} \propto {g'_1}^2$ (see (11.16)).

In order to evaluate the experimental limits on Little Z' models we have used the experimental data on the cross-section limits rather than performing our own fast detector MC simulations which could never be as reliable. Using this data we have generated exclusion plots in the $g'_1 - M_{Z'}$ plane. It is worth pointing out that such a compilation of the different limits from LEP, Tevatron and LHC in the $g'_1 - M_{Z'}$ plane is both novel and useful in identifying viable regions of parameters space for Little Z' models.

We emphasise that the narrow width approximation is particularly suitable for Little Z' models in which the reduced g' coupling leads to a correspondingly a reduced Z' boson width. It has been shown that limits in the case of narrow Z' resonances are very straightforward since they are free from finite width and interference effects [186]. Also, one should mention that, in the case of a narrow Z', the experimental mass resolution would be mainly determined by the calorimeter resolution. Therefore, taking into account these considerations, the estimation of the Z' limits we present below is essentially model-independent.

The procedure we follow in order to estimate limits in the $g'_1 - M_{Z'}$ plane is somewhat involved, since we have evaluated cross sections for Z' production at the Tevatron and the LHC collider taking into account QCD NNLO effects as implemented in the WZPROD program [218, 219, 220]. We have adopted this package for simulating the Z' production, and have linked it to an updated set of PDFs. This set includes in particular the most recent versions of CTEQ6.6 [157, 221] and MSTW08 [222] PDF's, which we use in our analysis. The code can be provided upon request.

Using this approach we have converted experimental limits on the $\sigma \times Br$ versus $M_{Z'}$ to limits on the coupling g'_1 versus $M_{Z'}$. In Figure 11.2 we show the results of our analysis for the cross section for lepton (e, μ) pair-production via Z' at LHC at $\sqrt{s} = 8$ TeV in the g'_1 – $M_{Z'}$ plane for the Little Z' models with charges corresponding to the E$_6$SSM. The horizontal, dashed line indicates the standard GUT predicted g'_1 value. The dash-dotted lines are cross section limits on the E$_6$SSM Z' from D$\emptyset$[223], CMS [213, 197] and ATLAS[224] that we have converted to limits on the coupling g'_1.

The estimated indirect exclusion limits from electro-weak precision tests (EWPT)[225, 18, 226], mostly by LEP, on the ratio $\frac{M_{Z'}}{g'_1}$ are plotted with red crosses. These are not available for the E$_6$SSM but the limit for the $U(1)_\chi$ Z' is

$$\frac{M_{Z'}}{g'_1} > 3.8 \text{ TeV},$$

$g_1'/0.46$	1	1/2	1/10	1/15	
$s >$	5.5	9.3	16.5	~ 11	[TeV]
$M_{Z'} >$	2	1.7	0.6	~ 0.2	[TeV]
$\Delta_{M_{Z'}} >$	192	139	17	~ 1	

Table 11.1: Scenarios with different values of g_1' for the Little Z' models with charges corresponding to the E$_6$SSM. The Z' mass and thus its source of fine-tuning, $\Delta_{M_{Z'}} = \frac{M_{Z'}^2}{M_Z^2}\frac{\partial M_Z^2}{\partial M_{Z'}^2}$, can be reduced by reducing g_1' at the cost of increasing the singlet VEV, s. Because experimental limits on the cross section get weaker in the low mass region the limit on s gets slightly weaker, hence the weaker limit on s in the case of $g_1' = 0.46/15$.

and the limit for the $U(1)_\psi$ Z' is

$$\frac{M_{Z'}}{g_1'} > 2.5 \text{ TeV}.$$

As an estimate of these limits for the E$_6$SSM, we plot with red crosses an intermediate limit

$$\frac{M_{Z'}}{g_1'} \gtrsim 3.0 \text{ TeV}.$$

Figure 11.2 also shows contours of constant values of the singlet VEV s, so it is possible to read off exclusions limits on s. At large masses the limits from ATLAS and CMS follow the cross section contours well but in the low mass regime the SM background is large which weakens the limits on the cross section. In this region, just above 200 GeV, the direct searches by the LHC and Tevatron experiments place the strongest bounds on the coupling and all place limits of about $g_1' < 0.03$.

It is obvious from Figure 11.2 that it is possible to lower the limit on $M_{Z'}$ by decreasing the coupling g_1' but by doing this the value of the singlet VEV, s, generally has to increase. The limit on s is however strongest for $M_{Z'}$ of about 500-800 GeV and gets slightly relaxed in the lowest mass region, 200-500 GeV. Examples of how the limits on $M_{Z'}$, s and the fine-tuning with respect to $M_{Z'}$ changes as the coupling g_1' decreases are tabulated in Table 11.1.

11.3 Higgs mass spectrum with reduced g_1'

Let us now investigate what happens to the Higgs sector of the E$_6$SSM in the case of a reduced g_1' coupling. If we use the fact that $g_1' \ll 1$ and also keep in mind that $s \gg v$ the tree level Higgs mass squared matrix elements in the $(v, 0, s)$-basis in (9.16) reduce

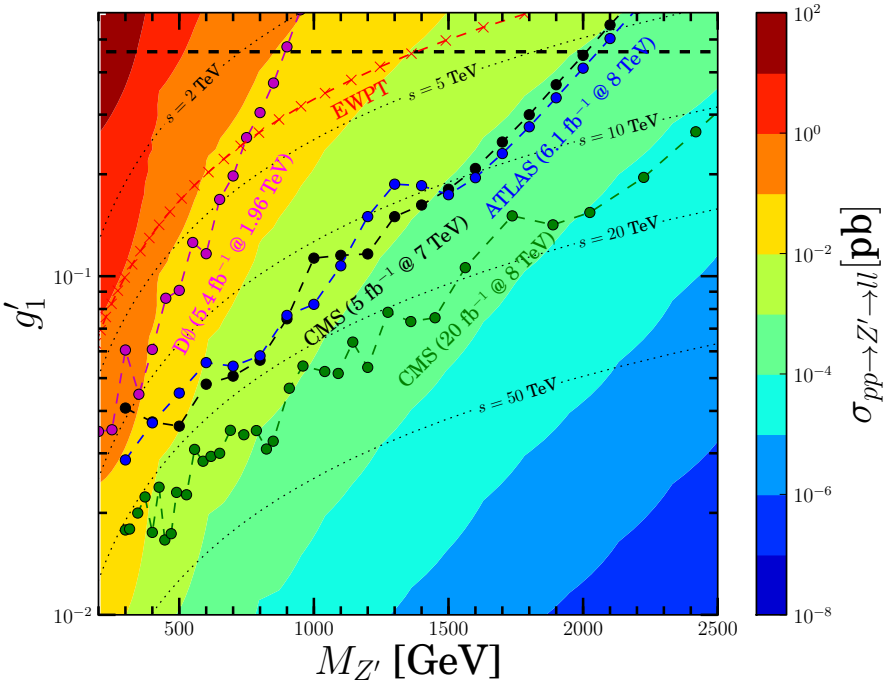

Figure 11.2: Cross section for lepton (e, μ) pair-production via Z' at LHC at $\sqrt{s} = 8$ TeV in the g'_1 – $M_{Z'}$ plane for Little Z' models with charges corresponding to the E$_6$SSM. The horizontal, dashed line indicates the standard GUT predicted g'_1 value. Exclusion limits from direct searches are plotted with dash-dotted lines in magenta, black, green and blue for DØ, CMS 7 TeV, CMS 8 TeV and ATLAS respectively. Indirect constraint on the mass-coupling ratio from electro-weak precision tests taking into account a fit of 18 EWPT parameters[18] are plotted with red crosses and coincides with the contour for the singlet VEV $s \approx 4$ TeV.

to

$$M_{11}^2 = \frac{\lambda^2 v^2}{2} \sin^2 2\beta + \frac{\bar{g}^2 v^2}{4} \cos^2 2\beta \tag{11.18}$$

$$M_{12}^2 = \left(\frac{\lambda^2}{4} - \frac{\bar{g}^2}{8} \right) v^2 \sin 4\beta \tag{11.19}$$

$$M_{22}^2 = M_A^2 + \left(\frac{\bar{g}^2}{4} - \frac{\lambda^2}{2} \right) v^2 \sin^2 2\beta \tag{11.20}$$

$$M_{23}^2 = -M_A^2 \frac{v}{s} \frac{\sin 4\beta}{4} \tag{11.21}$$

$$M_{13}^2 = -M_A^2 \frac{v}{s} \frac{\sin^2 2\beta}{2} + \lambda^2 v s \tag{11.22}$$

$$M_{33}^2 = M_A^2 \frac{v^2}{s^2} \frac{\sin^2 2\beta}{4} + M_{Z'}^2. \tag{11.23}$$

The upper bound on the mass of the SM-like Higgs boson is set by the element M_{11}^2. The value of λ determines what term in M_{11}^2 could be the largest.

One of the motivations for this model is that it is easier to achieve a large Higgs mass than in the MSSM, due to the extra tree-level contribution proportional to λ. If we want to keep this motivation, λ has to be large otherwise the MSSM tree-level bound holds. For $\lambda > \bar{g}/\sqrt{2} \approx 0.5$ the maximum upper bound is

$$M_{h_1}^{\max} = \frac{\lambda v}{\sqrt{2}} \tag{11.24}$$

and is achieved for $\tan\beta = 1$. If this occurs the heavy Higgs-like state, H, associated with the mass squared element M_{22}^2 decouples from the other two states, h and S, and gets a mass

$$M_H = \sqrt{M_A^2 + M_Z^2 - M_{h_1}^{\max\,2}}. \tag{11.25}$$

The remaining two eigenstates get a mass matrix,

$$\begin{pmatrix} \frac{\lambda^2 v^2}{2} & \frac{1}{\varepsilon}\left(\frac{\lambda^2 v^2}{2} - M_A^2\varepsilon^2\right) \\ \frac{1}{\varepsilon}\left(\frac{\lambda^2 v^2}{2} - M_A^2\varepsilon^2\right) & M_A^2\varepsilon^2 + M_{Z'}^2 \end{pmatrix}, \tag{11.26}$$

where $\varepsilon = \frac{v}{2s} \ll 1$. The matrix has the eigenvalues

$$\begin{aligned} M_{h_1,h_2}^2 =& \frac{1}{2}\Bigg[\frac{\lambda^2 v^2}{2} + M_A^2\varepsilon^2 + M_{Z'}^2 \\ & \mp \sqrt{\left(M_{Z'}^2 + M_A^2\varepsilon^2 - \frac{\lambda^2 v^2}{2}\right)^2 + \frac{4}{\varepsilon^2}\left(\frac{\lambda^2 v^2}{2} - M_A^2\varepsilon^2\right)^2}\Bigg]. \end{aligned} \tag{11.27}$$

The maximum $M_{h_1} = M_{h_1}^{\max}$ is achieved when

$$\frac{\lambda^2 v^2}{2} = M_A^2\varepsilon^2 \quad \Rightarrow \quad \lambda = \frac{M_A}{s\sqrt{2}}, \tag{11.28}$$

in which case mixing between the states vanish and their masses are

$$\begin{aligned} M_{h_1} =& \frac{\lambda v}{\sqrt{2}} \\ M_{h_2} =& \sqrt{M_{h_1}^2 + M_{Z'}^2}. \end{aligned} \tag{11.29}$$

Since the mass-squared splitting is inversely proportional to ε, the relation in (11.28) must approximately hold even away from the maximum to avoid negative eigenvalues. As one moves away from the small $\tan\beta$ limit or if $\lambda < \bar{g}/\sqrt{2} \approx 0.5$ the maximum of the lightest Higgs mass goes to the MSSM value, M_Z. This behaviour is shown in Figure 11.3 where the maximum mass of the lightest Higgs boson in the $\lambda - \tan\beta$-plane is plotted for $s = 50$ TeV, $M_{Z'} = 300$ GeV and M_A is numerically chosen to provide the maximum, under the condition that $M_A < 100$ TeV. The reason why large λ is disfavoured for large $\tan\beta$ is only due to the artificial bound on M_A. For $s = 50$ TeV

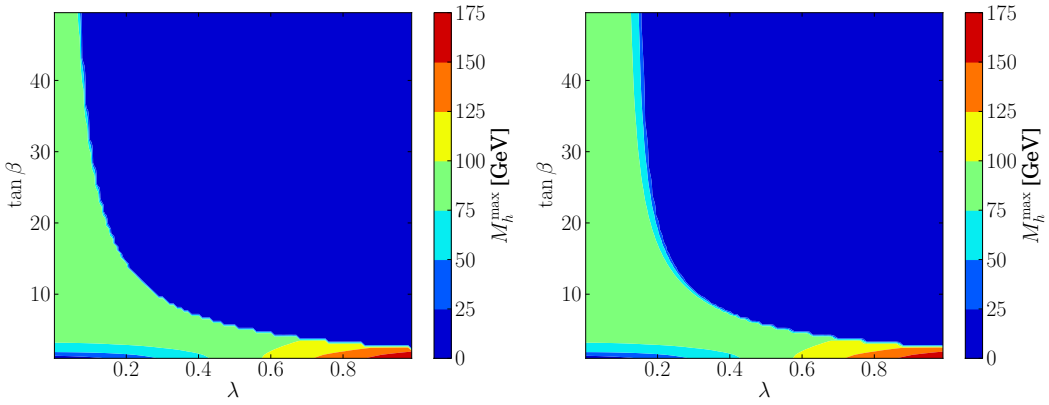

Figure 11.3: Contours for the maximum of the lightest Higgs mass for $s = 50$ TeV and $M_{Z'} = 300$ GeV (Left) and 3000 GeV (Right), where $M_A < 100$ TeV. The allowed region for large $\tan\beta$ is broaden somewhat by a larger $M_{Z'}$.

and $M_A < 100$ TeV the region of large $\tan\beta$ and large λ is not allowed since the lightest Higgs mass squared is negative there. To avoid generating a negative eigenvalue the mixing element M_{13}^2 must be close to zero. Generalising the condition (11.28) to include $\tan\beta$ gives the condition

$$\lambda \approx \frac{M_A}{s\sqrt{2}} \sin 2\beta \tag{11.30}$$

and since we assumed $M_A < 2s$ we need $\lambda \lesssim \sqrt{2} \sin 2\beta$. A large value of $M_{Z'}$ relaxes this condition slightly by making the diagonal element M_{33}^2 larger, which can be seen by comparison of the two plots in Figure 11.3. Leading order one- and two-loop contributions to the upper bound on the SM-like Higgs mass are independent of g_1' and will contribute at most around 20 GeV. The maximum is however no longer for the same ratio of M_A to s.

As the g_1' was taken small, a large region of parameter space which was motivated by an increased tree-level contribution to the Higgs mass due to D-terms from the $U(1)'$ group was lost. This loss is illustrated in Figure 11.4 where in the left plot the coupling has the standard value $g_1' \approx 0.46$ while in the right plot $g_1' \approx 0.0076$. The NMSSM-like region for small $\tan\beta$, which is motivated by providing a large tree-level Higgs mass, is shown in more detail in Figure 11.5.

11.4 Conclusion

In this chapter we have explicitly illustrated how the fine-tuning of E_6 inspired models depends on the Z' mass. The current experimental limits from the LHC on the Z' boson mass of 2-3 TeV raises the fine-tuning in these models to undesirably high levels. This is a generic property of SUSY models where the Higgs doublets carry a $U(1)'$ charge. In order to solve this problem we have proposed a new class of models called *Little*

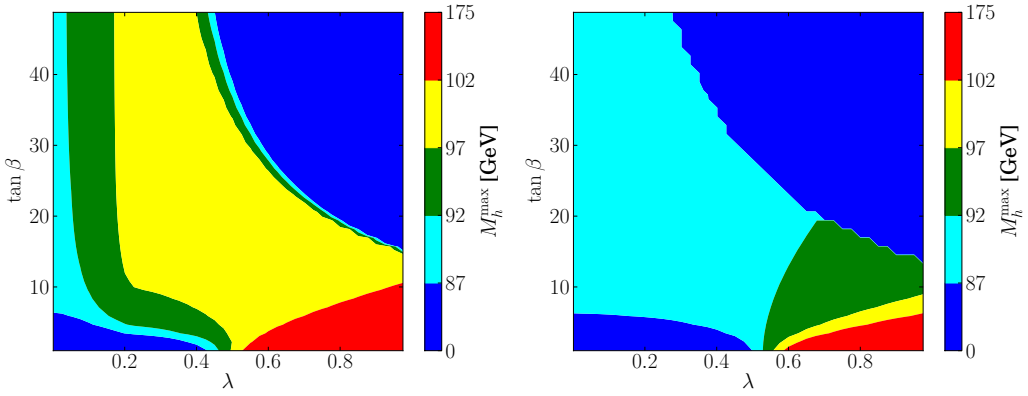

Figure 11.4: Contours for the maximum of the lightest Higgs mass for $s = 8.3$ TeV and $M_{Z'} = 3000$ GeV (Left), and for $s = 50$ TeV and $M_{Z'} = 300$ (Right). The maximum is chosen for a pseudoscalar mass $M_A < 10s$. In the blue regions the mass is essentially zero or imaginary. MSSM-like values close to M_Z are shown in cyan. The green region shows small enhancements ($\lesssim 5$ GeV) and the yellow region shows an additional small enhancement ($\lesssim 5$ GeV) in which the maximum D-term contribution occurs. The red region show the large enhancements of the NMSSM-like region at small $\tan\beta$ which is illustrated in more detail in Figure 11.5.

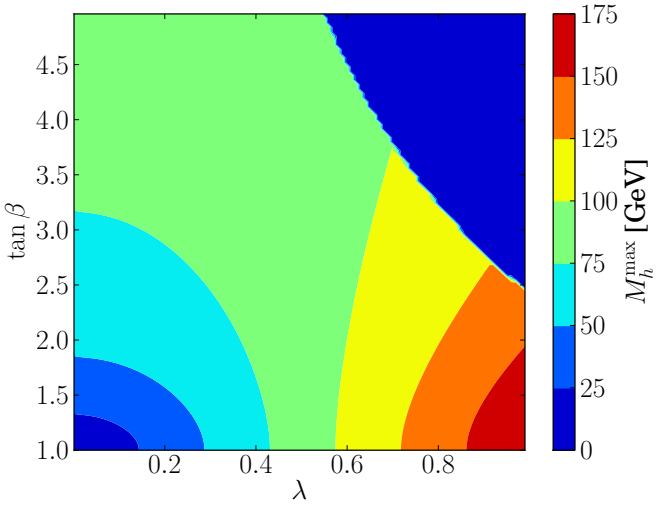

Figure 11.5: Contours for the maximum of the lightest Higgs mass for $s = 50$ TeV and $M_{Z'} = 300$ GeV, where $M_A < 100$ TeV.

Z' models involving a weakly coupled lower mass Z'. These models can originate from supersymmetric E_6 inspired supersymmetric models where the spontaneously broken extra $U(1)'$ gauge group has a reduced gauge coupling.

We have shown that reducing the value of the extra gauge coupling relaxes these limits, leading to the possibility of low mass Z' resonances, for example down to about 200 GeV, thereby reducing fine-tuning due to the Z' mass down to acceptable levels. Such

a reduced extra gauge coupling does not affect conventional gauge coupling unification of the strong, weak and electromagnetic gauge couplings and in fact is well motivated in certain classes of F-theory models. We emphasise the main experimental prediction of such Little Z' models which is the appearance of a low mass weakly coupled Z' which may yet appear in future LHC searches. Although the source of tree level fine-tuning due to the Z' mass is reduced in Little Z' models, it does so at the expense of increasing the singlet vacuum expectation value, leading to overall fine-tuning similar to that in the MSSM.

We have also investigated the consequences on the tree-level mass spectrum in the Higgs sector. The reduced extra gauge coupling narrows down the region of parameter space where one can achieve a larger tree-level Higgs mass than in the MSSM. The remaining attractive region is in the NMSSM-like part of the parameter space, with large λ and small $\tan\beta$. Furthermore, the pseudoscalar Higgs mass, is forced to be of about the same order as the singlet VEV to not cause significant mixing between h and S which would push a mass squared eigenvalue negative. A larger Z' mass relaxes this constraint slightly.

Chapter 12

Conclusions and outlook

In this thesis different aspects of distinguishing models of new physics at the LHC has been discussed. The work has been focused mainly on supersymmetric models, specifically the MSSM and the E_6SSM, but many arguments and methods could often be transferred to a wider class of BSM models. We have seen that even though the LHC has not yet confirmed the existence of BSM physics there is still hope for discoveries after the upgrade to a higher collision energy and acquisition of more data. The LHC has a great potential of revealing what physics lie behind the electro-weak scale and the properties of the recently discovered Higgs boson.

We have shown how the LHC, in some still plausible scenarios, has the capability of measuring the width of a heavy or pseudoscalar Higgs boson, which occurs in SUSY models. The measurement is made possible when an enhanced coupling to muons allows for detecting and analysing the comparatively rare di-muon events with the high-resolution muon detectors. The precise mass and width measurements of such a particle are important for determining the parameter $\tan\beta$ which is an essential ingredient to differentiate between certain scenarios and models.

The task of distinguishing between a minimal realisation of SUSY and a non-minimal one has also been investigated. We have studied benchmarks from the MSSM and E_6SSM and quantitatively shown how much they will differ in tri-lepton signatures from gluino cascade decays. The importance of multi-lepton channels for more complex models, with more low-energy matter and longer decay chains has been illustrated by a thorough analysis. The typical feature shown is that if gluinos are appearing in multi-jet channels the MSSM gluinos will not give any signal in the multi-lepton channels while gluinos from models with an extended particle content such as the E_6SSM will show a signal also in these channels. The basic reasons for this is that models with more particles cause the gluino decay chains to be longer with more final state particles and less missing transverse momentum from the LSP. This causes the 0-lepton searches where

cuts on missing transverse momentum are important to be less effective and multi-lepton searches to be more effective, due to the increased lepton-multiplicity.

Many BSM models predict a Z' boson, e.g. GUT inspired models, technicolour models and models of extra dimensions. The measurement of, or the limit on, the mass of the Z' boson is therefore undoubtedly an interesting piece of information. The mass is in many models a contribution to fine-tuning and thus a measure of how attractive a model is. Furthermore, in many models, e.g E_6-inspired models, the properties of the Z' connects to many other parts of the model. In the E$_6$SSM for example, the singlet VEV which is responsible for the Z' mass has a great influence in the chargino and neutralino sectors, it affects the Higgs sector and sets the scale for coloured exotics. By combining predictions and measurements from different sectors the Z' mass becomes an important ingredient when distinguishing models. We have investigated the possibility of low-mass, weakly coupled Z' bosons in E_6-inspired models with a reduced gauge coupling g'_1. The reduced coupling allows for a lower Z' mass, but is also removing the attractive D-term contributions to the Higgs mass, leaving only the NMSSM-like low $\tan\beta$ region as a motivation for larger tree-level Higgs mass. The existence of such a light Z' would typically also force the singlet VEV to be very large and consequently, if one wants to avoid huge fine-tuning with respect to the μ-parameter, the model would have to be very MSSM-like in many aspects.

The connection between LHC phenomenology and dark matter has been emphasised several times throughout the thesis. We have shown examples of how model predictions of the relic density and direct detection cross sections can influence the predictions at the LHC where you would expect to produce the DM particles and its properties are important. From another point of view we have also touched upon the possibility of making predictions of dark matter properties from measurements at colliders, when exploring the resonance annihilation of DM via di-muon signatures at LHC. Both theoretical predictions and detection measurements of dark matter are somewhat inconclusive since mechanisms of dark matter may be modified slightly and measurements disagree on observations. However, dark matter serves as an interesting test for models and may provide evidence which indicate what models are more attractive than others.

In this thesis only a few of the huge amount of proposed models of physics beyond the SM has been discussed. After a discovery there will be a long and difficult project to determine what models are ruled out and which ones that are more likely to explain the data. A first step in taking on such a project is the collection of models and their signatures, which has begun at the HEPMDB, where one also can compare models on the level of Monte Carlo event analysis. Not only is just few of all proposed BSM models discussed in this thesis but also just a few of all proposed methods of distinguishing peculiar features of models discussed here. A structured and systematic collection of methods on how to distinguish particular scenarios would be extremely useful. The collection and implementation of such methods and algorithms, which can distinguish

subtle differences between models, into a database like HEPMDB would benefit the exploration and validation of BSM models greatly.

Appendix A

Gluino Decay Diagrams for Benchmarks

This appendix displays the possible gluino decays of each benchmark in a more complete fashion. Horizontal lines representing particle states are separated proportionally to their mass difference. Some exceptions are made where states are closely degenerate, in which case the lines have been separated more. An arrow then connects lines where possible decays occur with the corresponding branching ratio written above. The gluino decays of the MSSM benchmark is shown in Figure A.1(a), E_6SSM-I in Figure A.1(b), E_6SSM-II in Figure A.1(c), E_6SSM-III in Figure A.1(d), E_6SSM-IV in Figure A.1(e), E_6SSM-V in Figure A.1(f) and E_6SSM-VI in Figure A.1(g).

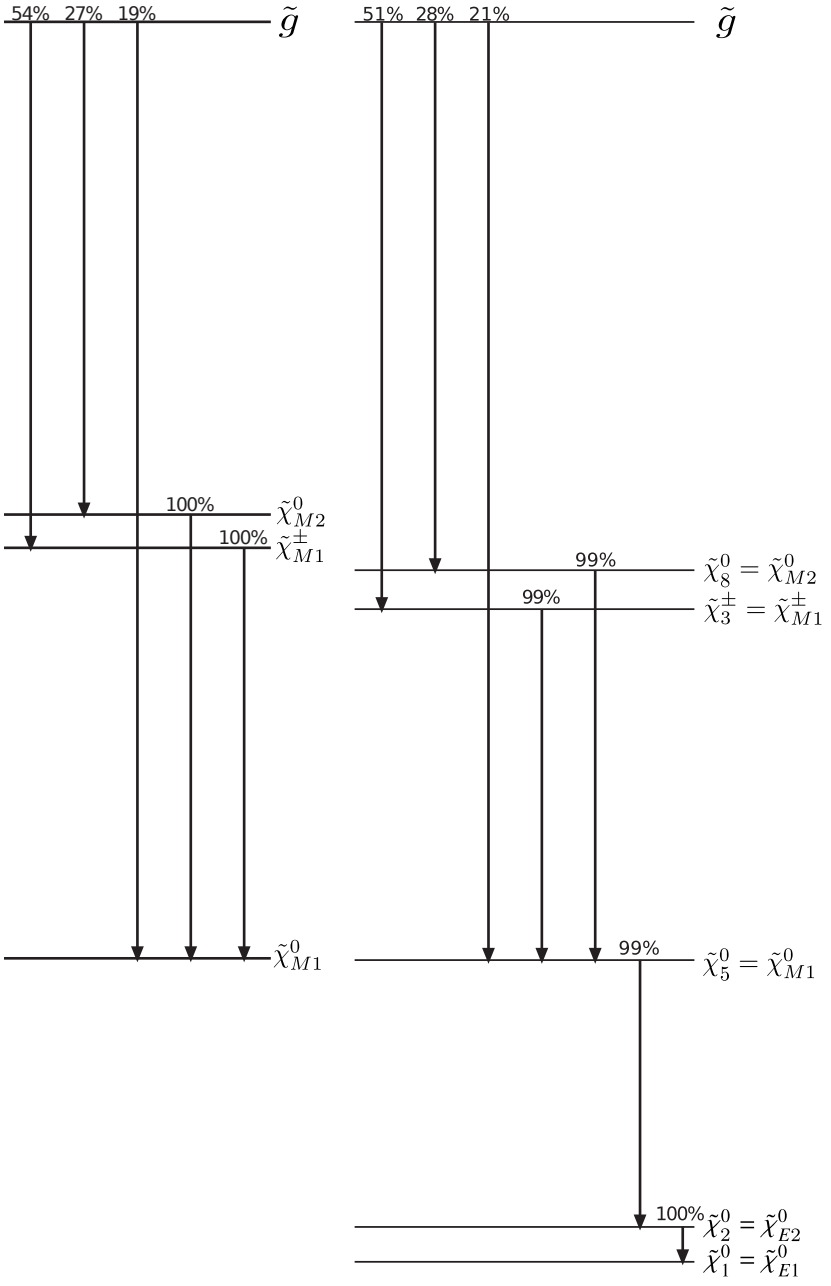

(a) MSSM (b) E_6SSM-I

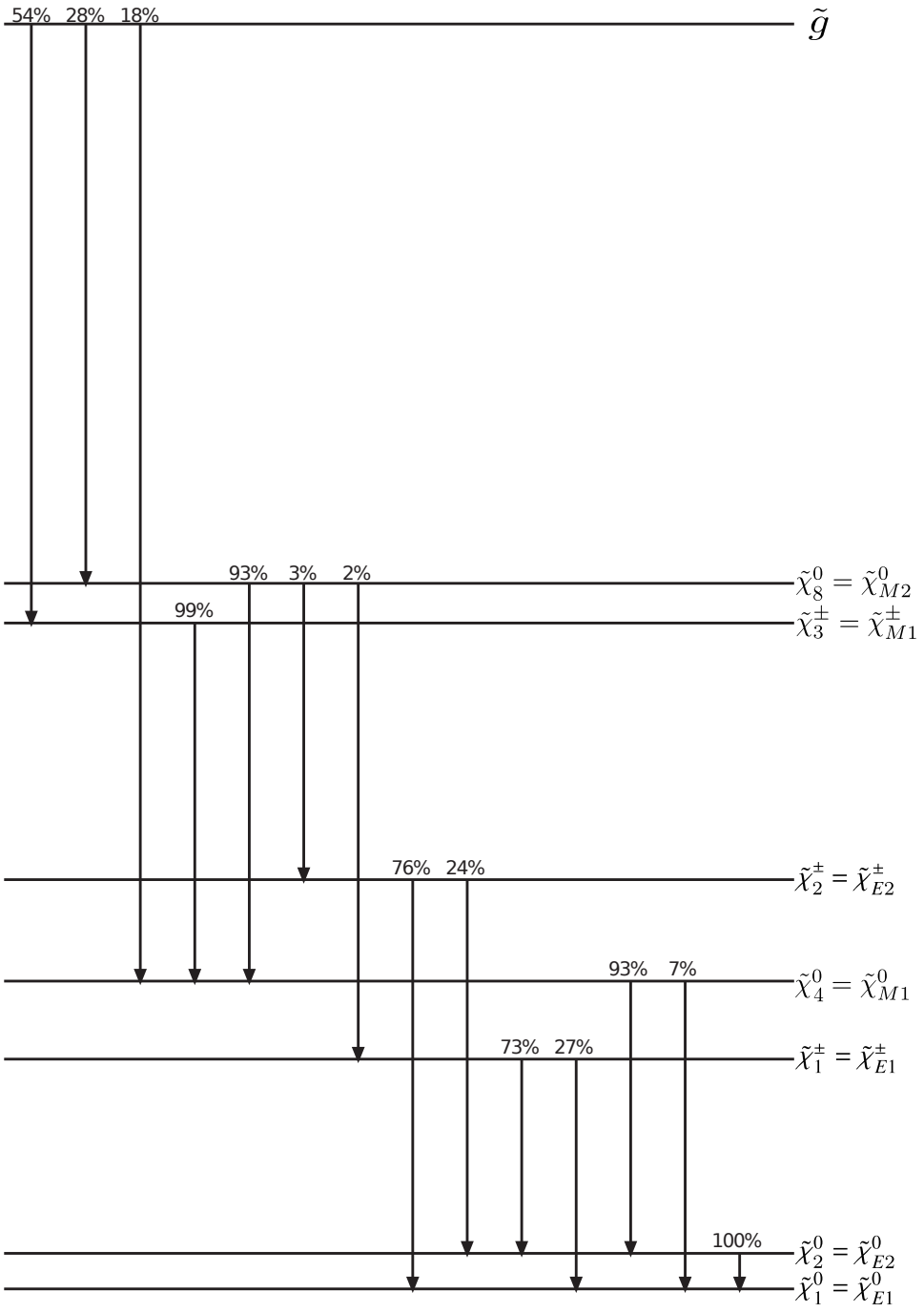
54%
28%
18%
$\tilde{g}$
93%
3%
2%
$\tilde{\chi}_8^0 = \tilde{\chi}_{M2}^0$
99%
$\tilde{\chi}_3^\pm = \tilde{\chi}_{M1}^\pm$
76%
24%
$\tilde{\chi}_2^\pm = \tilde{\chi}_{E2}^\pm$
93%
7%
$\tilde{\chi}_4^0 = \tilde{\chi}_{M1}^0$
73%
27%
$\tilde{\chi}_1^\pm = \tilde{\chi}_{E1}^\pm$
100%
$\tilde{\chi}_2^0 = \tilde{\chi}_{E2}^0$
$\tilde{\chi}_1^0 = \tilde{\chi}_{E1}^0$

(c) E_6SSM-II

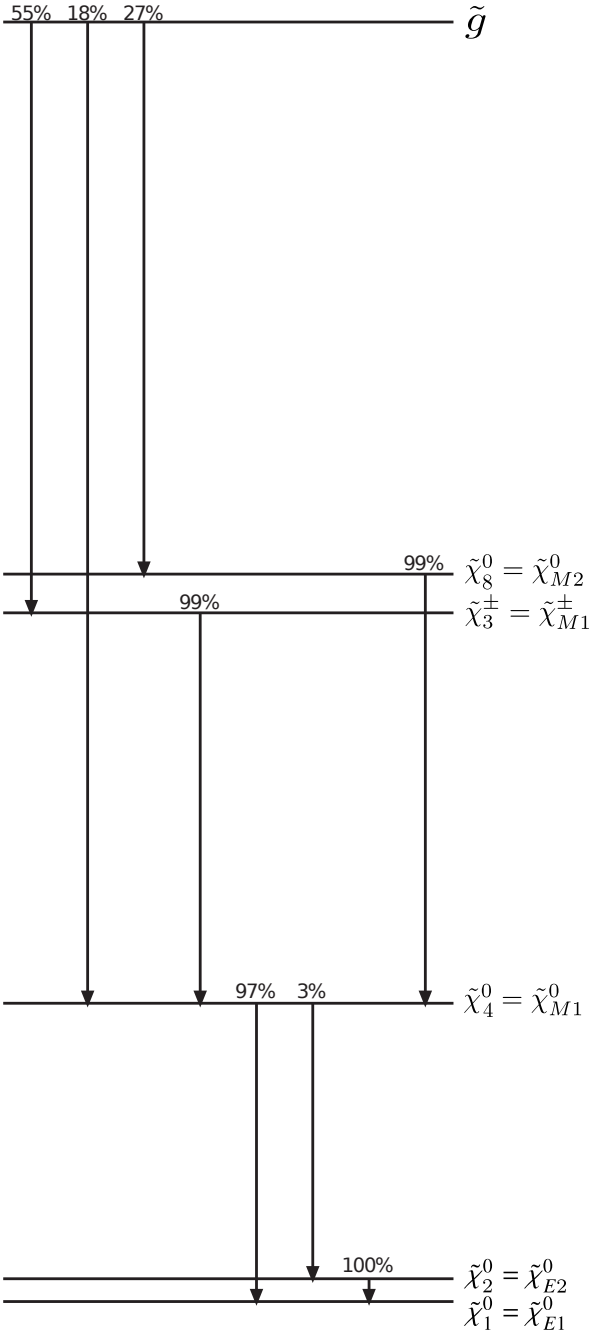

(d) E_6SSM-III

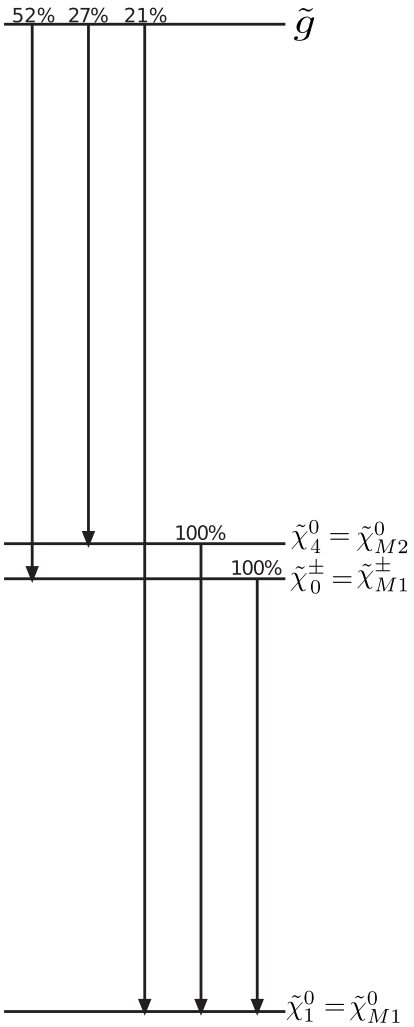

(e) E_6SSM-IV

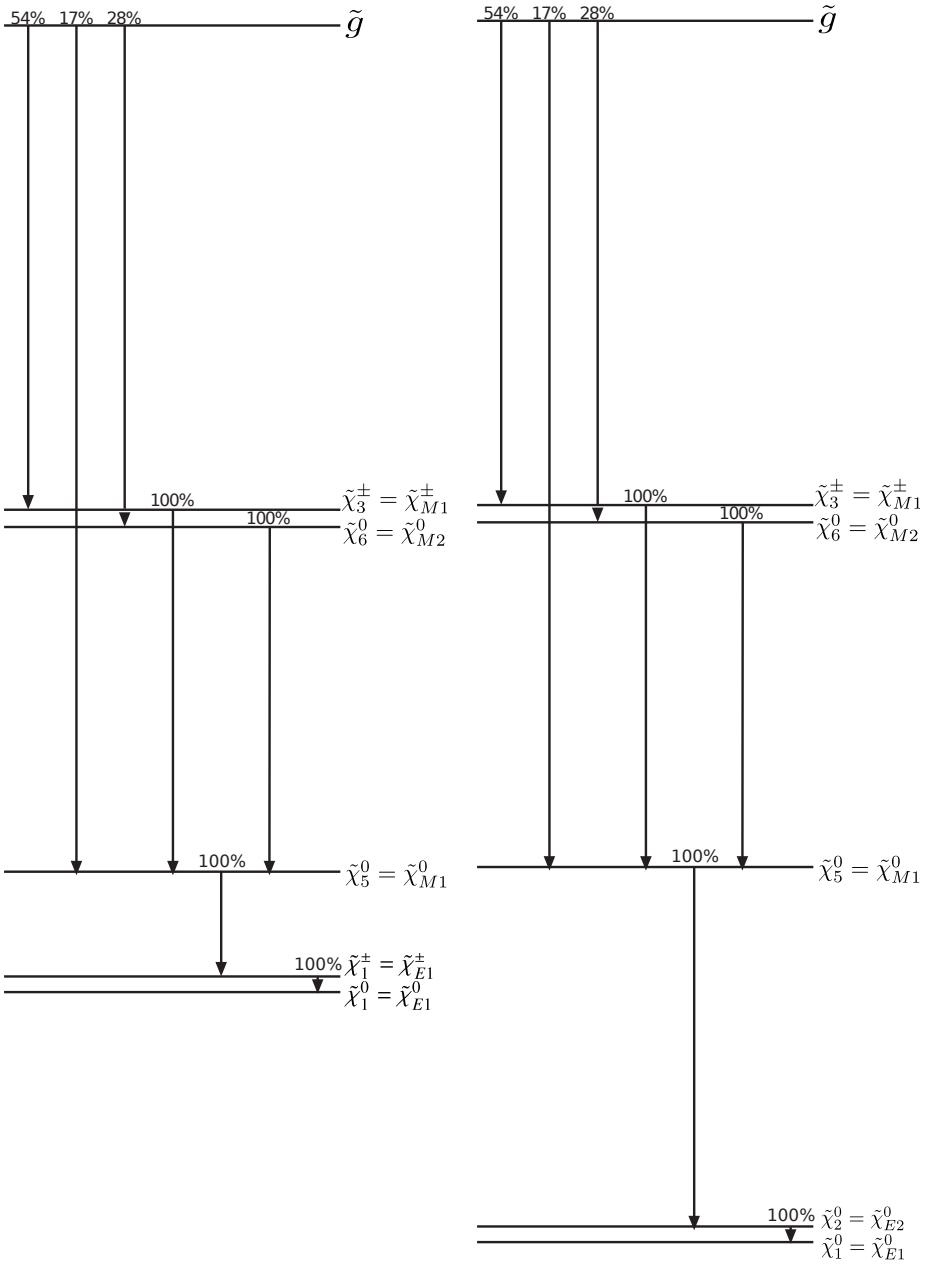

(f) E_6SSM-V (g) E_6SSM-VI

Figure A.1: Gluino decay diagrams for the MSSM and E_6SSM benchmarks, showing the leading decays (contributing more than 90%) for the involved sparticles. The vertical line spacings are proportional to the mass splitting among the particles.

Appendix B

Details about the E6SSM `CalcHEP` Model

In this Appendix the contents and properties of the `CalcHEP` models `E6SSM-12.02` (hepmdb:1112.0106) [188] and `E6SSM-12.02` (hepmdb:0413.0129) [189] are described in detail. The model files are accessible from HEPMDB [78] where one can either run it with `CalcHEP` on the IRIDIS cluster via the web interface or download it and run it on one's local `CalcHEP` installation. The model constitutes of four files; `varsNN.mdl`, `prtclsNN.mdl`, `funcNN.mdl`, and `lgrngNN.mdl`; for input variables, particle definitions, functions or constraints, and Feynman rules for vertices, respectively.

B.1 Particle content

The model shares many features and particles with the MSSM and its extensions, e.g. the USSM or NMSSM, but has a greater particle content. This `CalcHEP` version of the E_6SSM, `E6SSM-12.02`, includes particles from the three generations of 27 representations but not all. What is yet to be implemented is the full Higgs sector, including the *inert* Higgs *boson* states, and the coloured exotics. This is work in progress and will be added in a later version of the model. The extra particles included compared to the MSSM are a SM-singlet S, which mixes with the two MSSM-like CP-even Higgs particles; a Z'-boson; two extra chargino states from inert Higgsinos; and 8 extra neutralino states, two from the bino$'$ and the singlino and six from the inert neutral Higgsinos and singlinos. The `CalcHEP` particle names and properties as used in the `prtclsNN.mdl` file are shown in Table B.1. The table shows the full name of each particle followed by the symbols used in `CalcHEP` for it and its antiparticle. The PDG code is a positive number assigned to each particle for referencing in the code, the antiparticles have PDG codes equal to the negative of the particles' PDGs. The spin, mass, width and color properties are also given in `CalcHEP` notation. Following the convention from earlier SUSY models

in `CalcHEP`, superparters, i.e. particles which are odd under R-parity, are denoted with a ~ prefix. The conventions we use for the particle mass and width variables are `M`< particle symbol > and `w`< particle symbol >. If the particle is charged the particle symbol is modified with a suffix `-c` for "charged" to avoid confusion, e.g. `MHc` for the charged Higgs `H+`. In the case of superpartners the ~ is not used in the mass or width variable. Instead a prefix `S-` or suffix `-o` is attached to the particle name depending on whether the sparticle is a **S**fermion or a boson**o**, e.g. `MGo` for the gluino mass and `MSe1` for the first selectron mass. A number is added to the variable name whenever it refers to particles for which there are more than one of the same type, e.g. neutralinos or stops. We try to keep as close as possible to these conventions without departing too much from conventions used in earlier SUSY models. There are still some deviations from the set up conventions, e.g. the charged slepton sector, which we hope will not be too confusing until a more uniform way of naming the particles and variables is introduced. In future versions of the model the conventions will be used more strictly.

B.2 Input parameters

The input parameters used in the model, with the exception of some SM parameters, are listed in Table B.2. The pseudoscalar Higgs mass is used as an input variable instead of the soft trilinear lambda coupling from the term $A_\lambda \lambda S H_d H_u$. The electroweak soft gaugino masses M_1, M_2, and M_1' are denoted `MG1`, `MG2`, and `MG1b`, respectively. The physical gluino mass is denoted `MGo`. The soft squark masses for the first two generations are set by a common squark mass scale, `MSq`, by default. It is however easy to modify the model files by moving the soft squark masses `Mq1, Mq2, Mu1, Mu2, Md1, Md2` from the function file `funcNN.mdl` to the input parameter file `varsNN.mdl` and assigning them separate values.

B.3 Functions and dependent parameters

In the file `funcNN.mdl` all dependent parameters are listed in terms of input parameters and dependent parameters above themselves in the list. The dependence can be given as simple algebraic expressions or as functions of external functions. As an example, expressions for mass matrix elements are given in this file. These matrix elements are then used as inputs for numerical diagonalisation routines from the `SLHAplus` library, which comes with `CalcHEP`. `SLHAplus` then returns evaluated particle masses, which are defined in this file. As an example of what the contents of this file look likes, a few lines from it are presented in Table B.3.

Full Name	particle	antiparticle	PDG ID	2×spin	mass	width	color
gluon	G	G	21	2	0	0	8
neutrino	n1	N1	12	1	0	0	1
electron	e1	E1	11	1	Me1	0	1
muon-neutrino	n2	N2	14	1	0	0	1
muon	e2	E2	13	1	Me2	0	1
tau-neutrino	n3	N3	16	1	0	0	1
tau-lepton	e3	E3	15	1	Me3	0	1
u-quark	u	U	2	1	Mu	0	3
d-quark	d	D	1	1	Md	0	3
c-quark	c	C	4	1	Mc	0	3
s-quark	s	S	3	1	Ms	0	3
t-quark	t	T	6	1	Mt	!wt	3
b-quark	b	B	5	1	Mb	0	3
light Higgs	h1	h1	25	0	Mh1	!wh1	1
heavier Higgs	h2	h2	26	0	Mh2	!wh2	1
heaviest Higgs	h3	h3	27	0	Mh3	!wh3	1
pseudoscalar Higgs	ha	ha	28	0	Mha	!wha	1
charged Higgs	H+	H-	37	0	MHc	!wHc	1
photon	A	A	22	2	0	0	1
Z-boson	Z	Z	23	2	MZ	!wZ	1
W-boson	W+	W-	24	2	MW	!wW	1
Z-primed-boson	Zb	Zb	32	2	MZb	!wZb	1
chargino 1	~1+	~1-	1000024	1	MCo1	!wCo1	1
chargino 2	~2+	~2-	1000037	1	MCo2	!wCo2	1
chargino 3	~3+	~3-	1000038	1	MCo3	!wCo3	1
chargino 4	~4+	~4-	1000039	1	MCo4	!wCo4	1
neutralino 1	~o1	~o1	1000022	1	MNo1	0	1
neutralino 2	~o2	~o2	1000023	1	MNo2	!wNo2	1
neutralino 3	~o3	~o3	1000025	1	MNo3	!wNo3	1
neutralino 4	~o4	~o4	1000026	1	MNo4	!wNo4	1
neutralino 5	~o5	~o5	1000027	1	MNo5	!wNo5	1
neutralino 6	~o6	~o6	1000028	1	MNo6	!wNo6	1
neutralino 7	~o7	~o7	1000029	1	MNo7	!wNo7	1
neutralino 8	~o8	~o8	1000030	1	MNo8	!wNo8	1
neutralino 9	~o9	~o9	1000031	1	MNo9	!wNo9	1
neutralino 10	~oA	~oA	1000032	1	MNoA	!wNoA	1
neutralino 11	~oB	~oB	1000033	1	MNoB	!wNoB	1
neutralino 12	~oC	~oC	1000034	1	MNoC	!wNoC	1
gluino	~g	~g	1000021	1	MGo	!wGo	8
1st selectron	~e1	~E1	1000011	0	MSe1	!wSe1	1
2nd selectron	~e4	~E4	2000011	0	MSe2	!wSe2	1
1st smuon	~e2	~E2	1000013	0	MSmu1	!wSmu1	1
2nd smuon	~e5	~E5	2000013	0	MSmu2	!wSmu2	1
1st stau	~e3	~E3	1000015	0	MStau1	!wStau1	1
2nd stau	~e6	~E6	2000015	0	MStau2	!wStau2	1
e-sneutrino	~n1	~N1	1000012	0	MSn1	!wSn1	1
mu-sneutrino	~n2	~N2	1000014	0	MSn2	!wSn2	1
tau-sneutrino	~n3	~N3	1000016	0	MSn3	!wSn3	1
1st u-squark	~u1	~U1	1000002	0	MSu1	!wSu1	3
2nd u-squark	~u2	~U2	2000002	0	MSu2	!wSu2	3
1st d-squark	~d1	~D1	1000001	0	MSd1	!wSd1	3
2nd d-squark	~d2	~D2	2000001	0	MSd2	!wSd2	3
1st c-squark	~c1	~C1	1000004	0	MSc1	!wSc1	3
2nd c-squark	~c2	~C2	2000004	0	MSc2	!wSc2	3
1st s-squark	~s1	~S1	1000003	0	MSs1	!wSs1	3
2nd s-squark	~s2	~S2	2000003	0	MSs2	!wSs2	3
1st t-squark	~t1	~T1	1000006	0	MSt1	!wSt1	3
2nd t-squark	~t2	~T2	2000006	0	MSt2	!wSt2	3
1st b-squark	~b1	~B1	1000005	0	MSb1	!wSb1	3
2nd b-squark	~b2	~B2	2000005	0	MSb2	!wSb2	3

Table B.1: Particle content in the `E6SSM-12.02` with `CalcHEP` naming conventions and properties.

Name	Value	Comment
g1b	0.073	U(1)-primed coupling with sqrt(1/40)
hL	0.393	Yukawa coupling for S Hu Hd
hL22	-0.000357	Yukawa coupling for S Hd2 Hu2
hL21	0.04	Yukawa coupling for S Hd2 Hu1
hL12	0.0321	Yukawa coupling for S Hd1 Hu2
hL11	0.000714	Yukawa coupling for S Hd1 Hu1
hFd22	0.001	Yukawa coupling for S2 Hd Hu2
hFd21	0.6844	Yukawa coupling for S2 Hd Hu1
hFd12	0.65	Yukawa coupling for S1 Hd Hu2
hFd11	0.001	Yukawa coupling for S1 Hd Hu1
hFu22	0.001	Yukawa coupling for S2 Hu Hd2
hFu21	0.67	Yukawa coupling for S2 Hu Hd1
hFu12	0.64	Yukawa coupling for S1 Hu Hd2
hFu11	0.001	Yukawa coupling for S1 Hu Hd1
hXd2	0.000714	Yukawa coupling for S Hd Hu2
hXd1	0.000714	Yukawa coupling for S Hd Hu1
hXu2	0.000714	Yukawa coupling for S Hd2 Hu
hXu1	0.000714	Yukawa coupling for S Hd1 Hu
hZ2	0.001	Yukawa coupling for S2 Hd Hu
hZ1	0.001	Yukawa coupling for S1 Hd Hu
Svev	5180	SM-singlet VEV
Hvev	246	SM Higgs VEV
MSq	2000	Common soft squark mass scale for gen. 1 and 2 MSq= Mq1= Mq2= Mu1= Mu2= Md1= Md2
topA	-2200	soft trilinear A-coupling for top
botA	-2200	soft trilinear A-coupling for bottom
Mq3	2000	Soft squark mass for third gen. SU(2) doublet, q
Mu3	2000	Soft squark mass for third gen. right-handed u
Md3	2000	Soft squark mass for third gen. right-handed d
Ml1	2000	Soft slepton mass for 1st gen. SU(2) doublet, L
Ml2	2000	Soft slepton mass for 2nd gen. SU(2) doublet, L
Ml3	2000	Soft slepton mass for 3rd gen. SU(2) doublet, L
Mr1	2000	Soft slepton mass for 1st gen. right-handed e (selectron)
Mr2	2000	Soft slepton mass for 2nd gen. right-handed e (smuon)
Mr3	2040	Soft slepton mass for 3rd gen. right-handed e (stau)
tauA	-2200	soft trilinear A-coupling for tau
lsc	165	scale for Higgs loop corrections
lmt	165	top mass in Higgs loop corrections
Mha	2736	pseudoscalar Higgs mass
MG1	150	Soft gaugino mass for U(1) (hypercharge)
MG2	300	Soft gaugino mass for SU(2)
MG1b	151	Soft gaugino mass for U(1)'
Maux	1	mass of aux particles
tb	1.5	tangent beta
MGo	800	gluino mass

Table B.2: Input parameters for the `E6SSM-12.02` model in `CalcHEP` notation. Some SM parameters have been removed from this list. This is the format and content of the varsNN.mdl file that comes with the model. By default the parameter values of benchmark E_6SSM-I are given.

Name	Expression
⋮	⋮
MNE13	-MZ*SW*cb
MNE14	MZ*SW*sb
⋮	⋮
MNo1	MassArray(NeDiag, 1) % Neutralino mass 1
MNo2	MassArray(NeDiag, 2) % Neutralino mass 2
⋮	⋮

Table B.3: Example lines from the model file `funcNN.mdl`, where dependent parameters are specified. Comments are allowed at the ends of lines after a %. The lines shown are examples of simple expressions for matrix elements and masses defined by external numerical routines.

P1	P2	P3	P4	Factor	dLagrangian/ dA(p1) dA(p2) dA(p3)
A	H+	H-		-EE	m1.p2-m1.p3
G	W+	~C1	~b1	-EE*GG*Sqrt2*Vcb*Zd33/SW	m1.m2
W+	W+	W-	W-	-EE^2/SW^2	m1.m4*m2.m3-2*m1.m2*m3.m4+m1.m3*m2.m4

Table B.4: Example lines from the model file `lgrngNN.mdl`, where Feynman rules for all vertices in the model are listed.

B.4 Feynman rules

All of the vertices in the model are listed in the file `lgrngNN.mdl`. Some of the vertices include auxiliary particles, which are included for technical reasons, e.g. to construct a four-gluon vertex. Examples of vertices and Feynman rules from this file are given in Table B.4.

B.5 Updates in `E6SSM-13.04`

The latest updated version of the model, `E6SSM-13.04` [189], has recently been made public on HEPMDB. No significant changes is made in terms of structure. The main update concerns new implementations of 1-loop corrections to the CP-even Higgs mass matrix. Previous 1-loop corrections were taken from the USSM results referred to in [185]. In the updated version, the 1-loop corrections agree with [195] and has been cross-checked with an independent implementation by the authors of the same reference. Furthermore, minor typos have been corrected and the default parameter values have been adjusted slightly.

References

[1] J. Ellis, J.R. Espinosa, G.F. Giudice, A. Hoecker, and A. Riotto, "The Probable Fate of the Standard Model," Phys.Lett. **B679**, 369–375 (2009), arXiv:0906.0954 [hep-ph]

[2] M. Baak, M. Goebel, J. Haller, A. Hoecker, D. Kennedy, *et al.*, "The Electroweak Fit of the Standard Model after the Discovery of a New Boson at the LHC," Eur.Phys.J. **C72**, 2205 (2012), arXiv:1209.2716 [hep-ph]

[3] J. Beringer *et al.* (Particle Data Group), "Review of Particle Physics (RPP)," Phys.Rev. **D86**, 010001 (2012)

[4] Stephen P. Martin, "A Supersymmetry primer," (1997), arXiv:hep-ph/9709356 [hep-ph]

[5] O. Buchmueller and J. Marrouche, "Universal mass limits on gluino and third-generation squarks in the context of Natural-like SUSY spectra," (2013), arXiv:1304.2185 [hep-ph]

[6] E. Aprile *et al.* (XENON100 Collaboration), "Dark Matter Results from 225 Live Days of XENON100 Data," Phys.Rev.Lett. **109**, 181301 (2012), arXiv:1207.5988 [astro-ph.CO]

[7] *Search for squarks and gluinos with the ATLAS detector using final states with jets and missing transverse momentum and 5.8 fb^{-1} of $\sqrt{s}$=8 TeV proton-proton collision data*, Tech. Rep. ATLAS-CONF-2012-109 (CERN, Geneva, 2012)

[8] *A Search for Anomalous Production of Events with three or more leptons using 9.2 fb^{-1} of $\sqrt{s}$=8 TeV CMS data*, Tech. Rep. CMS-PAS-SUS-12-026 (CERN, Geneva, 2012)

[9] *Search for supersymmetry in events with same-sign dileptons*, Tech. Rep. CMS-PAS-SUS-12-017 (CERN, Geneva, 2012)

[10] *Search for Supersymmetry in pp collisions at 8 TeV in events with a single lepton, multiple jets and b-tags*, Tech. Rep. CMS-PAS-SUS-13-007 (CERN, Geneva, 2013)

[11] *Search for gluino-mediated bottom- and top-squark production in pp collisions at 8 TeV*, Tech. Rep. CMS-PAS-SUS-12-024 (CERN, Geneva, 2013)

[12] *Search for direct EWK production of SUSY particles in multilepton modes with 8TeV data*, Tech. Rep. CMS-PAS-SUS-12-022 (CERN, Geneva, 2012)

[13] *Higgs to tau tau (MSSM) (HCP)*, Tech. Rep. CMS-PAS-HIG-12-050 (CERN, Geneva, 2012)

[14] G. Belanger, F. Boudjema, A. Pukhov, and A. Semenov, "Micromegas: Version 1.3," (2004), hep-ph/0405253

[15] E. Komatsu *et al.* (WMAP Collaboration), "Seven-Year Wilkinson Microwave Anisotropy Probe (WMAP) Observations: Cosmological Interpretation," Astrophys.J.Suppl. **192**, 18 (2011), arXiv:1001.4538 [astro-ph.CO]

[16] E. Aprile *et al.* (XENON100 Collaboration), "Dark Matter Results from 100 Live Days of XENON100 Data," Phys.Rev.Lett. **107**, 131302 (2011), arXiv:1104.2549 [astro-ph.CO]

[17] W. Beenakker, R. Hopker, M. Spira, and P.M. Zerwas, "Squark and gluino production at hadron colliders," Nucl.Phys. **B492**, 51–103 (1997), arXiv:hep-ph/9610490 [hep-ph]

[18] G. Cacciapaglia, C. Csaki, G. Marandella, and A. Strumia, "The minimal set of electroweak precision parameters," Phys. Rev. **D74**, 033011 (2006), arXiv:hep-ph/0604111

[19] Alexander Belyaev, Jonathan P. Hall, Stephen F. King, and Patrik Svantesson, "Novel gluino cascade decays in E_6 inspired models," Phys.Rev. **D86**, 031702 (2012), arXiv:1203.2495 [hep-ph]

[20] Patrik Svantesson, Alexander Belyaev, Jonathan P. Hall, and Stephen F. King, "E6SSM vs MSSM Gluino Phenomenology," EPJ Web Conf. **28**, 12014 (2012), arXiv:1201.5141 [hep-ph]

[21] Alexander Belyaev, Jonathan P. Hall, Stephen F. King, and Patrik Svantesson, "Discovering E_6 SUSY models in gluino cascade decays at the LHC," Phys.Rev. **D87**, 035019 (2013), arXiv:1211.1962 [hep-ph]

[22] Howard Baer, Alexander Belyaev, Chung Kao, and Patrik Svantesson, "Exploring neutralino dark matter resonance annihilation via $bA(bH) \to b\mu^+\mu^-$ at the LHC," Phys.Rev. **D84**, 095029 (2011), arXiv:1106.5055 [hep-ph]

[23] Alexander Belyaev, Stephen F. King, and Patrik Svantesson, "Little Z' Models," (2013), arXiv:1303.0770 [hep-ph]

[24] Georges Aad *et al.* (ATLAS Collaboration), "Observation of a new particle in the search for the Standard Model Higgs boson with the ATLAS detector at the LHC," Phys.Lett. **B716**, 1–29 (2012), arXiv:1207.7214 [hep-ex]

[25] Serguei Chatrchyan *et al.* (CMS Collaboration), "Observation of a new boson at a mass of 125 GeV with the CMS experiment at the LHC," Phys.Lett. **B716**, 30–61 (2012), arXiv:1207.7235 [hep-ex]

[26] *Combined coupling measurements of the Higgs-like boson with the ATLAS detector using up to 25 fb^{-1} of proton-proton collision data*, Tech. Rep. ATLAS-CONF-2013-034 (CERN, Geneva, 2013)

[27] *Properties of the Higgs-like boson in the decay H to ZZ to 4l in pp collisions at sqrt s =7 and 8 TeV*, Tech. Rep. CMS-PAS-HIG-13-002 (CERN, Geneva, 2013)

[28] *Evidence for a particle decaying to W+W- in the fully leptonic final state in a standard model Higgs boson search in pp collisions at the LHC*, Tech. Rep. CMS-PAS-HIG-13-003 (CERN, Geneva, 2013)

[29] Peter W. Higgs, "Broken Symmetries and the Masses of Gauge Bosons," Phys.Rev.Lett. **13**, 508–509 (1964)

[30] Peter W. Higgs, "Broken symmetries, massless particles and gauge fields," Phys.Lett. **12**, 132–133 (1964)

[31] F. Englert and R. Brout, "Broken Symmetry and the Mass of Gauge Vector Mesons," Phys.Rev.Lett. **13**, 321–323 (1964)

[32] G.S. Guralnik, C.R. Hagen, and T.W.B. Kibble, "Global Conservation Laws and Massless Particles," Phys.Rev.Lett. **13**, 585–587 (1964)

[33] Philip W. Anderson, "Plasmons, Gauge Invariance, and Mass," Phys.Rev. **130**, 439–442 (1963)

[34] S. Schael *et al.* (ALEPH Collaboration, DELPHI Collaboration, L3 Collaboration, OPAL Collaboration, SLD Collaboration, LEP Electroweak Working Group, SLD Electroweak Group, SLD Heavy Flavour Group), "Precision electroweak measurements on the Z resonance," Phys.Rept. **427**, 257–454 (2006), arXiv:hep-ex/0509008 [hep-ex]

[35] C. Albajar *et al.* (UA1 Collaboration), "Studies of Intermediate Vector Boson Production and Decay in UA1 at the CERN Proton - Antiproton Collider," Z.Phys. **C44**, 15–61 (1989)

[36] J. Alitti *et al.* (UA2 Collaboration), "An Improved determination of the ratio of W and Z masses at the CERN $\bar{p}p$ collider," Phys.Lett. **B276**, 354–364 (1992)

[37] F. Abe *et al.* (CDF Collaboration), "Observation of top quark production in $\bar{p}p$ collisions," Phys.Rev.Lett. **74**, 2626–2631 (1995), arXiv:hep-ex/9503002 [hep-ex]

[38] S. Abachi *et al.* (D0 Collaboration), "Observation of the top quark," Phys.Rev.Lett. **74**, 2632–2637 (1995), arXiv:hep-ex/9503003 [hep-ex]

[39] "Combination of CDF and D0 Results on the Width of the W boson," (2010), arXiv:1003.2826 [hep-ex]

[40] F. Zwicky, "Spectral displacement of extra galactic nebulae," Helv.Phys.Acta **6**, 110–127 (1933)

[41] Mordehai Milgrom, "The MOND paradigm," (2008), arXiv:0801.3133 [astro-ph]

[42] Maxim Markevitch, A.H. Gonzalez, D. Clowe, A. Vikhlinin, L. David, *et al.*, "Direct constraints on the dark matter self-interaction cross-section from the merging galaxy cluster 1E0657-56," Astrophys.J. **606**, 819–824 (2004), arXiv:astro-ph/0309303 [astro-ph]

[43] P.A.R. Ade *et al.* (Planck Collaboration), "Planck 2013 results. XVI. Cosmological parameters," (2013), arXiv:1303.5076 [astro-ph.CO]

[44] Volker Springel, Simon D.M. White, Adrian Jenkins, Carlos S. Frenk, Naoki Yoshida, *et al.*, "Simulating the joint evolution of quasars, galaxies and their large-scale distribution," Nature **435**, 629–636 (2005), arXiv:astro-ph/0504097 [astro-ph]

[45] Mark Trodden, "Electroweak baryogenesis," Rev.Mod.Phys. **71**, 1463–1500 (1999), arXiv:hep-ph/9803479 [hep-ph]

[46] Ariel Goobar, Steen Hannestad, Edvard Mortsell, and Huitzu Tu, "A new bound on the neutrino mass from the sdss baryon acoustic peak," JCAP **0606**, 019 (2006), arXiv:astro-ph/0602155 [astro-ph]

[47] Zornitza Daraktchieva, "Search for neutrinoless double beta decay with NEMO 3 experiment," Nucl.Phys. **A827**, 495C–497C (2009), arXiv:0901.2720 [hep-ex]

[48] Jean-Loup Gervais and B. Sakita, "FIELD THEORY INTERPRETATION OF SUPERGAUGES IN DUAL MODELS," Nucl.Phys. **B34**, 632–639 (1971)

[49] Yu.A. Golfand and E.P. Likhtman, "Extension of the Algebra of Poincare Group Generators and Violation of p Invariance," JETP Lett. **13**, 323–326 (1971)

[50] D.V. Volkov and V.P. Akulov, "Possible universal neutrino interaction," JETP Lett. **16**, 438–440 (1972)

[51] Sidney R. Coleman and J. Mandula, "ALL POSSIBLE SYMMETRIES OF THE S MATRIX," Phys.Rev. **159**, 1251–1256 (1967)

[52] Rudolf Haag, Jan T. Łopuszański, and Martin Sohnius, "All possible generators of supersymmetries of the s-matrix," Nuclear Physics B **88**, 257 – 274 (1975), ISSN 0550-3213, http://www.sciencedirect.com/science/article/pii/0550321375902795

[53] Ali H. Chamseddine, Richard L. Arnowitt, and Pran Nath, "Locally Supersymmetric Grand Unification," Phys.Rev.Lett. **49**, 970 (1982)

[54] Riccardo Barbieri, S. Ferrara, and Carlos A. Savoy, "Gauge Models with Spontaneously Broken Local Supersymmetry," Phys.Lett. **B119**, 343 (1982)

[55] Luis E. Ibanez, "Locally Supersymmetric SU(5) Grand Unification," Phys.Lett. **B118**, 73 (1982)

[56] Lawrence J. Hall, Joseph D. Lykken, and Steven Weinberg, "Supergravity as the Messenger of Supersymmetry Breaking," Phys.Rev. **D27**, 2359–2378 (1983)

[57] Nobuyoshi Ohta, "GRAND UNIFIED THEORIES BASED ON LOCAL SUPERSYMMETRY," Prog.Theor.Phys. **70**, 542 (1983)

[58] John R. Ellis, Dimitri V. Nanopoulos, and K. Tamvakis, "Grand Unification in Simple Supergravity," Phys.Lett. **B121**, 123 (1983)

[59] Luis Alvarez-Gaume, J. Polchinski, and Mark B. Wise, "Minimal Low-Energy Supergravity," Nucl.Phys. **B221**, 495 (1983)

[60] Hans Peter Nilles, "Supersymmetry, Supergravity and Particle Physics," Phys.Rept. **110**, 1–162 (1984)

[61] G.F. Giudice and R. Rattazzi, "Theories with gauge mediated supersymmetry breaking," Phys.Rept. **322**, 419–499 (1999), arXiv:hep-ph/9801271 [hep-ph]

[62] L. Girardello and Marcus T. Grisaru, "Soft Breaking of Supersymmetry," Nucl.Phys. **B194**, 65 (1982)

[63] Herbert K. Dreiner and Graham G. Ross, "R-parity violation at hadron colliders," Nucl.Phys. **B365**, 597–613 (1991)

[64] C.G. Lester and D.J. Summers, "Measuring masses of semiinvisibly decaying particles pair produced at hadron colliders," Phys.Lett. **B463**, 99–103 (1999), arXiv:hep-ph/9906349 [hep-ph]

[65] Alan Barr, Christopher Lester, and P. Stephens, "m(T2): The Truth behind the glamour," J.Phys. **G29**, 2343–2363 (2003), arXiv:hep-ph/0304226 [hep-ph]

[66] A. Semenov, "LanHEP - a package for the automatic generation of Feynman rules in field theory. Version 3.0," Comput. Phys. Commun. **180**, 431–454 (2009), arXiv:0805.0555 [hep-ph]

[67] Neil D. Christensen and Claude Duhr, "FeynRules - Feynman rules made easy," Comput.Phys.Commun. **180**, 1614–1641 (2009), arXiv:0806.4194 [hep-ph]

[68] Florian Staub, "From Superpotential to Model Files for FeynArts and CalcHep-/CompHep," Comput.Phys.Commun. **181**, 1077–1086 (2010), arXiv:0909.2863 [hep-ph]

[69] Alexander Belyaev, Neil D. Christensen, and Alexander Pukhov, "CalcHEP 3.4 for collider physics within and beyond the Standard Model," Comput.Phys.Commun. **184**, 1729–1769 (2013), arXiv:1207.6082 [hep-ph]

[70] Johan Alwall, Michel Herquet, Fabio Maltoni, Olivier Mattelaer, and Tim Stelzer, "MadGraph 5 : Going Beyond," JHEP **1106**, 128 (2011), arXiv:1106.0522 [hep-ph]

[71] Thomas Hahn, "Generating Feynman diagrams and amplitudes with FeynArts 3," Comput.Phys.Commun. **140**, 418–431 (2001), arXiv:hep-ph/0012260 [hep-ph]

[72] R. Mertig, M. Bohm, and Ansgar Denner, "FEYN CALC: Computer algebraic calculation of Feynman amplitudes," Comput.Phys.Commun. **64**, 345–359 (1991)

[73] Torbjorn Sjostrand, Stephen Mrenna, and Peter Z. Skands, "A Brief Introduction to PYTHIA 8.1," Comput.Phys.Commun. **178**, 852–867 (2008), arXiv:0710.3820 [hep-ph]

[74] Tanju Gleisberg, Stefan Hoeche, Frank Krauss, Andreas Schalicke, Steffen Schumann, *et al.*, "SHERPA 1. alpha: A Proof of concept version," JHEP **0402**, 056 (2004), arXiv:hep-ph/0311263 [hep-ph]

[75] T. Gleisberg, Stefan. Hoeche, F. Krauss, M. Schonherr, S. Schumann, *et al.*, "Event generation with SHERPA 1.1," JHEP **0902**, 007 (2009), arXiv:0811.4622 [hep-ph]

[76] John Conway *et al.*, "Pgs 4," `http://www.physics.ucdavis.edu/~conway/research/software/pgs/pgs4-general.htm`

[77] S. Ovyn, X. Rouby, and V. Lemaitre, "DELPHES, a framework for fast simulation of a generic collider experiment," (2009), arXiv:0903.2225 [hep-ph]

[78] M. Bondarenko, A. Belyaev, L. Basso, E. Boos, V. Bunichev, *et al.*, "High Energy Physics Model Database : Towards decoding of the underlying theory (within Les Houches 2011: Physics at TeV Colliders New Physics Working Group Report)," (2012), arXiv:1203.1488 [hep-ph], `https://hepmdb.soton.ac.uk`

[79] Neil D. Christensen, Claude Duhr, Benjamin Fuks, *et al.*, "Feynrules model database," `http://feynrules.irmp.ucl.ac.be/wiki/ModelDatabaseMainPage`

[80] Valeria Bartsch and Gunter Quast, *Expected Signal Observability at Future Experiments*, Tech. Rep. CMS-NOTE-2005-004 (CERN, Geneva, 2005)

[81] S. I. Bityukov and N. V. Krasnikov, "On observability of signal over background," (2007), physics/9809037

[82] A.J. Barr, "Determining the spin of supersymmetric particles at the LHC using lepton charge asymmetry," Phys.Lett. **B596**, 205–212 (2004), arXiv:hep-ph/0405052 [hep-ph]

[83] Csaba Csaki, Johannes Heinonen, and Maxim Perelstein, "Testing gluino spin with three-body decays," JHEP **0710**, 107 (2007), arXiv:0707.0014 [hep-ph]

[84] O. Elgaroy, O. Lahav, W.J. Percival, J.A. Peacock, D.S. Madgwick, *et al.*, "A New limit on the total neutrino mass from the 2dF galaxy redshift survey," Phys.Rev.Lett. **89**, 061301 (2002), arXiv:astro-ph/0204152 [astro-ph]

[85] P. Gondolo, J. Edsjo, P. Ullio, L. Bergstrom, Mia Schelke, *et al.*, "DarkSUSY: Computing supersymmetric dark matter properties numerically," JCAP **0407**, 008 (2004), arXiv:astro-ph/0406204 [astro-ph]

[86] R. Bernabei *et al.* (DAMA Collaboration, LIBRA Collaboration), "New results from DAMA/LIBRA," Eur.Phys.J. **C67**, 39–49 (2010), arXiv:1002.1028 [astro-ph.GA]

[87] C.E. Aalseth *et al.* (CoGeNT collaboration), "Results from a Search for Light-Mass Dark Matter with a P-type Point Contact Germanium Detector," Phys.Rev.Lett. **106**, 131301 (2011), arXiv:1002.4703 [astro-ph.CO]

[88] Z. Ahmed *et al.* (CDMS-II Collaboration), "Results from a Low-Energy Analysis of the CDMS II Germanium Data," Phys.Rev.Lett. **106**, 131302 (2011), arXiv:1011.2482 [astro-ph.CO]

[89] C.E. Aalseth, P.S. Barbeau, J. Colaresi, J.I. Collar, J. Diaz Leon, *et al.*, "Search for an Annual Modulation in a P-type Point Contact Germanium Dark Matter Detector," Phys.Rev.Lett. **107**, 141301 (2011), arXiv:1106.0650 [astro-ph.CO]

[90] G. Angloher, M. Bauer, I. Bavykina, A. Bento, C. Bucci, *et al.*, "Results from 730 kg days of the CRESST-II Dark Matter Search," Eur.Phys.J. **C72**, 1971 (2012), arXiv:1109.0702 [astro-ph.CO]

[91] R. Agnese *et al.* (CDMS Collaboration), "Silicon Detector Results from the First Five-Tower Run of CDMS II," (2013), arXiv:1304.3706 [astro-ph.CO]

[92] R. Agnese *et al.* (CDMS Collaboration), "Dark Matter Search Results Using the Silicon Detectors of CDMS II," Phys.Rev.Lett.(2013), arXiv:1304.4279 [hep-ex]

[93] Mads T. Frandsen, Felix Kahlhoefer, Christopher McCabe, Subir Sarkar, and Kai Schmidt-Hoberg, "The unbearable lightness of being: CDMS versus XENON," (2013), arXiv:1304.6066 [hep-ph]

[94] Torsten Bringmann, Xiaoyuan Huang, Alejandro Ibarra, Stefan Vogl, and Christoph Weniger, "Fermi LAT Search for Internal Bremsstrahlung Signatures from Dark Matter Annihilation," JCAP **1207**, 054 (2012), arXiv:1203.1312 [hep-ph]

[95] Christoph Weniger, "A Tentative Gamma-Ray Line from Dark Matter Annihilation at the Fermi Large Area Telescope," JCAP **1208**, 007 (2012), arXiv:1204.2797 [hep-ph]

[96] Howard Baer and Andrew D. Box, "Fine-tuning favors mixed axion/axino cold dark matter over neutralinos in the minimal supergravity model," Eur.Phys.J. **C68**, 523–537 (2010), arXiv:0910.0333 [hep-ph]

[97] Howard Baer, Andrew D. Box, and Heaya Summy, "Neutralino versus axion/axino cold dark matter in the 19 parameter SUGRA model," JHEP **1010**, 023 (2010), arXiv:1005.2215 [hep-ph]

[98] Adam G. Riess, Lucas Macri, Stefano Casertano, Hubert Lampeitl, Henry C. Ferguson, *et al.*, "A 3Constant with the Hubble Space Telescope and Wide Field Camera 3," Astrophys.J. **730**, 119 (2011), arXiv:1103.2976 [astro-ph.CO]

[99] Adam G. Riess, Lucas Macri, Stefano Casertano, Megan Sosey, Hubert Lampeitl, *et al.*, "A Redetermination of the Hubble Constant with the Hubble Space Telescope from a Differential Distance Ladder," Astrophys.J. **699**, 539–563 (2009), arXiv:0905.0695 [astro-ph.CO]

[100] John R. Ellis, Toby Falk, and Keith A. Olive, "Neutralino - Stau coannihilation and the cosmological upper limit on the mass of the lightest supersymmetric particle," Phys.Lett. **B444**, 367–372 (1998), arXiv:hep-ph/9810360 [hep-ph]

[101] John R. Ellis, Toby Falk, Keith A. Olive, and Mark Srednicki, "Calculations of neutralino-stau coannihilation channels and the cosmologically relevant region of MSSM parameter space," Astropart.Phys. **13**, 181–213 (2000), arXiv:hep-ph/9905481 [hep-ph]

[102] M.E. Gomez, George Lazarides, and C. Pallis, "Supersymmetric cold dark matter with Yukawa unification," Phys.Rev. **D61**, 123512 (2000), arXiv:hep-ph/9907261 [hep-ph]

[103] M.E. Gomez, George Lazarides, and C. Pallis, "Yukawa unification, b to s gamma and Bino-Stau coannihilation," Phys.Lett. **B487**, 313–320 (2000), arXiv:hep-ph/0004028 [hep-ph]

[104] A.B. Lahanas, Dimitri V. Nanopoulos, and V.C. Spanos, "Neutralino relic density in a universe with nonvanishing cosmological constant," Phys.Rev. **D62**, 023515 (2000), arXiv:hep-ph/9909497 [hep-ph]

[105] Richard L. Arnowitt, Bhaskar Dutta, and Y. Santoso, "Coannihilation effects in supergravity and D-brane models," Nucl.Phys. **B606**, 59–83 (2001), arXiv:hep-ph/0102181 [hep-ph]

[106] Celine Boehm, Abdelhak Djouadi, and Manuel Drees, "Light scalar top quarks and supersymmetric dark matter," Phys.Rev. **D62**, 035012 (2000), arXiv:hep-ph/9911496 [hep-ph]

[107] John R. Ellis, Keith A. Olive, and Yudi Santoso, "Calculations of neutralino stop coannihilation in the CMSSM," Astropart.Phys. **18**, 395–432 (2003), arXiv:hep-ph/0112113 [hep-ph]

[108] Joakim Edsjo, Mia Schelke, Piero Ullio, and Paolo Gondolo, "Accurate relic densities with neutralino, chargino and sfermion coannihilations in mSUGRA," JCAP **0304**, 001 (2003), arXiv:hep-ph/0301106 [hep-ph]

[109] Kim Griest and David Seckel, "Three exceptions in the calculation of relic abundances," Phys.Rev. **D43**, 3191–3203 (1991)

[110] Joakim Edsjo and Paolo Gondolo, "Neutralino relic density including coannihilations," Phys.Rev. **D56**, 1879–1894 (1997), arXiv:hep-ph/9704361 [hep-ph]

[111] N. Arkani-Hamed, A. Delgado, and G.F. Giudice, "The Well-tempered neutralino," Nucl.Phys. **B741**, 108–130 (2006), arXiv:hep-ph/0601041 [hep-ph]

[112] Howard Baer, Azar Mustafayev, Eun-Kyung Park, and Xerxes Tata, "Target dark matter detection rates in models with a well-tempered neutralino," JCAP **0701**, 017 (2007), arXiv:hep-ph/0611387 [hep-ph]

[113] Howard Baer, Azar Mustafayev, Eun-Kyung Park, and Xerxes Tata, "Collider signals and neutralino dark matter detection in relic-density-consistent models without universality," JHEP **0805**, 058 (2008), arXiv:0802.3384 [hep-ph]

[114] Kwok Lung Chan, Utpal Chattopadhyay, and Pran Nath, "Naturalness, weak scale supersymmetry and the prospect for the observation of supersymmetry at the Tevatron and at the CERN LHC," Phys.Rev. **D58**, 096004 (1998), arXiv:hep-ph/9710473 [hep-ph]

[115] Jonathan L. Feng, Konstantin T. Matchev, and Takeo Moroi, "Multi - TeV scalars are natural in minimal supergravity," Phys.Rev.Lett. **84**, 2322–2325 (2000), arXiv:hep-ph/9908309 [hep-ph]

[116] Jonathan L. Feng, Konstantin T. Matchev, and Takeo Moroi, "Focus points and naturalness in supersymmetry," Phys.Rev. **D61**, 075005 (2000), arXiv:hep-ph/9909334 [hep-ph]

[117] Howard Baer, Chih-hao Chen, Frank Paige, and Xerxes Tata, "Signals for minimal supergravity at the CERN large hadron collider: Multi - jet plus missing energy channel," Phys.Rev. **D52**, 2746–2759 (1995), arXiv:hep-ph/9503271 [hep-ph]

[118] Howard Baer, Chih-hao Chen, Frank Paige, and Xerxes Tata, "Signals for minimal supergravity at the CERN large hadron collider. 2: Multi - lepton channels," Phys.Rev. **D53**, 6241–6264 (1996), arXiv:hep-ph/9512383 [hep-ph]

[119] Howard Baer, Chih-hao Chen, Manuel Drees, Frank Paige, and Xerxes Tata, "Probing minimal supergravity at the CERN LHC for large tan Beta," Phys.Rev. **D59**, 055014 (1999), arXiv:hep-ph/9809223 [hep-ph]

[120] Howard Baer, Tadas Krupovnickas, Stefano Profumo, and Piero Ullio, "Model independent approach to focus point supersymmetry: From dark matter to collider searches," JHEP **0510**, 020 (2005), arXiv:hep-ph/0507282 [hep-ph]

[121] Manuel Drees and Mihoko M. Nojiri, "The Neutralino relic density in minimal $N = 1$ supergravity," Phys.Rev. **D47**, 376–408 (1993), arXiv:hep-ph/9207234 [hep-ph]

[122] Howard Baer and Michal Brhlik, "Neutralino dark matter in minimal supergravity: Direct detection versus collider searches," Phys.Rev. **D57**, 567–577 (1998), arXiv:hep-ph/9706509 [hep-ph]

[123] Howard Baer, Michal Brhlik, Marco A. Diaz, Javier Ferrandis, Pedro Mercadante, *et al.*, "Yukawa unified supersymmetric SO(10) model: Cosmology, rare decays and collider searches," Phys.Rev. **D63**, 015007 (2000), arXiv:hep-ph/0005027 [hep-ph]

[124] John R. Ellis, Toby Falk, Gerardo Ganis, Keith A. Olive, and Mark Srednicki, "The CMSSM parameter space at large tan beta," Phys.Lett. **B510**, 236–246 (2001), arXiv:hep-ph/0102098 [hep-ph]

[125] Vernon D. Barger and Chung Kao, "Implications of new CMB data for neutralino dark matter," Phys.Lett. **B518**, 117–122 (2001), arXiv:hep-ph/0106189 [hep-ph]

[126] Leszek Roszkowski, Roberto Ruiz de Austri, and Takeshi Nihei, "New cosmological and experimental constraints on the CMSSM," JHEP **0108**, 024 (2001), arXiv:hep-ph/0106334 [hep-ph]

[127] A. Djouadi, Manuel Drees, and J.L. Kneur, "Constraints on the minimal supergravity model and prospects for SUSY particle production at future linear e^+e^- colliders," JHEP **0108**, 055 (2001), arXiv:hep-ph/0107316 [hep-ph]

[128] A.B. Lahanas and V.C. Spanos, "Implications of the pseudoscalar Higgs boson in determining the neutralino dark matter," Eur.Phys.J. **C23**, 185–190 (2002), arXiv:hep-ph/0106345 [hep-ph]

[129] Howard Baer, Azar Mustafayev, Stefano Profumo, Alexander Belyaev, and Xerxes Tata, "Neutralino cold dark matter in a one parameter extension of the minimal supergravity model," Phys.Rev. **D71**, 095008 (2005), arXiv:hep-ph/0412059 [hep-ph]

[130] Howard Baer, Azar Mustafayev, Stefano Profumo, Alexander Belyaev, and Xerxes Tata, "Direct, indirect and collider detection of neutralino dark matter in SUSY models with non-universal Higgs masses," JHEP **0507**, 065 (2005), arXiv:hep-ph/0504001 [hep-ph]

[131] Howard Baer, Chih-hao Chen, Manuel Drees, Frank Paige, and Xerxes Tata, "Collider phenomenology for supersymmetry with large tan Beta," Phys.Rev.Lett. **79**, 986–989 (1997), arXiv:hep-ph/9704457 [hep-ph]

[132] John M. Campbell, R. Keith Ellis, F. Maltoni, and S. Willenbrock, "Higgs-Boson production in association with a single bottom quark," Phys.Rev. **D67**, 095002 (2003), arXiv:hep-ph/0204093 [hep-ph]

[133] Chung Kao, Duane A. Dicus, Rahul Malhotra, and Yili Wang, "Discovering the Higgs bosons of minimal supersymmetry with tau leptons and a bottom quark," Phys.Rev. **D77**, 095002 (2008), arXiv:0711.0232 [hep-ph]

[134] Chung Kao, Shankar Sachithanandam, Joshua Sayre, and Yili Wang, "Discovering the Higgs Bosons of Minimal Supersymmetry with Bottom Quarks," Phys.Lett. **B682**, 291–296 (2009), arXiv:0908.1156 [hep-ph]

[135] Chung Kao and Nikita Stepanov, "Discovering the Higgs bosons of minimal supersymmetry with muons," Phys.Rev. **D52**, 5025–5030 (1995), arXiv:hep-ph/9503415 [hep-ph]

[136] Sally Dawson, Duane Dicus, Chung Kao, and Rahul Malhotra, "Discovering the Higgs bosons of minimal supersymmetry with muons and a bottom quark," Phys.Rev.Lett. **92**, 241801 (2004), arXiv:hep-ph/0402172 [hep-ph]

[137] Chung Kao and Yili Wang, "Detecting Higgs bosons with muons at hadron colliders," Phys.Lett. **B635**, 30–35 (2006), arXiv:hep-ph/0601004 [hep-ph]

[138] Howard Baer, Csaba Balazs, and Alexander Belyaev, "Neutralino relic density in minimal supergravity with coannihilations," JHEP **0203**, 042 (2002), arXiv:hep-ph/0202076 [hep-ph]

[139] Frank E. Paige, Serban D. Protopopescu, Howard Baer, and Xerxes Tata, "ISAJET 7.69: A Monte Carlo event generator for pp, anti-p p, and e+e- reactions," (2003), arXiv:hep-ph/0312045 [hep-ph]

[140] H. Baer, J. Ferrandis, S. Kraml, and W. Porod, "On the treatment of threshold effects in SUSY spectrum computations," Phys.Rev. **D73**, 015010 (2006), arXiv:hep-ph/0511123 [hep-ph]

[141] Howard Baer, Csaba Balazs, Alexander Belyaev, Tadas Krupovnickas, and Xerxes Tata, "Updated reach of the CERN LHC and constraints from relic density, $b \to s\gamma$ and a(μ) in the mSUGRA model," JHEP **0306**, 054 (2003), arXiv:hep-ph/0304303 [hep-ph]

[142] H. Baer, John R. Ellis, G.B. Gelmini, Dimitri V. Nanopoulos, and Xerxes Tata, "SQUARK DECAYS INTO GAUGINOS AT THE p anti-p COLLIDER," Phys.Lett. **B161**, 175 (1985)

[143] G. Gamberini, "HEAVY GLUINO AND SQUARK DECAYS AT P ANTI-P COLLIDER," Z.Phys. **C30**, 605–613 (1986)

[144] Howard Baer, Vernon D. Barger, Debra Karatas, and Xerxes Tata, "Detecting Gluinos at Hadron Supercolliders," Phys.Rev. **D36**, 96 (1987)

[145] Howard Baer, Xerxes Tata, and Jeffrey Woodside, "Multi - lepton signals from supersymmetry at hadron super colliders," Phys.Rev. **D45**, 142–160 (1992)

[146] Howard Baer and Jorge O'Farrill, "Probing neutralino resonance annihilation via indirect detection of dark matter," JCAP **0404**, 005 (2004), arXiv:hep-ph/0312350 [hep-ph]

[147] Howard Baer, Alexander Belyaev, Tadas Krupovnickas, and Jorge O'Farrill, "Indirect, direct and collider detection of neutralino dark matter," JCAP **0408**, 005 (2004), arXiv:hep-ph/0405210 [hep-ph]

[148] Howard Baer, Eun-Kyung Park, and Xerxes Tata, "Collider, direct and indirect detection of supersymmetric dark matter," New J.Phys. **11**, 105024 (2009), arXiv:0903.0555 [hep-ph]

[149] E. Aprile *et al.* (XENON100 Collaboration), "First Dark Matter Results from the XENON100 Experiment," Phys.Rev.Lett. **105**, 131302 (2010), arXiv:1005.0380 [astro-ph.CO]

[150] Howard Baer, Kaoru Hagiwara, and Xerxes Tata, "Gauginos as a Signal for Supersymmetry at p anti-p Colliders," Phys.Rev. **D35**, 1598 (1987)

[151] Howard Baer, Debra Dzialo Karatas, and Xerxes Tata, "GLUINO AND SQUARK PRODUCTION IN ASSOCIATION WITH GAUGINOS AT HADRON SUPERCOLLIDERS," Phys.Rev. **D42**, 2259–2264 (1990)

[152] Howard Baer, Chung Kao, and Xerxes Tata, "Aspects of chargino - neutralino production at the tevatron collider," Phys.Rev. **D48**, 5175–5180 (1993), arXiv:hep-ph/9307347 [hep-ph]

[153] Howard Baer, Chih-hao Chen, Frank Paige, and Xerxes Tata, "Trileptons from chargino - neutralino production at the CERN Large Hadron Collider," Phys.Rev. **D50**, 4508–4516 (1994), arXiv:hep-ph/9404212 [hep-ph]

[154] I. Hinchliffe, F.E. Paige, M.D. Shapiro, J. Soderqvist, and W. Yao, "Precision SUSY measurements at CERN LHC," Phys.Rev. **D55**, 5520–5540 (1997), arXiv:hep-ph/9610544 [hep-ph]

[155] I. Hinchliffe and F.E. Paige, "Measurements in gauge mediated SUSY breaking models at CERN LHC," Phys.Rev. **D60**, 095002 (1999), arXiv:hep-ph/9812233 [hep-ph]

[156] Henri Bachacou, Ian Hinchliffe, and Frank E. Paige, "Measurements of masses in SUGRA models at CERN LHC," Phys.Rev. **D62**, 015009 (2000), arXiv:hep-ph/9907518 [hep-ph]

[157] S. Kretzer, H.L. Lai, F.I. Olness, and W.K. Tung, "Cteq6 parton distributions with heavy quark mass effects," Phys.Rev. **D69**, 114005 (2004), arXiv:hep-ph/0307022 [hep-ph]

[158] Damien M. Pierce, Jonathan A. Bagger, Konstantin T. Matchev, and Ren-jie Zhang, "Precision corrections in the minimal supersymmetric standard model," Nucl.Phys. **B491**, 3–67 (1997), arXiv:hep-ph/9606211 [hep-ph]

[159] Howard Baer, Mike Bisset, Duane Dicus, Chung Kao, and Xerxes Tata, "The Search for Higgs bosons of minimal supersymmetry: Impact of supersymmetric decay modes," Phys.Rev. **D47**, 1062–1079 (1993)

[160] Howard Baer, Mike Bisset, Chung Kao, and Xerxes Tata, "Detecting Higgs boson decays to neutralinos at hadron supercolliders," Phys.Rev. **D50**, 316–324 (1994), arXiv:hep-ph/9402265 [hep-ph]

[161] Edward A. Baltz, Marco Battaglia, Michael E. Peskin, and Tommer Wizansky, "Determination of dark matter properties at high-energy colliders," Phys.Rev. **D74**, 103521 (2006), arXiv:hep-ph/0602187 [hep-ph]

[162] G.L. Bayatian *et al.* (CMS Collaboration), "CMS physics: Technical design report," (2006)

[163] G.L. Bayatian *et al.* (CMS Collaboration), "CMS technical design report, volume II: Physics performance," J.Phys. **G34**, 995–1579 (2007)

[164] A. Pukhov, "CalcHEP 2.3: MSSM, structure functions, event generation, batchs, and generation of matrix elements for other packages," (2004), arXiv:hep-ph/0412191 [hep-ph]

[165] Alan J. Barr and Christopher G. Lester, "A Review of the Mass Measurement Techniques proposed for the Large Hadron Collider," J.Phys. **G37**, 123001 (2010), arXiv:1004.2732 [hep-ph]

[166] Philip Bechtle, Torsten Bringmann, Klaus Desch, Herbi Dreiner, Matthias Hamer, *et al.*, "Constrained Supersymmetry after two years of LHC data: a global view with Fittino," JHEP **1206**, 098 (2012), arXiv:1204.4199 [hep-ph]

[167] O. Buchmueller, R. Cavanaugh, M. Citron, A. De Roeck, M.J. Dolan, *et al.*, "The CMSSM and NUHM1 in Light of 7 TeV LHC, B_s to mu+mu- and XENON100 Data," Eur.Phys.J. **C72**, 2243 (2012), arXiv:1207.7315 [hep-ph]

[168] C. Strege, G. Bertone, F. Feroz, M. Fornasa, R. Ruiz de Austri, *et al.*, "Global Fits of the cMSSM and NUHM including the LHC Higgs discovery and new XENON100 constraints," JCAP **1304**, 013 (2013), arXiv:1212.2636 [hep-ph]

[169] G.F. Giudice and A. Masiero, "A Natural Solution to the mu Problem in Supergravity Theories," Phys.Lett. **B206**, 480–484 (1988)

[170] Ulrich Ellwanger, Cyril Hugonie, and Ana M. Teixeira, "The Next-to-Minimal Supersymmetric Standard Model," Phys.Rept. **496**, 1–77 (2010), arXiv:0910.1785 [hep-ph]

[171] Ulrich Ellwanger, Michel Rausch de Traubenberg, and Carlos A. Savoy, "Particle spectrum in supersymmetric models with a gauge singlet," Phys.Lett. **B315**, 331–337 (1993), arXiv:hep-ph/9307322 [hep-ph]

[172] Ulrich Ellwanger, Michel Rausch de Traubenberg, and Carlos A. Savoy, "Higgs phenomenology of the supersymmetric model with a gauge singlet," Z.Phys. **C67**, 665–670 (1995), arXiv:hep-ph/9502206 [hep-ph]

[173] Ulrich Ellwanger, "Radiative corrections to the neutral Higgs spectrum in supersymmetry with a gauge singlet," Phys.Lett. **B303**, 271–276 (1993), arXiv:hep-ph/9302224 [hep-ph]

[174] P.N. Pandita, "Radiative corrections to the scalar Higgs masses in a nonminimal supersymmetric Standard Model," Z.Phys. **C59**, 575–584 (1993)

[175] T. Elliott, S.F. King, and P.L. White, "Radiative corrections to Higgs boson masses in the next-to-minimal supersymmetric Standard Model," Phys.Rev. **D49**, 2435–2456 (1994), arXiv:hep-ph/9308309 [hep-ph]

[176] S.F. King and P.L. White, "Resolving the constrained minimal and next-to-minimal supersymmetric standard models," Phys.Rev. **D52**, 4183–4216 (1995), arXiv:hep-ph/9505326 [hep-ph]

[177] F. Franke and H. Fraas, "Neutralinos and Higgs bosons in the next-to-minimal supersymmetric standard model," Int.J.Mod.Phys. **A12**, 479–534 (1997), arXiv:hep-ph/9512366 [hep-ph]

[178] C. Panagiotakopoulos and K. Tamvakis, "Stabilized NMSSM without domain walls," Phys.Lett. **B446**, 224–227 (1999), arXiv:hep-ph/9809475 [hep-ph]

[179] S.F. King, S. Moretti, and R. Nevzorov, "Theory and phenomenology of an exceptional supersymmetric standard model," Phys.Rev. **D73**, 035009 (2006), arXiv:hep-ph/0510419 [hep-ph]

[180] S.F. King, S. Moretti, and R. Nevzorov, "Exceptional supersymmetric standard model," Phys.Lett. **B634**, 278–284 (2006), arXiv:hep-ph/0511256 [hep-ph]

[181] S.F. King, S. Moretti, and R. Nevzorov, "Gauge coupling unification in the exceptional supersymmetric standard model," Phys.Lett. **B650**, 57–64 (2007), arXiv:hep-ph/0701064 [hep-ph]

[182] S.F. King, R. Luo, 2 Miller, D.J., and R. Nevzorov, "Leptogenesis in the Exceptional Supersymmetric Standard Model: Flavour dependent lepton asymmetries," JHEP **0812**, 042 (2008), arXiv:0806.0330 [hep-ph]

[183] D.J.H. Chung, L.L. Everett, G.L. Kane, S.F. King, Joseph D. Lykken, *et al.*, "The Soft supersymmetry breaking Lagrangian: Theory and applications," Phys.Rept. **407**, 1–203 (2005), arXiv:hep-ph/0312378 [hep-ph]

[184] Jonathan P. Hall and Stephen F. King, "Neutralino Dark Matter with Inert Higgsinos and Singlinos," JHEP **0908**, 088 (2009), arXiv:0905.2696 [hep-ph]

[185] J. Kalinowski, S.F. King, and J.P. Roberts, "Neutralino Dark Matter in the USSM," JHEP **0901**, 066 (2009), arXiv:0811.2204 [hep-ph]

[186] Elena Accomando, Alexander Belyaev, Luca Fedeli, Stephen F. King, and Claire Shepherd-Themistocleous, "Z' physics with early LHC data," Phys.Rev. **D83**, 075012 (2011), arXiv:1010.6058 [hep-ph]

[187] A. Semenov, "Lanhep - a package for automatic generation of feynman rules from the lagrangian. updated version 3.1," (May 2010), 1005.1909

[188] Jonathan P. Hall and Patrik Svantesson, "E6ssm-12.02," CalcHEP model, `http://hepmdb.soton.ac.uk/hepmdb:1112.0106`

[189] Jonathan P. Hall and Patrik Svantesson, "E6ssm-13.04," CalcHEP model, `http://hepmdb.soton.ac.uk/hepmdb:0413.0129`

[190] G. Belanger, Neil D. Christensen, A. Pukhov, and A. Semenov, "Slhaplus: a library for implementing extensions of the standard model," Comput.Phys.Commun. **182:763-774,2011** (Aug. 2010), 1008.0181

[191] *Search for gluino pair production in final states with missing transverse momentum and at least three b-jets using 12.8 fb-1 of pp collisions at sqrt(s) = 8 TeV with the ATLAS Detector.*, Tech. Rep. ATLAS-CONF-2012-145 (CERN, Geneva, 2012)

[192] Georges Aad *et al.* (ATLAS Collaboration), "Search for squarks and gluinos using final states with jets and missing transverse momentum with the ATLAS detector in sqrt(s) = 7 TeV proton-proton collisions," (2011), arXiv:1109.6572 [hep-ex]

[193] Hideki Okawa and for the ATLAS Collaboration, "Interpretations of susy searches in atlas with simplified models," (Oct. 2011), 1110.0282

[194] P. Athron, S.F. King, 2 Miller, D.J., S. Moretti, R. Nevzorov, *et al.*, "Predictions of the Constrained Exceptional Supersymmetric Standard Model," Phys.Lett. **B681**, 448–456 (2009), arXiv:0901.1192 [hep-ph]

[195] P. Athron, S.F. King, D.J. Miller, S. Moretti, and R. Nevzorov, "The Constrained Exceptional Supersymmetric Standard Model," Phys.Rev. **D80**, 035009 (2009), arXiv:0904.2169 [hep-ph]

[196] P. Athron, S.F. King, D.J. Miller, S. Moretti, and R. Nevzorov, "LHC Signatures of the Constrained Exceptional Supersymmetric Standard Model," Phys.Rev. **D84**, 055006 (2011), arXiv:1102.4363 [hep-ph]

[197] *Search for Resonances in the Dilepton Mass Distribution in pp Collisions at sqrt(s) = 8 TeV*, Tech. Rep. CMS-PAS-EXO-12-061 (CERN, Geneva, 2013)

[198] P. Athron, S.F. King, D.J. Miller, S. Moretti, and R. Nevzorov, "Constrained Exceptional Supersymmetric Standard Model with a Higgs Near 125 GeV," (2012), arXiv:1206.5028 [hep-ph]

[199] Serguei Chatrchyan *et al.* (CMS Collaboration), "Search for Resonances in the Dijet Mass Spectrum from 7 TeV pp Collisions at CMS," Phys.Lett. **B704**, 123–142 (2011), arXiv:1107.4771 [hep-ex]

[200] J.P. Hall, S.F. King, R. Nevzorov, S. Pakvasa, M. Sher, *et al.*, "Novel Higgs Decays and Dark Matter in the E(6)SSM," Phys.Rev. **D83**, 075013 (2011), arXiv:1012.5114 [hep-ph]

[201] Jonathan P. Hall and Stephen F. King, "Bino Dark Matter and Big Bang Nucleosynthesis in the Constrained E_6SSM with Massless Inert Singlinos," JHEP **1106**, 006 (2011), arXiv:1104.2259 [hep-ph]

[202] Stephen F. King and Alexander Merle, "Warm Dark Matter from keVins," (2012), arXiv:1205.0551 [hep-ph]

[203] J. Pumplin *et al.*, "New generation of parton distributions with uncertainties from global QCD analysis," JHEP **07**, 012 (2002), arXiv:hep-ph/0201195

[204] A. Kulesza and L. Motyka, "Soft gluon resummation for the production of gluino-gluino and squark-antisquark pairs at the LHC," Phys.Rev. **D80**, 095004 (2009), arXiv:0905.4749 [hep-ph]

[205] Wim Beenakker, Silja Brensing, Michael Kramer, Anna Kulesza, Eric Laenen, *et al.*, "Soft-gluon resummation for squark and gluino hadroproduction," JHEP **0912**, 041 (2009), arXiv:0909.4418 [hep-ph]

[206] W. Beenakker, S. Brensing, M.n Kramer, A. Kulesza, E. Laenen, *et al.*, "Squark and Gluino Hadroproduction," Int.J.Mod.Phys. **A26**, 2637–2664 (2011), arXiv:1105.1110 [hep-ph]

[207] Serguei Chatrchyan *et al.* (CMS Collaboration), "Search for supersymmetry in all-hadronic events with missing energy," (2011), CMS-PAS-SUS-11-004

[208] Georges Aad *et al.* (ATLAS Collaboration), "Search for supersymmetry in final states with jets, missing transverse momentum and one isolated lepton in sqrts = 7 TeV pp collisions using 1 fb^{-1} of ATLAS data," Phys.Rev. **D85**, 012006 (2012), 18 pages plus author list (30 pages total), 9 figures, 4 tables, final version to appear in Physical Review D, arXiv:1109.6606 [hep-ex]

[209] Georges Aad *et al.* (ATLAS Collaboration), "Searches for supersymmetry with the ATLAS detector using final states with two leptons and missing transverse momentum in sqrts = 7 TeV proton-proton collisions," (2011), arXiv:1110.6189 [hep-ex]

[210] Serguei Chatrchyan *et al.* (CMS Collaboration), "Multileptonic SUSY searches," (2011), CMS-PAS-SUS-11-013

[211] *Search for supersymmetry in events with four or more leptons and missing transverse momentum in pp collisions at* $\sqrt{s} = 7$ *TeV with the ATLAS detector*, Tech. Rep. ATLAS-CONF-2012-001 (CERN, Geneva, 2012)

[212] Howard Baer, Harrison Prosper, and Heaya Summy, "Early susy discovery at lhc without missing e_t: the role of multi-leptons," Phys.Rev.D **77:055017,2008** (Jan. 2008), 0801.3799

[213] Serguei Chatrchyan *et al.* (CMS Collaboration), "Search for narrow resonances in dilepton mass spectra in pp collisions at sqrt(s) = 7 TeV," (2012), arXiv:1206.1849 [hep-ex]

[214] Jonathan P. Hall and Stephen F. King, "NMSSM+," JHEP **1301**, 076 (2013), arXiv:1209.4657 [hep-ph]

[215] Peter Athron, Maien Binjonaid, and Stephen F. King, "Fine Tuning in the Constrained Exceptional Supersymmetric Standard Model," (2013), arXiv:1302.5291 [hep-ph]

[216] James C. Callaghan and Stephen F. King, "E6 Models from F-theory," (2012), arXiv:1210.6913 [hep-ph]

[217] John R. Ellis, K. Enqvist, Dimitri V. Nanopoulos, and F. Zwirner, "Observables in Low-Energy Superstring Models," Mod.Phys.Lett. **A1**, 57 (1986)

[218] R. Hamberg, W. L. van Neerven, and T. Matsuura, "A Complete calculation of the order $\alpha - s^2$ correction to the Drell-Yan K factor," Nucl. Phys. **B359**, 343–405 (1991)

[219] W. L. van Neerven and E. B. Zijlstra, "The O $(alpha - s^{2)}$ corrected Drell-Yan K factor in the DIS and MS scheme," Nucl. Phys. **B382**, 11–62 (1992)

[220] R. Hamberg, T Matsuura, and W.L. van Neerven, ZWPROD program (1989-2002), http://www.lorentz.leidenuniv.nl/research/neerven/DECEASED/Welcome.html

[221] Pavel M. Nadolsky *et al.*, "Implications of CTEQ global analysis for collider observables," Phys. Rev. **D78**, 013004 (2008), arXiv:0802.0007 [hep-ph]

[222] A. D. Martin, W. J. Stirling, R. S. Thorne, and G. Watt, "Parton distributions for the LHC," Eur. Phys. J. **C63**, 189–285 (2009), arXiv:0901.0002 [hep-ph]

[223] Victor Mukhamedovich Abazov *et al.* (D0), "Search for a heavy neutral gauge boson in the dielectron channel with 5.4 fb^{-1} of $\mathbf{p\bar{p}}$ collisions at $\sqrt{\mathbf{s}} = \mathbf{1.96}$ TeV," (2010), arXiv:1008.2023 [hep-ex]

[224] "Search for high-mass dilepton resonances in 6.1/fb of pp collisions at sqrt(s)= 8 TeV with the ATLAS experiment," (2012)

[225] Riccardo Barbieri, Alex Pomarol, Riccardo Rattazzi, and Alessandro Strumia, "Electroweak symmetry breaking after lep1 and lep2," Nucl. Phys. **B703**, 127–146 (2004), hep-ph/0405040

[226] Ennio Salvioni, Giovanni Villadoro, and Fabio Zwirner, "Minimal Z' models: present bounds and early LHC reach," JHEP **11**, 068 (2009), arXiv:0909.1320 [hep-ph]